ABSTRACT

LOKITZ, STEPHEN JARED. A High-Resolution Study of p + ^{44}Ca Reactions. (Under the direction of Dr. Gary E. Mitchell and Dr. John F. Shriner, Jr.)

A high resolution measurement of the cross-sections of the ^{44}Ca(p,p$_0$) and ^{44}Ca(p,p$_1$) reactions was performed over the energy range E_p = 2.50–3.53 MeV to improve the purity and completeness of the ^{45}Sc level sequences. A specific goal was the investigation of possible parity-dependence of the level densities of ^{45}Sc. This research was performed at the High Resolution Laboratory at Triangle Universities Nuclear Laboratory. The data were measured at five angles and the observed cross-sections were fit with the multilevel, multichannel, R-matrix code MULTI6. Many levels were observed for the first time, and many levels were reassigned different quantum numbers. A total of $\sim$800 resonances were observed.

The purity and completeness of the ^{45}Sc data were tested via several statistical analyses: the nearest-neighbor spacing distribution, the reduced width distribution, and the Dyson-Mehta Δ_3 statistic. The results of the statistical analyses were mixed. The s-wave resonance sequence compares very well with random matrix predictions. The other sequences do not agree well with GOE predictions, suggesting missing and/or misassigned levels.

The experimental nearest-neighbor spacings were compared to the Wigner distribution to identify anomalously large (small) spacings which imply missing (misassigned) levels. The number of anomalous spacings has been reduced, indicating improved purity and completeness of the data. In particular the small spacing anomalies proved to be a very useful and practical analysis tool. The level densities were determined using two methods to correct for missing levels. Uncertainties in the level densities have been significantly reduced. No evidence of parity dependence in the level densities of ^{45}Sc was observed.

A HIGH RESOLUTION STUDY OF p + ^{44}Ca REACTIONS

by

STEPHEN JARED LOKITZ

A dissertation submitted to the Graduate Faculty of

North Carolina State University

in partial fulfillment of the

the requirements for the Degree of

Doctor of Philosophy

PHYSICS

Raleigh

2004

APPROVED BY:

John H. Kelley

Mohamed Bourham

Gary E. Mitchell,

Co-chair of Advisory Committee

John F. Shriner, Jr.,

Co-chair of Advisory Committee

To Kyla

and away we go...

Biography

Stephen Jared Lokitz

Personal

Born June 5, 1976, San Diego, CA

Married to Kyla Eve Leleux, June 19, 1999

Education

B.S. Physics, Mathematics, Millsaps College, 1998

M.S. Physics, North Carolina State University, 2000

Academic Positions

Teaching Assistant, North Carolina State University, 1998–2004

Research Assistant, North Carolina State University, 2001–2004

Memberships

Phi Beta Kappa

American Physical Society

Acknowledgments

Many people have made contributions to this endeavor. All deserve my sincere gratitude and appreciation.

It has been a privilege to study under the wings of Dr. Gary Mitchell. He has generously shared his experience, knowledge, and wisdom, and he has been an invaluable mentor throughout my graduate career. I also want to acknowledge Dr. John Shriner, Jr. He always responded to frantic e-mails with patience and suggestions. These two professors helped me overcome obstacles that I thought were insurmountable. They have my admiration and respect. Without them, my project could not have been successfully completed.

Dr. Undraa Agvaanluvsan formulated many of the theoretical issues that provided the groundwork for this research. She took the time to explain trivial, and not so trivial details, even when she was busy with her own responsibilities. I would also like to thank Dr. Daniel McDevitt for his assistance with data collection.

I want to thank Dr. Mohamed Bourham and Dr. John Kelly for serving on my committee.

I am confident that I could not have coaxed the HRL to produce high quality data without the skill and expertise of Chris Westerfeldt. His mastery of the HRL is phenomenal. He always offered suggestions to solve any problem that I encountered and was available far more often than I could reasonably expect him to be. The assistance of Bret Carlin, Paul Carter, John Dunham, Sidney Edwards, Patrick Mulkey and Richard O'Quinn has also been immeasurable. I am indebted to them for their willingness to drop everything to help me.

I also would like to give a special message to Dr. Sharon Stephenson. As my undergraduate physics professor at Millsaps College, her enthusiasm for nuclear physics was part of the motivation that directed me to pursue nuclear physics and to attend North

Carolina State University. Her guidance and encouragement have and continue to be greatly appreciated.

In addition, I would like to recognize my colleagues, Bill Beal and Lance McLean. Their knowledge and skill in the lab have been a tremendous resource. I relied heavily on their support and encouragement. Whether discussing sports, music or how to fix the ESA, their friendship and camaraderie will not be easily replaced or replicated.

Special thanks go to my parents and family. I owe them much more than words can express. I hope they take as much pride in this accomplishment as I do.

Finally, this achievement would not be as meaningful without my wife, Kyla, in my life.

This project was supported in part by the United States Department of Energy and the Triangle Universities Nuclear Laboratory.

Contents

List of Tables

List of Figures

Chapter 1

Introduction

Level densities have been investigated experimentally and theoretically for more than 50 years. The many practical applications of level densities have attracted interest from a variety of fields. Many experiments at the High Resolution Laboratory at the Triangle University Nuclear Laboratory have been performed over the last thirty years to determine the level densities of many different nuclei.

Level densities are usually determined by direct counting of observed nuclear states. Because experimental limitations have always produced imperfect data, even the best data may not allow precise determination of the level densities. However, recent research has produced improved analytic techniques that better determine the fraction of missing levels in a sequence. A better estimate of the completeness of a sequence will allow a more accurate determination of the level densities [Agv03b]. The application of these methods to several sets of data previously measured has produced improved results. However, the application to one data set resulted in results which have caused a reassessment of the quality of the previous data.

The p + ^{44}Ca reaction has been very well studied. The quality of the measurements made in these experiments was considered excellent. However, the application of the level density corrections to the ^{45}Sc compound nucleus data has produced interesting results. The corrected level densities of the compound nucleus ^{45}Sc suggested a parity-dependence of the level densities [Agv03a]. The uncertainties in these level densities precluded definitive conclusions.

A by-product of the observed fraction corrections is an analysis method (the spacing anomaly analysis method) which provides a qualitative assessment of the purity and completeness of experimental sequences. By comparing the nearest-neighbor spacing distribution, anomalous spacings which indicate potential misassigned or missing levels are revealed. This analysis indicated many specific suspected misassigned levels and many suspected general locations of unobserved resonances in the ^{45}Sc data. The apparent parity dependence of the level densities in ^{45}Sc can be questioned because of the large number of anomalies present in the data.

One goal of the present experiment was to investigate the specific resonances that the spacing anomaly analysis indicated were problematic. If the spacing anomalies can be removed, then the level densities will be better determined. Several factors have led to the conclusion that the experimental conditions have improved sufficiently to justify a re-investigation of the p + ^{44}Ca reactions. Recent experiments at the High Resolution Laboratory have shown that the beam resolution of the system has been improved. Passivated implanted planar silicon charged-particle detectors can measure the cross-sections of the inelastic channels with greatly reduced background. Faster computers allow a more detailed analysis of the cross-section data. Thus weaker resonances should be observed, and more accurate J^π assignments should be made. With higher quality resonance parameters, the level densities should be determined more accurately. With the level densities determined with reduced uncertainties, the observed parity dependence of the level densities can be evaluated more precisely.

The previous experiments that investigated the p + ^{44}Ca reactions were performed over a period of fifteen years [Wil75, Shr82, Shr83, Smi89] with vastly different experimental conditions and different methods of analysis. The different data sets are of uneven quality and reliability. The present experiment remeasured the ^{44}Ca(p,p$_0$) and ^{44}Ca(p,p$_1$) cross-sections over the chosen energy range to produce one continuous data set of consistent quality.

This experiment measured the differential cross-sections for the ^{44}Ca(p,p$_0$) and ^{44}Ca(p,p$_1$) reactions for five angles over the energy range E$_p$ = 2.50–3.53 MeV using 1.1–1.5 μg/cm^2 thick ^{44}Ca targets. The experiment was performed using the modified KN-3000 Van de Graaff proton accelerator at the High Resolution Laboratory at the Triangle University Nuclear Laboratory. Excellent results were obtained. The observed resonances were sorted into sequences which were tested statistically for completeness and purity. The level densities were determined with improved precision. The parity-dependence of the level densities with improved uncertainties was investigated, and the validity of the spacing anomaly analysis method was examined.

This work consists of seven chapters and four appendices. In the next chapter, an overview of the relevant parts of random matrix theory will be presented along with a discussion of two methods that estimate the observed fraction of levels in a sequence. Statistical tests of data quality are also described. Chapter 3 presents a brief description of the R-matrix theory used to analyze the cross-section data. Chapter 4 describes the experimental apparatus used to perform this experiment.

Chapter 5 describes the determination of resonance parameters and gives a comparison of the resonances observed in this experiment with those from the previous work. Chapter 6 shows the results of several of the statistical analyses of the data. The nearest-neighbor spacing distributions and reduced width distributions are compared to theoretical predictions. The J-dependence and parity-dependence of the corrected level densities are investigated. Chapter 7 presents a summary of this experiment and the results.

Four appendices are included in this thesis. In Appendix A, the observed differential cross-section data and the theoretical fits for the ^{44}Ca(p,p$_0$) and the ^{44}Ca(p,p$_1$) reactions are presented. Appendix B lists the resonance parameters both in order of E$_p$ and sorted by J$^\pi$. Appendix C lists the adopted levels of ^{45}Ca used to identify analog resonances in ^{45}Sc. Appendix D presents the results of the procedure which unfolds the energy dependence of the level densities.

Chapter 2

Statistical Analyses

The goal of the present experiment is to obtain pure and complete ^{45}Sc level sequences to measure accurately the level densities of ^{45}Sc and to test the applicability of the spacing analysis postulated by Agvaanluvsan [Agv02]. Agvaanluvsan analyzed the ^{45}Sc level sequences measured by Smith [Smi89]. The analysis produced evidence of a possible parity dependence of the level densities [Agv03a]. However, this analysis also suggested a large number of possible quantum number misassignments and missing levels. This chapter describes the relevant theoretical issues for such an analysis. Section 2.1 describes random matrix theory (RMT) and several statistics used to analyze nuclear spectra. Section 2.2 discusses the determination of f, the fraction of states observed for an experimental sequence. Section 2.3 describes the spacing anomaly analysis and a new method to evaluate a mixed distribution of two GOE sequences.

2.1 Random Matrix Theory

RMT is the theory used to describe statistical properties of nuclear resonances. A comprehensive review was presented by Guhr *et al.* [Guh98]; the general theory is described by Mehta [Meh91]. The Gaussian orthogonal ensemble (GOE) is the appropriate version of RMT when the system is time-reversal-invariant and rotationally symmetric. The GOE introduces an ensemble of random Hamiltonian matrices H which are real and symmetric. The nuclear Hamiltonian is treated as a random variable with a probability distribution $P(H)$. To obtain the explicit form of the probability distribution, the distribution is assumed to be independent of the choice of basis vectors and the independent elements of H are assumed to be statistically independent. The explicit form of $P(H)$ can be shown to be

$$P(H) = e^{-a\,\mathrm{tr}(H^2)+b\,\mathrm{tr}(H)+c} \tag{2.1}$$

where $a, b,$ and c are constants, and

$$\mathrm{tr}(H^j) = \sum_{k=1}^{N} \lambda_k^j; \tag{2.2}$$

here the λ_k are the eigenvalues of the nuclear Hamiltonian H. Each matrix H is assumed to describe equally probable interactions between particles. The GOE does not account for the dynamical properties of the nuclear Hamiltonian. However, statistical properties of nuclear level sequences can be investigated by examining the fluctuations about the averages of certain observables. The GOE makes parameter-free predictions about the fluctuation properties of nuclear spectra but says nothing about the dynamical properties.

2.1.1 Reduced Width Distribution

The probability distribution of the reduced widths (γ^2) of a sequence of levels is one test used to investigate the completeness of a nuclear sequence. A sequence of levels is defined as a set of levels all having the same quantum numbers (in this work, J and π). The GOE prediction for the distribution of the reduced widths of a sequence is called the Porter-Thomas distribution [Por56] and has the form

$$P(y) = \frac{1}{\sqrt{2\pi y}} e^{-\frac{y}{2}}. \tag{2.3}$$

Here $y = \frac{\gamma_\lambda^2}{\langle\gamma^2\rangle}$, where γ_λ^2 is the reduced width for level λ and $\langle\gamma^2\rangle$ is the average reduced width for all levels in the sequence. The Porter-Thomas distribution predicts a large probability for obtaining very small widths. The distribution is not valid globally because the distribution is energy independent and requires a constant average reduced width. To describe this property globally, another quantity, the strength function S is used

$$S = \frac{\langle \gamma^2 \rangle}{D} \tag{2.4}$$

where D is the mean level spacing. Alternatively, the spreading width $\Gamma^{\downarrow} = 2\pi S$ can be used to describe the global characteristics of the reduced widths of a sequence. Since the mean level spacing changes exponentially with increasing energy, the characterization "global" may be questionable. However, $\langle \gamma^2 \rangle$ also effectively changes exponentially with increasing energy because the complexity of the eigenstates grows strongly with increasing energy [Guh98] such that these exponential dependencies cancel in $\Gamma^{\downarrow}$ and S. These parameters are then suitable for describing the global properties of the reduced width distribution.

2.1.2 Nearest-Neighbor Spacing Distribution

The nearest-neighbor spacing distribution (NNSD) represents one of the key results of any of the ensembles of RMT. The NNSD provides information about the short-range order of the eigenvalues. The probability density function describes the probability of finding two adjacent levels with a spacing s [Guh98]. It is convenient and conventional to work with the dimensionless variable x, defined as the ratio of the spacing between adjacent levels (s) and the average spacing between levels (D)

$$x = \frac{s}{D}. \tag{2.5}$$

A system that follows the GOE statistics has a probability distribution approximately of the form

$$P_{GOE}(x) = \frac{\pi}{2} x e^{-\frac{\pi x^2}{4}}. \tag{2.6}$$

This distribution is the Wigner distribution [Wig57]. As illustrated in Figure 2.1, $P_{GOE}(x)$ approaches zero as x approaches zero. This "level repulsion" is one of the key predictions of the GOE for the nearest-neighbor spacing distribution.

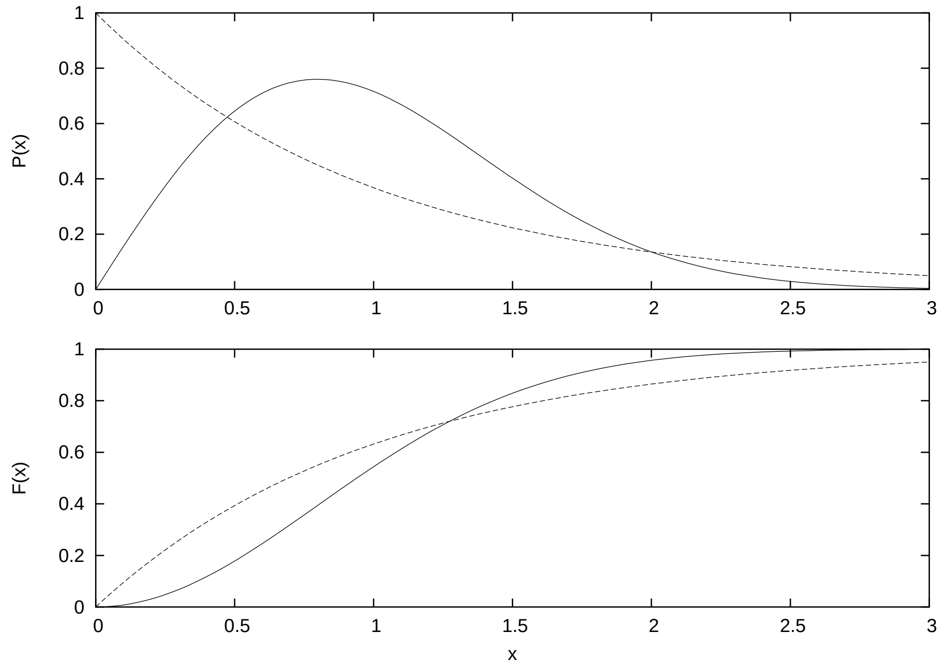

Figure 2.1: Nearest neighbor spacing distributions. The upper graph shows the probability function, $P(x)$. The lower graph shows $F(x)$, the integral of $P(x)$. The solid lines represent the GOE distribution and the dashed lines represent the Poisson distribution.

If a sequence contains a random set of uncorrelated energy levels with no special symmetries, the system will obey Poisson statistics. This distribution has the form

$$P_{Poisson}(x) = e^{-x}. \tag{2.7}$$

This Poisson distribution has behavior quite different from the Wigner distribution at $x = 0$; the probability density function has its maximum at $x = 0$.

Histograms can in some cases be very sensitive to the choices of bins, and therefore the integral of the probability density function is also used to compare NNSD data with the predicted distributions. The integral of $P(x)$ is defined as $F(x)$, the definite integral over an intermediate variable x' from zero to x,

$$F(x) = \int_0^x P(x')dx'. \tag{2.8}$$

Integrating Equations 2.7 and 2.6 gives:

$$F_{Poisson}(x) = 1 - e^{-x} \tag{2.9}$$

$$F_{GOE}(x) = 1 - e^{-\frac{\pi x^2}{4}} \tag{2.10}$$

Figure 2.1 illustrates the differences in $P(x)$ and $F(x)$ for the Poisson and GOE distributions.

2.1.3 Dyson-Mehta Δ_3 Statistic

The Dyson-Mehta Δ_3 statistic [Dys63] was developed to investigate long-range order. The Dyson-Mehta Δ_3 statistic for a sequence of levels from E_{min} to E_{max} is

$$\Delta_3 = \min_{A,B}\left(\frac{1}{E_{max} - E_{min}} \int_{E_{min}}^{E_{max}} [N(E) - AE - B]^2 dE\right), \tag{2.11}$$

where the parameters A and B are parameters of the best straight line fit to the integral of the level density, $N(E)$:

$$N(E) = \int_0^E \rho(E) dE. \tag{2.12}$$

This statistic can be expressed as a function of L, the number of average spacings in an interval. For Poisson statistics

$$\Delta_{3_{poisson}}(L) = \frac{L}{15}. \tag{2.13}$$

For GOE statistics, Δ_3 must be evaluated numerically. For large values of L, Δ_3 approaches the value

$$\Delta_{3_{GOE}} \approx \frac{1}{\pi^2}(\ln L - 0.0687). \tag{2.14}$$

Figure 2.2 illustrates Δ_3 for Poisson and GOE distributions.

2.2 Missing Level Analysis

Level densities are often measured by direct counting of compound nuclear states. However, because no experiment will ever produce perfect data, corrections must be made

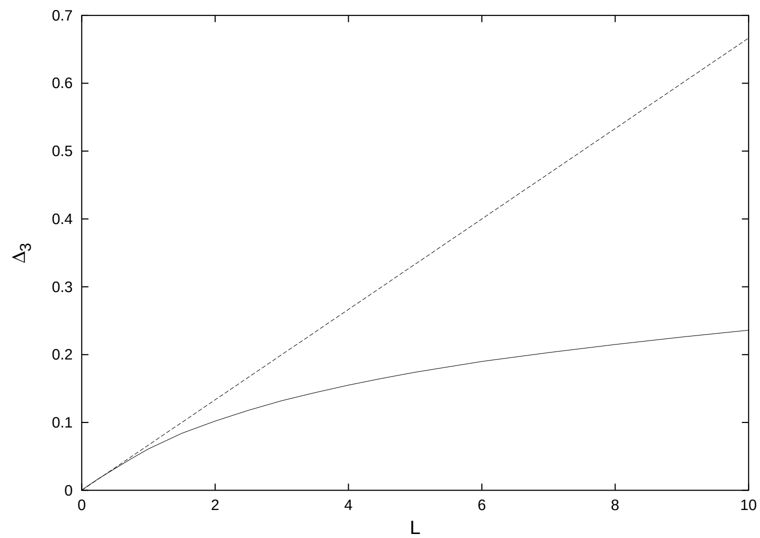

Figure 2.2: The Dyson-Mehta Δ_3 statistic is plotted as a function of L, the number of average spacings. Theoretical predictions are shown for Poisson (dashed line) and GOE (solid line) distributions.

to the data to account for unobserved levels and to estimate the uncertainties introduced by the corrections. Two methods to estimate the number of missing levels in a sequence were described by Agvaanluvsan *et al.* [Agv02, Agv03b], a standard width analysis method and a new spacing analysis method. A brief description of both methods is presented here.

2.2.1 Width Analysis Method

The width analysis method uses the reduced widths, γ^2, to estimate the observed fraction of levels in a sequence. Some levels will remain unobserved due to the finite experimental threshold of observation. A perfect sequence (no missing or spurious levels) follows the Porter-Thomas distribution (Equation 2.3). An imperfect sequence can be described by a modified Porter-Thomas distribution which accounts for the distorted experimental distribution. This method includes only the effects of missing levels.

The width analysis method that Agvaanluvsan [Agv02] follows is that of Fröhner [Frö80]. The distribution of reduced widths is assumed to be a truncated Porter-Thomas distribution,

$$P_f(y) = \begin{cases} 0 & : \quad y < y_0 \\ \dfrac{1}{\mathrm{erfc}\left(\sqrt{y_0/2}\right)} \dfrac{\mathrm{e}^{-y/2}}{\sqrt{2\pi y}} & : \quad y \geq y_0 \end{cases} . \tag{2.15}$$

Applying the maximum likelihood technique to this distribution leads to the equation

$$\langle \gamma^2 \rangle = \langle \gamma^2 \rangle_{obs} \Big(1 + \sqrt{\frac{2y_0}{\pi}} \frac{e^{-y_0/2}}{\mathrm{erfc}\sqrt{y_0/2}} \Big)^{-1}. \tag{2.16}$$

The solution to Equation 2.16 is obtained by calculating $\langle \gamma_1^2 \rangle$ from the experimentally obtained value of $\langle \gamma_{obs}^2 \rangle$. The calculated value of $\langle \gamma_1^2 \rangle$ is entered into the right-hand side of Equation 2.16 as $\langle \gamma_{obs}^2 \rangle$ and a new value $\langle \gamma_2^2 \rangle$ is computed. The process is repeated until the value entered into the right-hand side of Equation 2.16, $\langle \gamma_{n-1}^2 \rangle$, and the calculated result $\langle \gamma_n^2 \rangle$ converge. This final value of $\langle \gamma_n^2 \rangle$ is then compared with the observed value, $\langle \gamma_{obs}^2 \rangle$, to obtain the observed fraction of levels in a sequence.

2.2.2 Spacing Analysis Method

The nearest-neighbor spacing distribution for a perfect GOE sequence follows the Wigner distribution. Experimental data are almost always incomplete. Unlike the reduced width distribution where widths are usually missed because they are too small to observe, the missing levels in the spacing analysis are randomly distributed. When levels are missing, the nearest-neighbor spacing distribution will not be described accurately by the Wigner distribution since some observed nearest neighbors are not actually nearest neighbors.

The distribution for the spacing of an imperfect sequence can be written as

$$P(z) = \sum_{k=0}^{\infty} a_k \lambda p(k; \lambda z). \tag{2.17}$$

The parameter z is defined as $z \equiv fx$, where f is defined as $f = N_{observed}/N_{true}$. The relative contributions of the k-th nearest-neighbor spacing distribution $p(k; \lambda z)$ are given by the parameters a_k. The parameter λ describes the incompleteness of the sequence.

Several conditions are imposed upon Equation 2.17. The total probability of $P(z)$ must be normalized to unity, and the average value of z must be 1. The functions $P(k; \lambda z)$

must also be normalized to one and have average values of $k+1$ when expressed in terms of the variable x. These conditions are expressed by the two constraints

$$\sum_{k=0}^{\infty} a_k = 1, \tag{2.18}$$

$$\sum_{k=0}^{\infty} a_k(k+1) = \lambda. \tag{2.19}$$

The parameters a_k can be determined by defining an entropy

$$S\{a_k\} = -\sum_{k=0}^{\infty} a_k \ln a_k \tag{2.20}$$

along with two Lagrange multipliers α and β for the two constraints (Equation 2.18 and Equation 2.19). Maximizing the entropy requires

$$\delta \left\{ -\sum_{k=0}^{\infty} a_k \ln a_k - \alpha \sum_{k=0}^{\infty} a_k - \beta \sum_{k=0}^{\infty} (k+1) a_k \right\} = 0. \tag{2.21}$$

The values that maximize the entropy are $a_k = f(1-f)^k$ and $\lambda = 1/f$. These values yield the expression

$$P(x) = \sum_{k=0}^{\infty} f(1-f)^k P(k;x). \tag{2.22}$$

The maximum likelihood method is then applied to Equation 2.22 which generates a value of f and a value for the uncertainty in f for a sequence. The two methods, spacing and width, complement each other and provide independent tests of the missing fraction of levels in a sequence.

2.3 Spacing Anomaly Analysis

If the expected distribution is known, information can be gained by comparing the expected and experimental distributions. Section 2.2.2 described the comparison of the nearest-neighbor spacing distributions of a sequence to the Wigner distribution to provide an estimate of the percentage of missing levels in the sequence. While this is necessary for accurate calculations of the nuclear level densities, the percentage of missing levels does not indicate specific regions where the missing levels are likely to be found. Section 2.3.1 describes a method that uses the nearest-neighbor spacing distributions to locate suspected spacing anomalies, and Section 2.3.2 explains a new method that uses the value of the nearest-neighbor spacing distribution at $x = 0$ to estimate the number of spurious levels in a sequence.

2.3.1 Spacing Anomalies

The nearest-neighbor spacing distributions for nuclear level sequences are expected to follow the Wigner distribution (Equation 2.6). Observed nearest-neighbor spacing distributions for level sequences can be expressed in terms of the variable $x \equiv \frac{s}{D}$ and compared directly to the Wigner distribution. As shown in Section 2.2.2, this comparison to observed data gives an indication of the percentage of missing levels. However, the locations of the missing levels are unknown.

An anomalous spacing is defined as a nearest-neighbor spacing that has a value of x that is either so small or so large as to be very unlikely given the Wigner distribution. Large values of x suggest a missing (unobserved) level. Listed in Table 2.1 are the values of x for a given confidence level. Sufficiently large spacings strongly suggest missing levels. However, experimental evidence may be very difficult to obtain, since the resonance probably would have already been observed if it were easy to detect. Some of the missing resonances will be observed in the current experiment, but some will remain unobserved due to the finite experimental threshold. Also, there is only limited information regarding the locations of suspected missing levels. The energy interval suggested by a large spacing anomaly can be large and may contain many other resonances with different quantum numbers. Thus, correcting all large spacing anomalies with the current experimental methods is unlikely.

Corrections involving small spacing anomalies are more promising. Small values of x indicate levels that are too close together and suggest a level with a misassigned quantum number. Figure 2.3 shows the Wigner distribution and the values of x that are too small for a given confidence level. To investigate small values of x, for convenience the inverse, $1/x$,

Table 2.1: Percentage of levels with spacings $\geq x$.

$x = \frac{s}{D}$	% of levels $\geq x$
1.95	5 %
2.23	2 %
2.42	1 %
3.00	0.1 %

is considered. Table 2.2 lists the values of $1/x$ for a given confidence level. Small spacing anomalies can be more easily investigated since the locations of both levels are already known. Studying the pair of resonances that produced the small spacing with improved resolution and determining the resonance parameters of these resonances with improved confidence may produce a quantum number reassignment and eliminate the small spacing anomaly. Thus, a small spacing anomaly should be easier to correct experimentally than a large spacing anomaly, because the levels that produce a small spacing anomaly have always been previously observed.

Table 2.2: Percentage of levels with spacings $\geq 1/x$.

$x = \frac{s}{D}$	$1/x$	% of levels $\geq 1/x$
0.25	4.00	5 %
0.16	6.25	2 %
0.11	8.84	1 %
0.04	25.00	0.1 %

To identify the anomalous spacings, plots of x and $1/x$ are prepared. The normalized nearest-neighbor spacings are plotted successively to identify anomalous spacings. These plots also provide an immediate qualitative measure of the completeness and purity of a sequence. Fewer anomalies in a sequence generally indicate fewer possible mistakes and omissions. The x plots indicate specific regions where missing levels are likely to occur while the $1/x$ plots indicate specific pairs of levels that may have a misassigned quantum

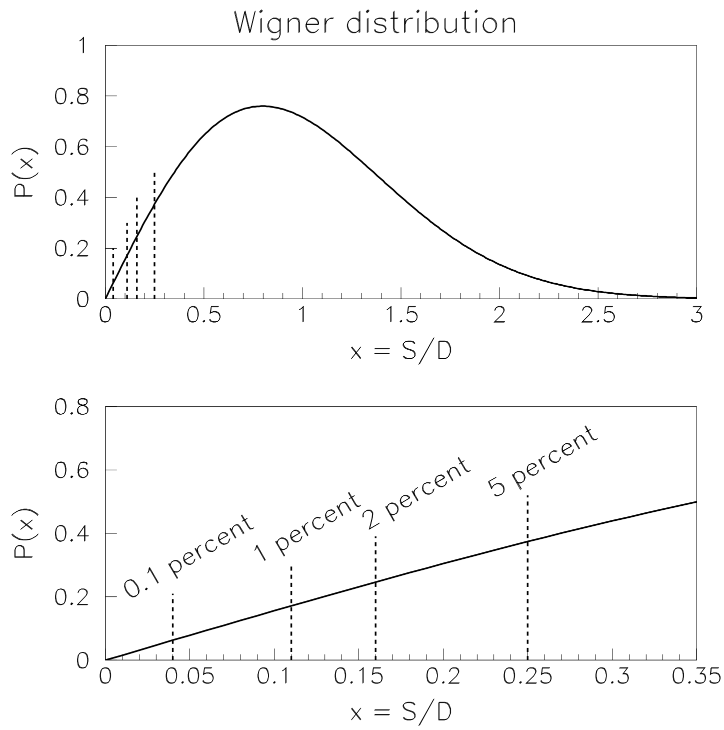

Figure 2.3: The relative probability of small spacings for a Wigner distribution. The upper graph shows the Wigner distribution. The dashed lines indicate the values of x for which the probability of finding a value smaller than that value of x are 0.1%, 1%, 2%, and 5%. The lower graph shows the small-x portion of the upper graph in greater detail.

number.

Figure 2.4 is the combined data for $J^\pi = \frac{1}{2}^-$ resonances in ^{45}Sc from previous work [Wil75, Shr82, Shr83, Smi89]. This figure illustrates the usefulness of this spacing analysis method. The anomalies in the x plot are very likely to be produced by unobserved levels in the sequence; $x \geq 4.0$ has a probability of $\sim \frac{1}{10^6}$. A value of $1/x \geq 25$ has a probability $\sim \frac{1}{10^3}$. The x and $1/x$ plots provide an approximate measure of the overall quality of a sequence while suggesting specific levels that may be misassigned or energy regions where levels may be missed.

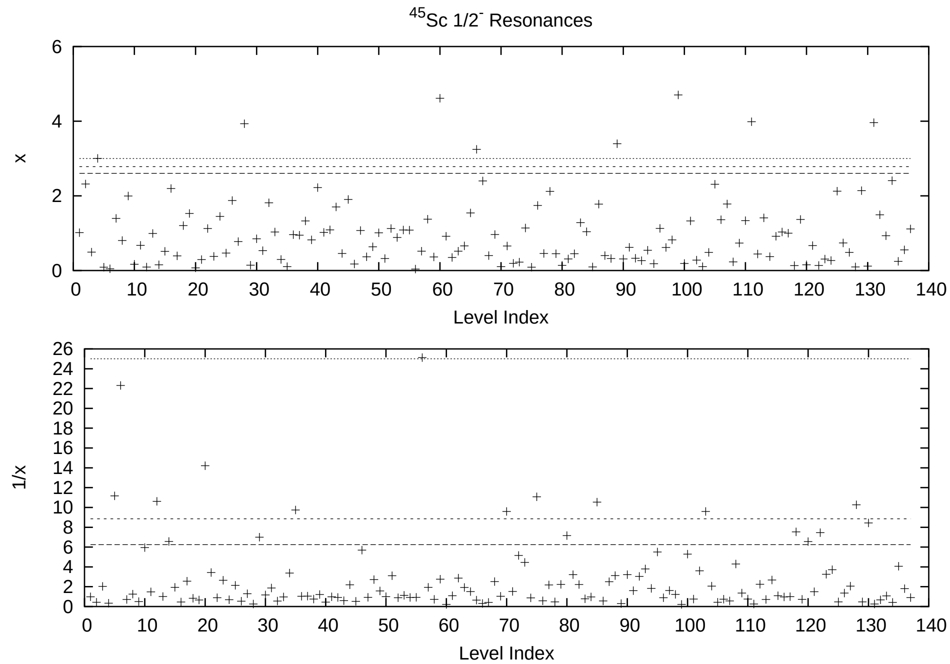

Figure 2.4: x and $1/x$ plots for the $J^{\pi} = \frac{1}{2}^{-}$ sequence before the current measurements. The dashed lines represent the 2%, 1% and 0.1% confidence level.

2.3.2 $P(0)$ Analysis

One flaw of the spacing anomaly analysis described in Section 2.3.1 is that only levels with extreme spacings will be indicated by plotting x and $1/x$. The method does not identify misassignments or missing levels if the nearest-neighbor spacings are not anomalously large or small. A method that does not depend on spacing anomalies to quantify the purity of a sequence has been considered.

Spurious levels in a sequence are levels that have misassigned quantum numbers and are placed in a sequence in which the level does not belong. The resulting nearest-neighbor spacing distribution will be a mixture of GOE sequences instead of one as in the pure and complete case. The nearest-neighbor spacing distribution for the mixing of GOE sequences was formulated by Mehta [Meh91]. Although the general distribution is extremely complicated, it reduces to a very simple form at $x = 0$:

$$P(0) = 1 - \sum_{i}^{n} f_i^2, \tag{2.23}$$

with f_i being the relative probability of the mixed sequences. For proton resonance data, the ambiguity in the fitting analysis reduces to mixing only two sequences, i.e., $n = 2$. $P(0)$ can then be written

$$P(0) = 1 - f_1^2 - f_2^2. \tag{2.24}$$

Since $f_1 + f_2 = 1$, Equation 2.24 reduces to a quadratic of the form:

$$f_1^2 - f_1 + \frac{P(0)}{2} = 0. \tag{2.25}$$

Thus, if $P(0)$ can be determined for experimental data, then the number of spurious levels in the sequence can also be determined. The number of spurious levels in a sequence will be directly related to the overall quality of the sequence.

Chapter 3

Reaction Formalism

The most useful formalism for describing compound nuclear resonances is the R-matrix theory, formulated by Wigner and Eisenbud [Wig46b, Wig46a, Wig47]. R-matrix theory has been used very successfully to describe the charged-particle scattering cross-sections measured at the High Resolution Laboratory. Section 3.1 contains a brief description of R-matrix theory as formulated by Lane and Thomas [Lan58] and presented in many theses [Wil73, Wat80, Nel83, Smi89]. Section 3.2 describes isobaric analog resonances (IAR).

3.1 R-Matrix Formalism

R-matrix theory makes several assumptions. R-matrix theory only describes non-relativistic quantum mechanical systems. Three-body systems are not allowed unless considered as a succession of two-body reactions. Only reactions in which the initial and final states consist of two particles are considered in this description of R-matrix theory. There must be a distance beyond which the interaction between the two particles ceases. This distance is called the "channel radius".

For the present experiment, all of the above assumptions are valid. Since the nucleon kinetic energy inside the nucleus is a few percent of the rest mass, non-relativistic quantum mechanics is sufficient to describe the system. This experiment involved only the ^{44}Ca(p,p$_0$)

and ^{44}Ca(p,p$_1$) reactions, and thus the two-body requirement is met. Finally, since nuclear forces are short range, a "channel radius" a_c can be defined.

R-matrix theory can be formulated in different representations. When used to describe the interaction of an unpolarized beam and target, the channel spin representation is normally used. The spin of the target and the spin of the projectile are coupled to form a channel spin, which is then coupled with the relative angular momentum of the target and projectile to form the spin of the compound state. This method is used since the cross-sections are incoherent in channel spin, and the total cross-section can be expressed as a weighted sum of the cross-sections for each channel spin. The compound nucleus is created via an "entrance" channel which consists of the projectile and target. The compound nucleus then decays through an "exit" channel. Channels which are not allowed by some conservation law are called "closed" while allowed channels are called "open".

A pair of interacting nuclei is labelled by the letter α which specifies the quantum states of each nucleus in the pair. The two nuclei have spins, I_1 and I_2, which are vector-coupled to form the channel spin s. The resultant channel spin can assume values between $\mid I_1 - I_2 \mid$ and $\mid I_1 + I_2 \mid$. The two nuclear spins also have corresponding projections i_1 and i_2, and the channel spin has a projection ν. The relative orbital angular momentum ℓ and its projection m are also specified for the pair α. The channel spin, s, and the relative angular momentum, ℓ, are combined to give a resultant total angular momentum, J (with projection M). A channel c for the pair α is then defined by the angular momentum coupling $\{\alpha(I_1, I_2)s\ell JM\}$. For variables that do not depend on angular momentum, we can use either the channel label c or the pair label α without confusion. However, some variables will refer only to a specific channel, and for those we must maintain the channel label. In what follows, every effort is made to indicate this distinction.

Before solving the Schroedinger equation, the following quantities are useful to define. The interaction radius beyond which the nuclei labeled by c feel no mutual nuclear intereaction is $a_c = a_\alpha$, and the energy of the relative motion is $E_c = E_\alpha$. The relative position of particle two with respect to particle one is denoted by $\mathbf{r}_\alpha = \mathbf{r_c}$. Other convenient definitions are:

$$
\begin{aligned}
\text{the reduced mass of the system} \quad M_c &= M_\alpha = \frac{M_{\alpha_1} M_{\alpha_2}}{M_{\alpha_1} + M_{\alpha_2}}, \\
\text{the wave number} \quad k_c &= k_\alpha = \left[\frac{2M_\alpha E_\alpha}{\hbar^2}\right]^{\frac{1}{2}}, \\
\text{the relative velocity} \quad v_c &= v_\alpha = \frac{\hbar k_c}{M_c}, \\
\text{the Coulomb field parameter} \quad \eta_c &= \eta_\alpha = \frac{Z_{\alpha_1} Z_{\alpha_2} e^2}{\hbar v_\alpha}, \\
\text{and a dimensionless parameter} \quad \rho_c &= \rho_\alpha = k_c r_c.
\end{aligned}
$$

To solve the Schroedinger equation, the radial space is separated into an external region ($r_c > a_c$) and internal region ($r_c < a_c$). Only the Coulomb force is present in the external region, and the Schroedinger equation can be solved exactly. The resulting external wave functions are

$$\psi_c^{ext} = \frac{\chi_c(\mathbf{r_c}) u_{\alpha\ell}(r_c)}{\sqrt{v_c}}, \tag{3.1}$$

where

$$\chi_c(\mathbf{r_c}) = \left[\frac{i^\ell Y_\ell^m(\theta_\alpha, \phi_\alpha)}{r_c}\right] \psi_{\alpha s\nu} \tag{3.2}$$

are the surface wave functions which are mutually orthogonal and normalized at $r_c = a_c$. The Y_ℓ^m are the usual spherical harmonics, and $\psi_{\alpha s\nu}$ are the channel spin wave functions formed by the vector coupling of the spin wave functions of the two interacting nuclei. The function $u_{\alpha\ell}$ is the radial wave function which satisfies the following:

$$\frac{d^2 u_{\alpha\ell}}{dr_c^2} + \left[\frac{2M_\alpha}{\hbar^2}\right] \left[E_c - V_c\right] u_{\alpha\ell}(r_c) = 0. \tag{3.3}$$

The potential V_c includes both the Coulomb and "centrifugal" potential energies and has the form:

$$V_c = \frac{Z_{\alpha_1} Z_{\alpha_2} e^2}{r_c^2} + \frac{\hbar^2 \ell(\ell+1)}{2M_c r_c^2}. \tag{3.4}$$

Obtaining the solutions to the radial wave functions by considering only the open channels ($E_c > 0$) yields two linearly independent solutions, F_c and G_c. These solutions are the regular and irregular Coulomb functions [Jah60]. The general solutions of the radial wave function are linear combinations of the regular and irregular Coulomb functions and represent incoming and outgoing waves:

$$I_c^+ = [G_c - F_c]\, e^{i\omega_c} \tag{3.5}$$

and

$$O_c^+ = [G_c + F_c]\, e^{-i\omega_c}. \tag{3.6}$$

The parameter ω_c takes the form:

$$\omega_c = \omega_{\alpha\ell} = \sum_{n=1}^{\ell} \tan^{-1}\left(\frac{\eta_\alpha}{n}\right) \tag{3.7}$$

The complete channel wave functions which represent incoming and outgoing waves of unit flux in the external region are then

$$I_c = \frac{\chi_c(r_c) I_c^+}{\sqrt{v_c}} \tag{3.8}$$

and

$$O_c = \frac{\chi_c(r_c) O_c^+}{\sqrt{v_c}}. \tag{3.9}$$

A collision matrix $U_{cc'}$ can be introduced in the general solution of the wave function in the external region. The general solution can be expressed as a linear combination of I_c and O_c. The solution chosen represents the external wave function for a particular incoming wave and has the form

$$\psi_c^{ext} = I_c - \sum_{c'} U_{cc'} O_{c'}. \tag{3.10}$$

The collision matrix is the amplitude of the outgoing wave in channel c' which is associated with a particular incoming wave in channel c. One example would be elastic scattering which is described by Equation 3.10 when $c = c'$. All the information necessary to solve the reaction problem is contained in the collision matrix. The collision matrix must be expressed as an analytical function since the differential cross-sections can be calculated from the collision matrix ($\frac{d\sigma}{d\Omega} \propto \mid U_{cc'} \mid^2$).

Several methods have been considered to obtain $U_{cc'}$. One method would be to assume a nuclear potential in the internal region. With a nuclear potential, the Schroedinger equation could be solved to generate a wave function for the internal region which could then be matched to the external wave function at the nuclear surface ($r_c = a_c$). However, the results of this method would rely on the parameters chosen to describe the nuclear potential. The R-matrix theory instead proposes a complete set of states which are eigenstates of the Hamiltonian in the internal region. This postulate covers all possible resonances of the compound nuclear system and has the form

$$H_\lambda \psi_\lambda = E_\lambda \psi_\lambda \tag{3.11}$$

with

$$\int \psi_\lambda^* \psi_{\lambda'} dr = \delta_{\lambda\lambda'}. \tag{3.12}$$

The channel wave functions can then be expressed in terms of the overlap of the internal λ states with the appropriate surface wave functions χ_c. Integrating over the nuclear surface of radius a_c gives

$$\chi_\lambda(r_c) = \int_{a_c} \chi_c^* \psi_\lambda dS, \tag{3.13}$$

which are eigenfunctions with eigenenergies E_λ in channel c and have arbitrary, real, energy-independent boundary conditions

$$\left[\rho_c \frac{\chi_c'}{\chi_c}\right]_{r_c=a_c} = B_c. \tag{3.14}$$

Here the prime indicates differentiation with respect to ρ_c.

The wave functions in the internal region for any energy E can be expressed in terms of an expansion of the eigenfunctions $\chi_\lambda(r_c)$. The coefficients of the expansion can be determined by applying Green's theorem. The resulting internal wave function can be written as

$$\psi_c^{int}(r_c) = R_{cc'} \left[a_c \frac{d\psi_c^{int}(r_c)}{dr} - B_c \psi_c^{int}(r_c)\right]_{r_c=a_c} \tag{3.15}$$

where the Green's function, $R_{cc'}$, that relates the value of the wave function in the internal region to its derivative on the surface is

$$R_{cc'} = \sum_{\lambda} \frac{\gamma_{\lambda c}\gamma_{\lambda c'}}{E_{\lambda} - E}. \tag{3.16}$$

The reduced widths, $\gamma_{\lambda c}$, take the form

$$\gamma_{\lambda c} = \left[\frac{\hbar^2}{2M_c a_c}\right]^{\frac{1}{2}} \chi_{\lambda}(a_c) = \left[\frac{\hbar^2}{2M_c a_c}\right]^{\frac{1}{2}} \int_{a_c} \chi_c^* \psi_{\lambda} dS. \tag{3.17}$$

Equations 3.16 and 3.17 define the elements of the R-matrix and the reduced widths. The collision matrix (U-matrix) may be expressed in terms of the R-matrix by equating the logarithmic derivatives of the internal and external wave functions at $r_c = a_c$. The result can be shown to be

$$U_{cc'} = e^{i(\omega_c + \omega_{c'} - \phi_c - \phi_{c'})} \left[\delta_{cc'} + 2iP_c^{\frac{1}{2}} \frac{1}{1 - R_{cc'}L_{c'}} R_{cc'} P_{c'}^{\frac{1}{2}}\right] \tag{3.18}$$

where

$$L_c = \left[\rho_c \frac{O_c'}{O_c}\right]_{r_c = a_c} - B_c = \left[S_c^{\lambda} - B_c\right] + iP_c. \tag{3.19}$$

P_c is called the penetrability; it is proportional to the transmission probability through the external barrier and can be expressed as

$$P_c = \left[\frac{\rho_c}{F_c^2 + G_c^2}\right]_{r_c = a_c}. \tag{3.20}$$

S_c is the shift function and has the form

$$S_c = \left[\rho_c \frac{F_c F_c' + G_c G_c'}{F_c^2 + G_c^2}\right]_{r_c = a_c}. \tag{3.21}$$

The quantity ϕ_c is called the hard-sphere phase shift and has the form

$$\phi_c = \tan^{-1}\left(\frac{F_c}{G_c}\right). \tag{3.22}$$

The quantity ω_c is the Coulomb phase shift for channel c.

A quantity that represents the total energy shift from the eigenenergy E_{λ} and results from a mismatch of the external and internal boundary conditions is

$$\Delta_{\lambda} = -\sum_{c'} \left[S_{c'}^{\lambda} - B_{c'}\right] \gamma_{\lambda c'}^2. \tag{3.23}$$

The total laboratory width for a level is

$$\Gamma_\lambda = \sum_c \Gamma_{\lambda c}, \tag{3.24}$$

where the partial laboratory width for a channel,

$$\Gamma_{\lambda c} = 2P_c\gamma^2_{\lambda c}, \tag{3.25}$$

is the transition probability from the state λ via the channel c. The partial laboratory width contains a factor from both the external region (penetrability) and internal region (reduced width). The penetrability is a measure of the kinematic effects in the external region. The penetrability decreases as ℓ increases. Thus high ℓ states will generally have smaller values of laboratory partial widths than low ℓ states. The reduced widths have the external region effect removed which allows for a comparison of the strength of the nuclear coupling to the entrance channel.

The R-matrix and collision matrix are both diagonal in total spin and in parity. The cross-section includes contributions from all spins and parities. The relationship between the differential cross-section and collision matrix is derived by Lane and Thomas and is programmed in the FORTRAN code MULTI6. The equation is

$$\begin{aligned}
\frac{d\sigma_{\alpha s,\alpha' s'}}{d\Omega_{\alpha'}} &= \frac{\pi}{k^2_\alpha}\left|C_{\alpha'}(\theta_{\alpha'})\right|^2 \delta_{\alpha' s',\alpha s} \\
&+ \frac{1}{k^2_\alpha(2s+1)}\sum_L B_L(\alpha' s',\alpha s)P_L(\cos\theta_{\alpha'}) \\
&+ \frac{\pi^{\frac{1}{2}}}{k^2_\alpha(2s+1)}\sum_{J\ell}(2J+1)\delta_{\alpha' s'\ell',\alpha s\ell}Re\left[iT^J_{\alpha' s'\ell',\alpha s\ell}\right]C_{\alpha'}(\theta_{\alpha'})P_\ell(\cos\theta),
\end{aligned} \tag{3.26}$$

where

$$\begin{aligned}
B_L(\alpha' s',\alpha s) &= \frac{1}{4}(-1)^{(s-s')}\sum_{J_1J_2\ell_1\ell_2\ell'_1\ell'_2}\overline{Z}(\ell_1J_1\ell_2J_2,sL) \\
&\times\ \overline{Z}(\ell'_1J_1\ell'_2J_2,s'L)\left(T^{J_1}_{\alpha' s'\ell'_1,\alpha s\ell_1}\right)\left(T^{J_2}_{\alpha' s'\ell'_2,\alpha s\ell_2}\right)^*,
\end{aligned} \tag{3.27}$$

$$T^J_{\alpha' s'\ell',\alpha s\ell} = e^{2i\omega_{\alpha'\ell'}}\delta_{\alpha' s'\ell',\alpha s\ell} - U^J_{\alpha' s'\ell',\alpha s\ell}, \tag{3.28}$$

and

$$C_\alpha = \frac{1}{[4\pi]^{\frac{1}{2}}} \eta_\alpha \csc^2\left(\frac{\theta_\alpha}{2}\right) e^{-2i\eta_\alpha \log[\sin(\frac{\theta_\alpha}{2})]}. \tag{3.29}$$

The $\overline{Z}$ coefficients are the Z coefficients of Biedenharn *et al.* [Bie52] with the phase convention of Huby [Hub54]. The $P_\ell(\cos\theta)$ are the Legendre polynomials with the phase convention of Condon and Shortley [Con51].

The first term in Equation 3.26 represents pure Coulomb scattering, the second term represents resonance scattering and reaction, and the third term represents the interference between the first two terms. The Coulomb and interference terms vanish except for elastic scattering. To obtain the experimentally measured cross-sections for unpolarized beam and target, Equation 3.26 must be summed over s' and averaged over s. The summing and averaging is also performed by MULTI6; the result is

$$\frac{d\sigma_{\alpha,\alpha'}}{d\Omega_{\alpha'}} = \frac{1}{(2I_1+1)(2I_2+1)} \sum_{ss'} \frac{d\sigma_{\alpha s,\alpha' s'}}{d\Omega_{\alpha'}}. \tag{3.30}$$

3.2 Isobaric Analog Resonances

Isobaric analog states are defined as nuclear states that are multiplets of a given isospin, T. These nuclei differ by the exchange of a neutron for a proton. In an analog parent-daughter system, both nuclei have A nucleons, but the daughter has one more proton and one less neutron than the parent. If the nuclear force is charge independent and charge symmetric, then the isospin quantum number $T = \frac{N-Z}{2}$ is a good quantum number, and the energy difference between parent and daughter is $\Delta E_c - \delta$, where ΔE_c is the Coulomb energy difference and δ is the proton-neutron mass difference. Corresponding states in the parent and daughter have the same values of J$^\pi$. The energy differences between parent and daughter are illustrated in Figure 3.1.

From Figure 3.1, an the excitation energy of the parent (E_x) and the center of mass proton energy (E_{cm}) are related by

$$\Delta E_c = B_n + E_{cm} - E_x, \tag{3.31}$$

where B_n is the binding energy of the last neutron in the parent nucleus, and B_p is the binding energy of the last proton in the daughter nucleus. Analog resonances were used to determine values of ΔE_c. Jänecke has determined a semi-empirical approximation for ΔE_c given by [Jän69]

$$\Delta E_c = \frac{C_1 Z_< + C_2}{A^{\frac{1}{3}}}, \tag{3.32}$$

where A is the mass of the parent system, $Z_<$ is the proton number of the target and C_1 and C_2 are constants. For the $A = 45$ system, $B_n = 7.41479$ MeV, $B_p = 6.8882$ MeV, and Jänecke's estimate gives $\Delta E_c = 7.238$ MeV. Therefore, the approximate relation between E_{cm} for p + ^{44}Ca resonances and E_x in ^{45}Ca is $E_{cm} = E_x$ - 0.177 MeV. ΔE_c can vary significantly; thus the uncertainty in this calculation can be large.

The analog state is a non-statistical effect and can be extremely strong compared to the background resonances. Because an analog state has a non-statistical effect on γ^2, analog resonances must be considered before statistical analyses of the reduced width distribution, calculations of the strength function, or width analysis level density corrections can proceed. In addition, analog states can fragment. Fragmentation occurs when an analog resonance enhances the strength of the nearby resonances. Some resonances may be obviously enhanced while other resonances may be so weak that the enhancement may not be noticeable. The fine structure of the fragment distribution can be fit and the total contribution of the analog level enhancement determined [Bil76]. However, this detailed analysis is unnecessary for the current experiment. For the present purposes the primary goal is to identify the strong analogs and to remove their contributions to the strength. Otherwise, the strong analogs will distort the statistical width analyses.

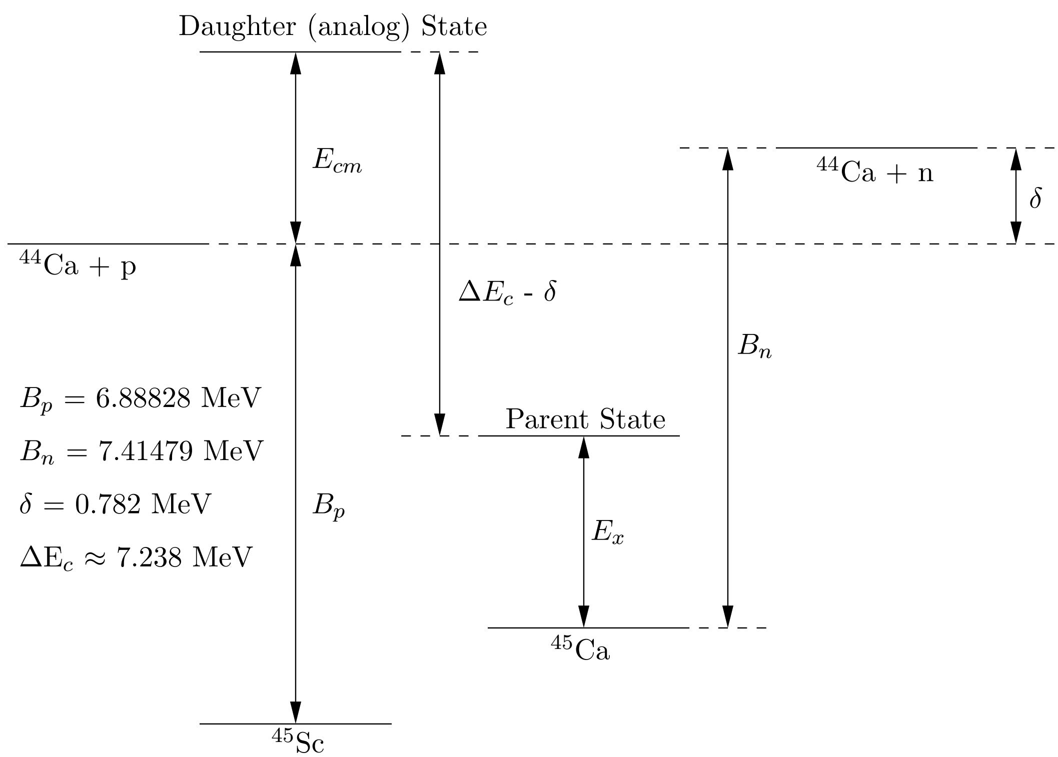

Figure 3.1: Analog state energy schematic for the ^{45}Ca and ^{45}Sc system. B_p, the binding energy of the last proton in the daughter nucleus, and B_n, the binding energy of the last neutron in the parent nucleus, are from the 2003 mass evaluation of the National Nuclear Data Center [Nud03]. ΔE_c, the estimated Coulomb energy difference between the parent and daughter nucleus, is from Jänecke [Jän69].

Chapter 4

Experimental Setup

The data for this experiment were collected at the High Resolution Laboratory (HRL) of the Triangle Universities Nuclear Laboratory (TUNL). The HRL is shown schematically in Figure 4.1. The main component of the HRL is a modified KN-3000 Van de Graaff positive ion accelerator. Recent experiments have produced tunable proton beams over the energy range 0.9–4.0 MeV. Combined with the laboratory's unique electrostatic analyzer (ESA), this accelerator produces a proton beam with excellent beam energy resolution (200–300 eV) which allows the investigation of weak, closely spaced nuclear resonances. The accelerator and ESA will be discussed in Section 4.1. The detectors and the data acquisition system will be explained in Section 4.2. The experimental procedure will be outlined in Section 4.3 and the target fabrication described in Section 4.4.

4.1 Accelerator

The modified KN-3000 Van de Graaff positive ion accelerator (illustrated in Figure 4.2) is a single-ended, belt-driven particle accelerator. This machine has been refitted to operate at accelerating potentials up to four million volts [Wes88, Wes95]. The entire accelerator column is encased inside a steel tank that is pressurized to 270–300 psi with a

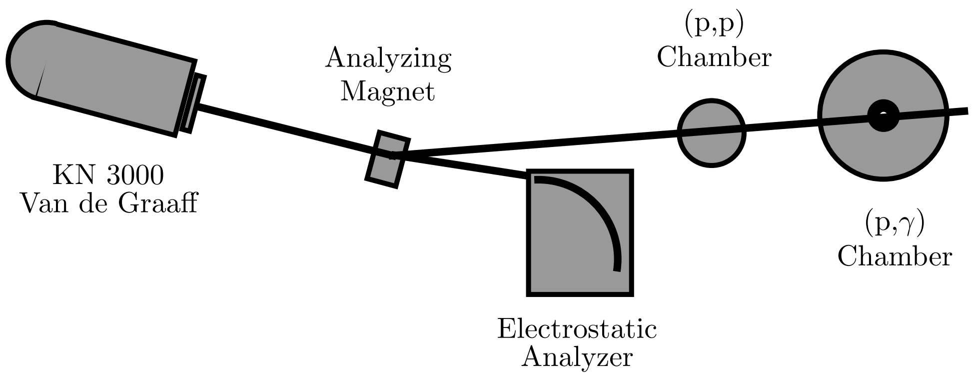

Figure 4.1: Floorplan of the High Resolution Laboratory at TUNL (not to scale). The (p,p) chamber was used in this experiment.

combination of dry CO_2 and N_2 for electrical insulation. Along this column runs a 190-inch vulcanized rubber belt which carries positive charge to the dome. Beside the column is a stainless steel accelerator tube rated for potentials as high as four million volts. Some of the charge deposited on the dome flows through a series of column-mounted 600-MΩ resistors, resulting in a series of equipotential planes which produce constant acceleration over the length of the tube. To maintain constant charge on the dome, a set of corona needles are mounted on the inside of the tank between the dome and the tank wall. Current flows from the dome through the needles, which allows the amount of positive charge on the dome to be altered. The corona controller is partially driven by a capacitive pickoff signal (CPO). The CPO is an electrically isolated metal plate which monitors the AC components of the dome voltage. The CPO generates a signal which is used as feedback to reduce low frequency AC fluctuations (20 Hz or less).

During normal operation, two ion beams are produced by a radio frequency (RF) ion source, which sits at the unsupported end of the cantilevered column. High purity H_2 gas is leaked into a glass source bottle. An RF field applied to this bottle results in the gas becoming a plasma. The disassociation of the H_2 results in protons (H^+) and singly ionized hydrogen molecules (H_2^+). The two beams are then extracted from the source bottle, focused, and accelerated. At the base of the accelerator tank is an analyzing magnet. The

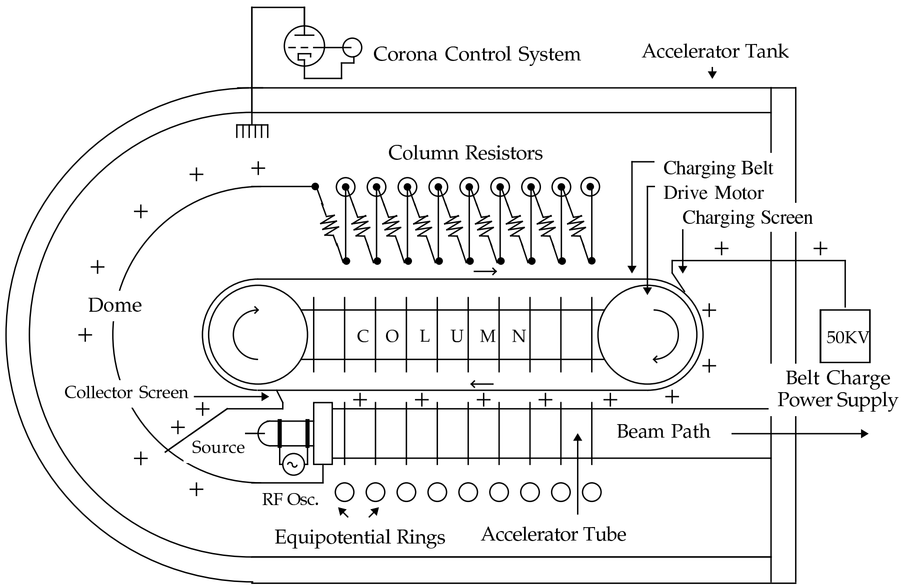

Figure 4.2: Schematic of the modified KN-3000 Van de Graaff accelerator.

two species are deflected by different amounts due to the difference in their charge-to-mass ratios. The magnet is set so that the H^+ beam is deflected by 25° into a beam line that terminates at the target chambers and the H_2^+ beam is deflected 17° into the ESA to be used for diagnostic purposes.

The ESA is basically a pair of curved metal plates. This system is designed to monitor and correct the energy fluctuations of the accelerated proton beam. The plates are separated by 4.57 mm and form a 90° arc. The plates are biased to voltages of equal magnitude but opposite polarities such that the H_2^+ beam can only pass through the ESA if it is within a certain energy tolerance. The total voltage difference between the plates is set to the desired proton beam energy divided by 111.37. The voltage settings are monitored by a high precision voltmeter and a control PC to ensure that the proper voltage is maintained. There are also two sets of lateral slits, the corona slits at the entrance and the image slits at the exit of the ESA. Figure 4.3 shows the various feedback loops used by the ESA.

The corona signal is used to drive the corona controller to reduce fluctuations in the

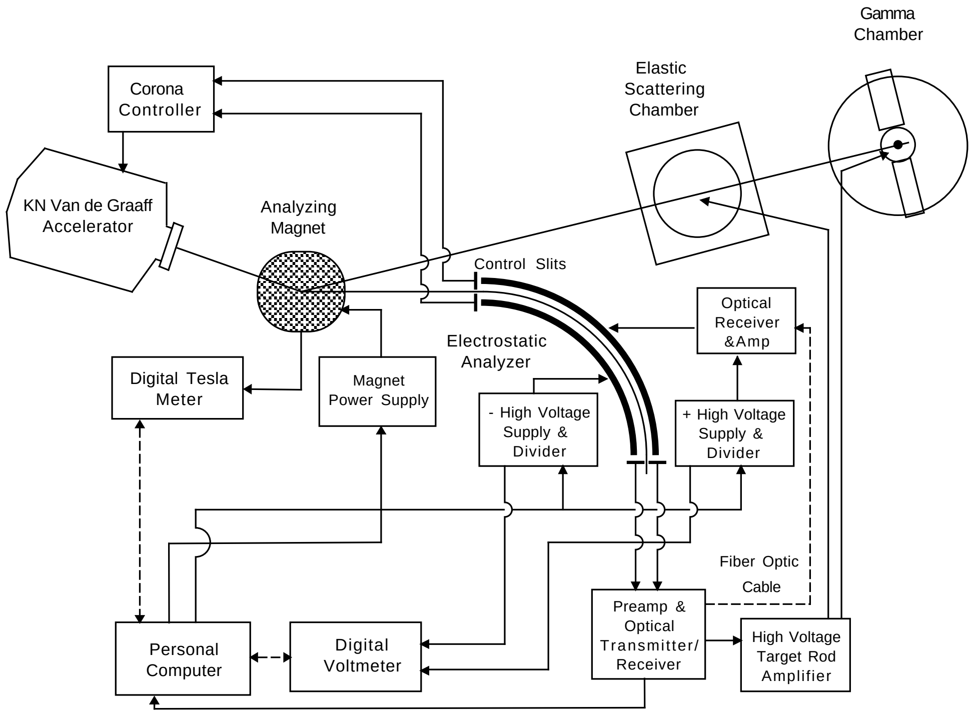

Figure 4.3: High Resolution Laboratory Control Loops. A current difference signal from the corona control slits is used to regulate voltage on the terminal. A current difference signal from the image slits located at the end of the ESA is used to regulate the magnetic field, the potential on the outer plate, and to adjust the target rod voltage.

terminal voltage. A slit difference signal is measured by sampling the difference in the H_2^+ beam current on the left and right corona slits. This signal is a direct indication of the slow energy fluctuations inherent in a belt-driven accelerator. The corona controller attempts to minimize this slit difference signal in order to maintain a mono-energetic proton beam. Used in conjunction with the CPO feedback, this system dramatically decreases the amplitude of the dome voltage fluctuations (to a value ≈ 1 kV$_{p-p}$). The corona slits are also used in the automated creation of yield curves which will be discussed shortly.

The image slits are also used to create a difference signal. This signal is a real time indication of the energy fluctuations. This signal is used by three control loops simultaneously: the analyzing magnet, the ESA outer plate driver, and the target rod driver. To regulate the magnet, this slit difference signal is sent to the control PC. The control

PC adjusts the magnet setting to minimize the slit difference signal. This increases the stability of the beam and is crucial when automating the generation of yield curves. The slit difference signal is also applied to the outer plate of the ESA which slightly alters the voltage difference between the ESA plates. This is done to increase the H_2^+ beam stability by accounting for the small fluctuations in beam energy measured by the slit difference signal. Finally, the slit difference signal is sent to the target rod driver. The target rod is normally biased at 3 kV; the slit difference signal is amplified by the target rod driver and added to the bias voltage. In this manner, the proton beam energy is corrected for dome voltage fluctuations as it approaches the target. The result of these control loops is to create a nearly mono-energetic beam with outstanding resolution and reduced energy drift.

The control loops are also used for the critical function of automating the generation of yield curves. This is accomplished by the TUNL XSYS data acquisition software system, which can change the energy of the proton beam automatically. First the VAX and control PC change the voltage of the ESA to the voltage that corresponds to the new proton beam energy. Because the molecular beam will no longer be properly centered in the ESA, the image slit difference will increase. The control PC will then adjust the analyzing magnet to minimize the image slit difference signal. As this is accomplished, the H_2^+ beam will now generate a slit difference signal at the corona slits. The corona driver will alter the dome voltage to minimize this signal, and the proton beam will now be at a new energy without any operator involvement. This process is monitored by the control PC to inhibit data acquisition if problems arise.

4.2 Detectors and Data Acquisition System

The target chamber is on the 25° beam line into which the H^+ beam is steered and is shown schematically in Figure 4.4. The protons are deflected by the analyzing magnet and steered and focused to this chamber by two sets of quadrupole magnets and two sets of dipole magnets. The beam is highly collimated by a series of three in-line collimators located just in front of the target chamber. The ^{44}Ca targets are mounted on a target rod which holds four targets and a tuning ring. The beam current is measured with a Faraday cup at the rear of the target chamber. For this experiment, a typical beam was 6-8 μA with less than 5 nA on the tuning ring and last collimator.

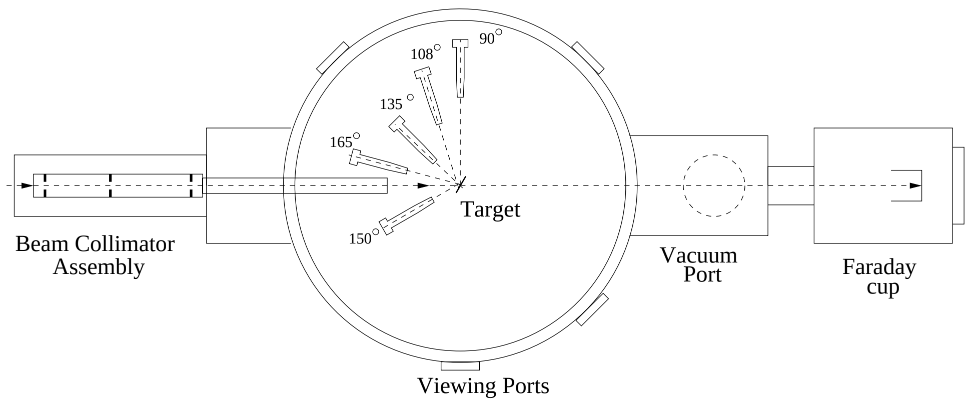

Figure 4.4: High Resolution Laboratory charged particle target chamber. The beam is collimated before striking the target, which is set at 330°. The beam is measured at the Faraday cup. This chamber was designed by Westerfeldt [Wes82, Wes83].

Mounted inside the target chamber were five passivated implanted planar silicon (PIPS) detectors manufactured by Canberra. The PIPS detectors were the partially depleted (PD50-13-300AM) model with 50 mm^2 active area and 300 micron depth. The detectors are factory tested to have a resolution of $\leq$ 13 keV (FWHM) for ^{241}Am-5.486 MeV alpha particles. Each detector was mounted on its own stand in the horizontal plane of the target and with a collimator in front of the detector. Dipole magnets were placed on the collimator snouts to reduce noise from electrons attracted to the positively biased detector. The detectors were located such that the count rates for all five detectors were approximately equal. The detector solid angles are listed in Table 4.1.

The data acquisition system is illustrated in Figure 4.5. Scattered charged particles with energies used in this experiment (a few MeV) deposit all of their energy in the depletion zone of the biased (+40 V) PIPS detector. This generates a pulse proportional to the energy of the scattered particle. The pulse is amplified by a pre-amplifier (Ortec 142) in order to transmit the signal from the target chamber to the control room. The signal is

Table 4.1: Detector solid angles for the five detectors used in this experiment. Solid angles were chosen such that there were approximately equal count rates in each detector.

Detector Angle	Ω (msr)
90°	0.53
108°	0.90
135°	1.54
150°	1.84
165°	2.04

then amplified by a linear amplifier (Ortec 572) which outputs both a bipolar (timing) and unipolar (energy) signal. Both outputs are used to process the signal. The unipolar singal is digitized and displayed in a spectrum via the VAX unless prevented by the bipolar signal discrimination process, which is used to eliminate carbon scattering events and to reduce electronic dead time.

The unipolar signal is sent to the multiplexer (Ortec 476-8) after an appropriate delay and then sent to the ADC (Northern NS-621). The delay allows electronic discrimination of the bipolar signal. The bipolar signal is split, with one line entering a Timing Single Channel Analyzer (TSCA) (Ortec 551 or Ortec 420A) and the other delayed to arrive simultaneously at a Gated Single Channel Analyzer (SCA) (Hewlett-Packard 5583A) with the output of the TSCA. The TSCA is used to discriminate against carbon scattering events. The TSCA examines the signal to determine if it falls within a window which is calibrated to the energy of a carbon scattering event. If the signal is identified as a carbon event, then the SCA is inhibited from accepting the delayed bipolar signal. In turn, no signal is sent to the multiplexer gate box from the SCA, and the unipolar signal is not accepted by the multiplexer. If the signal is identified as a non-carbon event, the gated SCA accepts the bipolar signal and generates and transmits a gate to the multiplexer gate box. The multiplexer then accepts the delayed unipolar signal and the ADC digitizes this signal.

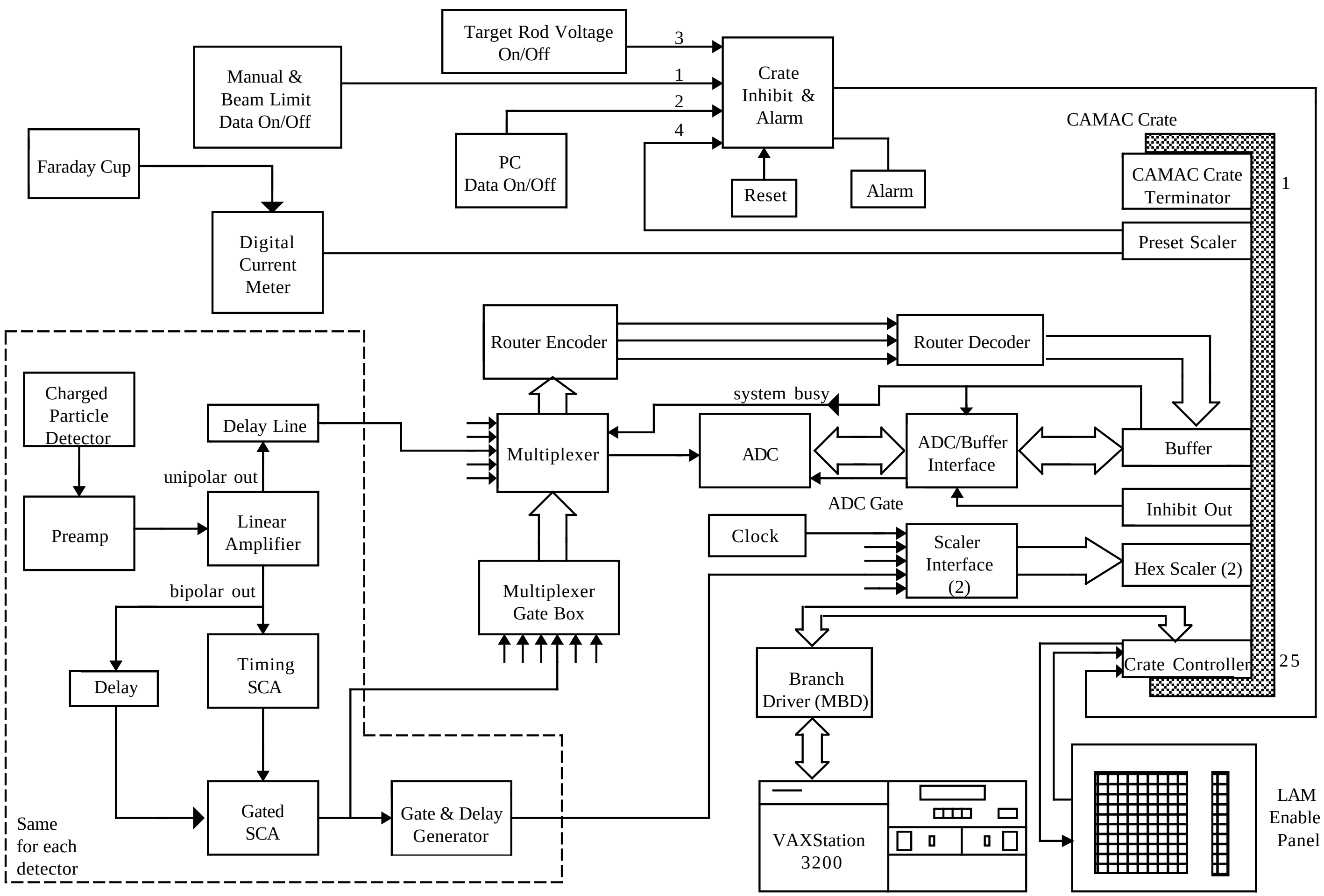

Figure 4.5: Data acquisition electronics for the PIPS detectors.

The SCA also serves as a discriminator to eliminate low and high energy noise by setting upper and lower limits on the signals. When an event is to be processed, the gated SCA also sends a signal to a Gate and Delay Generator (Ortec 416A). This creates a signal which is sent directly to the scalar interface to count the number of acceptable events. Thus, the signals that are determined acceptable exclude carbon scattering events and events with too low or too high an amplitude.

The unipolar signal is sent directly to the multiplexer after a 900-ns delay, which corresponds to the processing time of the bipolar signal. When the multiplexer is given the command to accept a signal, it also generates a routing signal which indicates the detector from which the digitized signal came. This signal is decoded and sent to the buffer interface, where the digitized signal is tagged to maintain the detector identification. This information accumulates in the buffer in the CAMAC crate to await transfer to the Microprogrammable Branch Driver (MBD) and then to the VAX. A final piece of information waits in the CAMAC crate as well. The Gate and Delay Generator signal is sent to the scalar interface and then to a hex scalar. The number of signals sent to the hex scalar for each detector is compared to the number of digitized events to calculate the dead time for each detector. Typical dead times for this experiment were between 3–10%.

Finally, there is a series of inhibits to prevent data from accumulating during unacceptable conditions. Such conditions include the target rod being unbiased, large fluctuations of the beam currents, or the ESA voltage being outside acceptable limits. The last is the most important as it prevents data accumulation when the proton beam energy is fluctuating abnormally or while energy steps are being performed.

The data collected are stored in 512-channel spectra. The TUNL XSYS data acquisition softare allows data acquisition until a preset amount of charge has been accumulated. A typical spectrum is shown in Figure 4.6 with the peaks of interest corresponding to ^{44}Ca(p,p$_0$), ^{44}Ca(p,p$_1$), and ^{44}Ca(p,p$_2$). The ^{16}O(p,p$_0$) peak is identified and used for calibrating the spectra. To generate yield curves, windows were set around the peaks of interest and the counts were summed. The sums are then corrected for background and dead time

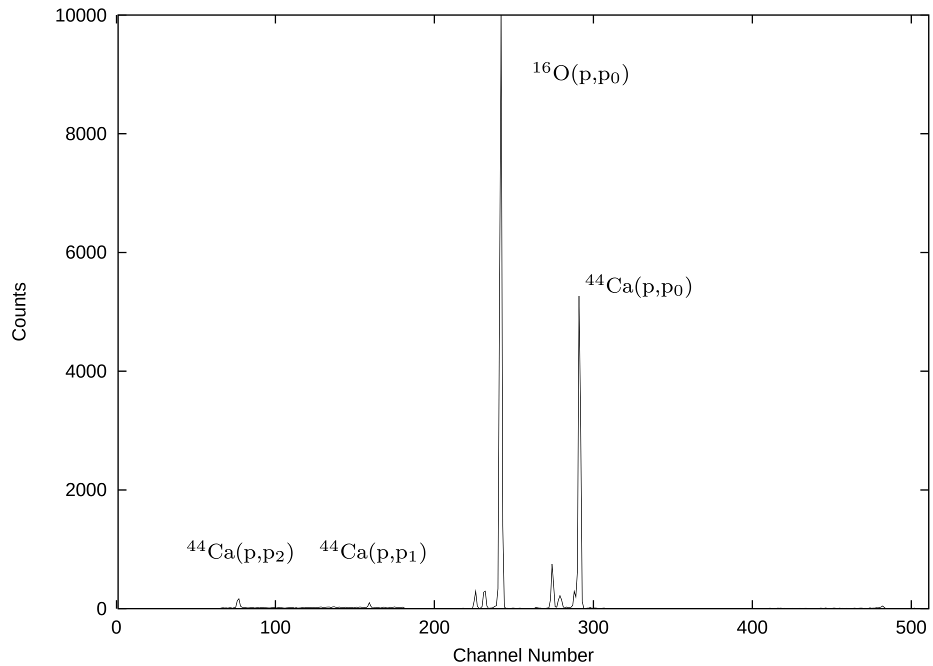

Figure 4.6: Charged particle spectrum for $E_p = 3.0938$ MeV. The ^{44}Ca(p,p) peaks were gated and summed to produce yield curves. Note the flat area near channel 200 where the ^{12}C(p,p$_0$) peak has been removed electronically.

and stored as a function of energy. The system automatically increments the energy on reaching the preset amount of charge and begins a new set of spectra. For this experiment, the preset charge was generally 400 or 500 μC, which required run times of 90–180 seconds. The preset value was chosen to provide acceptable statistics ($\sim$ 1%) for the ^{44}Ca(p,p$_0$) reaction.

4.3 Experimental Procedure

To obtain the data for this experiment, the beam is first extracted from the accelerator. With stable H_2^+ beam in the ESA and acceptable H^+ beam tuned to the scattering chamber, the experiment can proceed. The XSYS data acquisition software is run on the

VAX using a set of interactive command codes. Before the automated generation of yield curves begins, the spectra must be energy calibrated. Calibration is accomplished by identifying the peaks in the spectra — usually ^{44}Ca(p,p$_0$), ^{44}Ca(p,p$_1$), and ^{16}O(p,p$_0$) — and determining the energy of the scattered protons from kinematic considerations. With this information, the VAX can track the peaks of interest as they change with bombarding energy.

When the calibrations are complete and the electronics properly set, the starting energy, energy step size, and total amount of charge to be collected per point are entered into the VAX. For this experiment, data were collected over the energy range 2.5–3.5 MeV in 100-eV energy steps. As noted above, the total charge collected per point was 400 or 500 μC. The VAX will collect data until the preset amount of charge is reached, sum the data for the on-line yield curves, and increment the energy to continue the experiment. Data collection continues until manually halted. Halting occurs when experimental conditions deteriorate for such reasons as target degradation, erratic beam fluctuations, or equipment failure. The data is thus taken in segments. To ensure sufficient overlap between segments for identification and energy calibration purposes, the energy is stepped back a sufficient amount to provide an overlap in the two neighboring segments. This experiment was taken in many segments ($\sim$ 30) over two one-week periods.

The VAX displays the spectra described above as well as real-time yield curves for monitoring data quality. However, only the spectra are stored by the VAX on a hard drive. At the completion of the experiment, the data is moved from the laboratory VAX to an analysis VAX and copied to CD-ROM for secure storage. Yield curves are generated off-line in a similar manner. Without experimental time constraints, the off-line yield curve generation can be monitored very closely to ensure optimal results. A sample yield curve generated off-line is shown in Figure 4.7.

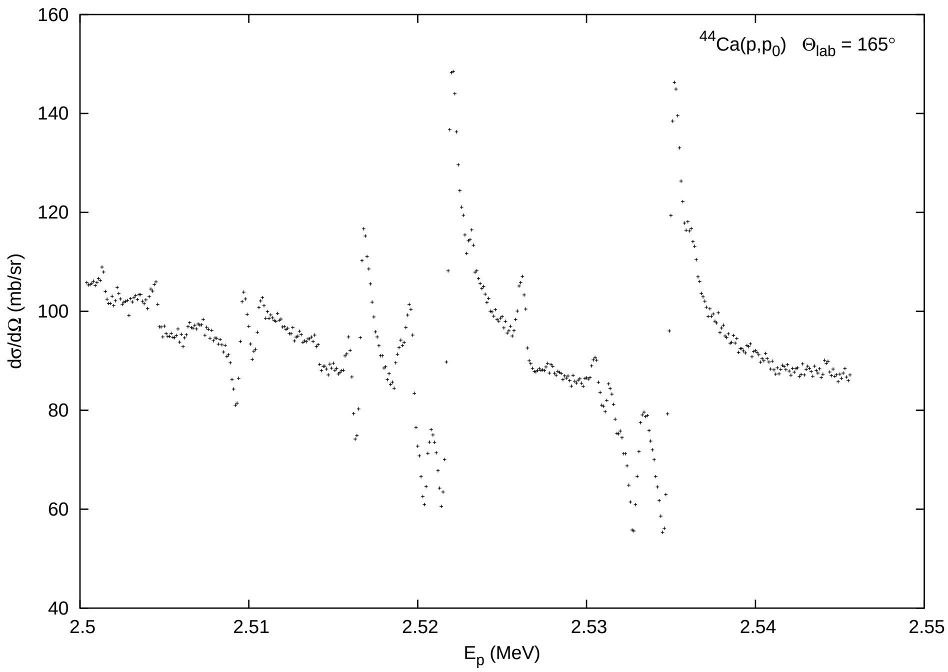

Figure 4.7: $^{44}Ca(p,p_0)$ yield curve over the energy range E_p = 2.50-2.55 MeV.

4.4 Targets

Two types of targets were used for this study, ^{44}Ca and ^{56}Fe. The ^{44}Ca targets were used for the collection of new data, while the ^{56}Fe targets were used to provide an absolute beam energy calibration [Nel83]. Both targets were thin films evaporated onto carbon foils. For ^{44}Ca the target thickness was 1.1–1.5 μg/cm^2, which corresponds to 70–120 eV average energy loss. This is well below the machine energy resolution. The ^{56}Fe targets did not have to be as thin, since they were only used for energy calibration. The thickness for the iron targets was $\sim$ 2.5 μg/cm^2, which corresponded to $\sim$ 200 eV energy loss.

Fabrication of both types of targets began by placing a carbon backing onto stainless steel target rings. The 5.0-μg/cm^2 carbon foils were floated off slides using distilled water. The target rings were then placed in a frame above an evaporation boat in a bell jar (illustrated in Figure 4.8). An evaporation boat was placed between two high current electrodes and the bell jar was evacuated to $\leq$ 2.0 μTorr. The boat was then heated by current flowing between the electrodes. There was also a shutter and aperture to allow the boats to be heated without deposition on the targets. Clean glass slides were placed on top of the target rings in the frame to prevent the target material from depositing on the back of the targets.

For ^{44}Ca target fabrication, a 0.01" closed tantalum boat was used. The calcium was in the form of $CaCO_3$ enhanced to 95.9% ^{44}Ca. To reduce the carbonate and obtain calcium targets, tantalum powder was added at a 1:6 calcium carbonate to tantalum ratio to provide sufficient reducing agent. This mixture is then inserted into the closed boat and placed inside the bell jar. The current was slowly raised using the high current electrodes to $\sim$ 70 A at which point reduction occurs. Reduction was indicated by rapidly increasing pressure inside the bell jar and typically lasted for 5 minutes. After reduction, the current was raised to $\sim$ 150 A and evaporation occurred. The deposition was monitored via a quartz crystal thickness monitor and calibrated using Coulomb scattering measurements. The proper thickness was easier to achieve when the evaporation process was performed slowly. To produce a batch of targets, the evaporation process lasted $\sim$ 15 minutes.

For ^{56}Fe target fabrication, a 0.005" open tungsten boat was used. Each evaporation used 0.02 g of Fe_2O_3 enriched to 99.87% ^{56}Fe. The boat and isotope were placed into the evaporation chamber, sealed with a miniature bell jar, and evacuated. After the jar was evacuated ($\leq$ 1 μTorr), the system was filled to $\sim$ 300 Torr with hydrogen gas. The hydrogen was used as a reducing agent. The current was raised to $\sim$ 100 A; reduction was characterized by the red powder form of Fe_2O_3 turning black and melting onto the boat. The reduction occurred rapidly ($\sim$ 2 minutes). The mini-bell jar was replaced with the standard bell jar, and targets were installed in the chamber. The current was raised to 110 A, and the deposition was monitored using the same thickness monitor.

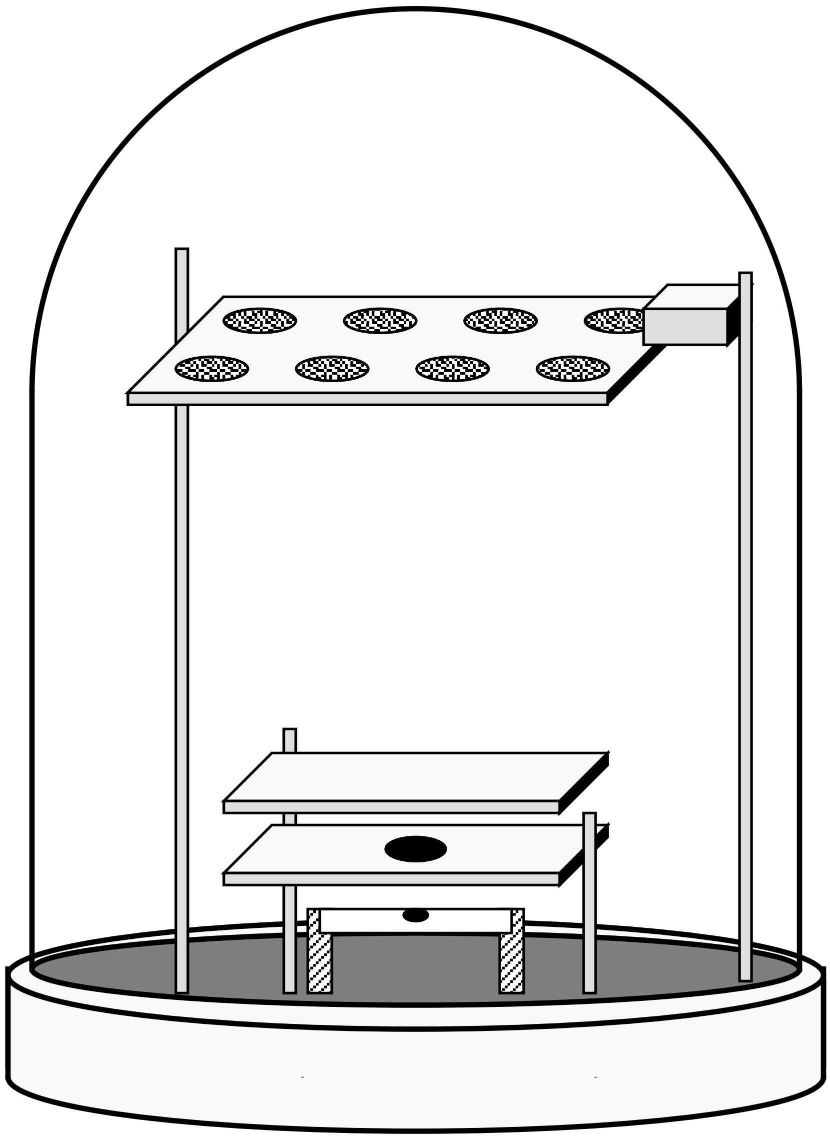

Figure 4.8: Schematic of the high current evaporator system used to fabricate targets.

Chapter 5

Determination of Resonance Parameters

The ^{44}Ca(p,p$_0$) and ^{44}Ca(p,p$_1$) differential cross-sections were measured at five angles, Θ_{lab} = 90°, 108°, 135°, 150°, and 165°, over the energy range E$_p$ = 2.500–3.534 MeV in 100-eV steps. ^{44}Ca targets were prepared with a thickness of 1.1–1.5 μg/cm^2. Resonance parameters were determined for 809 resonances. Figure 5.1 shows the cross-sections and fits for several angles and reactions. This chapter describes the identification and assignments of the observed resonances. Section 5.1 explains both the FORTRAN code MULTI6 which was used to fit the data and the angular momentum coupling scheme used in the fitting procedure. Section 5.2 discusses the energy calibration. Section 5.3 provides specific examples of the fitting procedure, and Section 5.4 presents the results of the differential cross-section analysis.

5.1 MULTI6

The R-matrix theory described in Section 3.1 has been coded in FORTRAN to analyze the charged-particle scattering data taken at the HRL. MULTI6 is a multi-level, multi-channel R-Matrix code used to determine resonance parameters from experimental

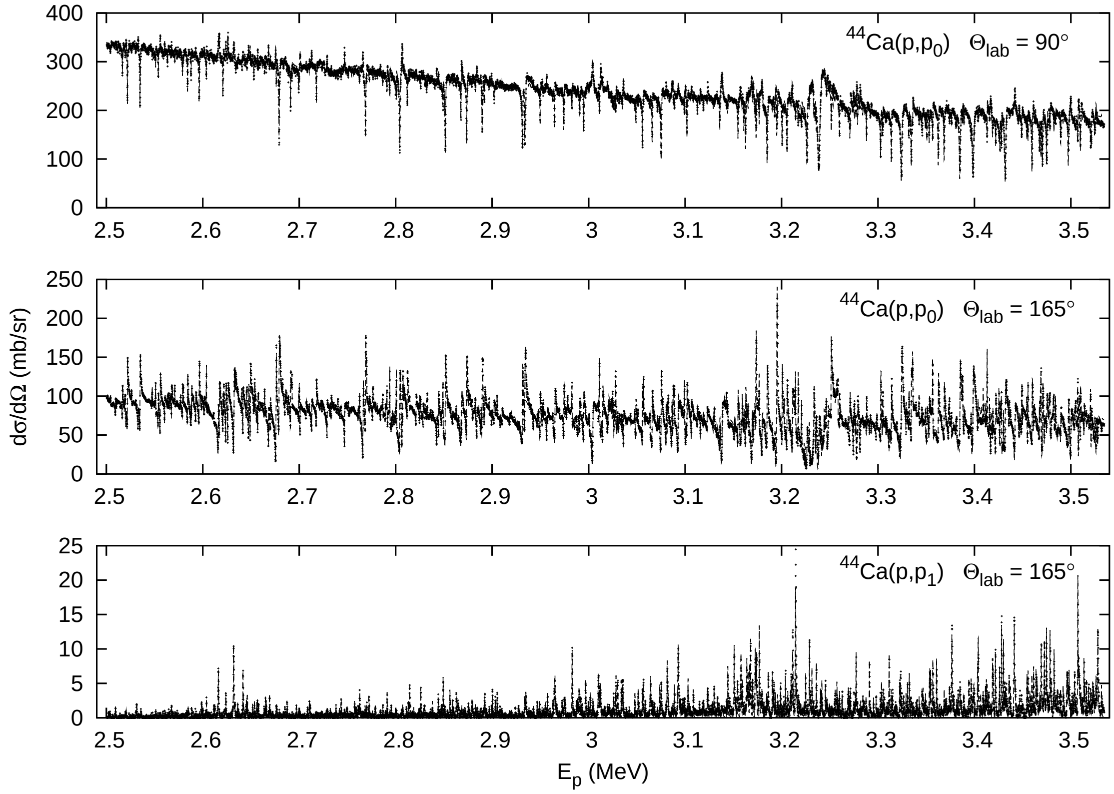

Figure 5.1: Cross-sections and fits for ^{44}Ca(p,p$_0$) and ^{44}Ca(p,p$_1$) at $\Theta_{lab} = 165°$ and ^{44}Ca(p,p$_0$) at $\Theta_{lab} = 90°$.

cross sections. MULTI6 calculates theoretical cross-sections based on many input parameters and can calculate simultaneously the differential cross-sections for both reactions at all five observed angles. The calculated cross-sections are visually compared to the normalized experimental cross-sections. Input parameters are adjusted until the experimental cross-sections and calculated cross-sections compare well. Typically, many executions of MULTI6 are necessary for each observed resonance.

The theoretical cross-section calculations require many input parameters. Each resonance requires specification of the resonance energy E_p, compound state angular momentum J, compound state parity π, channel spin s in the elastic channel, elastic channel orbital angular momentum ℓ, and laboratory resonance width Γ_p for elastic scattering. When a resonance is observed in inelastic scattering, each channel c for inelastic scattering must have

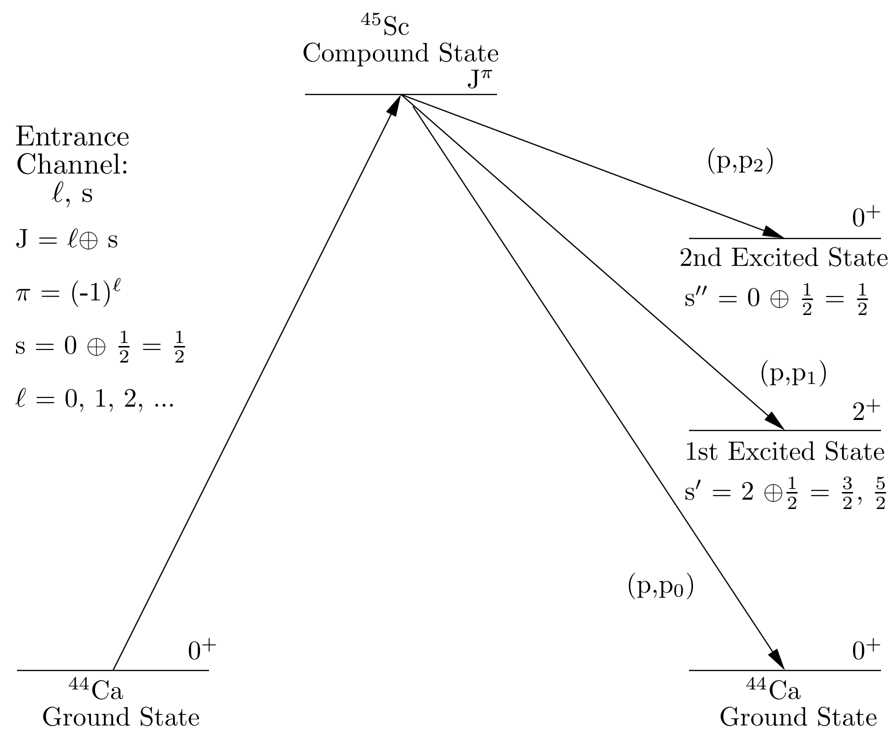

Figure 5.2: Angular momentum coupling scheme for the ^{44}Ca(p,p$_0$), ^{44}Ca(p,p$_1$), and ^{44}Ca(p,p$_2$) reactions in the channel spin representation.

an exit channel spin s$'$ and an orbital angular momentum ℓ' as well as a laboratory width Γ_c. All resonances are observed in the elastic reaction channel, and many are also observed in the inelastic reaction channel. The angular momentum coupling is illustrated in Figure 5.2. In addition to calculating the cross-sections, MULTI6 also calculates the reduced widths, γ^2, for each channel from the expression $\Gamma = 2P\gamma^2$ where P is the penetrability for that channel computed from Coulomb wave functions.

MULTI6 also requires a resolution function as input. MULTI6 will adjust the calculated cross-sections by convoluting the cross-sections to simulate the effects of beam energy resolution. The choice of resolution function is very important, as it is possible to obtain several combinations of input parameters and resolution functions that agree with experimental data. One procedure for determining the resolution parameters is to fit a resonance with extremely well-known parameters and adjust the resolution function until the calculated cross-section compares well with the experimental cross-section. Another method is to fit a large segment of data. This method ensures that a suitable resolution function is chosen since a large data segment will have resonances with a wide variation in resonance shape and width. Only one resolution function will be suitable for an entire data segment. For this experiment, a resolution of 300-400 eV produced reasonable results. This value is similar to the function used in other recent scattering experiments at the HRL and slightly better than the function used in previous studies of ^{44}Ca(p,p).

Angular momentum is very important in charged-particle elastic scattering; the orbital angular momentum of the compound state strongly influences the resonance shape, while the total angular momentum has a lesser but significant effect. Shown in Figure 5.3 are sample shapes for the ^{44}Ca(p,p_0) reaction calculated by MULTI6. Sample shapes are shown only for those spin-parity combinations that were observed experimentally and fitted. The spin and parity of each resonance can usually be determined by fitting the shapes of the elastic resonances. The sample shapes shown illustrate this process. From the 90° data, the parity can be determined; positive and negative parity states are clearly differentiated. From the 165° and 150° data, s-wave and p-wave resonances can be distinguished from the other resonance shapes. The 108° data can, in practice, usually discriminate $J^\pi = \frac{1}{2}^-$ resonances from $J^\pi = \frac{3}{2}^-$ resonances. However, for very weak resonances, the elastic shapes at this angle are very similar, and assigning J^π unambiguously is difficult. Similarly, the 135° data can distinguish between the d-wave resonance shapes. However, the shapes are still similar, and assignments based solely on the 135° data are not made with a high confidence level.

Since MULTI6 is a multi-level, multi-channel R-matrix code, cross-sections for inelastic scattering are calculated in the same way that the elastic cross-sections are calculated. The analysis proceeds in the same manner except now cross-section data from two

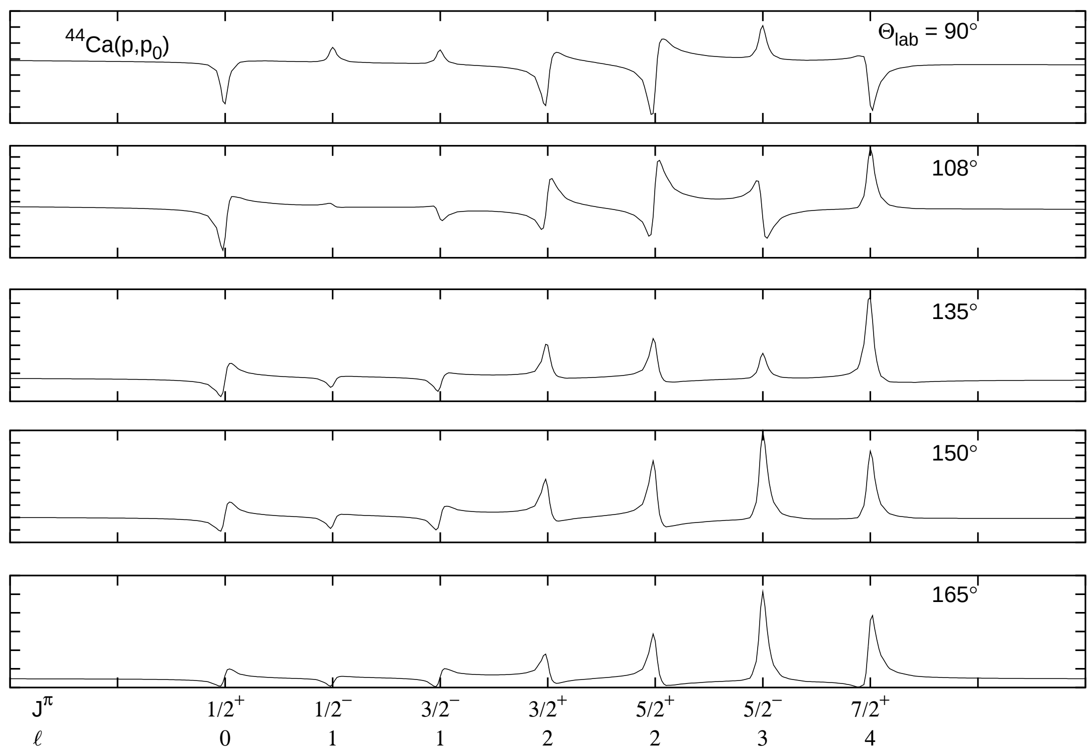

Figure 5.3: Sample elastic scattering shapes for all J^{π} combinations observed in this study. Each sample resonance has the same laboratory width, $\Gamma_p = 100$ eV.

reactions must compare well to two calculated sets of cross-sections. The data for inelastic scattering is sometimes useful in making J assignments when the elastic data is ambiguous. Shown in Figure 5.4 are sample p-wave resonance shapes for the inelastic scattering channel. From the p-wave resonance elastic scattering sample shapes in Figure 5.3, the difficulty in determining J is apparent. If an isolated resonance in the inelastic reaction channel has an anisotropic angular distribution and is already identified as a p-wave resonance, then the $J = \frac{3}{2}$ assignment is obvious. If the resonance in the inelastic reaction channel has an isotropic angular distribution, then the resonance can have either $J = \frac{1}{2}$ or $\frac{3}{2}$. Similarly,

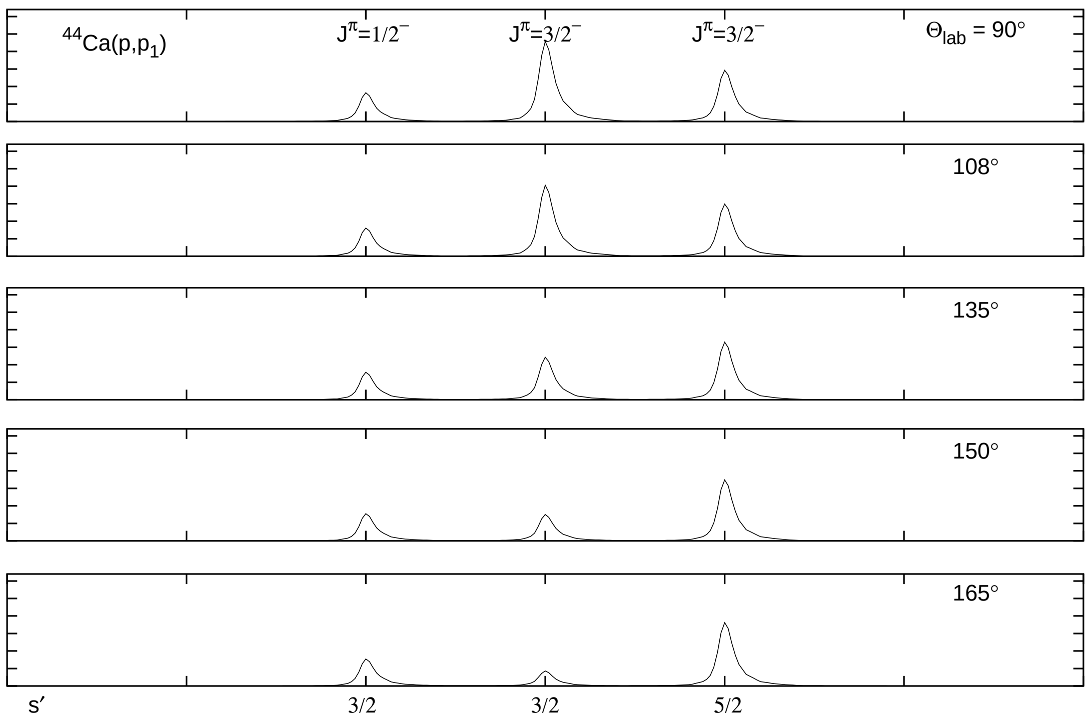

Figure 5.4: Sample ^{44}Ca(p,p$_1$) angular distributions for $\ell = 1$ resonances. Results are shown only for $\ell' = 1$. No $\ell' \geq 3$ contributions to resonances in the inelastic reaction channel were observed. Each resonance shown has the same laboratory width in the inelastic reaction channel ($\Gamma_{p'}$ = 100 eV) as well as the elastic reaction channel (Γ_p = 100 eV) .

the ^{44}Ca(p,p$_1$) reaction can provide information useful in making J$^\pi$ assignments for the d-wave resonances.

Finally, resonance interference must be considered when analyzing high density resonance data such as ^{44}Ca(p,p). The examples shown in Figures 5.3 and 5.4 do not demonstrate interference effects because the resonances are too far apart. While the elastic and inelastic shapes are obvious when shown in this manner, experimental cross-section data can have very closely spaced resonances which dramatically interfere. Interference effects in certain situations can help differentiate between d-wave resonances and less frequently between p-wave resonances. In these cases, the interference effects can be beneficial when making assignments.

5.2 Energy Calibration

While the HRL has superior beam energy resolution, the system is subject to global energy shifts. Therefore, the accelerator energy must be regularly calibrated. Calibration is accomplished by finding a well-known resonance and setting the machine energy to the resonance energy. There are two resonances typically used for calibration in this laboratory, a ^{44}Ca(p,p$_0$) resonance at $E_p = 1.8440$ MeV and a ^{56}Fe(p,p$_0$) resonance at $E_p = 3.2369$ MeV. The p + ^{56}Fe resonance was used for calibration for this experiment.

The calibration procedure is described by Nelson [Nel83]. The calibration resonance is a d-wave resonance with $J^\pi = \frac{3}{2}^+$ and a laboratory width of $\Gamma_p = 44$ eV. This resonance is a secondary energy standard determined to be at $E_p = 3.2369$ MeV by measuring the ^{13}C(p,n) threshold at 0°. This d-wave resonance was initially observed at an energy setting of $E_p = 3.2361$ MeV as shown in Figure 5.5. To calibrate the ^{44}Ca(p,p) data, calcium data were taken immediately after the iron resonance without altering any accelerator settings. By locating the d-wave resonance at $E_p = 3.2363$ MeV in ^{44}Ca(p,p$_0$) relative to the secondary standard, the energies of the ^{44}Ca(p,p) data are scaled linearly to match the calibration point.

With a known energy as a reference point, ^{44}Ca(p,p) data not measured at the same time can be calibrated as well. Due to the nature of the experimental procedure, the data are taken in segments. Each segment has sufficient overlap with neighboring segments to mate the segments. By establishing the energy of each segment relative to the neighboring segments, the energy calibration will scale the entire data set. While one energy calibration point is not typically adequate for a data set, the present data set did not extend to a low enough energy to include the low-energy calibration point. However, the combination of a one-point calibration of the accelerator system and careful calibration of the rest of the homogenizer system prior to data collection should provide good energy determination. The

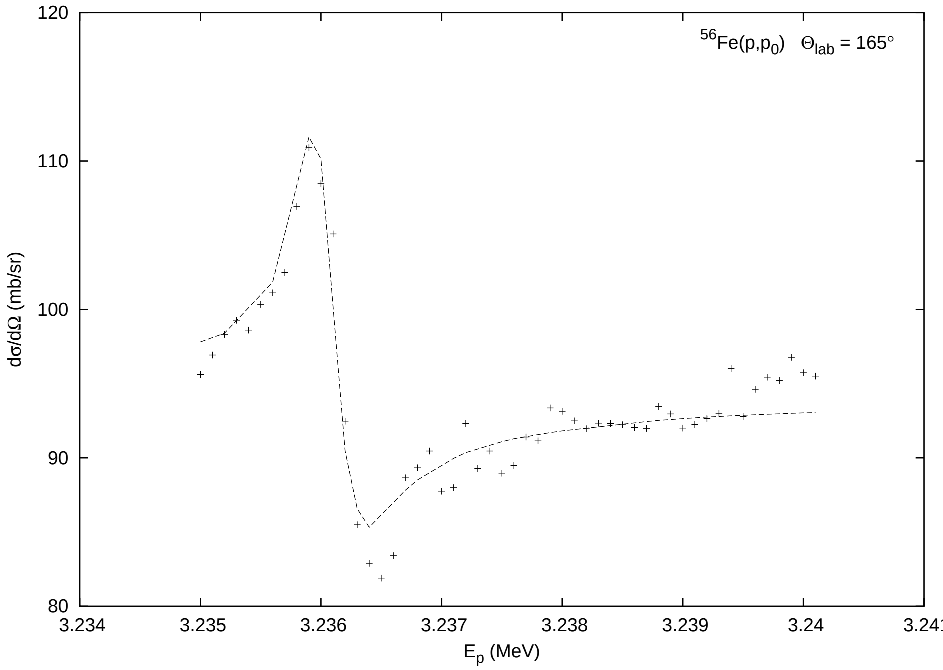

Figure 5.5: ^{56}Fe(p,p$_0$) data and fits for $\Theta_{lab} = 165°$. The d-wave calibration resonance which appears to be at $E_p = 3.2361$ MeV in this figure has a known energy of $E_p = 3.2369$ MeV. All ^{44}Ca(p,p) data from this experiment was calibrated to this energy point.

energies of the observed resonances agree reasonably well with the data taken by Wilson [Wil75]. Thus this calibration method was sufficient for this data set.

5.3 Examples of Fits

From the analysis of the cross-section data, many J^π assignments made during previous experiments were changed, and a large number of new resonances were observed. Although many assignments were unique, here we consider specific data and fits which exemplify common problems and successes. First, a few comments on Figure 5.1 are necessary. Figure 5.1 shows the experimental cross-sections and fits for ^{44}Ca(p,p$_0$) at $\Theta_{lab} = 165°$ and $\Theta_{lab} = 90°$ as well as ^{44}Ca(p,p$_1$) at $\Theta_{lab} = 165°$ for the entire energy range observed in this experiment. Although most of the weak, newly observed resonances cannot be seen in Figure 5.1, the sheer volume of resonances is evident. Figure 5.1 is also a useful illustration

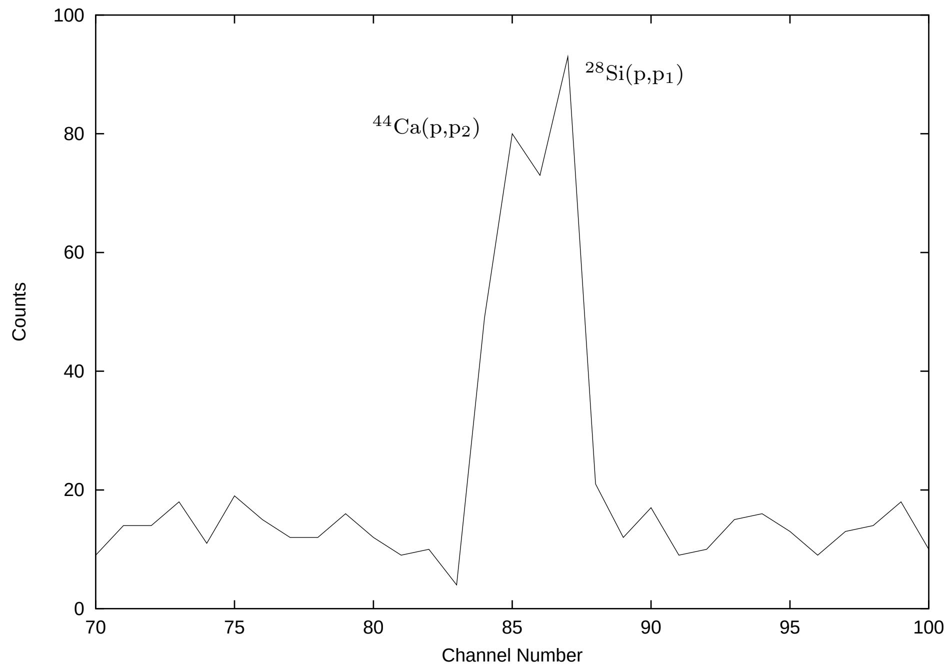

Figure 5.6: Partial charged particle spectrum for $E_p = 3.0921$ MeV. The contaminant ^{28}Si(p,p$_1$) reaction prevented clear identification of the ^{44}Ca(p,p$_2$) reaction.

of how the parity of a resonance is determined. The 90° elastic data show that positive parity resonances can be easily be distinguished from negative parity resonances. While the J ambiguity exists for resonances with $\ell \neq 0$, the 90° elastic data is a very good indicator of ℓ and therefore π. The cross-sections for inelastic scattering are also presented in Figure 5.1. More than 350 additional resonances were observed in the ^{44}Ca(p,p$_1$) reaction than in previous work.

The ^{44}Ca(p,p$_2$) reaction could also be observed over part of this energy range. However, as shown in Figure 5.6, a contaminant peak from the ^{28}Si(p,p$_1$) reaction was extremely close energetically to the ^{44}Ca(p,p$_2$) peak in the spectrum. Although Figure 5.6 clearly shows that both reactions were observed, the separation between the two peaks was never large enough to gate unambiguously on the calcium peak. This observation of the ^{44}Ca(p,p$_2$)

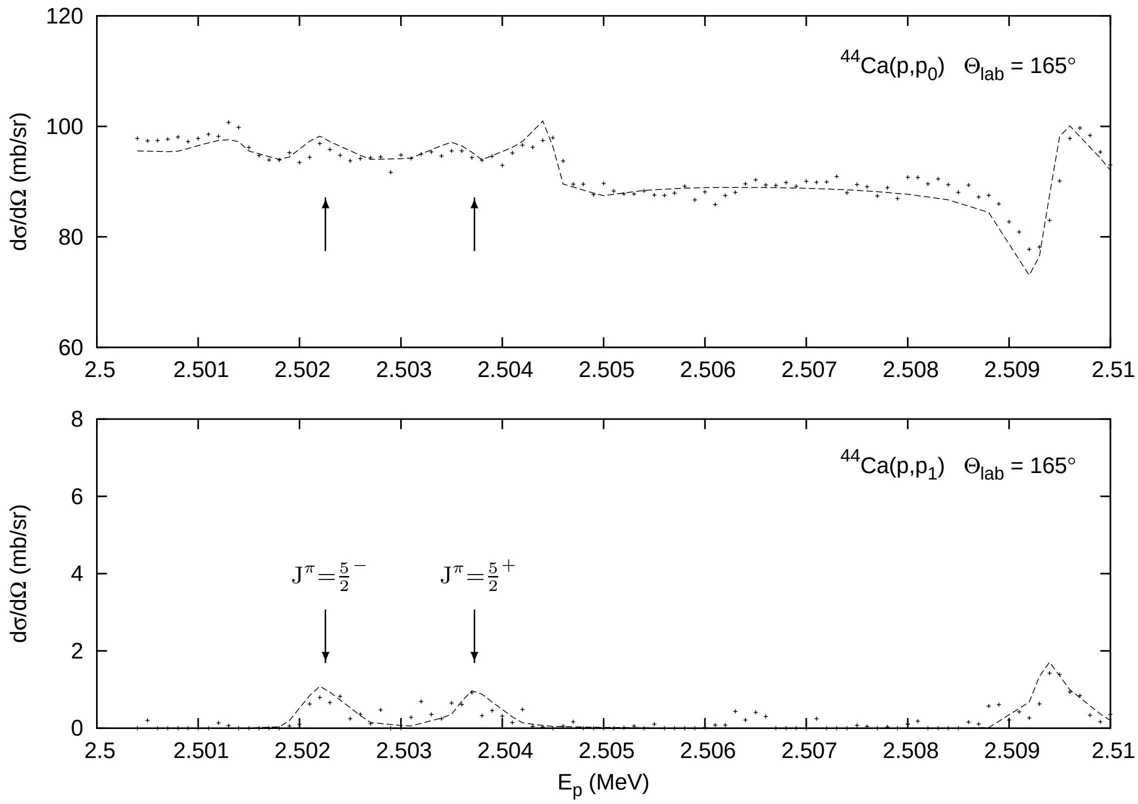

Figure 5.7: Differential cross-sections for the ^{44}Ca(p,p$_0$) reaction and the ^{44}Ca(p,p$_1$) reaction for $\Theta_{lab} = 165°$. The resonances labeled were first observed in this study. This example illustrates how the observance of a resonance in the inelastic channel helped to identify new resonances. The J$^\pi$ = $\frac{5}{2}^-$ level is located at E$_p$ = 2.5022 MeV and the J$^\pi$ = $\frac{5}{2}^+$ level is located at E$_p$ = 2.5037 MeV.

peak is one indicator of the improvement in data quality, even though resonance parameters were not obtained for this channel.

Many new resonances were observed in this experiment. The vast majority of the newly observed resonances were identified due to the dramatically improved cross-section data in the inelastic reaction channel. The arrows in Figure 5.7 indicate two resonances that were not observed in previous experiments. In both cases, it would have been difficult to obtain unambiguous resonance parameters for the very weak (Γ_p = 3 eV) resonances in the elastic reaction channel. Even though the resonances in the inelastic reaction channel were also weak ($\Gamma_{p'} \sim 3$ eV), J^π assignments were made with increased confidence because of the very low background. Most of the new resonances identified in this study are weak resonances that would not have been noticed or accurately assigned without a resonance in the inelastic reaction channel.

The ^{44}Ca(p,p$_1$) reaction also provided the evidence for many of the J reassignments. In this study, the higher quality cross-section data for the inelastic reaction channel showed anisotropic angular distributions for many resonances in the inelastic reaction channel that were previously fit with an isotropic distribution. The resonance indicated in Figure 5.8 is a p-wave resonance. This resonance was previously assigned J = $\frac{1}{2}$. The associated angular distribution in the inelastic reaction channel was previously observed to be isotropic and fit accordingly. In this study, the angular distribution of the cross-section in the inelastic reaction channel was clearly anisotropic. Since a J = $\frac{1}{2}$ resonance must have an isotropic distribution, reassignment was necessary. Many of the reassignments (> 30) in this study were reassignments of p-wave resonances from J = $\frac{1}{2}$ to J = $\frac{3}{2}$ due to the angular distribution of the cross-sections of the inelastic reaction channel.

Another common change made in this study was reassigning d-wave resonances as f-wave resonances. Previous experimentalists argued that f-wave and g-wave resonances would not be observed due to the decreased penetrability of the higher exit angular orbital momentum resonances. However, it is clear from the present work that some resonances previously labelled d-waves are actually f-wave resonances. The arrows in Figure 5.9 show

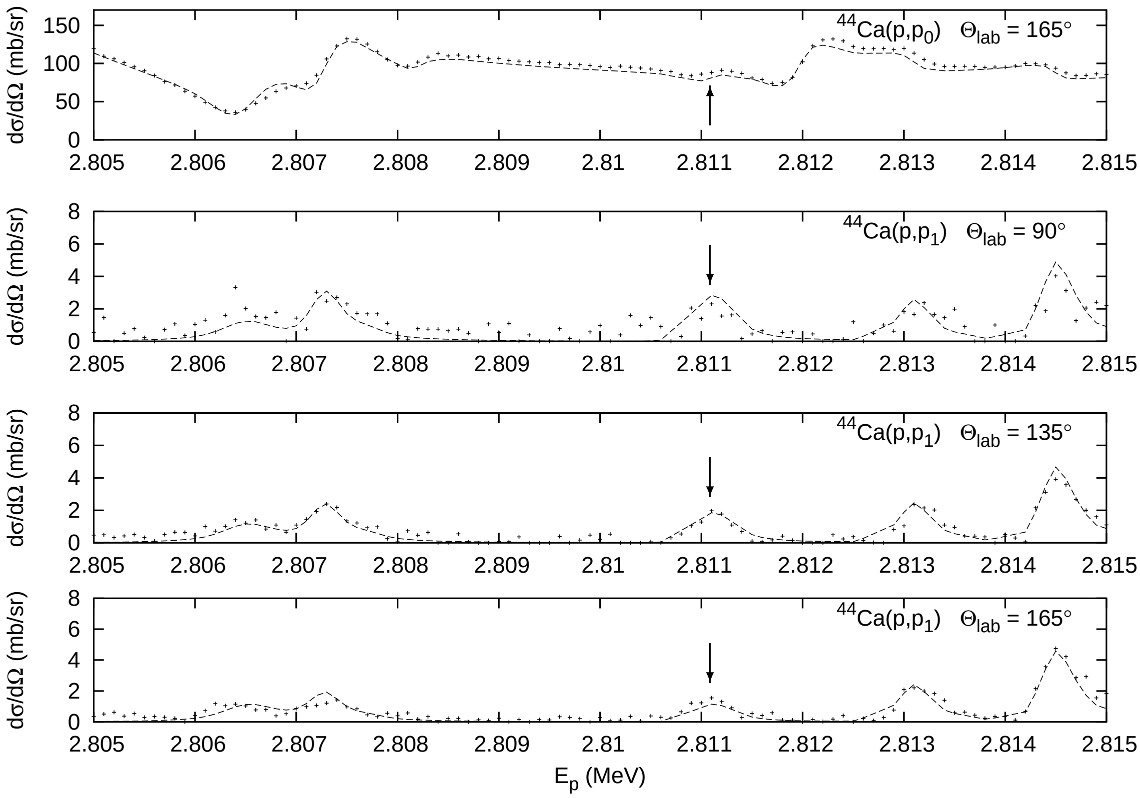

Figure 5.8: Differential cross-sections for the ^{44}Ca(p,p$_0$) reaction for $\Theta_{lab} = 165°$ and the ^{44}Ca(p,p$_1$) reaction for $\Theta_{lab} = 165°$, 135°, and 90°. The shape in the elastic reaction channel at $\Theta_{lab} = 165°$ allowed the resonance near $E_p = 2.811$ MeV to be identified as an s-wave or p-wave resonance. The angular distribution of the inelastic channel excluded $J = \frac{1}{2}$. Thus, the labeled resonance was reassigned $J^\pi = \frac{3}{2}^-$ from $J^\pi = \frac{1}{2}^-$.

a resonance that was assigned $J^\pi = \frac{5}{2}^+$ by Smith [Smi89]. In this study, assigning $J^\pi = \frac{5}{2}^-$ agrees much better with the observed cross-section at 90°. To fit the indicated resonance in Figure 5.9 with a positive parity resonance, the calculated cross-section at 90° would have a clearly visible shape. Not only were there many (40) previously unobserved f-wave resonances identified in this study, there were also many (30) f-wave resonances that had been misassigned as d-wave resonances in the earlier work. The difference in shape between the two f-wave resonance elastic shapes is very small, and many observed f-wave resonances could also be fit with $J = \frac{7}{2}$. Therefore, all observed f-wave resonances were arbitrarily assigned $J = \frac{5}{2}$.

The last major category of reassignments in the study were d-wave resonance spins. The spins of over 60 d-wave resonances were reassigned for a variety of reasons. In previous work, most d-wave resonances are identified as $\ell = 2$ resonances unambiguously, but the J assignment is less conclusive. The J value assignment for d-wave resonances is difficult because the shapes in the elastic channel are similar and the inelastic reaction channel does not prove as useful as when assigning J for p-wave resonances. Therefore, it is not surprising that there were many reassignments of this type. The majority of reassignments were made either because the cross sections of the inelastic reaction channel compared better to the other J^π choice or because the elastic reaction channel cross-section was larger at some angles than at others. Although the current assignments are reasonable, the assignments often are not definitive.

5.4 Results of Cross-Section Analysis

This experiment was performed in order to improve the overall data quality and quantum number assignments for the resonances observed in the p + ^{44}Ca reactions. With improved resolution and better inelastic scattering data, many small, previously undetected resonances were observed. The improved data also allowed correction of previous misassignments. Experimental cross-sections and fits were shown in Figure 5.1. A more detailed

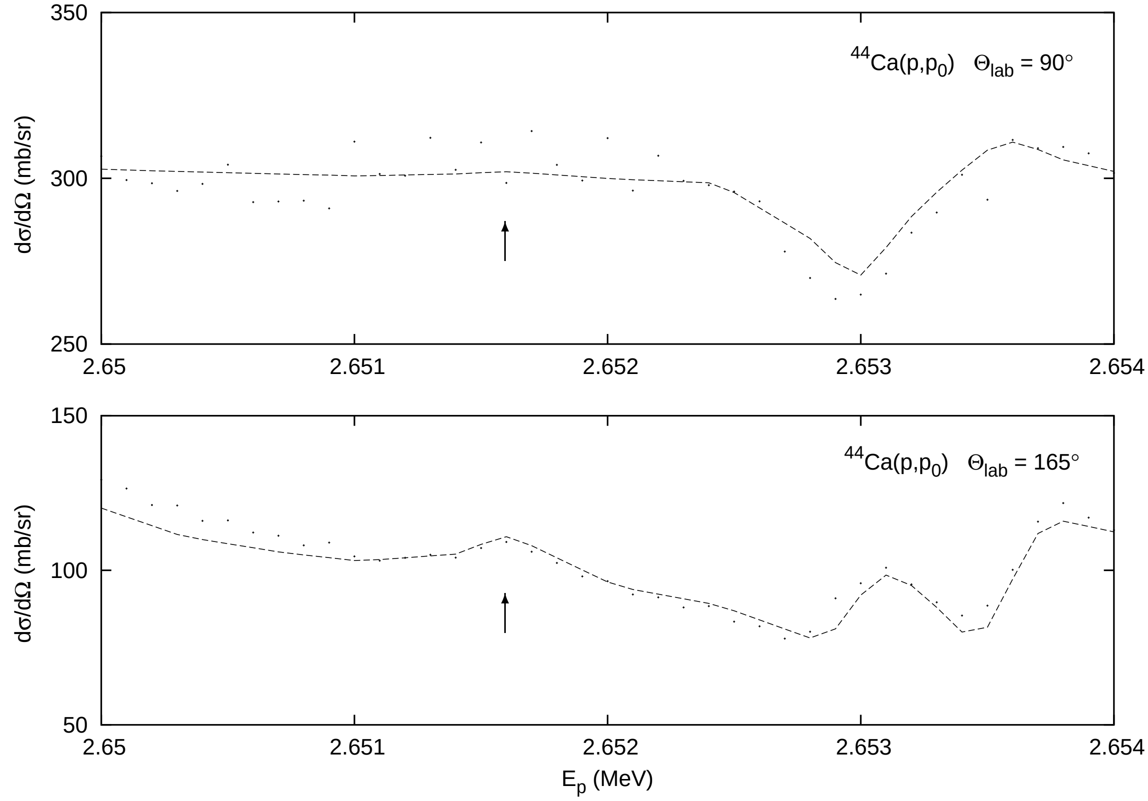

Figure 5.9: ^{44}Ca(p,p$_0$) data for $\Theta_{lab} = 165°$ and $90°$. The resonance indicated was reassigned $J^\pi = \frac{5}{2}^-$ from $J^\pi = \frac{5}{2}^+$. $J^\pi = \frac{5}{2}^-$ and $J^\pi = \frac{5}{2}^+$ resonances can now be distinguished due to improved resolution.

presentation of the experimental cross-sections and fits are shown in Appendix A. As shown by the examples in Section 5.3, the cross-section data collected in this experiment and the resulting resonance parameters appear to be superior to the cross-section data and resonance parameters from previous experiments.

From the experimental differential cross-sections, 809 resonances were identified and fit. Most of the newly observed resonances and reassignments resulted from excellent inelastic scattering data. Analysis identified 375 resonances that were not observed previously in

Table 5.1: Observed resonances by J^π.

Data Set	Resonance J^π							
	$\frac{1}{2}^+$	$\frac{1}{2}^-$	$\frac{3}{2}^-$	$\frac{3}{2}^+$	$\frac{5}{2}^+$	$\frac{5}{2}^-$	$\frac{7}{2}^+$	Total
Previous Work†	129	138	125	121	141	0	0	654
Present Work	121	116	178	203	117	72	2	809

† [Wil75, Shr82, Shr83, Smi89]

the inelastic reaction channel. Many are associated with previously observed resonances. The resonance parameters are listed in Table B.1 (see Appendix B) in sequential order and in Tables B.2–B.8 separately by J^π values. In this experiment, 23% of the resonances had not been observed in past studies and 26% of the previously observed resonances were assigned different quantum numbers. The percentage of newly identified resonances is similar to those observed in recent studies of other targets at the HRL. The number of quantum number reassignments is surprisingly large. However, many misassignments were predicted by the spacing analysis of Agvaanluvsan [Agv02], and many of the reassignments in the current analysis correspond to those spacing anomalies. A comparison between the resonances observed in this study and those of previous work is presented in Table 5.1.

Table 5.2: Summary of changes to previous assignments.

Resonance J^π	$\frac{1}{2}^+$	$\frac{1}{2}^-$	$\frac{3}{2}^-$	$\frac{3}{2}^+$	$\frac{5}{2}^+$	$\frac{5}{2}^-$	$\frac{7}{2}^+$	Total
New Resonances	4	7	43	65	27	40	0	186
Resonances Removed	3	13	3	5	7	0	0	31
Reassignments	12	35	22	29	70	0	0	168

Table 5.2 gives a more detailed summary of the differences between the present work and the previous compilation. "New Resonances" are resonances that were observed in the present work but not in the previous work. "Resonances Removed" are previously identified resonances not observed in the current work, and "Reassignments" are previously observed

resonances that have had spin and/or parity reassigned in the current work.

Chapter 6

Analysis and Results

From the extracted resonance parameters of ^{45}Sc, six statistically significant J$^{\pi}$ sequences were formed. A variety of statistical tests were applied to these sequences, and the results are presented in this chapter. Section 6.1 describes the spacing analyses including the x and $1/x$ analysis and the nearest-neighbor spacing distribution analysis. Section 6.2 describes the results of the $P(0)$ analysis. Section 6.3 presents the results of the Dyson-Mehta Δ_3 analysis. Identification of analog resonances is detailed in Section 6.4, and the reduced width distribution analysis and the strength function results are presented in Section 6.5. The missing level corrections are applied to the data, and the resulting level densities are investigated in Section 6.6.

6.1 Spacing Analyses

The x and $1/x$ spacing analyses were described in Section 2.2.2. The application of these methods to the previous data [Wil75, Shr82, Shr83, Smi89] provided part of the motivation for the present experiment. The x and $1/x$ plots were generated from the previous data and the present data and analyzed in an iterative manner. However, before creating the x and $1/x$ plots and the nearest-neighbor spacing distributions from the J$^{\pi}$ sequences, the energy dependence of the level densities must be unfolded since random matrix theory assumes a uniform level density.

The nuclear level density increases exponentially with energy. When the energy interval under consideration is large, the change in the nuclear level density must be unfolded in order to make comparison with theory meaningful. If the energy dependence is not unfolded, the spacings at the high end of the energy interval will appear to be much smaller when compared to the spacings at the low end of the energy interval. The procedure used to unfold the energy dependence was described by Shriner *et al.* [Shr90]. In this approach, the constant-temperature form of the theoretical level density is assumed, and the integrated level density,

$$N_{theo}(E) = \int_0^E \rho(E)dE = e^{E-\frac{E_0}{T}} - e^{-\frac{E_0}{T}} + N_0, \tag{6.1}$$

is compared to the experimental $N(E)$. The best fit to $N(E)$ is obtained and a new sequence of energies is generated:

$$E_{new} = E_{min} + (E_{max} - E_{min})\frac{F(E) - F(E_{min})}{F(E_{max}) - F(E_{min})}. \tag{6.2}$$

The function $F(E)$ is the best fit to $N(E)$. The endpoints of the energy interval E_{max} and E_{min} do not change during the procedure. The parameter T is defined as a temperature, although not in the usual nuclear sense. This temperature is related only to the empirical fit to the data and is specific to each sequence. All the sequences were unfolded using this technique, and plots of the experimental and unfolded sequences are shown in Appendix D.

A summary of the level sequences observed in ^{45}Sc is presented in Figure 6.1. Figure 6.1 also gives an indication of the spacing of the levels in the sequences. Large gaps in the sequences can be seen and provide a measure of the completeness of the sequences. Investigation of these large spacings can improve data quality.

Before calculating the nearest-neighbor spacing distribution of a sequence, the quality of the sequence can be evaluated using the spacing anomaly method described in Section 2.3.1. The previous data [Wil75, Shr82, Shr83, Smi89] were analyzed for spacing anomalies. Although the previous data and analysis were considered to be of very good quality, the number of spacing anomalies was higher than expected. Because part of the

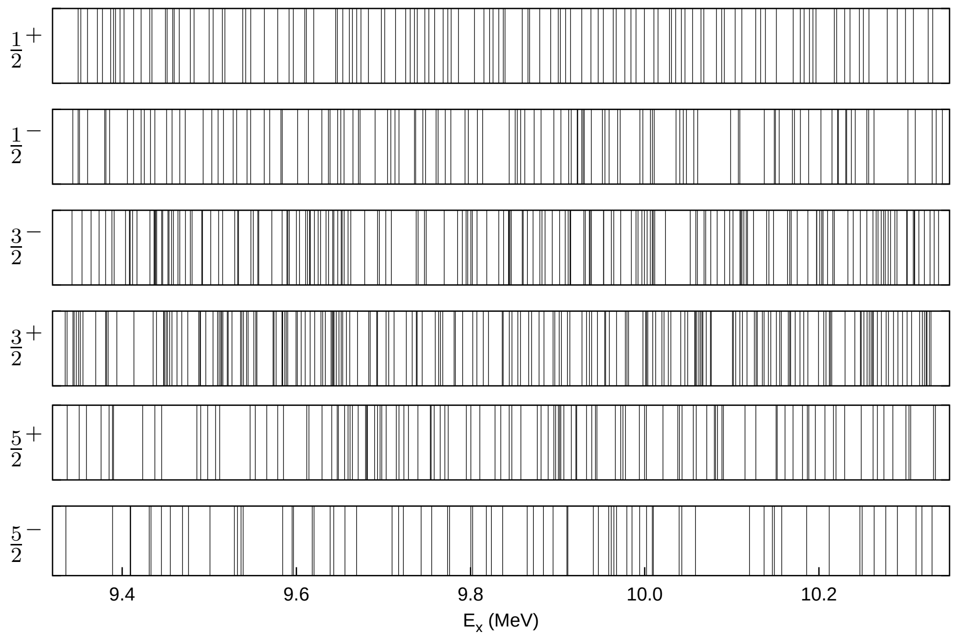

Figure 6.1: Summary of the level sequences observed in ^{45}Sc for excitation energy $E_x = 9.3$–10.4 MeV.

motivation for this experiment resulted from the spacing anomaly analysis of the previous data, the results of that analysis are instructive.

Figures 6.2–6.4 show the spacing anomaly analysis (x and $1/x$) for the previous measurements. This analysis indicated many spacing anomalies which represent possible missing or misassigned levels. The large spacing anomalies in the x plot indicate possible missing levels. The small spacing anomalies in the $1/x$ plot indicate levels with possible quantum number misassignments. The anomalies in the previous data can be examined using the resonance parameters obtained in the current work. Also shown in Figures 6.2–6.4 are those anomalies that were corrected either by observation of a new resonance or a resonance with a J^π reassignment in the current analysis.

Investigation of the small spacing anomalies in the previous data using the ^{44}Ca(p,p$_0$)

and ^{44}Ca(p,p$_1$) reactions was not expected to be very fruitful. Although the location of the pair of resonances that produced the spacing anomaly is known, the experimental resolution was not expected to be improved enough to provide many corrections to previous J$^\pi$ assignments. However, as shown in Chapter 5, the observation of a cross-section for inelastic scattering with very low background often allowed more conclusive J$^\pi$ determination than in previous J$^\pi$ measurements. Small spacing anomalies were corrected in two ways; either one of the pair of resonances that produced the anomaly was reassigned a new J$^\pi$ value (based on the cross-section data), or one of the pair was not observed in the present experiment. In a few cases, both resonances in the pair were reassigned a different J$^\pi$ or were unobserved in this experiment. For this experiment, a spacing was considered anomalous if the spacing was at the 2% confidence level or worse. The percentage of small spacing anomalies that have been removed for all sequences is 71%.

A large spacing anomaly indicates a probable missing level in a sequence, because a large value of x is statistically very unlikely. Unfortunately, a large spacing does not provide precise information about the location of the missing resonance. The large spacing anomaly is produced by two levels which form the endpoints of an energy region with a suspected missing level. Because the size of the energy region identified by a large spacing anomaly can be large, locating a resonance which corresponds to a large spacing anomaly can be very difficult. Also, finding a previously unobserved level in an energy region identified as a large spacing anomaly does not necessarily remove the anomaly. If the new level is close to either of the original resonances that produced the large spacing anomaly, one of the two new spacings can still be anomalous. For some large spacing anomalies investigated in this study, multiple new or reassigned resonances were observed in the energy region of the large spacing anomaly. Since the high number of J$^\pi$ reassignments made in this experiment have affected the large spacing anomalies, a direct comparison between the present experiment and the previous measurements is difficult. In fact, some of the resonances that created the large spacing anomalies were reassigned a J$^\pi$ which now puts the level in a different sequence. For this experiment, a large spacing anomaly was marked as removed in Figures 6.2–6.4 if

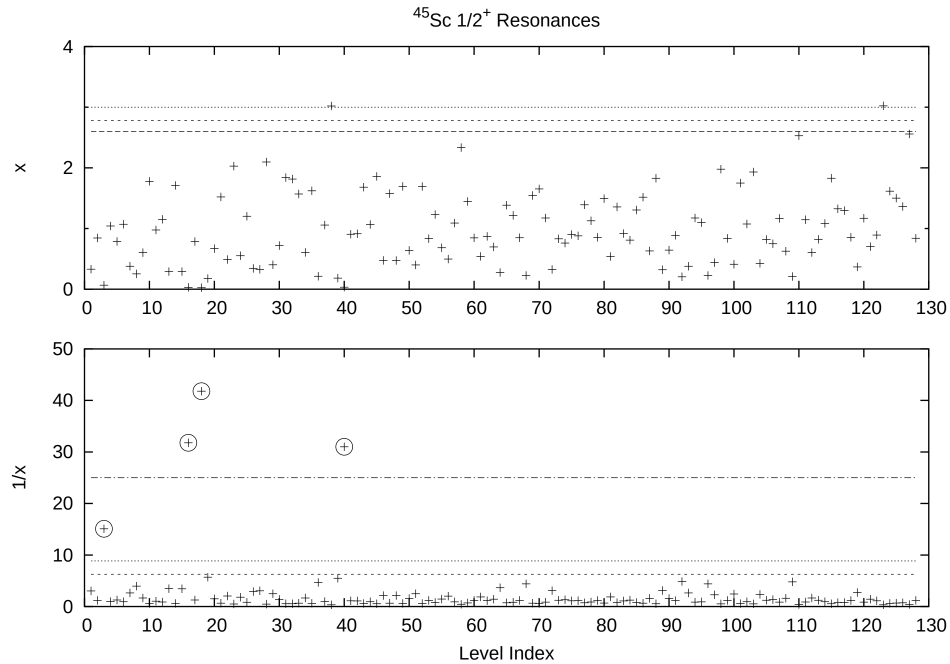

Figure 6.2: Spacing analysis for the s-wave resonance sequence for previous data [Wil75, Shr82, Shr83, Smi89]. The dotted lines from lowest to highest represent the 2%, 1%, and 0.1% values for $1/x$ and x. Data points enclosed by a circle indicate anomalies removed in the present work.

at least one level of the appropriate J$^\pi$ was introduced into the energy region of the large spacing anomaly either by reassignment or observation of a new level. Many large spacings were removed, but not at as high a percentage as for the small spacings. Only the spacing analysis of the current sequences will determine if the large spacing anomalies have truly been resolved.

The spacing analyses for the current data are presented in Figures 6.5–6.8. The spacing analysis provides a qualitative measure of the completeness and purity of a sequence. The large spacing analysis assesses the completeness of the sequence while the small spacing analysis indicates the purity of the sequence. Each J$^\pi$ sequence from the current experiment has been analyzed in this manner. Listed in Table 6.1 are the total spacing anomalies by sequence. Qualitatively, Table 6.1 provides evidence that the J$^\pi$ assignments from this

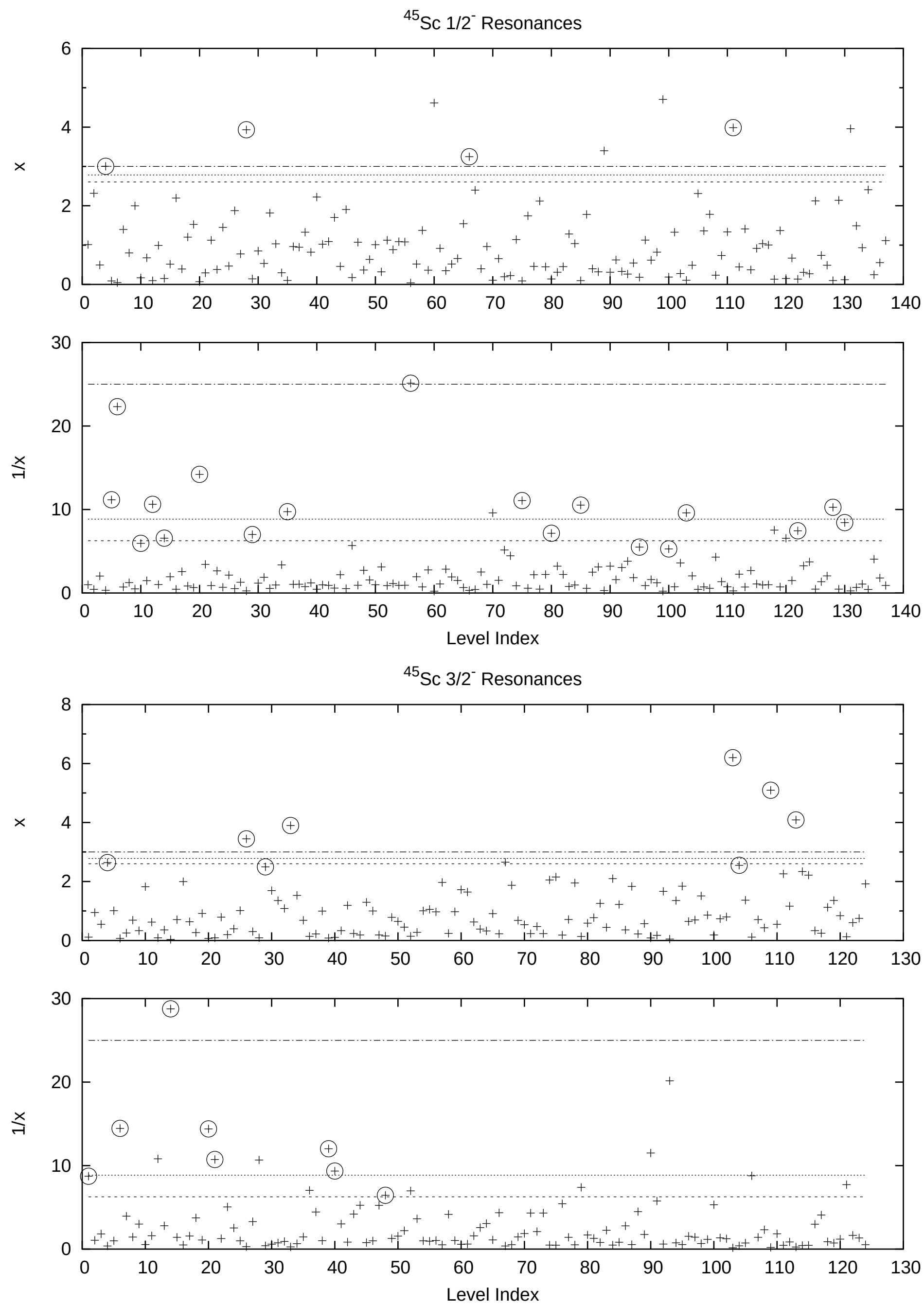

Figure 6.3: Spacing analysis for the p-wave resonance sequences for previous data [Wil75, Shr82, Shr83, Smi89]. The dotted lines from lowest to highest represent the 2%, 1%, and 0.1% values for $1/x$ and x. Data points enclosed by a circle indicate anomalies removed in the present work.

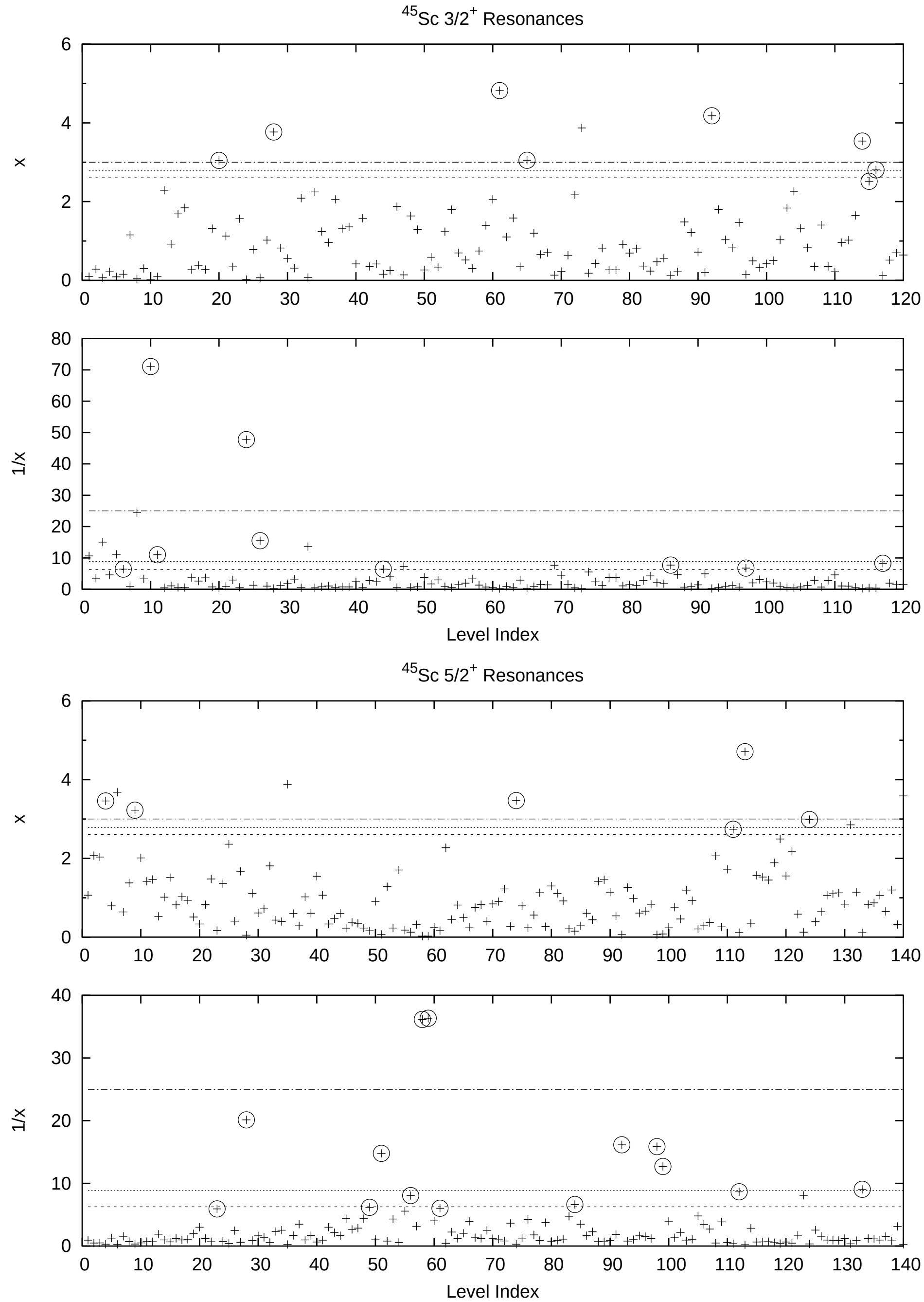

Figure 6.4: Spacing analysis for the d-wave resonance sequences for previous data [Wil75, Shr82, Shr83, Smi89]. The dotted lines from lowest to highest represent the 2%, 1%, and 0.1% values for $1/x$ and x. Data points enclosed by a circle indicate anomalies removed in the present work.

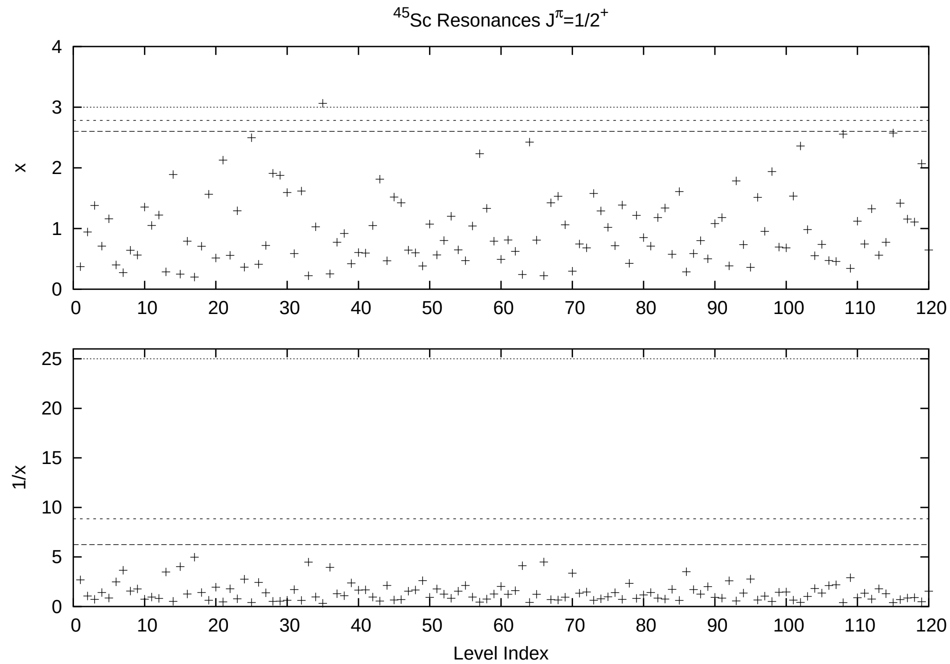

Figure 6.5: Spacing analysis for the s-wave resonance sequence for the present data. The dotted lines from lowest to highest represent the 2%, 1%, and 0.1% values for $1/x$ and x.

experiment are improved from the previous experiments. While some sequences are more improved than others, the number of anomalies was reduced in the current experiment by $\sim \frac{1}{3}$. The sequences derived from the current experiment are not perfect, but this experiment has provided significant improvement.

Figure 6.5 presents the spacing anomaly analysis for the s-wave resonance sequence. The extremely low number of spacing anomalies in Figure 6.5 implies that the s-wave resonance sequence obtained in this experiment is very pure with no spurious levels. The s-wave resonances are the easiest to assign unambiguously, since there is only one J$^{\pi}$ possibility. Few spurious levels are expected because few resonances are expected to be misassigned J$^{\pi}$ = $\frac{1}{2}^{+}$, and few small spacing anomalies were observed. One large spacing anomaly is presented. Thus, the sequence would also appear to be nearly complete.

The p-wave resonance spacing anomaly analysis is shown in Figure 6.6. The p-wave

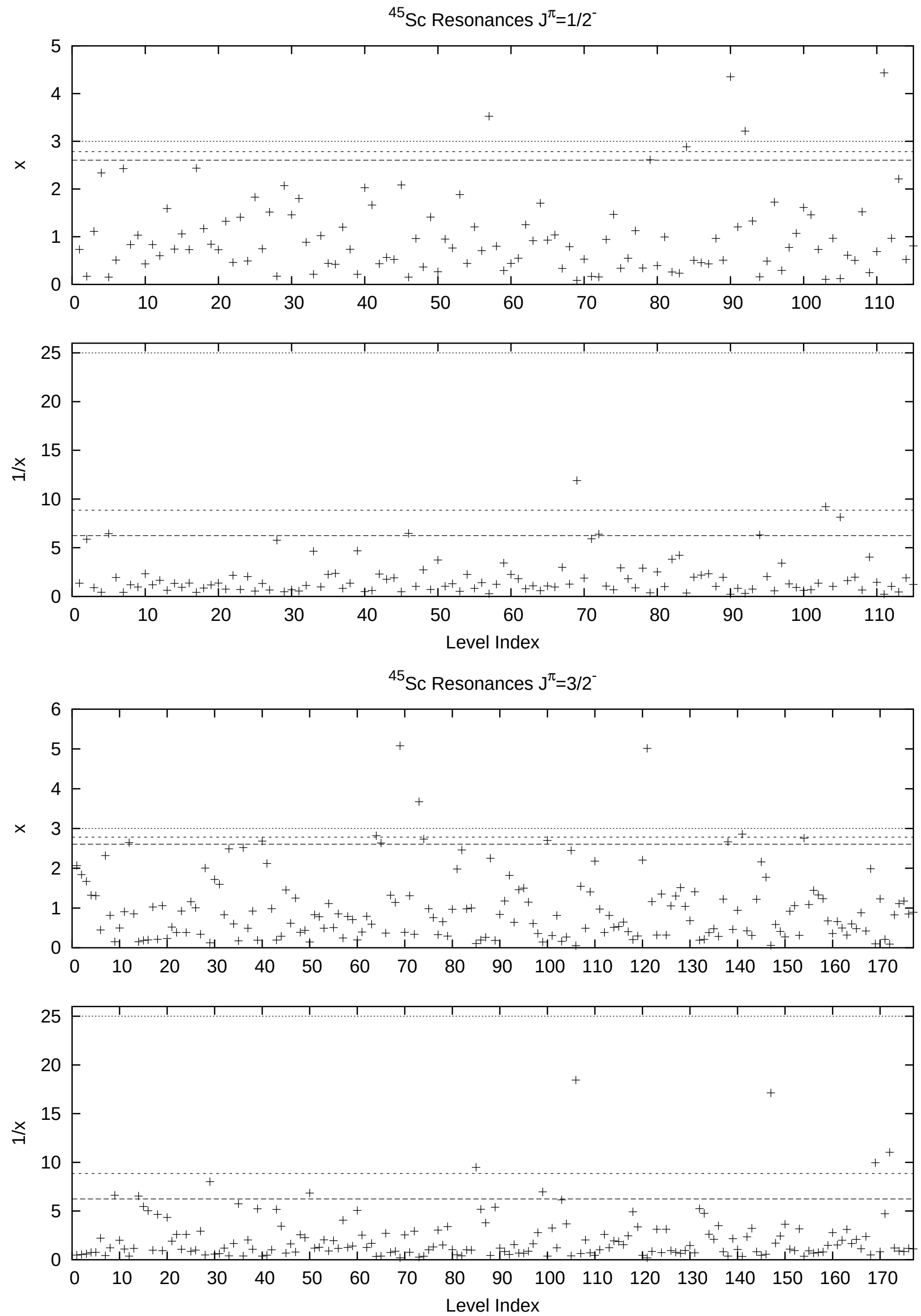

Figure 6.6: Spacing analysis for the p-wave resonance sequences for the current data. The dotted lines from lowest to highest represent the 2%, 1%, and 0.1% values for $1/x$ and x.

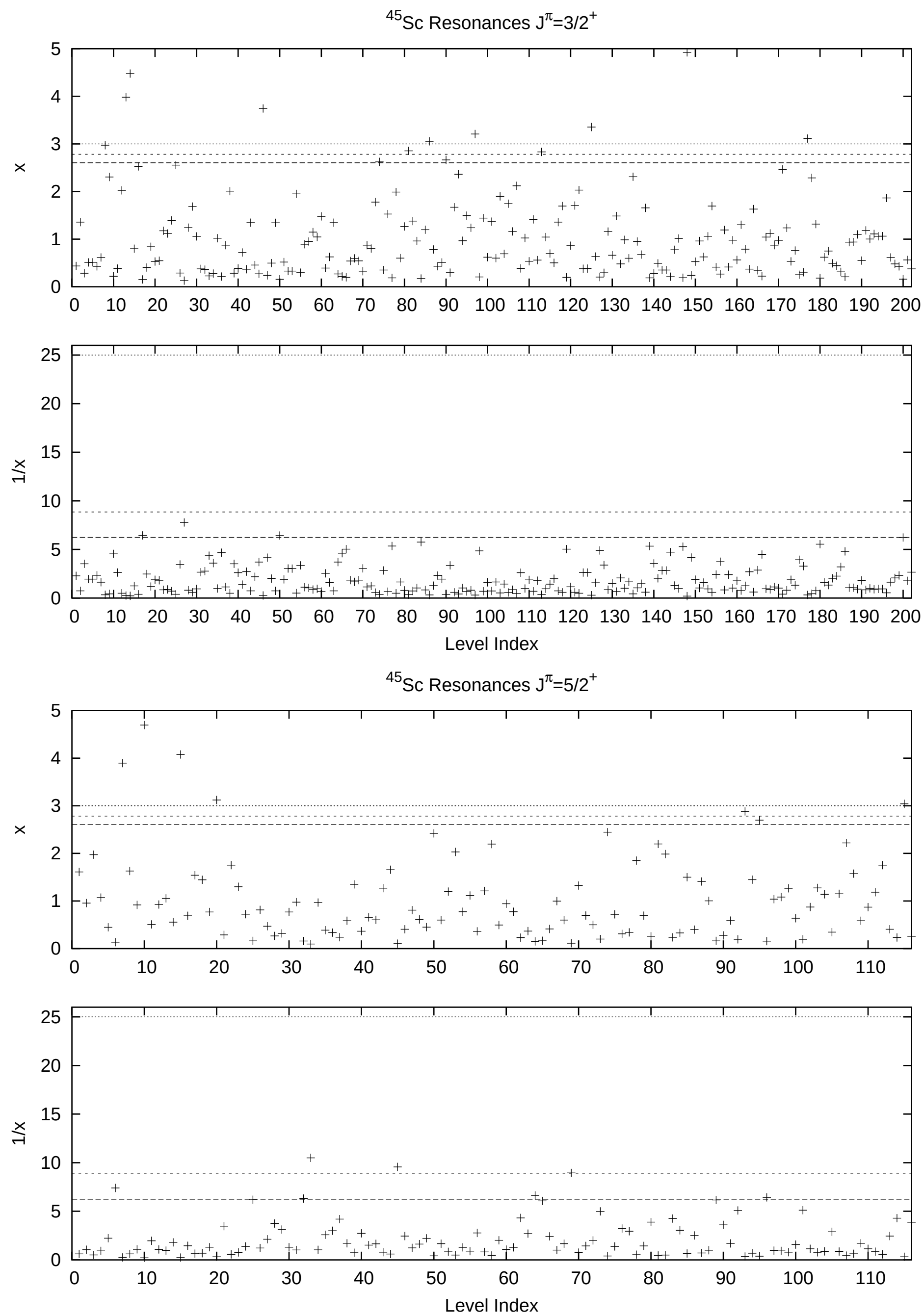

Figure 6.7: Spacing analysis for the d-wave resonance sequences for current data. The dotted lines from lowest to highest represent the 2%, 1%, and 0.1% values for $1/x$ and x.

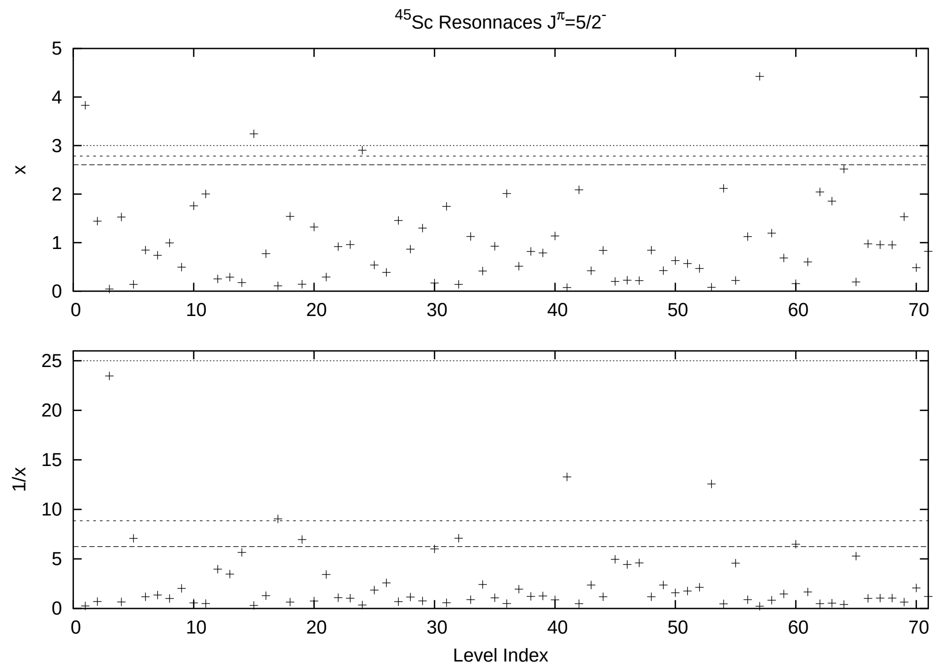

Figure 6.8: Spacing analysis for f-wave resonance sequence for current data. The dotted lines from lowest to highest represent the 2%, 1%, and 0.1% values for $1/x$ and x.

Table 6.1: Spacing anomalies. Anomalies are combined large and small spacing anomalies at the 2% confidence level. The values in parenthesis are the total number of spacings in the sequence.

Data Set	Resonance J^π						
	$\frac{1}{2}^+$	$\frac{1}{2}^-$	$\frac{3}{2}^-$	$\frac{3}{2}^+$	$\frac{5}{2}^+$	$\frac{5}{2}^-$	Total
Previous Work†	6(128)	26(137)	24(124)	24(120)	24(140)		104(649)
Present Work	1(120)	13(116)	22(178)	16(202)	14(116)	12(71)	66(803)

† [Wil75, Shr82, Shr83, Smi89]

resonance spacing analysis is not as impressive as is the s-wave resonance spacing analysis. The spacing analyses for the p-wave resonances show many spacing anomalies. Lower quality statistical results are anticipated due to the difficulty in distinguishing between $J = \frac{3}{2}$ and $J = \frac{1}{2}$ for p-wave resonances. Even with the improved quality cross-section data, J assignments can be difficult. The reduction in total spacing anomalies between Figure 6.3 and Figure 6.6 indicates the improvement in the quality of the current data. However, there are a few unexplained results apparent in these figures. One interesting result is the increase in large spacing anomalies for $J^\pi = \frac{3}{2}^-$. A possible explanation is that ∼50 more $J^\pi = \frac{3}{2}^-$ resonances were observed in this study than in the previous measurements. Since the energy range is unchanged, the average spacing is decreased. This results in large spacing anomalies being produced by smaller average spacings. Spacings that did not appear anomalous in the analysis of the previous measurements may now appear anomalous.

The d-wave resonance spacing anomaly analysis is shown in Figure 6.7. These results are very similar to the results from the p-wave resonance spacing anomaly analysis. The J assignment for d-wave resonances is even more difficult than the J assignment for p-wave resonances. However, the total spacing anomalies for the d-wave resonance sequences have been reduced. Spurious levels have been significantly reduced (11 versus 31). These remaining spacing anomalies arise from the difficulty in assigning J for d-wave resonances and the difficulty in observing very weak d-wave resonances. However, the d-wave resonance sequences also appear to be of improved quality.

The f-wave resonance spacing anomaly analysis is shown in Figure 6.8. With the difficulty in assigning J for f-wave resonances, little useful information is expected from the spacing anomaly analysis. The spacing anomalies analysis would be more useful if the J assignments for f-wave resonances could be determined more accurately from the cross-section data. All observed f-wave resonances were arbitrarily assigned J $= \frac{5}{2}$. The fact that 72 f-wave resonances were observed is unexpected. Previous charged particle scattering experiments at the HRL have observed few f-wave resonances. The unambiguous observation of many f-wave resonances only increases the confidence level of the other J^π sequences since one source of spurious levels in the other sequences has been removed.

In principle, the spacing anomaly analysis described can be used iteratively to reduce certain spacing anomalies. Small spacing anomalies indicate spurious levels in a sequence. A spurious level in the $J^\pi = \frac{1}{2}^-$ sequence is most likely a misassigned $J^\pi = \frac{3}{2}^-$ resonance. A J^π reassignment can remove a spacing anomaly from one sequence but introduce a spacing anomaly into another. Future work could possibly improve the quality of the assignments by using the spacing analysis to help assign J^π.

To consider the statistical properties of the distributions, the nearest-neighbor spacings distributions are compared to theoretical predictions. Random-matrix theory predicts the Wigner distribution while a pure uncorrelated sequence is described by the Poisson distribution. The nearest-neighbor spacing distributions are given in Equations 2.6 and 2.7. Shown in Figures 6.9–6.12 are the nearest-neighbor spacing distributions, $P(x)$, and the integral of the nearest-neighbor spacing distributions, $F(x)$, for the current sequences compared to the GOE and Poisson predictions. By comparing the nearest-neighbor spacing distributions to the theoretical predictions, information can be obtained about the short-range order of the system.

Figure 6.9 shows the nearest-neighbor spacing distribution for the s-wave resonance sequence. As expected, the nearest-neighbor spacing distribution of the s-wave resonance sequence appears to obey the GOE prediction, the Wigner distribution. The behavior of

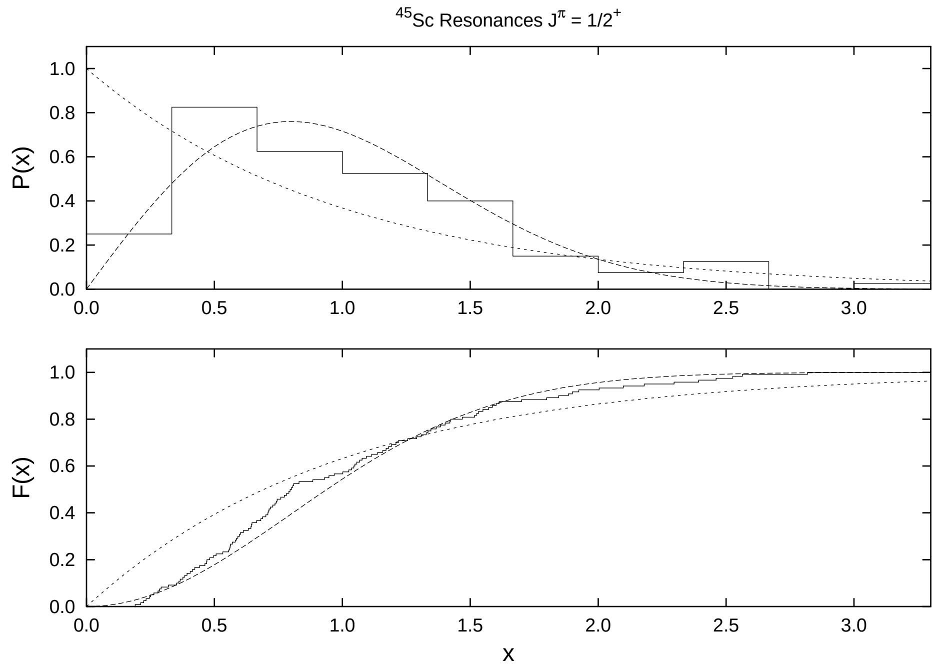

Figure 6.9: Nearest-neighbor spacing distributions for the $J^{\pi} = \frac{1}{2}^{+}$ sequence from the current work. The upper plot shows the nearest-neighbor distribution while the lower plot shows the integral, $F(x)$, of the nearest-neighbor spacing distribution. The dashed line shows the GOE predictions while the dotted line shows the Poisson predictions for the distribution and integrated distribution.

the nearest-neighbor spacing distribution at $x = 0$ is the easiest way to distinguish the two theoretical predictions. The integral, $F(x)$, also shown in Figure 6.9, agrees better with the GOE prediction. Aside from the discrepancy in Figure 6.9 near $x = 0.75$, the $F(x)$ for the s-wave resonances follows the GOE prediction quite well. With the expected result agreeing with the GOE prediction, the confidence in the overall quality of the s-wave resonance sequence is reinforced.

The nearest-neighbor spacing distributions of the other J^{π} sequences do not agree well with the GOE prediction (Figures 6.10–6.12). The nearest-neighbor spacing distributions are between the GOE and Poisson predictions. The integral of the spacing distribution for these sequences agrees better with the Poisson prediction. Even though the present data

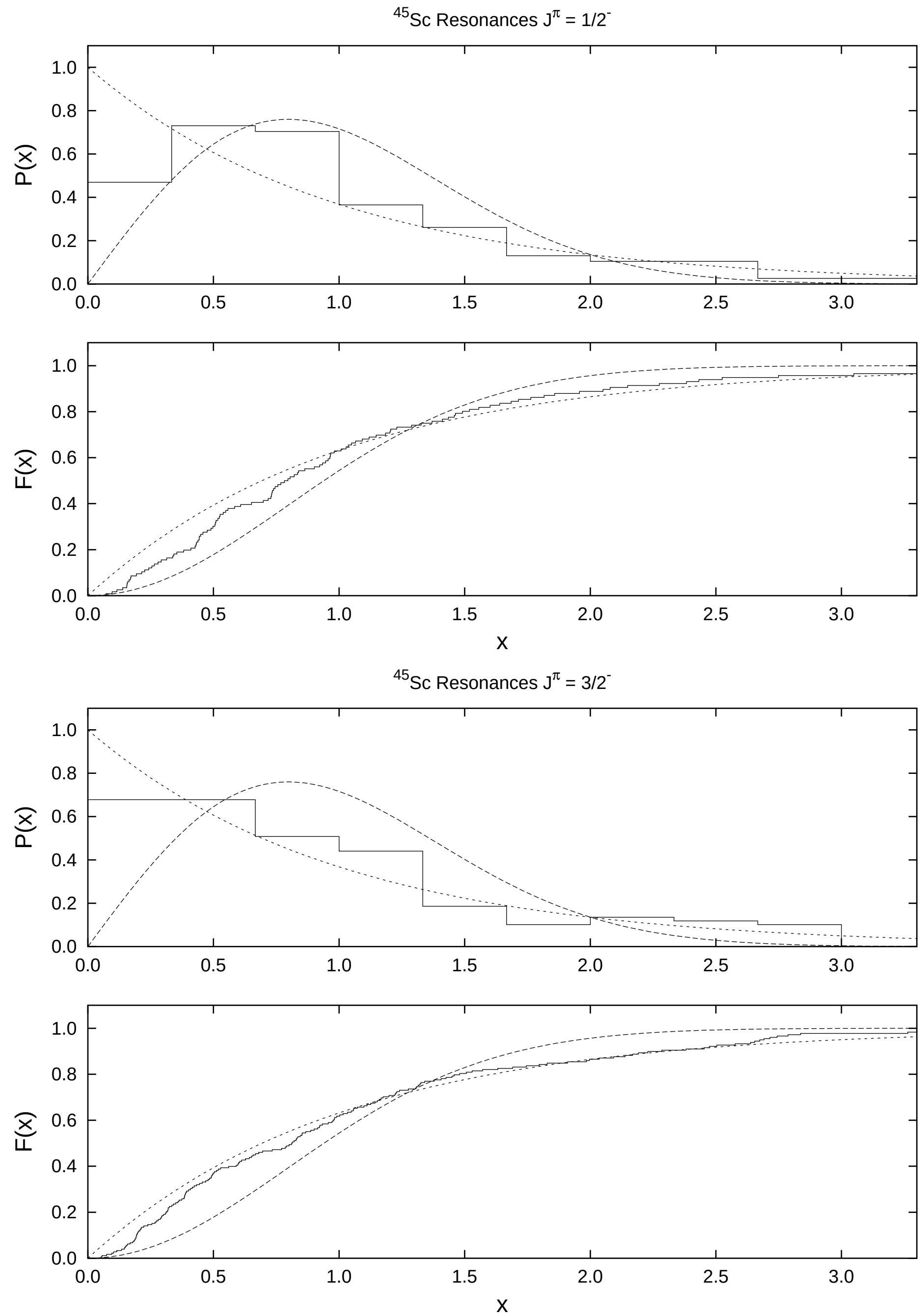

Figure 6.10: Nearest-neighbor spacing distributions for the p-wave resonance sequences for current work. The upper plot in each pair shows the nearest-neighbor spacing distribution while the lower plot shows the integral, $F(x)$, of the nearest-neighbor spacing distribution. The dashed line shows the GOE predictions while the dotted line shows the Poisson predictions for the distribution and integrated distribution.

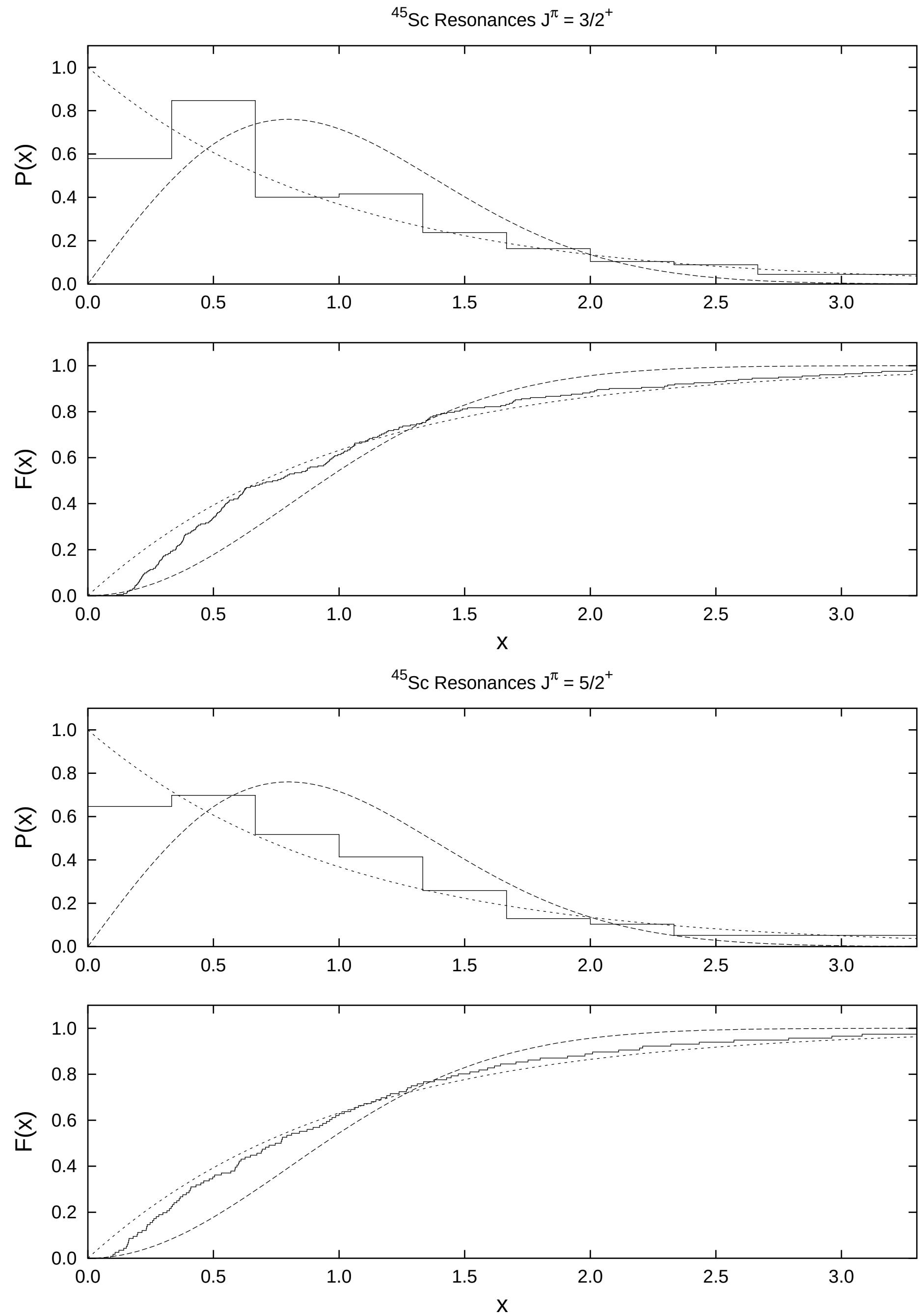

Figure 6.11: Nearest-neighbor spacing distributions for the d-wave resonance sequences for current work. The upper plot in each pair shows the nearest-neighbor spacing distribution while the lower plot shows the integral, $F(x)$, of the nearest-neighbor spacing distribution. The dashed line shows the GOE predictions while the dotted line shows the Poisson predictions for the distribution and integrated distribution.

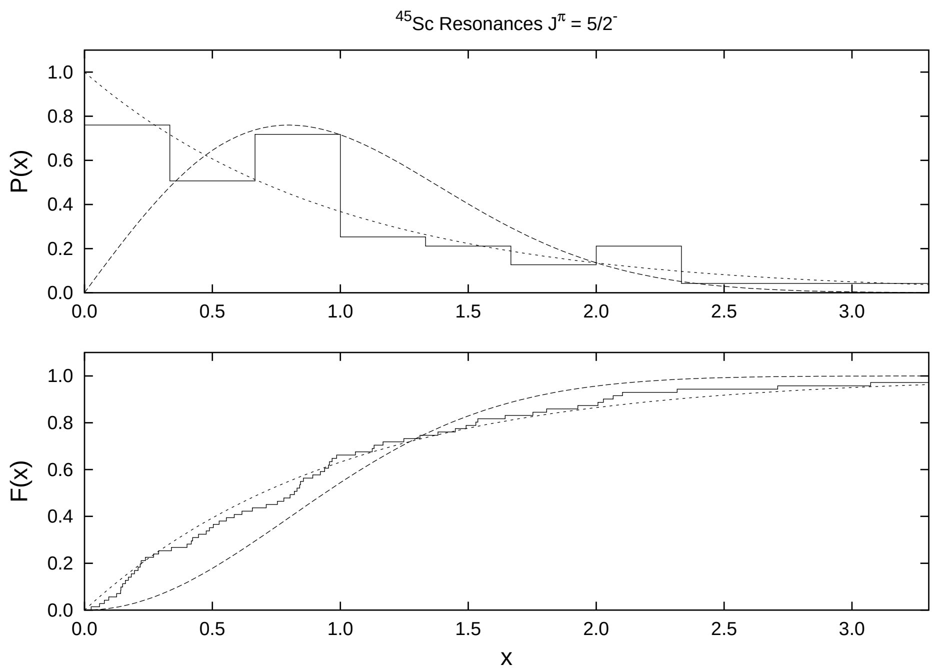

Figure 6.12: Nearest-neighbor spacing distributions for the f-wave resonance sequence for current work. The upper plot shows the nearest-neighbor spacing distribution while the lower plot shows the integral, $F(x)$, of the nearest-neighbor spacing distribution. The dashed line shows the GOE predictions while the dotted line shows the Poisson predictions for the distribution and integrated distribution.

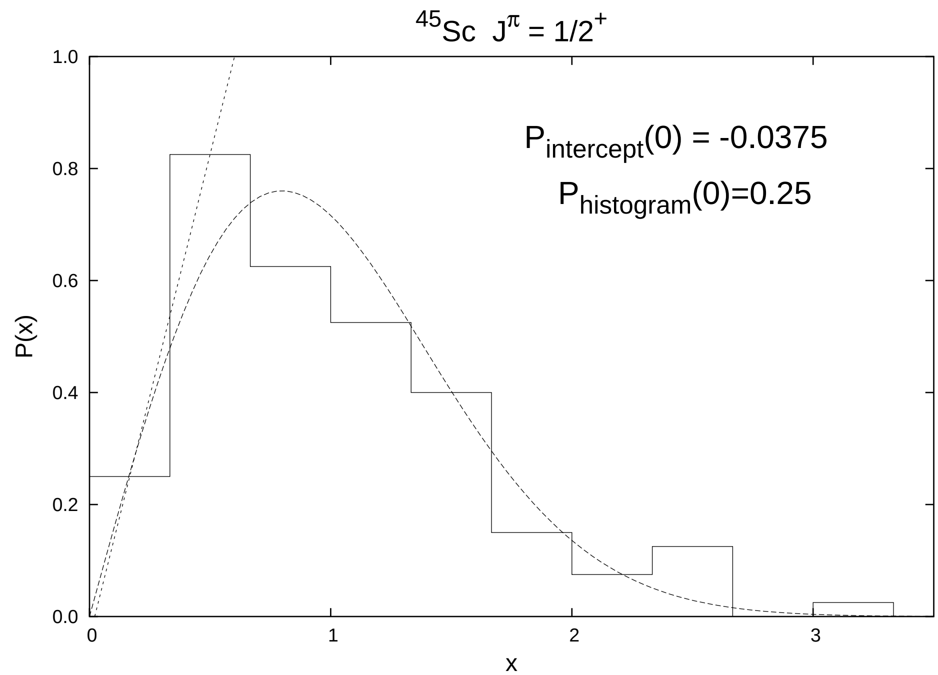

Figure 6.13: $P(0)$ analysis for the J$^{\pi}$ = $\frac{1}{2}^{+}$ sequence. $P_{intercept}(0)$ was determined by fitting the slope of the histogram for $x < 0.66$. The value from this method is effectively zero. $P_{histogram}(0)$ was set equal to the value of $P(x)$ for the first bin in the histogram.

have been shown to be of improved quality, the improvement is not sufficient to claim that the sequences are pure or complete enough to compare well to the expected GOE predictions. This statistical test is too sensitive for most of the sequences of the present experiment.

6.2 $P(0)$ Analysis

As shown in Section 2.3.2, the value of $P(0)$ from a nearest-neighbor spacing distribution provides information about the total number of spurious levels in a sequence. The spacing anomaly analysis also provides this information, but only spurious levels that produce a small spacing anomaly will be identified. Some spurious levels will not be identified using the small spacing anomaly method. The $P(0)$ analysis in principle can provide an overall assessment of the purity of a sequence.

Unfortunately, obtaining values of $P(0)$ from the nearest-neighbor spacing distributions is very difficult. Two procedures were used to interpolate a value of $P(0)$, neither of which produced satisfactory results. The first method was to simply take the value of first bin in the histogram as the value of $P(0)$. While determining the value in this manner clearly produces a larger value than is accurate, a rough estimate is determined.

Table 6.2: $P(0)$ analysis for J $= \frac{1}{2}$ determined using two methods. Spurious levels are determined by the solution to Equation 2.25.

Jπ	Number Levels	$P(0)$ Intercept	$P(0)$ Histogram	Spurious Levels Intercept	Spurious Levels Histogram
$\frac{1}{2}^+$	121	0	0.25	0	18
$\frac{1}{2}^-$	117	0.49	0.47	51	44

Another method used to obtain an estimate of the value of $P(0)$ is illustrated in Figure 6.13. The slope of the nearest-neighbor spacing distribution as $x \to 0$ is determined. The y-intercept of a line with that slope is a measure of $P(0)$. The difficulty lies in choosing which bins to include in the slope determination. For this attempt, only the first two bins were used. The slope is determined by creating two points with the bin height as the y-value and the center of the bin as the x-value. The slope is then determined. The decision to use only the first two bins was arbitrary.

Table 6.2 shows the results of the $P(0)$ analysis for J $= \frac{1}{2}$. The $P(0)$ analysis was performed for the other sequences, but reliable results were not obtained due to the difficulties described above. The $P(0)$ analysis indicated that there are more than 40 spurious levels in the $J^\pi = \frac{1}{2}^-$ sequence. No other statistical test performed implies that many spurious levels in that sequence. Thus, while in principle the $P(0)$ analysis should be a useful tool, better methods of determining $P(0)$ are required to utilize this analysis method.

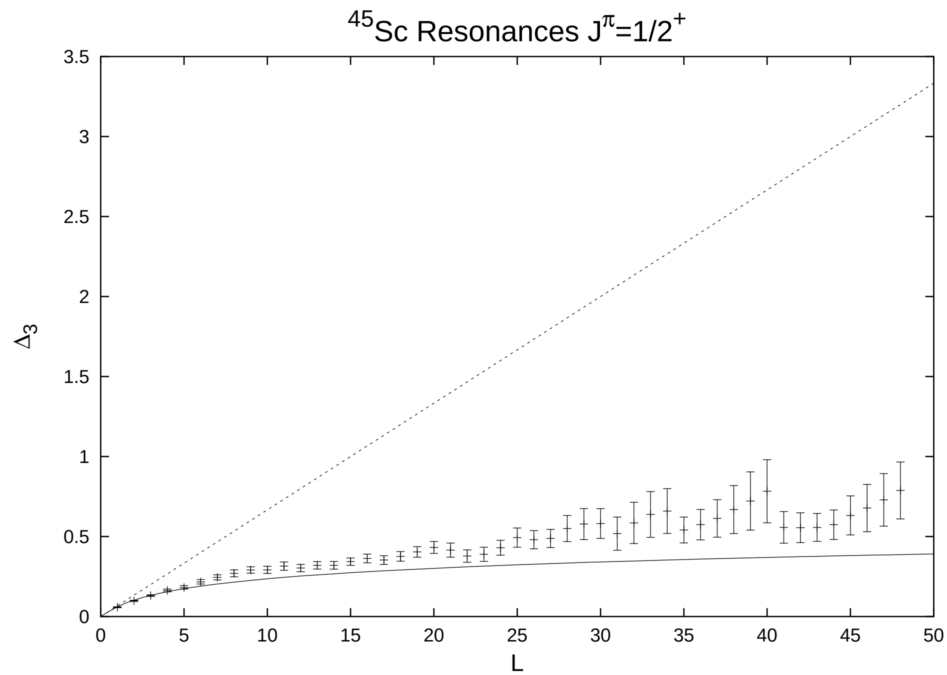

Figure 6.14: The Δ_3 statistic for the s-wave resonance sequence. The upper line represents the Poisson prediction while the lower curve represents the GOE prediction.

6.3 Dyson-Mehta Δ_3 Statistic

The Dyson-Mehta Δ_3 statistic is a measure of the long-range order of a sequence and is defined in Equation 2.11. The Δ_3 statistic is presented as a function of L. The Δ_3 statistic has been calculated for the present data and is shown in Figures 6.14–6.17. There are sufficient levels in the current sequences to provide enough statistics to calculate Δ_3 for relatively large values of L.

The results of the Δ_3 test are consistent with the results obtained by the spacing analysis tests. Figure 6.14 shows the Δ_3 for the s-wave resonance sequence, which agrees reasonably well with the GOE prediction. The other J^{π} sequences do not agree well with the GOE prediction. These sequences agree far better with the Poisson prediction. As previously stated, the nuclear sequences should agree with the GOE prediction. One reason

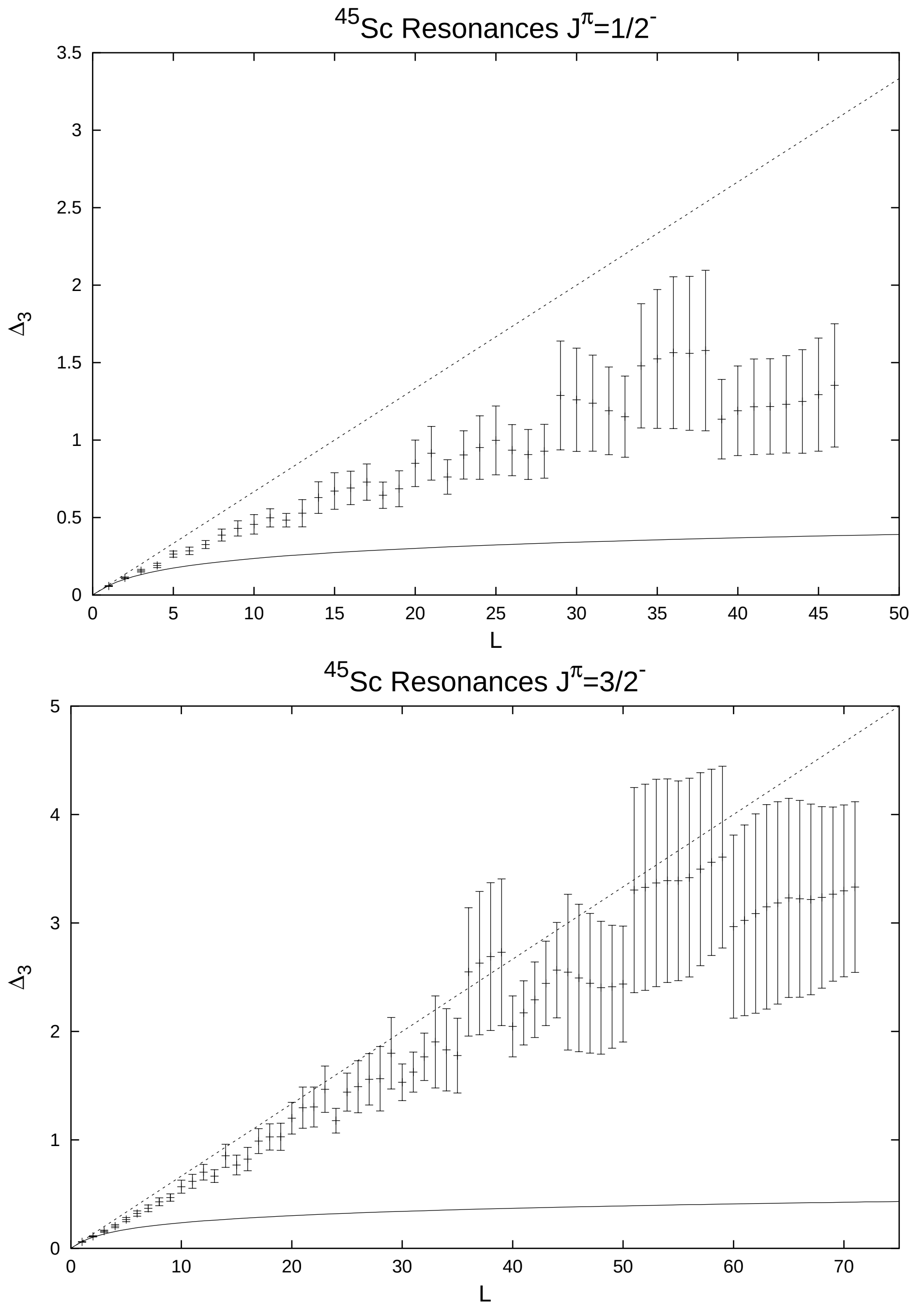

Figure 6.15: The Δ_3 statistic for the p-wave resonance sequences. The upper line represents the Poisson prediction while the lower curve represents the GOE prediction.

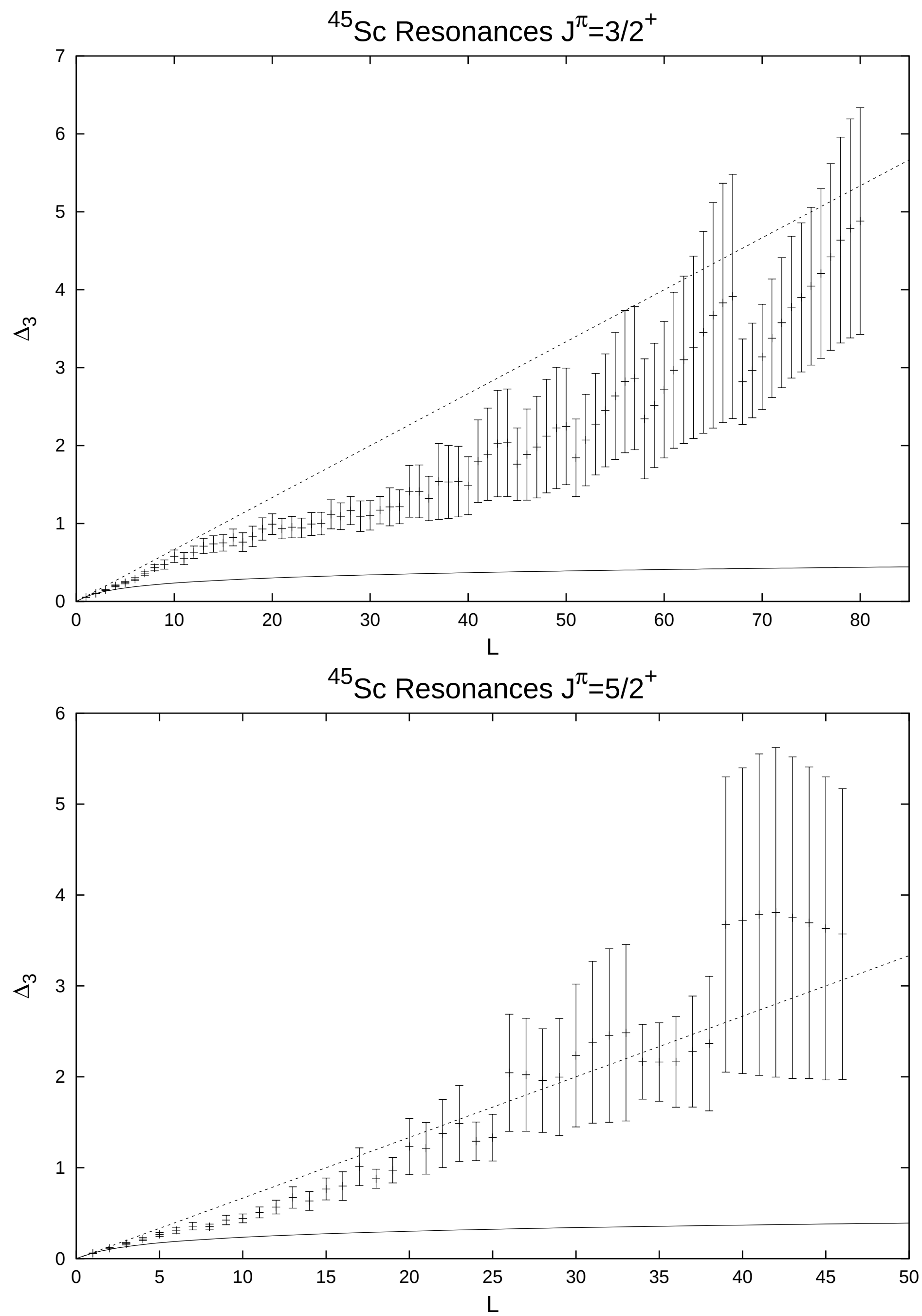

Figure 6.16: The Δ_3 statistic for the d-wave resonance sequences. The upper line represents the Poisson prediction while the lower curve represents the GOE prediction.

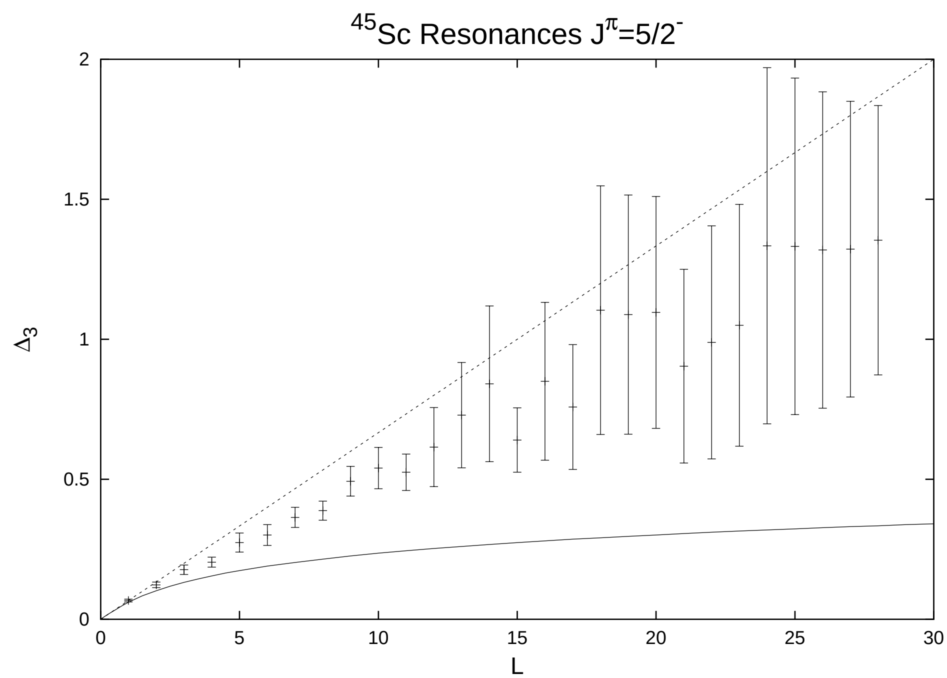

Figure 6.17: The Δ_3 statistic for the f-wave resonance sequence. The upper line represents the Poisson prediction while the lower curve represents the GOE prediction.

for the lack of agreement with the GOE prediction is that the Δ_3 statistic is very sensitive to missing and spurious levels. As shown by the spacing analysis, aside from the s-wave resonance sequence, there are many probable missing and spurious levels. Also, the nearest-neighbor spacing distributions also do not agree well with GOE predictions. Thus, the percentage of missing or spurious levels in the current data is probably large enough to prevent the Δ_3 statistic from agreeing with the GOE predictions. As already shown, the s-wave resonance sequence is of very high quality with very few missing or spurious levels. The rest of the sequences have more missing and spurious levels.

6.4 Analog Resonance Identification

As discussed in Section 3.2, analog resonances must be considered before statistical analysis of the reduced width distributions is performed. An analog resonance is a non-statistical effect which will enhance the reduced width of a resonance and then distort the reduced width distribution and the determination of the strength functions. Thus the analog resonances must be identified and removed from the sequences prior to statistical analysis of the reduced widths.

The method used to identify possible analog resonances in the present data was to prepare plots of γ^2 and $\sum\gamma^2$ for each J^π sequence. Values of the reduced width which result from non-statistical effects often appear much larger than the surrounding background resonance reduced widths and appear as a sharp rise in the $\sum\gamma^2$ plots. Possible analog resonances in ^{45}Sc will then be compared to the accepted levels of ^{45}Ca, the parent nucleus (presented in Appendix C). If a level exists in ^{45}Ca with the appropriate J^π in the appropriate energy range, the resonance will be labeled as an analog and removed from the sequence prior to the reduced width analysis. If the analog resonance is fragmented, the fragmentation may be indicated in the $\sum\gamma^2$ plot. A single enhanced level of a fragmented analog resonance may not be visible about the background levels since the enhancement is spread over many levels. However, the $\sum\gamma^2$ plot will indicate if many levels in a small

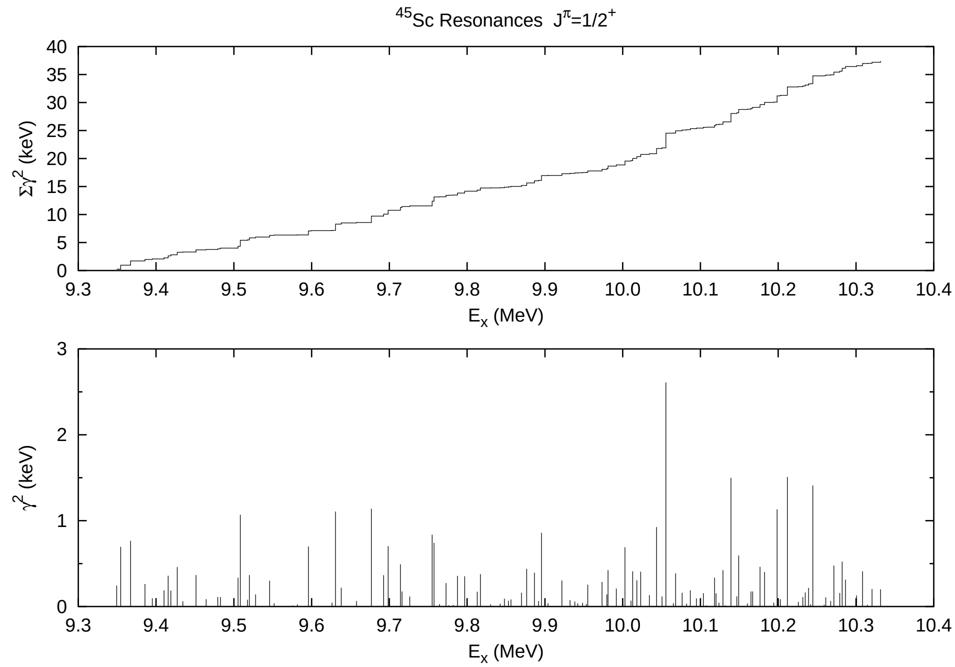

Figure 6.18: γ^2 and $\sum\gamma^2$ plots for ^{45}Sc s-wave resonances. No analog resonances were identified in this sequence.

energy region combine to produce an obvious enhancement effect.

Six sequences were analyzed in this manner resulting in the identification of three fragmented analog resonances which are listed in Table 6.3 and are shown in Figures 6.18–6.21. The three identified analog resonances were all p-wave resonances, one with J$^{\pi}$ $= \frac{1}{2}^{-}$ and two with J$^{\pi}$ $= \frac{3}{2}^{-}$. The J$^{\pi}$ $= \frac{1}{2}^{-}$ analog resonance at E$_x$ $\sim$ 10.05 MeV (see Figure 6.19) was previously identified by Smith [Smi89]. Smith removed the six strong resonances in this energy region. Although removing only the strongest levels will certainly remove most of the analog resonance enhancement effect on the reduced widths, for this experiment, all resonances in the vicinity of the analog resonance were identified as fragments and were removed from the sequence prior to the reduced width analysis. This fragmented analog resonance was identified as the analog of the state in ^{45}Ca at E$_x$ $= 3.442$ MeV. This analog resonance enhanced the widths of $\sim$ 20 resonances which had a total reduced width of

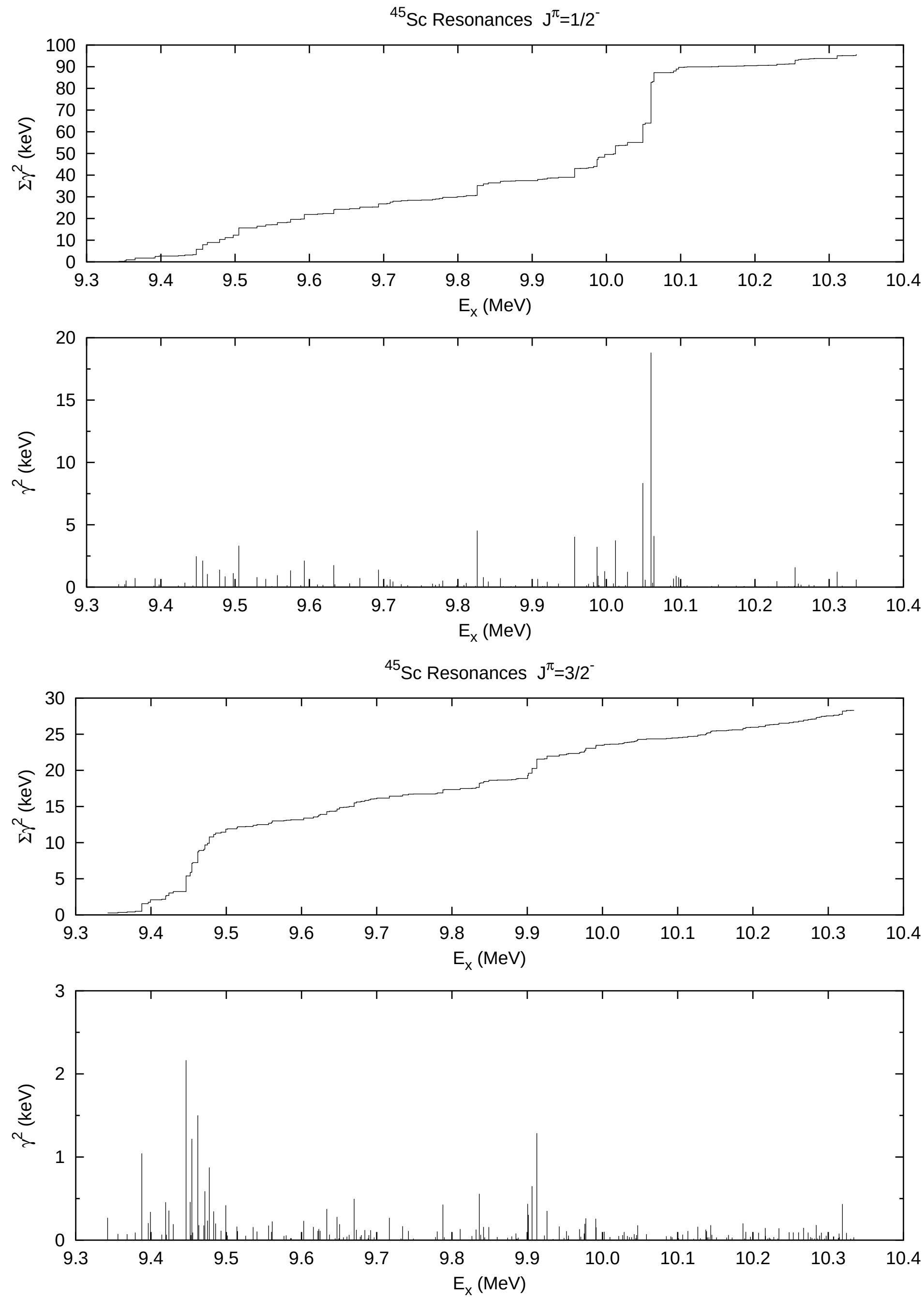

Figure 6.19: γ^2 and $\sum \gamma^2$ plots for ^{45}Sc p-wave resonances. The group of resonances near E_x = 10.05 MeV in the upper plots was identified as an analog resonance of the state in ^{45}Ca at E_x = 3.442 MeV. The group of resonances near E_x = 9.45 MeV in the lower plots was identified as an analog resonance of the state in ^{45}Ca at E_x = 2.84207 MeV. The group of resonances near E_x = 9.9 MeV in the lower plots was identified as an analog of the state in ^{45}Ca at E_x = 3.24134 MeV.

$\sim$ 48 keV.

Table 6.3: Analog resonances identified in ^{45}Sc.

Analog Number	J^π	^{45}Sc Resonances (MeV)	^{45}Ca Parent (MeV)	# of Resonances Removed	$\Sigma\Gamma$ (keV)	$\Sigma\gamma^2$ (keV)
1	$\frac{1}{2}^-$	3.1383–3.2476	3.442	20	19.88	48.22
2	$\frac{3}{2}^-$	2.5559–2.6476	2.842	19	1.66	10.28
3	$\frac{3}{2}^-$	3.0805–3.1068	3.241	7	1.28	3.65

The second analog resonance was previously identified and the fine structure fit by Wilson [Wil75]. Although the fragmented analog resonance was clearly observed (see Figure 6.19), no attempt was made in the present analysis to obtain the fine structure parameters. Instead the same procedure used in identifying the first analog resonance was used for all analog resonances identified. The fragmented analog resonance observed was identified as the analog of the state in ^{45}Ca at E_x = 2.842 MeV. The analog resonance enhancement affected 19 resonances and the total strength of the analog resonance was $\sim$ 10 keV.

The final analog resonance was misidentified by Smith. Information available at that time indicated that the state in ^{45}Ca at E_x = 3.241 MeV was assigned $J^\pi = \frac{1}{2}^-$. Hence, Smith identified the strong $J^\pi = \frac{1}{2}^-$ resonance at E_p = 3.0042 MeV as an analog resonance. A recent reassignment of the state in ^{45}Ca at E_x = 3.241 MeV to $J^\pi = \frac{3}{2}^-$ invalidated that identification. The group of $J^\pi = \frac{3}{2}^-$ resonances observed near $E_p \sim$ 3.090 MeV are now identified as this analog resonance. This analog resonance enhanced 7 resonances.

This procedure used to identify and remove analog resonances is not ideal. From Table C.1 it is apparent that the adopted levels of ^{45}Ca are not very well determined. Without an unambiguous level identification in the parent, identification of analog resonances is very difficult unless there is an obvious enhancement effect in the γ^2 or $\sum\gamma^2$ plot. Although there are other possible candidates for analog resonances in Figures 6.18, 6.20, and 6.21, positive identification as an analog resonance was not possible for these candidates. Some resonances observed in this study are probably unidentified analog resonances. However,

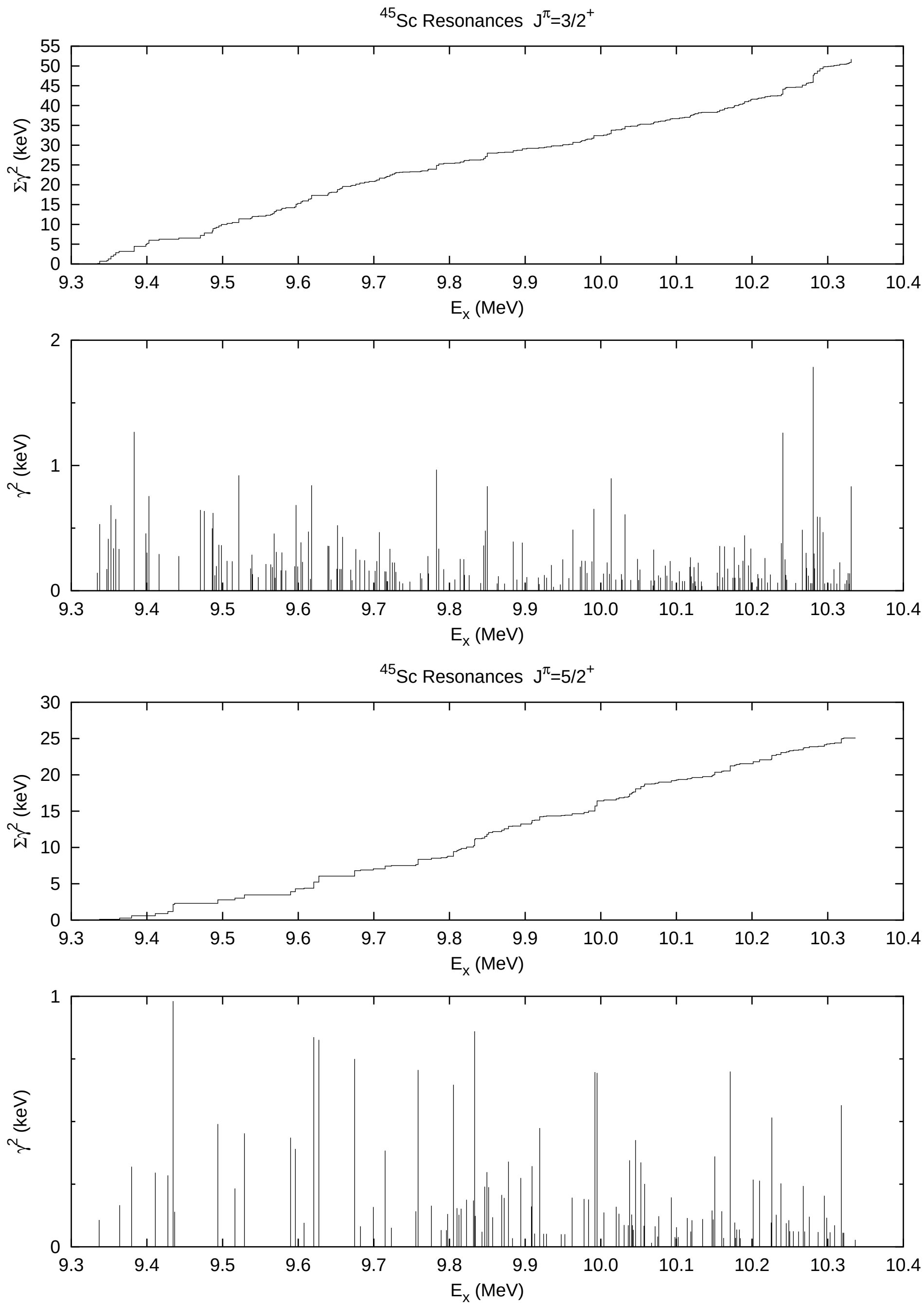

Figure 6.20: γ^2 and $\sum \gamma^2$ plots for ^{45}Sc d-wave resonances. No analog resonances were identified in these sequences.

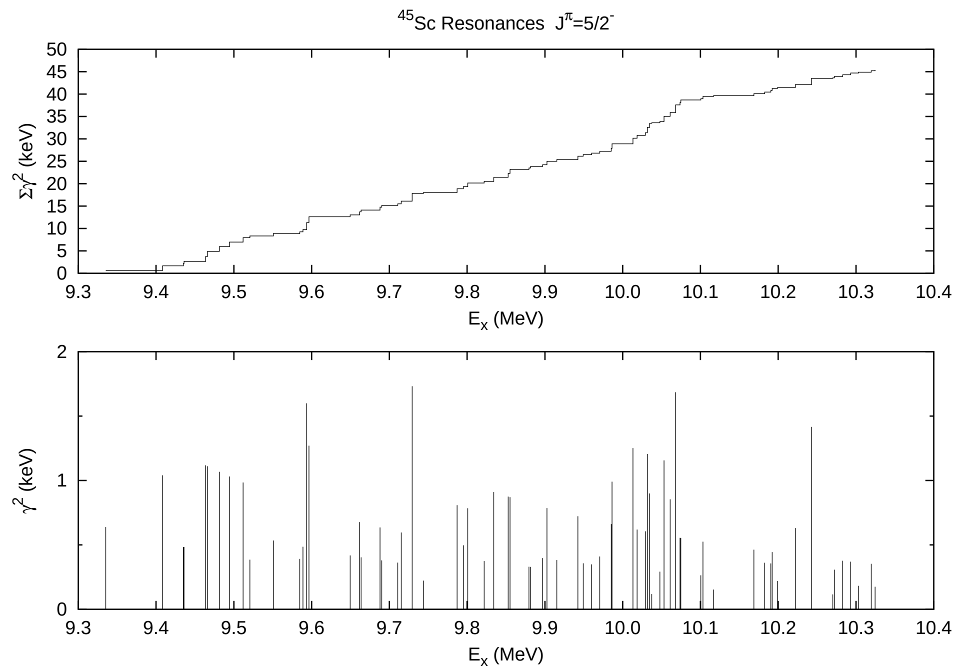

Figure 6.21: γ^2 and $\sum \gamma^2$ plots for ^{45}Sc f-wave resonances. No analog resonances were identified in this sequence.

the goal of this procedure was to remove the non-statistical effects introduced by analog resonances. If the other analog resonances are not obvious in the presented plots, then the reasonable assumption is that the unidentified analog resonances are not enhanced enough to distort the reduced width distributions significantly.

6.5 Reduced Width Distribution and Strength Functions

The reduced width distribution is another statistical property that reveals information about the completeness of a sequence. The behavior of the reduced width distribution for small values of y provides an assessment of the weakest resonances observed in a sequence. As shown in Section 2.1.1, the Porter-Thomas distribution predicts that very weak resonances are the most probable in a sequence. These weak resonances are also the most likely to remain unobserved due to inherent experimental limitations. The reduced width distribution should obey the Porter-Thomas distribution if non-statistical effects are removed from a sequence. Thus, the analog resonances identified in Section 6.4 are removed from the sequences before the reduced width distributions are plotted.

Shown in Figure 6.22 is the reduced width distribution for the s-wave resonance sequence. The reduced width distribution agrees very well with the Porter-Thomas distribution. The agreement implies that the s-wave resonance sequence is missing only a few weak levels. Although the weaker resonances seem to be slightly under represented in the reduced width distribution, the s-wave resonance sequence has the best agreement for $y < 0.1$ of any sequence constructed from the present experimental data. Thus, the s-wave resonance sequence is the most complete of the observed sequences, which independently confirms the results of the spacing analysis and Δ_3 tests.

The reduced width distributions for the other J^π sequences are shown in Figures 6.23, 6.24, and 6.25. While the large y behavior typically obeys the Porter-Thomas distribution, the cut-off value for small y varies from sequence to sequence. As the Porter-Thomas distribution predicts many weak levels, the obvious conclusion is that there are weak resonances

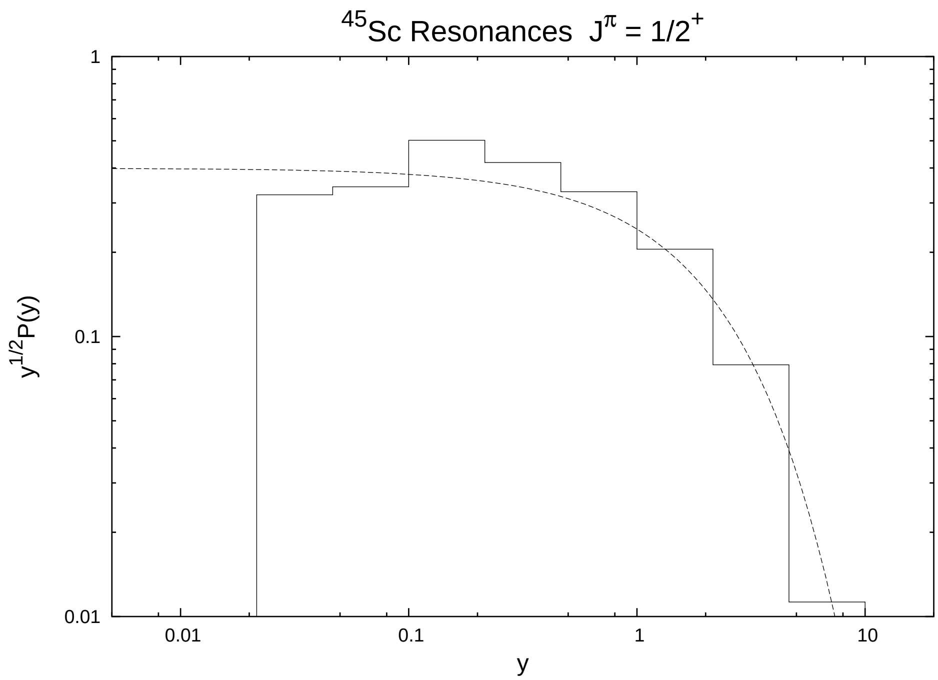

Figure 6.22: Reduced width distribution for the ^{45}Sc s-wave resonance sequence. The dashed line represents the Porter-Thomas distribution.

that were not observed in this experiment. The results of the spacing analysis and Δ_3 tests also imply that there are missing and spurious levels in these sequences. Thus, all statistical analyses seem to agree with the results of the reduced width distributions.

The strength functions, S, for each J$^{\pi}$ can be calculated using Equation 2.4. As with the reduced width distributions, the non-statistical analog resonances must be removed prior to the calculation of the strength functions. Shown in Table 6.4 are the strength functions determined from the present experiment and the strength functions determined from the measurements of Smith [Smi89]. The uncertainty ΔS was determined by the expression

$$\Delta S_J = S_J\sqrt{\frac{2}{N}} \tag{6.3}$$

The strength functions are not a primary concern of this experiment and are presented only for completeness.

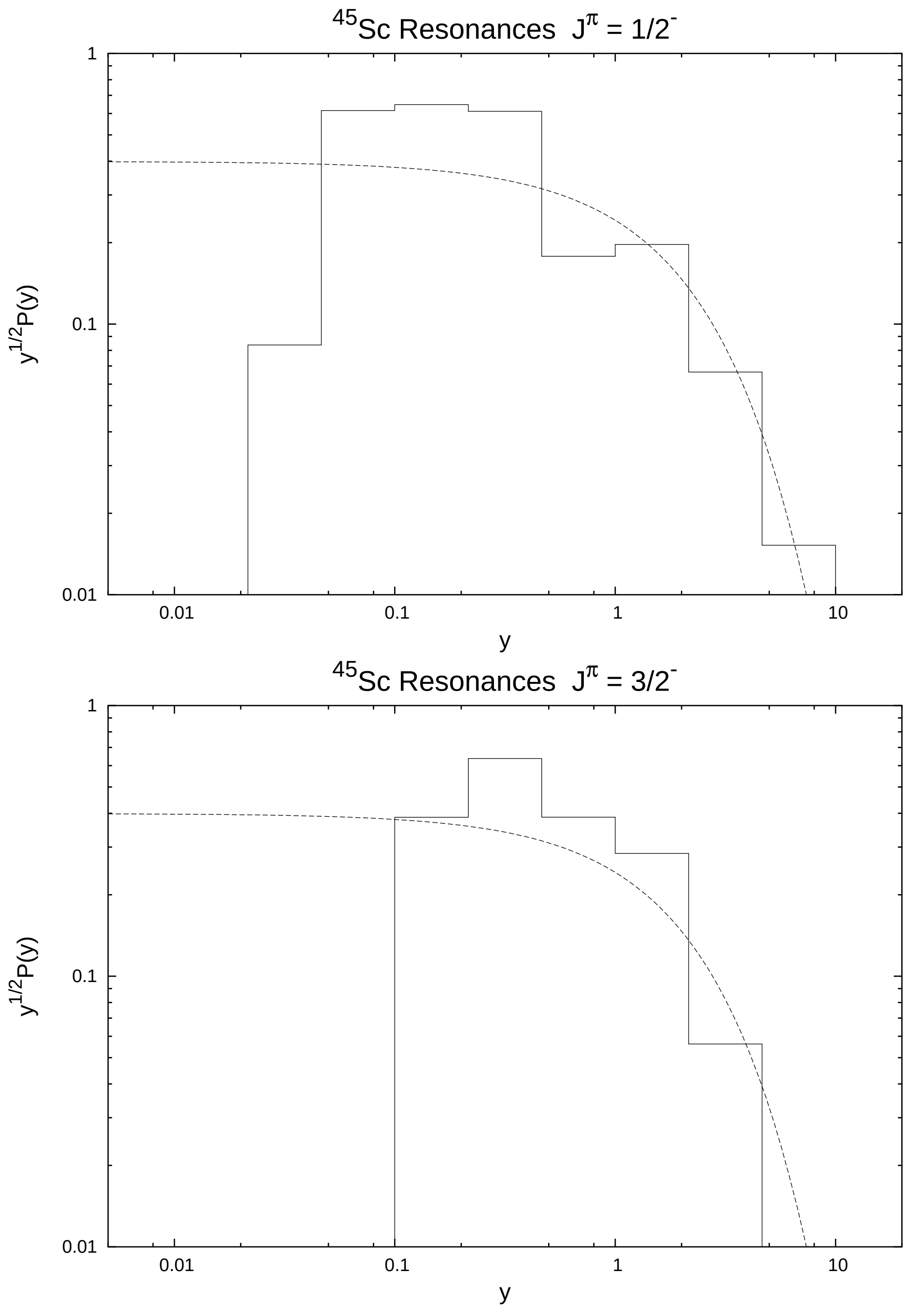

Figure 6.23: Reduced width distribution for p-wave resonances. The dashed line represents the Porter-Thomas distribution.

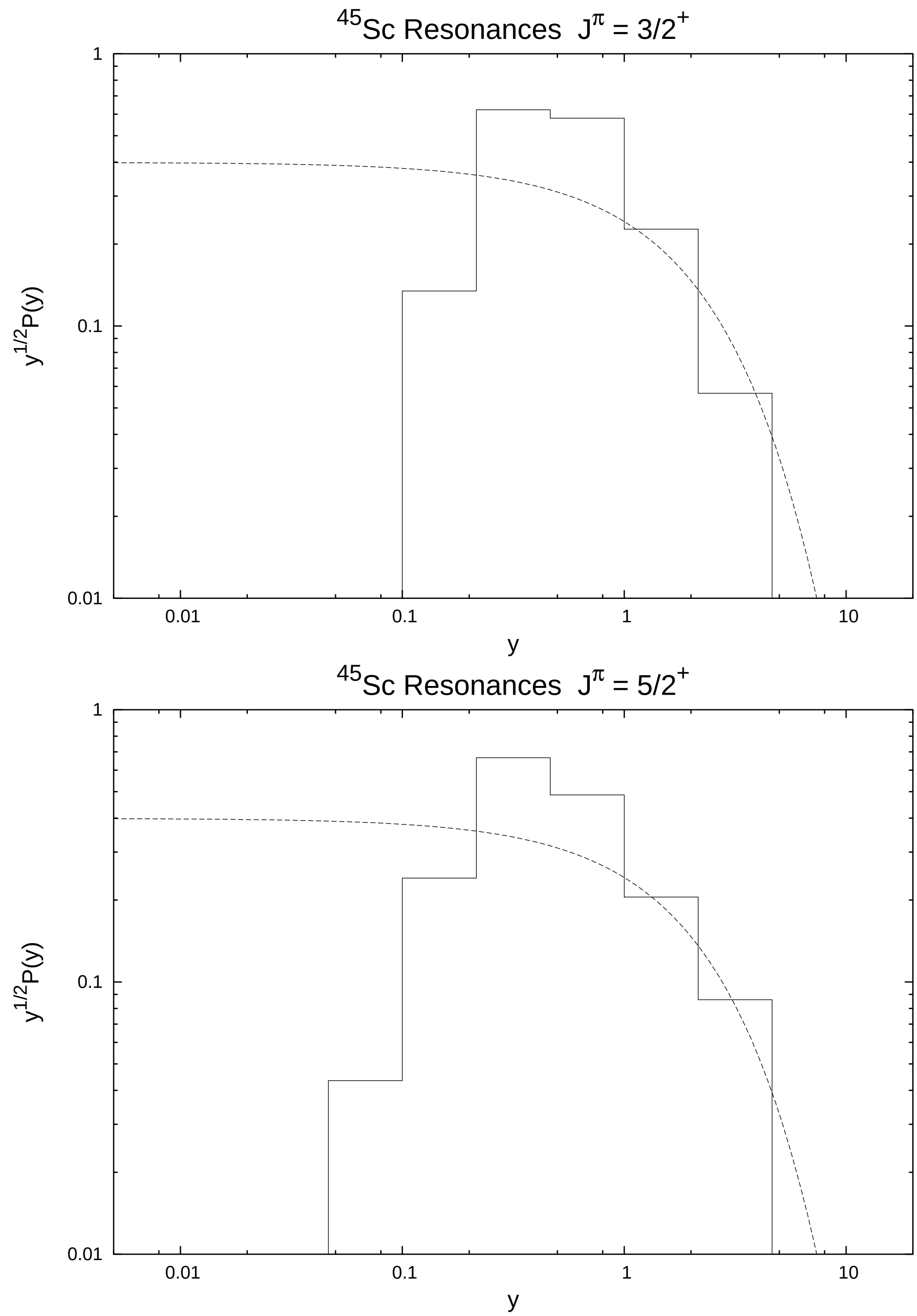

Figure 6.24: Reduced width distribution for d-wave resonances. The dashed line represents the Porter-Thomas distribution.

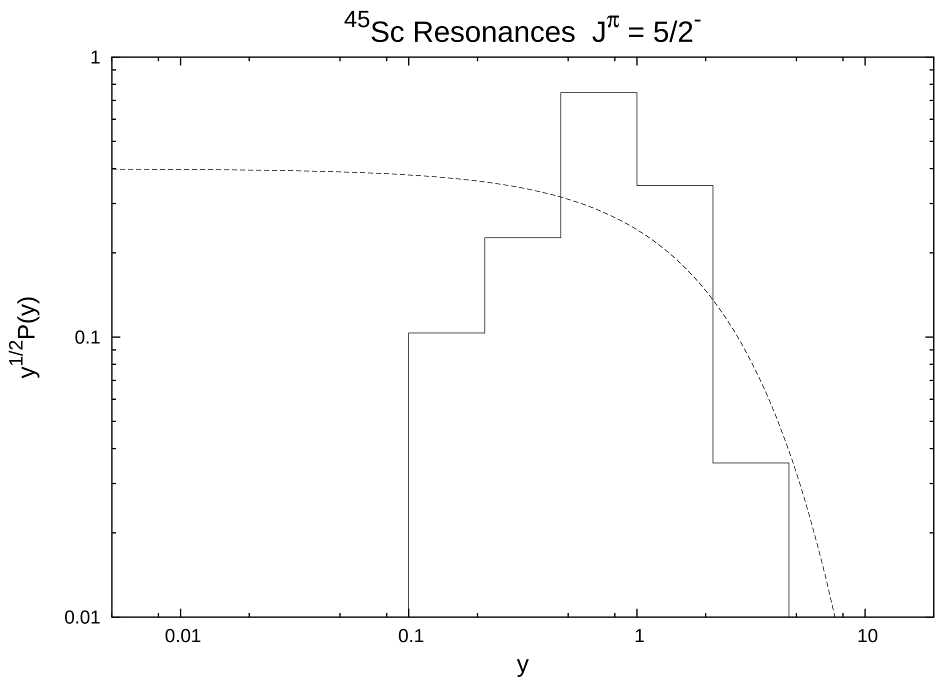

Figure 6.25: Reduced width distribution for f-wave resonances. The dashed line represents the Porter-Thomas distribution.

Table 6.4: Calculated strength functions for the J^π sequences observed in this experiment. The strength functions calculated from previous work only consider the energy range E_p = 2.95–3.72 MeV and were determined by Agvaanluvsan [Agv02].

J^π	$\sum \gamma^2_{obs}$ [keV] (current work)	$\sum \gamma^2_{obs}$ [keV] (previous work)†	S (current work)	S (previous work)†
$\frac{1}{2}^+$	37.50	33.6	0.036 ± .005	0.045 ± .006
$\frac{1}{2}^-$	48.15	36.6	0.047 ± .007	0.049 ± .006
$\frac{3}{2}^-$	15.14	14.3	0.015 ± .002	0.019 ± .003
$\frac{3}{2}^+$	43.94	35.7	0.043 ± .004	0.047 ± .006
$\frac{5}{2}^+$	25.22	26.8	0.025 ± .003	0.035 ± .006
$\frac{5}{2}^-$	45.74		0.044 ± .007	

† [Agv02]

6.6 Level Densities

Level densities were calculated for the six experimentally observed sequences. The spacing and width corrections (see Section 2.2.1 and 2.2.2) for the observed fraction are calculated independently. The two observed fractions, $f_{spacing}$ and f_{width}, are combined to produce a total observed fraction. The total observed fraction is the weighted average of these two values.

After calculating the corrected number of levels $N_{cor} = \frac{N_{obs}}{f}$, the level density is simply $\rho = N_{cor}/\Delta E$ where ΔE is the energy interval. The uncertainties in ρ arise from two sources; the statistical error due to the finite number of resonances in each sequence ($\Delta\rho_1$) and the statistical error due to the uncertainty in f, ($\Delta\rho_2$). The two uncertainties have the form

$$\Delta\rho_1 = \rho\sqrt{\frac{0.27}{N_{cor}}} \tag{6.4}$$

and

$$\Delta\rho_2 = \rho\frac{\Delta f}{f}, \tag{6.5}$$

where $\Delta\rho_1$ is taken according to Lynn [Lyn68]. The two uncertainties are combined to calculate an uncertainty for ρ:

$$\Delta\rho = \sqrt{(\Delta\rho_1)^2 + (\Delta\rho_2)^2} \tag{6.6}$$

Shown in Table 6.5 are the observed fractions and corrected level densities with uncertainties for each observed sequence. The $J^\pi = \frac{1}{2}^+$ sequence has the largest observed fraction and had the best agreement with the GOE predictions. The other sequences have a lower observed fraction and poor agreement with the GOE predictions as shown previously.

Table 6.5: Summary of level densities for ^{45}Sc resonances.

J^π	N_{obs}	$f_{spacing}$	f_{width}	f_{total}	N_{cor}	ρ [MeV]$^{-1}$
$\frac{1}{2}^+$	121	$0.95^{+.03}_{-.04}$	$0.86^{+.12}_{-.10}$	$0.94^{+.03}_{-.04}$	128	127^{+7}_{-8}
$\frac{1}{2}^-$	116	$0.87\pm .04$	$0.83^{+.13}_{-.11}$	$0.87\pm.04$	134	132^{+8}_{-9}
$\frac{3}{2}^-$	178	$0.85\pm .03$	$0.66^{+.08}_{-.07}$	$0.82\pm.03$	216	215 ± 11
$\frac{3}{2}^+$	203	$0.86\pm .03$	$0.69^{+.07}_{-.06}$	$0.83\pm.03$	245	242 ± 12
$\frac{5}{2}^+$	117	$0.85\pm .04$	$0.76^{+.10}_{-.09}$	$0.84\pm.04$	140	138 ± 9
$\frac{5}{2}^-$	72	$0.85\pm .05$	$0.61^{+.10}_{-.08}$	$0.79\pm.04$	91	90^{+6}_{-7}

A potential problem with the two methods of calculating the observed fractions is the failure of the two results to overlap for the given uncertainties for some of the sequences. The two methods should agree within uncertainties.

To investigate the J dependence of the level densities, the level densities are compared with the conventional spin dependence of the level density. This formula is:

$$f(J) \simeq \frac{2J+1}{2\sigma^2} e^{-\frac{J(J+1)}{2\sigma^2}}. \tag{6.7}$$

Figure 6.26 shows the level densities compared to Equation 6.7 with the spin cut-off parameter σ taken to be 2.9 [Gil65]. There is a large discrepancy between Equation 6.7 and the current level densities. The level densities have been fit to determine the value of the spin cut-off parameter required to fit these data. This fit is shown in Figure 6.27 with the value of the spin cut-off parameter $\sigma = 1.75$. This value is anomalously low and probably just reinforces the results of the statistical tests; there are missing and spurious levels in

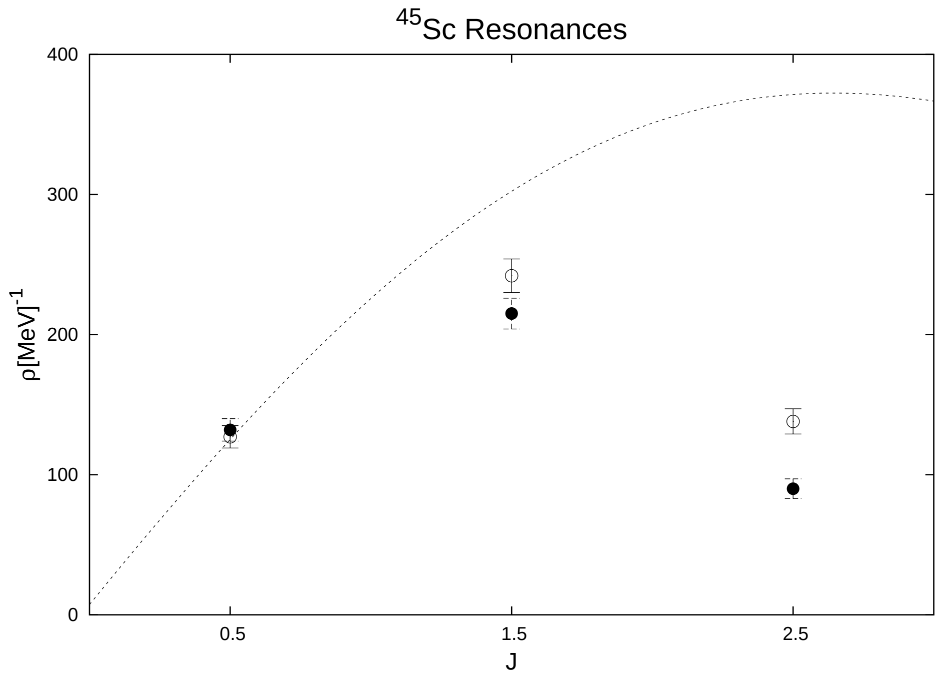

Figure 6.26: J dependence of the level densities of ^{45}Sc. The hollow circles represent π = + sequences while the solid circles represent π = - sequences. The dashed line is the conventional spin dependence $f(J)$ of the level density given by Equation 6.7 with the parameter $\sigma = 2.9$.

the p-wave, d-wave, and f-wave resonance sequences. Since the value of the spin cut-off parameter depends on accurate measurements of the level densities for J = $\frac{3}{2}$ and J = $\frac{5}{2}$, this value of the spin cut-off parameter is not realistic.

To investigate the parity dependence of the level densities, it is convenient to introduce a parameter α for the parity asymmetry of the level density:

$$\alpha = \frac{\rho_+ - \rho_-}{\rho_+ + \rho_-}, \tag{6.8}$$

where ρ_+ and ρ_- are the positive and negative parity level densities for a given value of J. The parameter α will be zero if there is no parity dependence. The parameter α will be positive if there are more positive parity states than negative parity states. The parity asymmetry is listed in Table 6.6 and shown in Figure 6.28. The J = $\frac{1}{2}$ value of α is

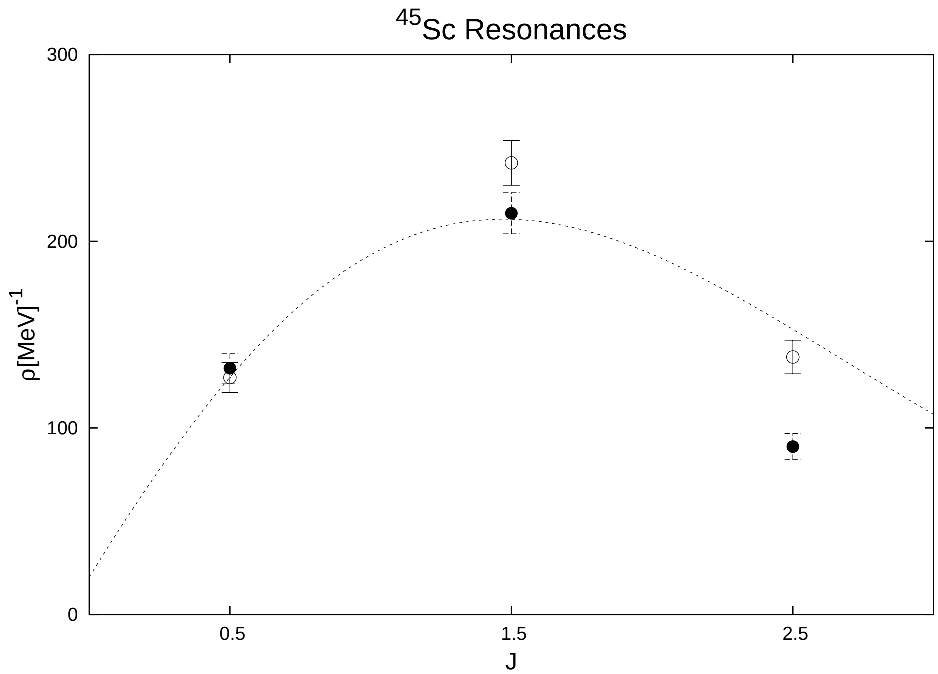

Figure 6.27: The spin cut-off parameter of ^{45}Sc. The hollow circles represent $\pi = +$ sequences while the solid circles represent $\pi =$ - sequences. The dashed line is the conventional spin dependence $f(J)$ of the level density given by Equation 6.7. The value of the spin cut-off parameter is $\sigma = 1.75$.

-0.02 ± 0.04. This is by far the most accurate value of α since the J $= \frac{1}{2}$ sequences have been determined to be the most pure and complete. While there is a large asymmetry for J $= \frac{5}{2}$ and a slight asymmetry for J $= \frac{3}{2}$, these results are not reliable due to the missing and spurious levels that the statistical tests indicate. Thus, the analysis of the highest quality sequences in ^{45}Sc indicates no parity dependence of the level density.

Table 6.6: Parity asymmetry in the ^{45}Sc resonance level densities.

J	α
$\frac{1}{2}$	-0.02 $\pm$ 0.04
$\frac{3}{2}$	$0.06\ ^{+0.03}_{-0.04}$
$\frac{5}{2}$	$0.21\ ^{+0.05}_{-0.04}$

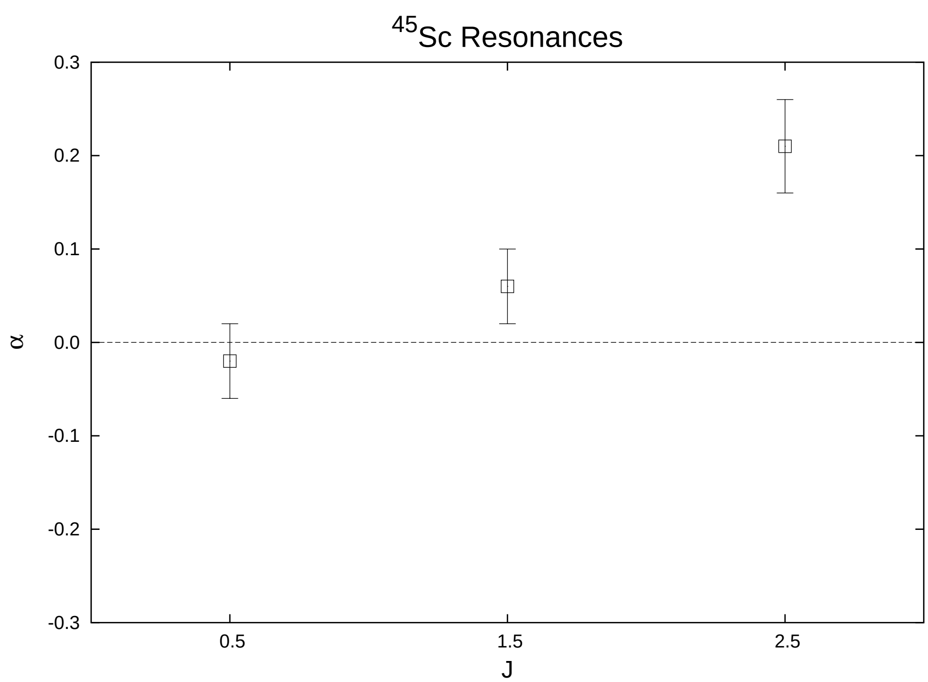

Figure 6.28: The parity asymmetry, α, in the ^{45}Sc level densities.

Chapter 7

Summary and Conclusion

The research presented in this thesis was motivated in part by the results of an analysis of the parity-dependence of the level densities of ^{45}Sc [Agv02, Agv03a]. The apparent observation of parity-dependence was suggestive although with large uncertainties. An additional test of the purity and completeness of a sequence indicated many probable misassigned and missing levels in ^{45}Sc [Agv02, Agv03b]. A measurement that improved the completeness and purity of the ^{45}Sc levels seemed appropriate.

High-resolution proton scattering measurements of the ^{44}Ca(p,p$_0$) and ^{44}Ca(p,p$_1$) reactions were performed in the energy range E_p = 2.50–3.53 MeV to identify all levels and to improve the assignments of the quantum numbers J and π. The observed cross-sections were analyzed using the multichannel, multilevel, R-matrix code MULTI6. A total of 809 resonances were observed. A large number (186) of previously unobserved levels were identified, and the spin and/or parity of many (168) resonances were reassigned.

Statistical tests were performed on the sequences formed from the observed levels. The Dyson-Mehta Δ_3 statistic, the nearest-neighbor spacing distribution, and the reduced width distribution were all compared to theoretical predictions. The results of the statistical analyses were mixed. The s-wave resonances were determined very well and agreed with the predictions of GOE for all statistical tests. The other J^π sequences did not agree well with the GOE predictions, presumably due to missing and misassigned levels.

The ^{45}Sc sequences were tested for purity and completeness using the spacing anomaly analysis method. This method compares the nearest-neighbor spacings to the Wigner distribution to identify anomalously large and small spacings. The anomalous spacings suggest missing or misassigned levels in a sequence. The number of anomalous spacings has been reduced, indicating the improved quality of the data. Remeasurement and reanalysis of the experimental data indicated that the small spacings are an excellent indicator for spin misassignment. Analysis of the two resonances involved in the anomalously small spacing usually led to a reassignment of the spin of one of the resonances. Anomalously large spacings are reliable indicators of a missing level but only define an energy region of interest. Reexamination of these regions sometimes led to the observation of a new resonance with the appropriate spin and parity. However, often no new resonance of the same J^π was observed, presumably because the level was too small to be observed.

The introduction of levels with the "wrong" quantum number into a sequence can be treated as producing a combination of two GOE sequences with appropriate weights. The general expression is rather complicated [Meh91] but reduces to a very simple form at $x = 0$. If the value of the nearest-neighbor spacing distribution at $x = 0$ can be determined, one can estimate the number of spurious levels in a sequence. The results of the $P(0)$ analysis were inconclusive. In practice, it appears difficult to determine an accurate value of $P(0)$.

The observed fraction of levels for each sequence was determined using two methods. The width analysis method uses a modified Porter-Thomas distribution to estimate the observed fraction of levels of a sequence, while the spacing analysis method produces an estimate of the observed fraction using the nearest-neighbor spacing distribution. The level densities were determined using the observed fraction estimates. The parity and J-dependence of the level densities were considered. The experimental J-dependence does not agree with the conventional spin dependence and the standard value of the spin cut-off parameter. This probably reflects a significant number of missing levels with higher J values.

The failure of most of the sequences to agree with the GOE predictions emphasizes the experimental limitations. Although the data is of very high quality, it was still difficult to assign J in many cases. Thus, many of the sequences are not of sufficient purity to show GOE behavior. No parity dependence is observed in the level densities of the J $= \frac{1}{2}$ sequences. Since these sequences are the most pure and complete of all of the measured sequences, there is no evidence for parity dependence effect for the level densities in ^{45}Sc.

Appendix A

p + ^{44}Ca Data and Fits

This appendix presents the experimentally observed differential cross-sections and the theoretical fits produced by MULTI6. Each figure consists of a 100-keV energy range of data for the measured cross-sections at five angles. The ^{44}Ca(p,p_0) reaction cross-sections are presented first, with the ^{44}Ca(p,p_1) reaction cross-sections following.

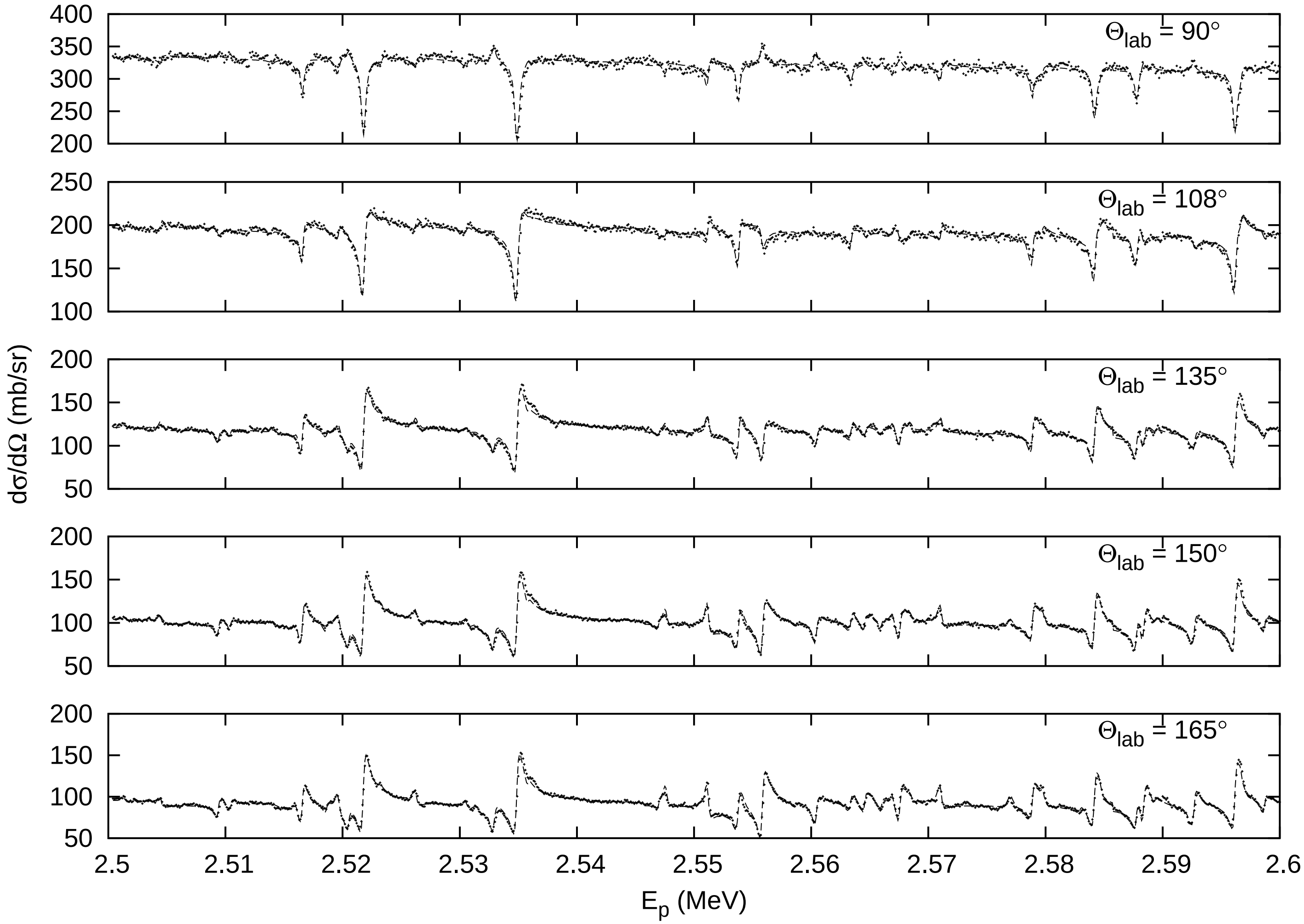

Figure A.1: The ^{44}Ca(p,p$_0$) reaction cross-sections and fits for E_p = 2.5–2.6 MeV.

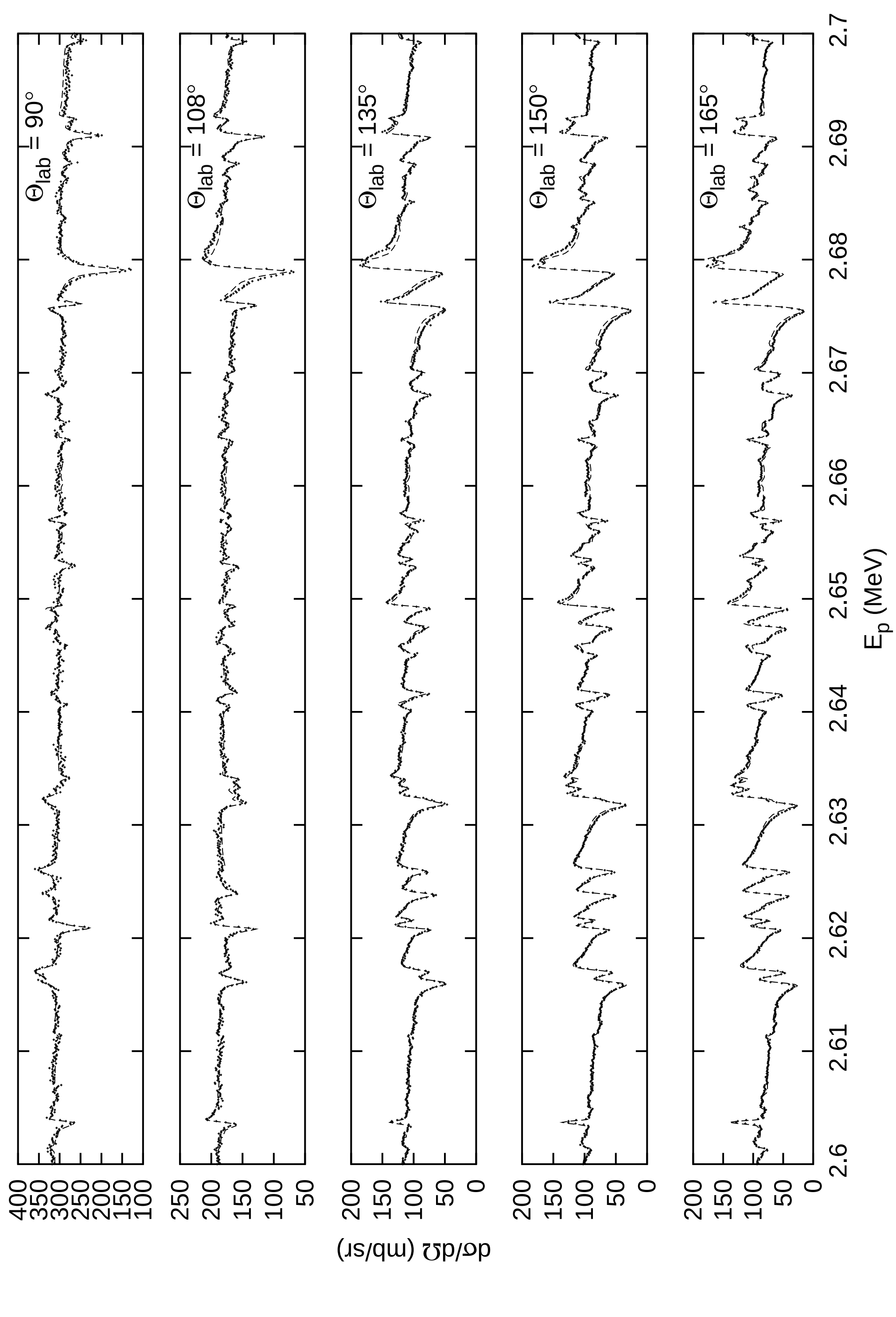

Figure A.2: The $^{44}Ca(p,p_0)$ reaction cross-sections and fits for E_p = 2.6–2.7 MeV.

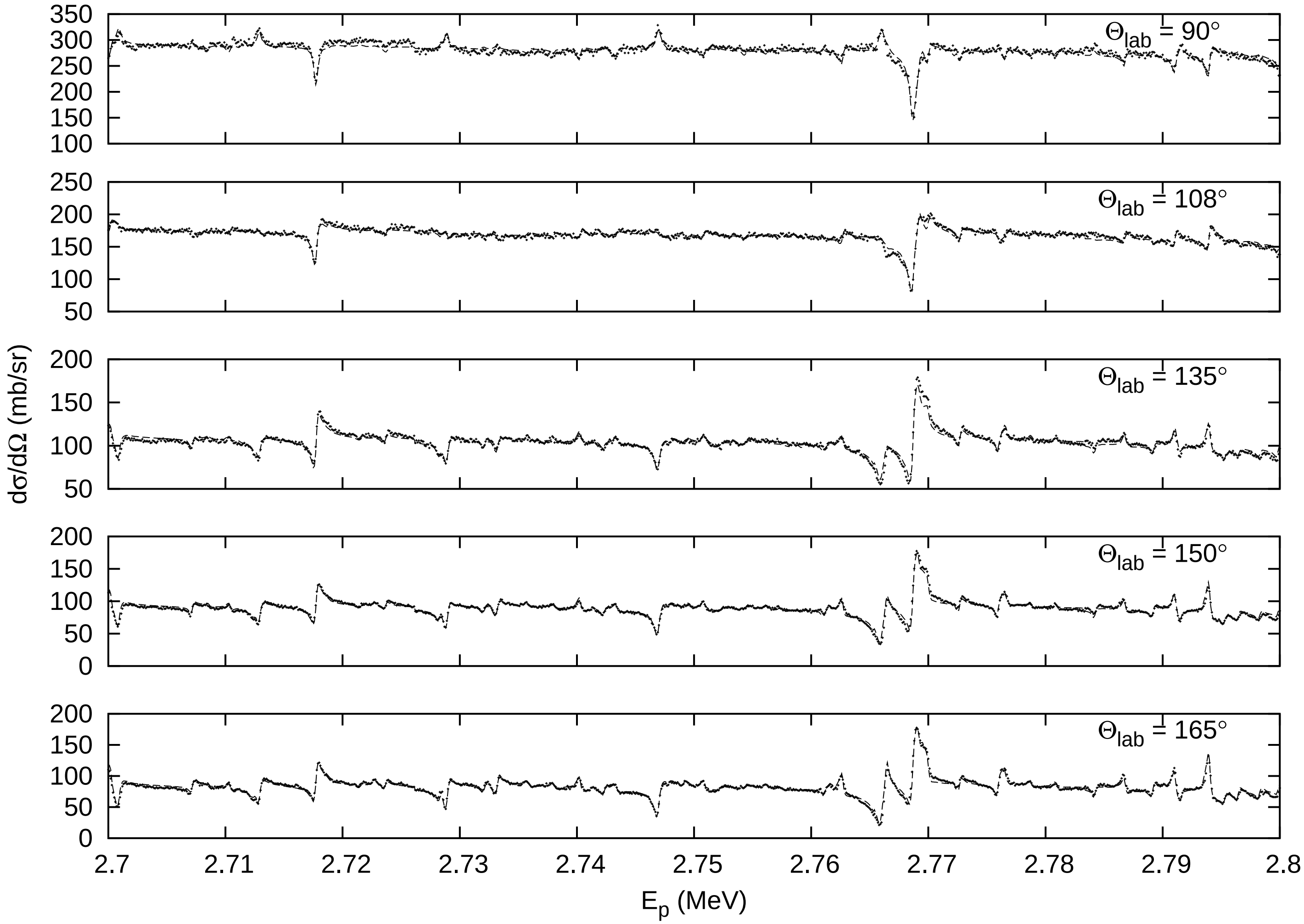

Figure A.3: The ^{44}Ca(p,p$_0$) reaction cross-sections and fits for E_p = 2.7–2.8 MeV.

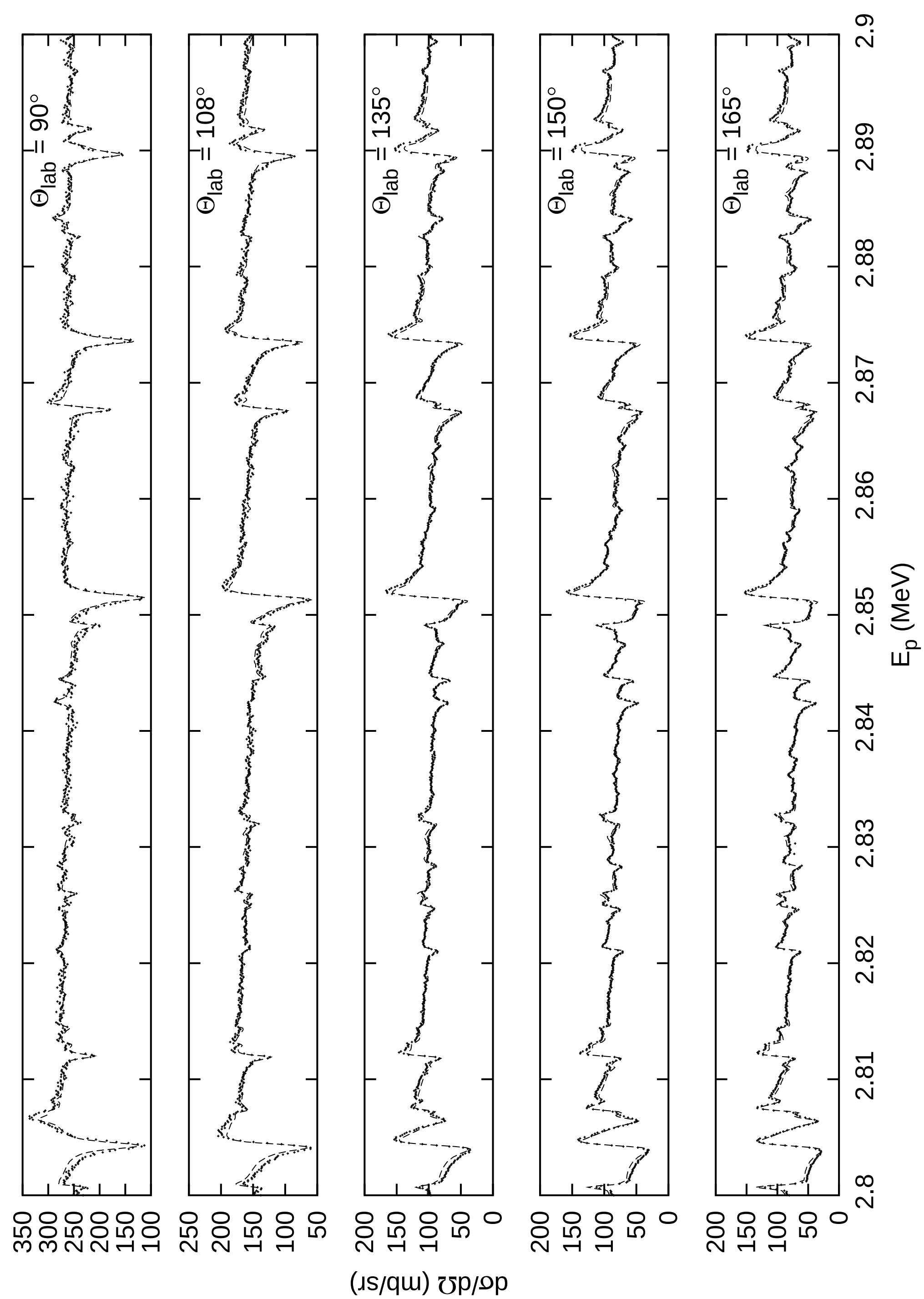

Figure A.4: The ${}^{44}Ca(p,p_0)$ reaction cross-sections and fits for E_p = 2.8–2.9 MeV.

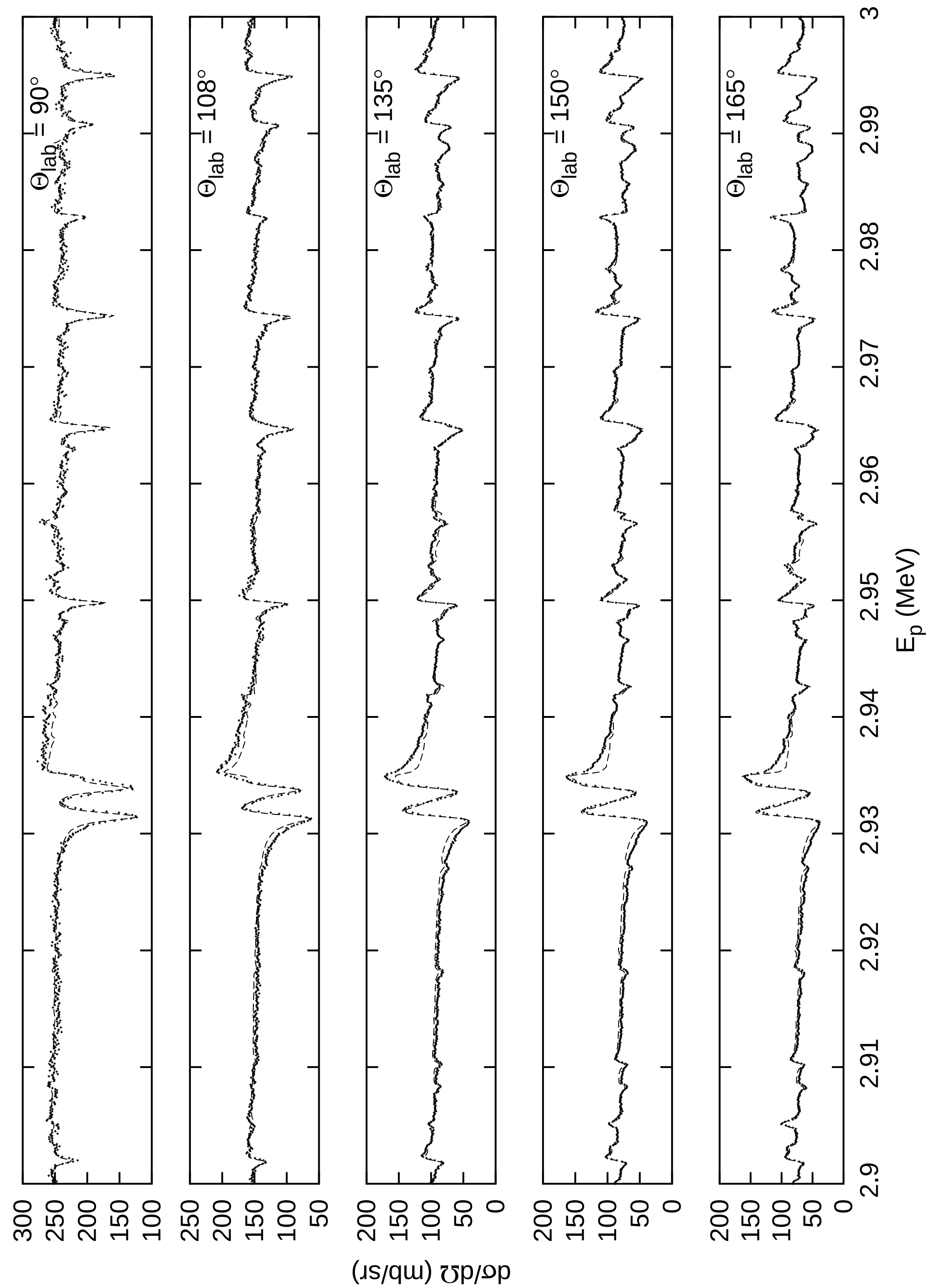

Figure A.5: The ^{44}Ca(p,p$_0$) reaction cross-sections and fits for $E_p = 2.9$–3.0 MeV.

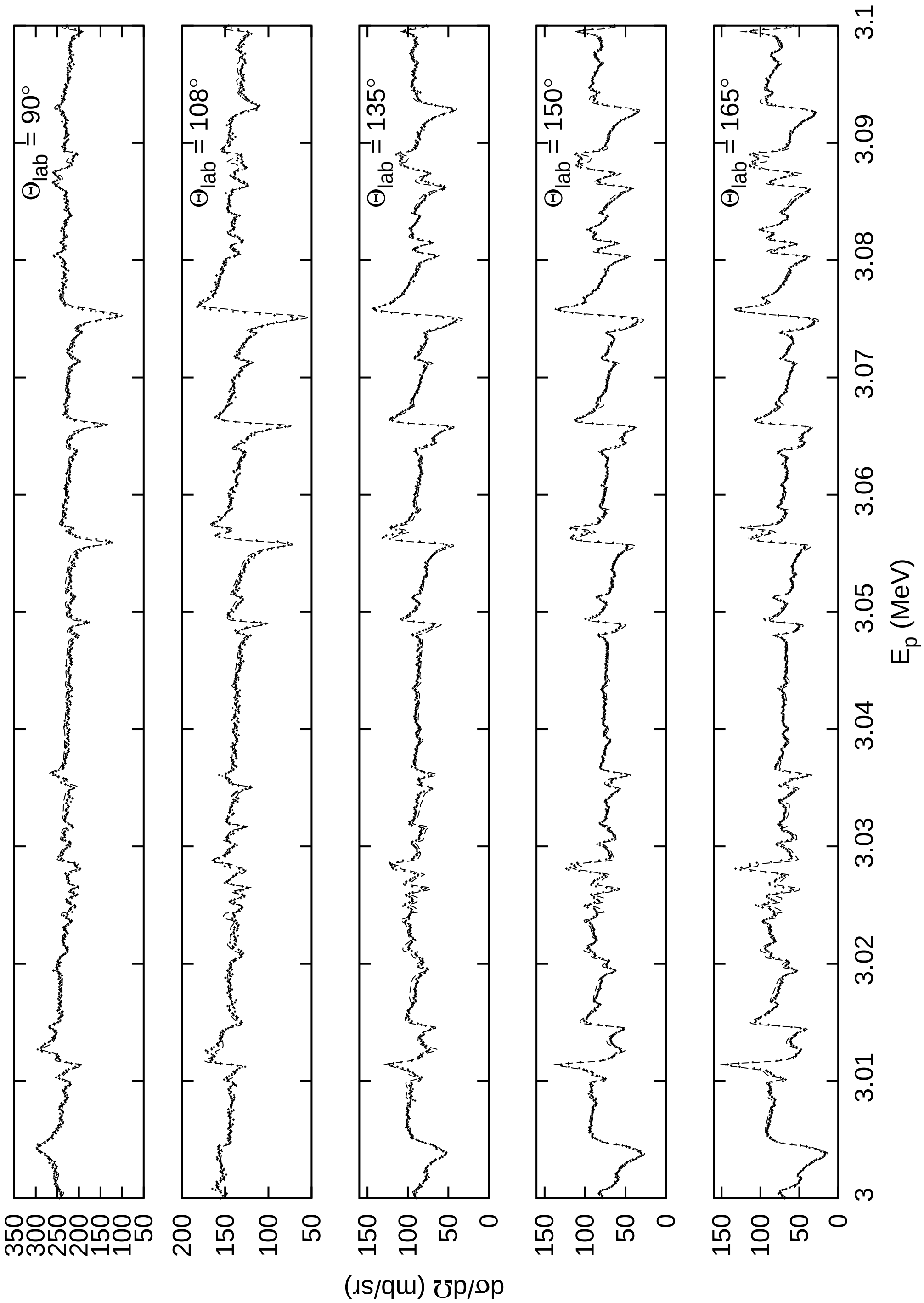

Figure A.6: The ^{44}Ca(p,p$_0$) reaction cross-sections and fits for E$_p$ = 3.0–3.1 MeV.

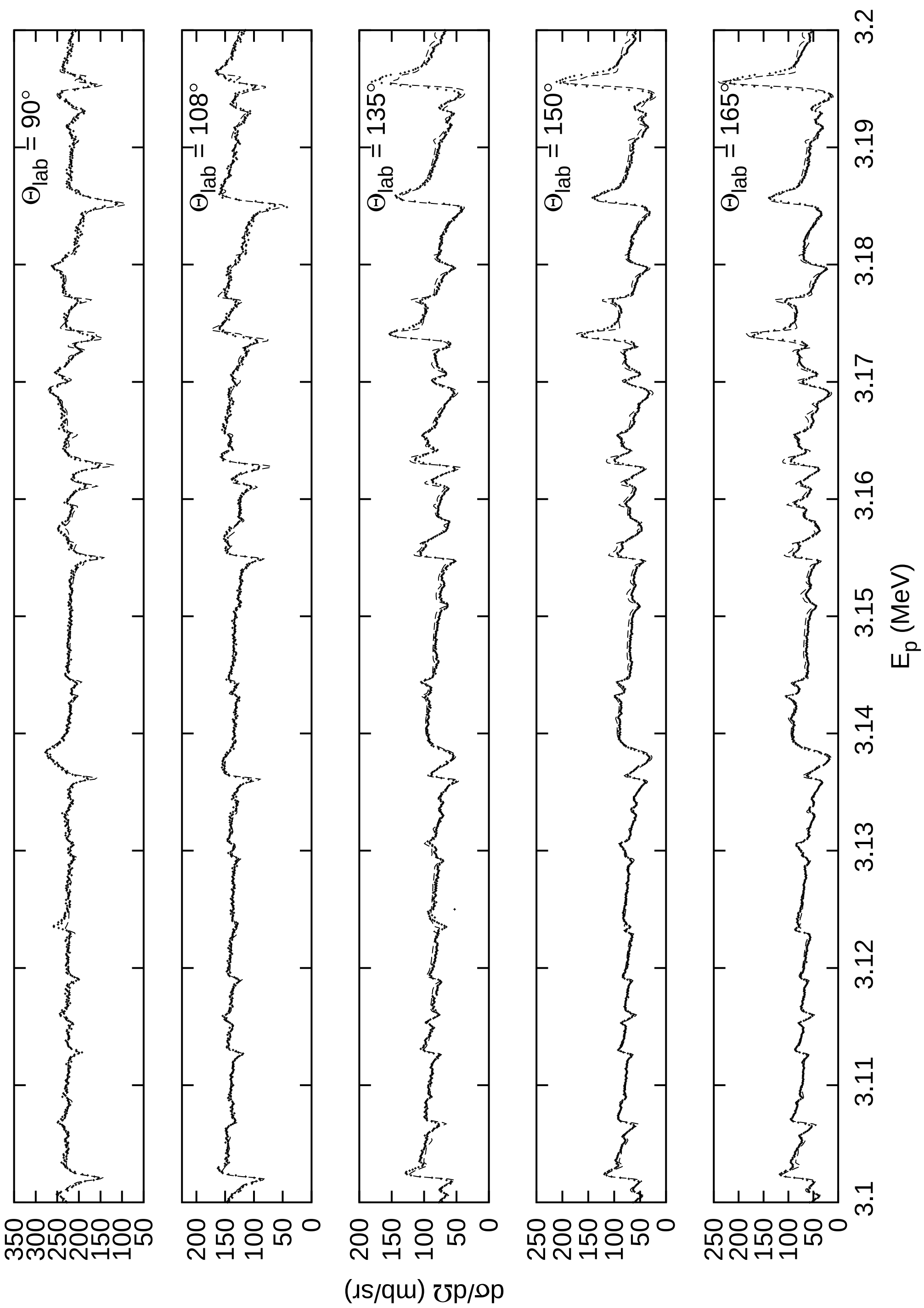

Figure A.7: The ^{44}Ca(p,p$_0$) reaction cross-sections and fits for E$_p$ = 3.1–3.2 MeV.

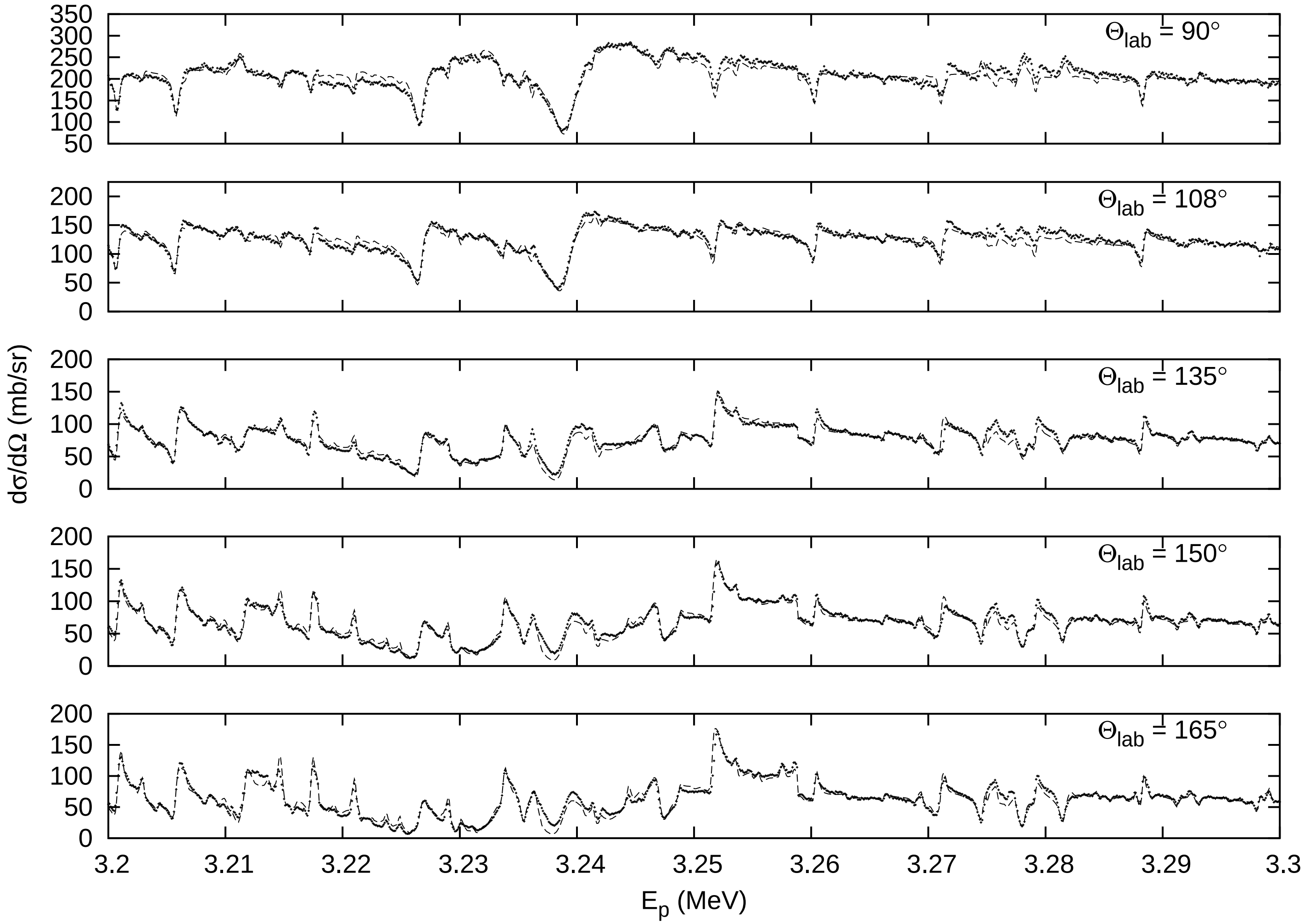

Figure A.8: The ${}^{44}Ca(p,p_0)$ reaction cross-sections and fits for E_p = 3.2–3.3 MeV.

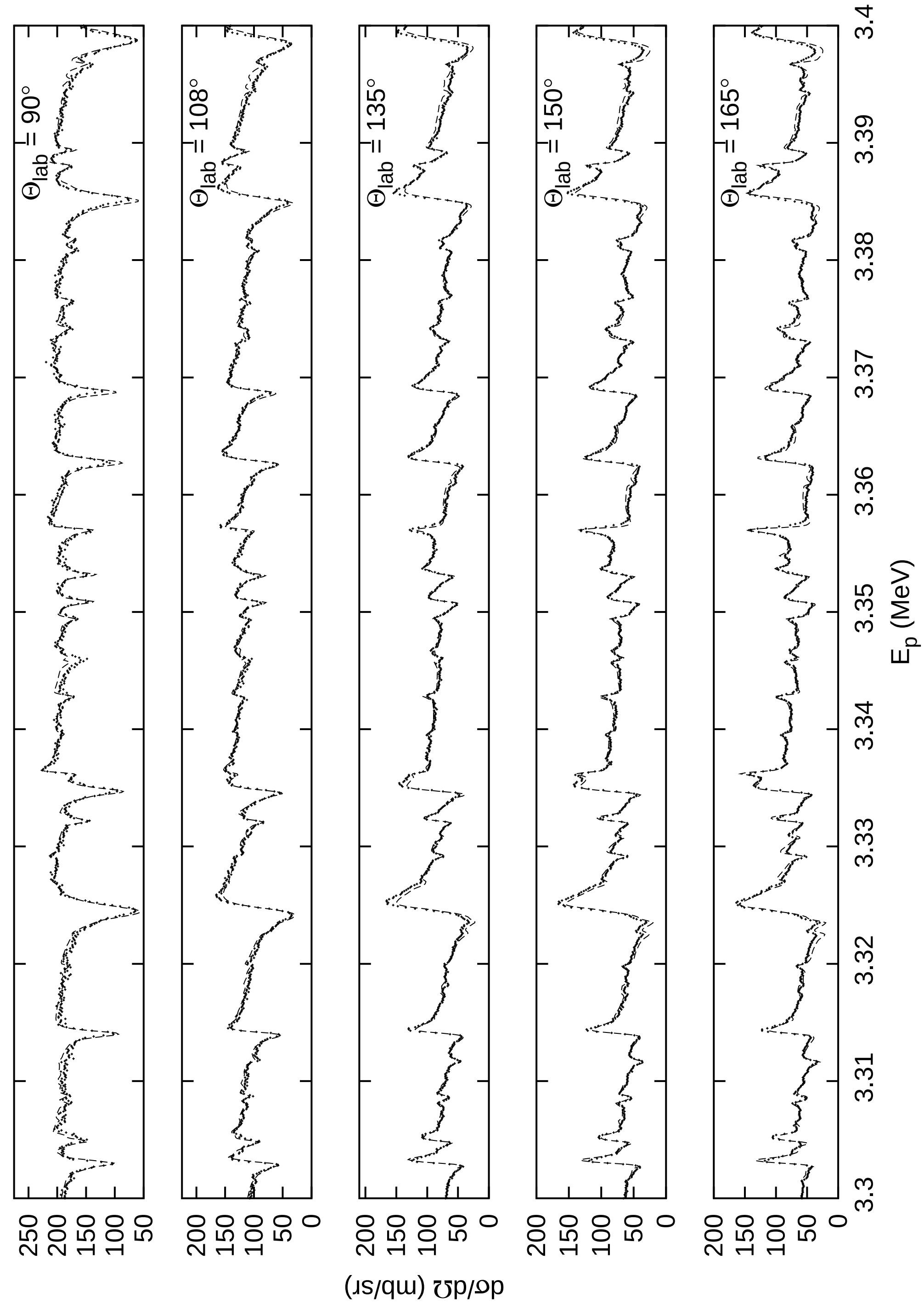

Figure A.9: The ^{44}Ca(p,p$_0$) reaction cross-sections and fits for E_p = 3.3–3.4 MeV.

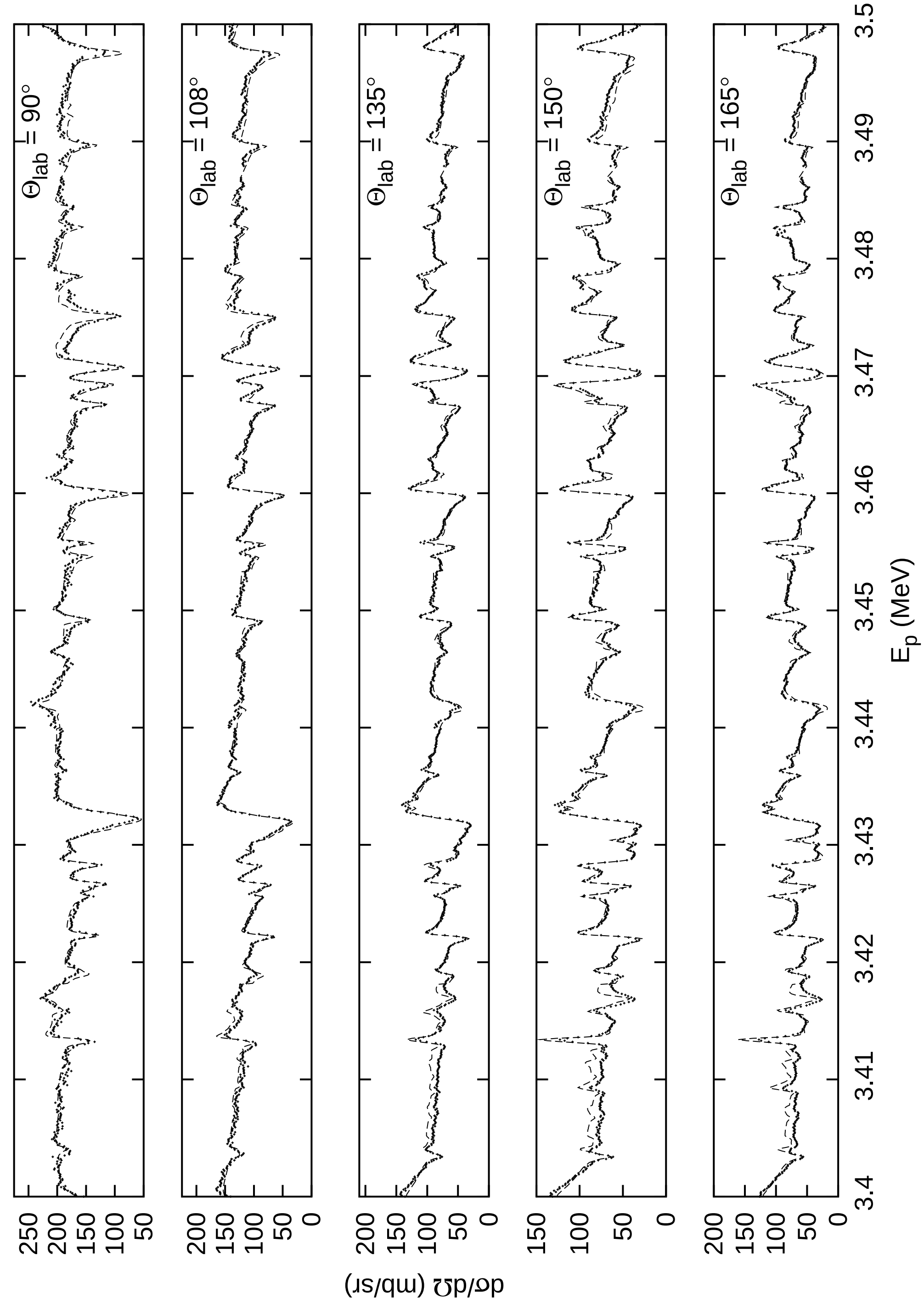

Figure A.10: The ${}^{44}Ca(p,p_0)$ reaction cross-sections and fits for E_p = 3.4–3.5 MeV.

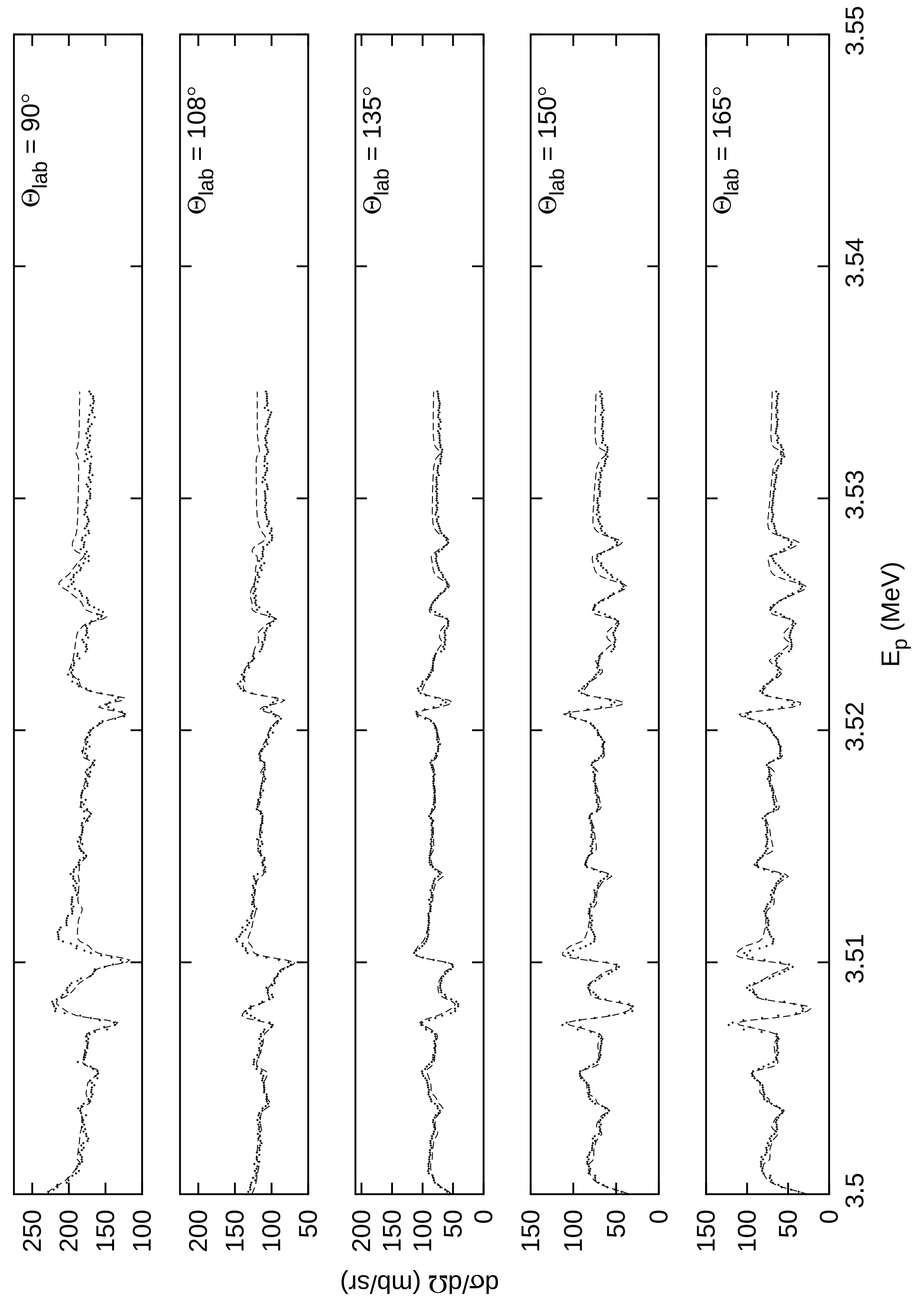

Figure A.11: The ^{44}Ca(p,p$_0$) reaction cross-sections and fits for E_p = 3.50–3.53 MeV.

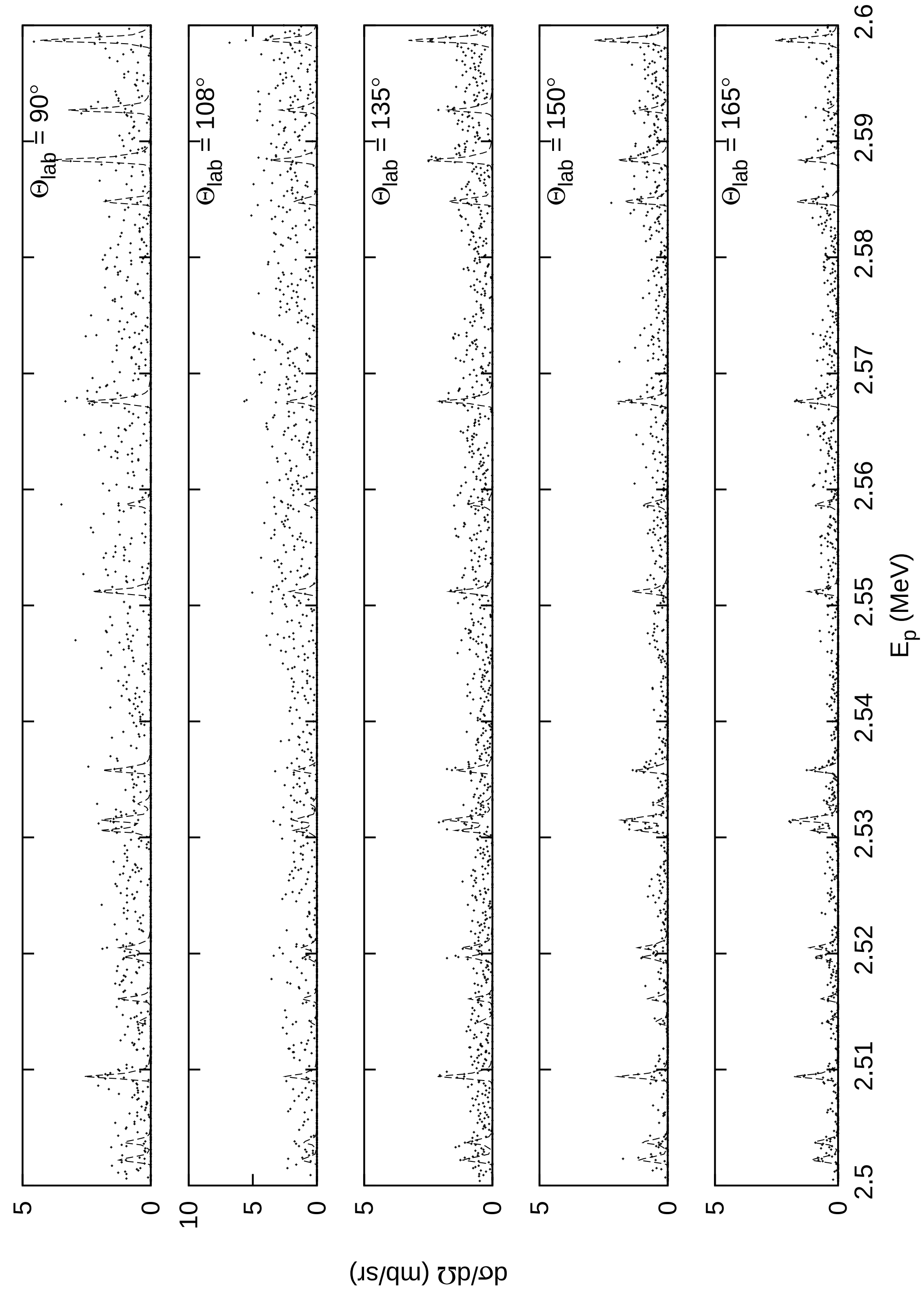

Figure A.12: The ${}^{44}Ca(p,p_1)$ reaction cross-sections and fits for E_p = 2.5–2.6 MeV.

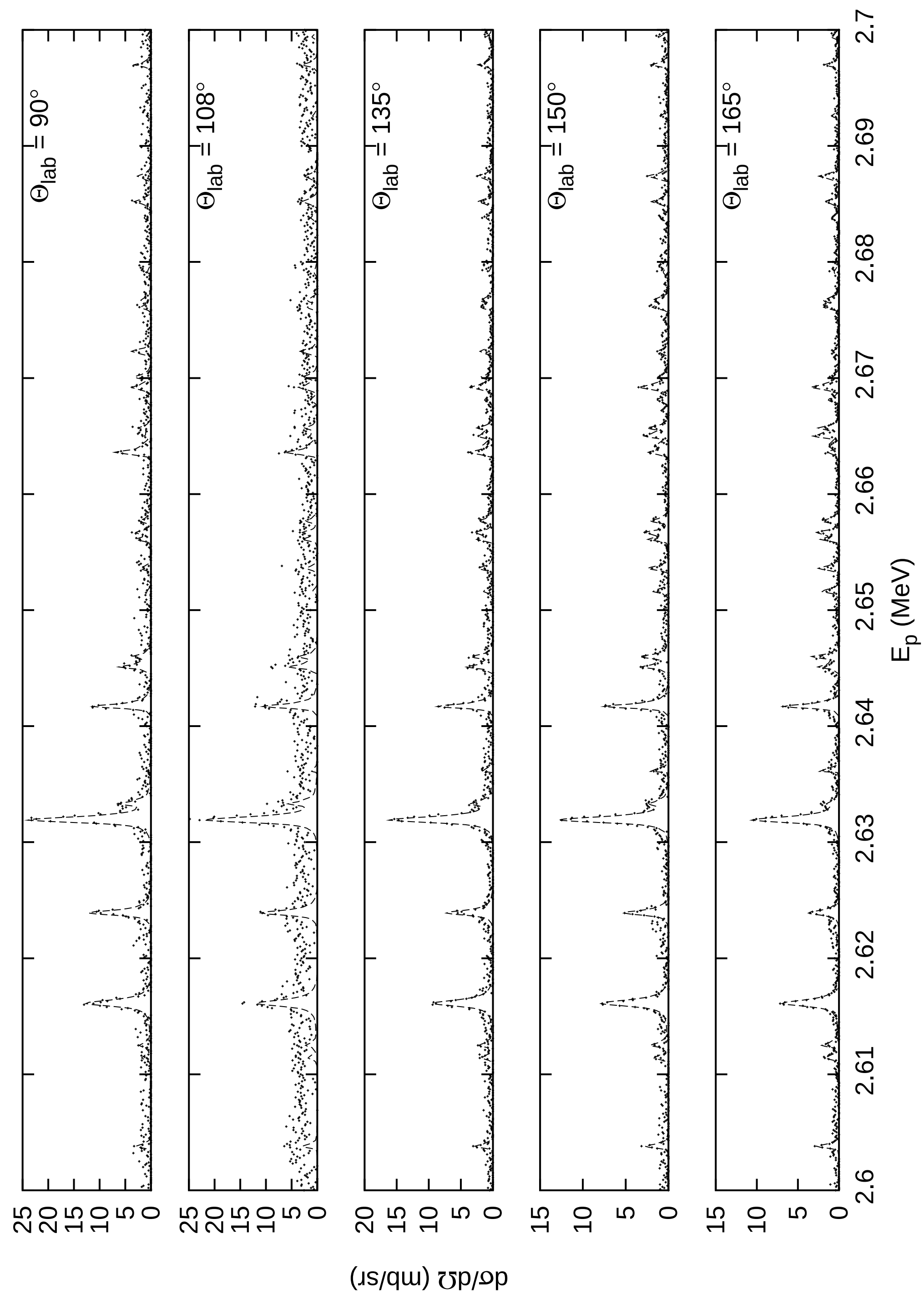

Figure A.13: The ^{44}Ca(p,p$_1$) reaction cross-sections and fits for E$_p$ = 2.6–2.7 MeV.

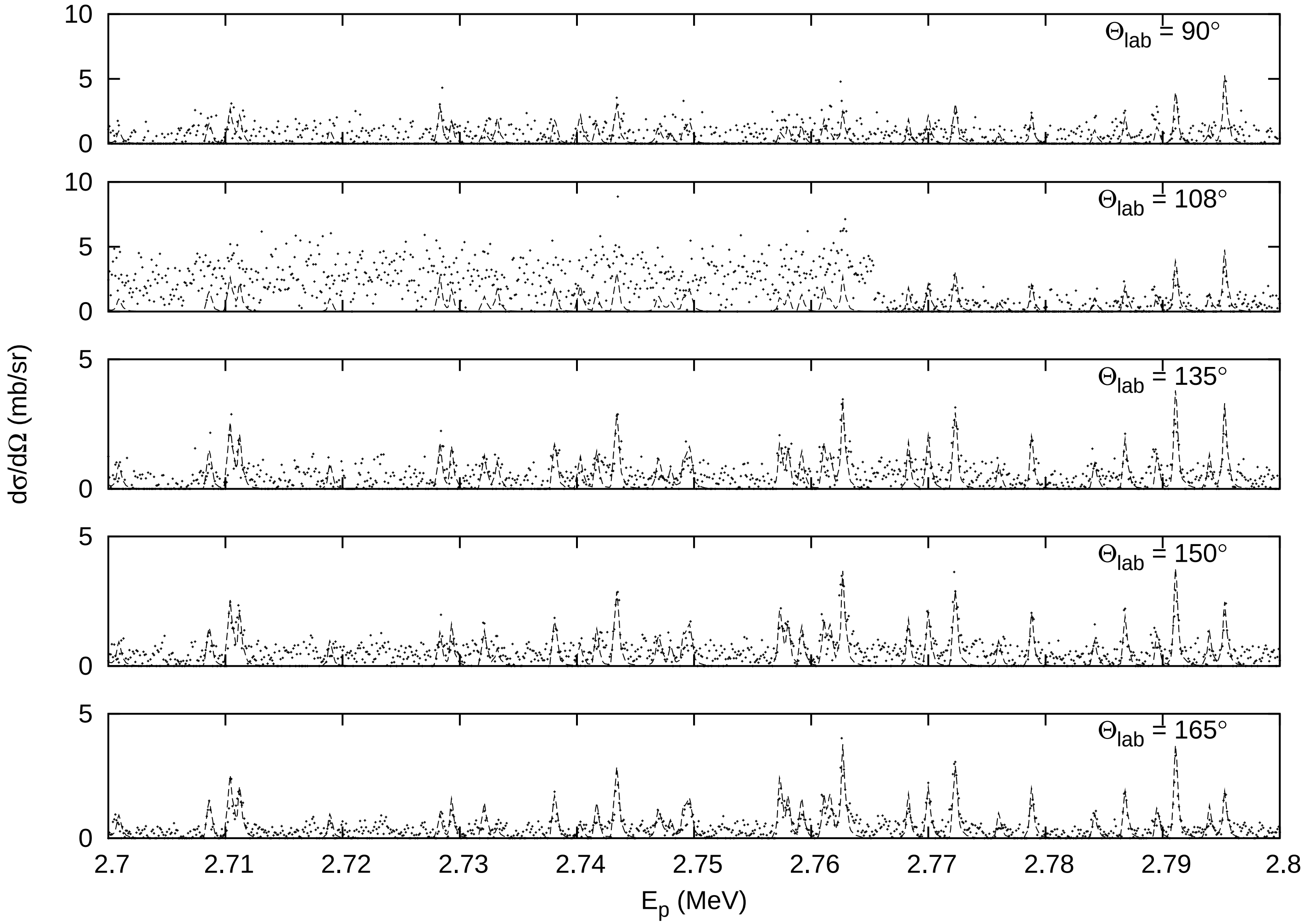

Figure A.14: The ^{44}Ca(p,p$_1$) reaction cross-sections and fits for $E_p = 2.7$–2.8 MeV.

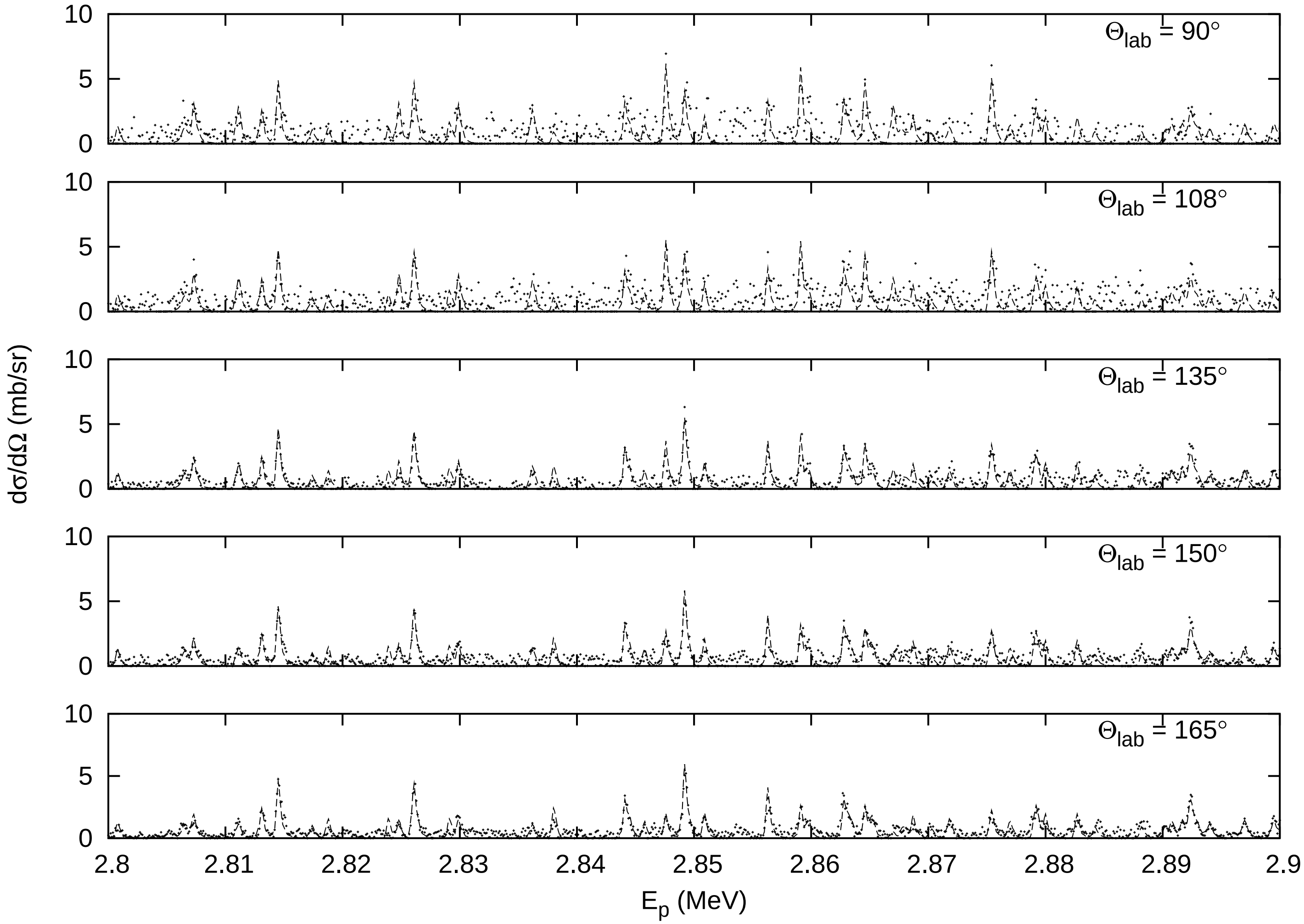

Figure A.15: The ${}^{44}Ca(p,p_1)$ reaction cross-sections and fits for $E_p = 2.8$–2.9 MeV.

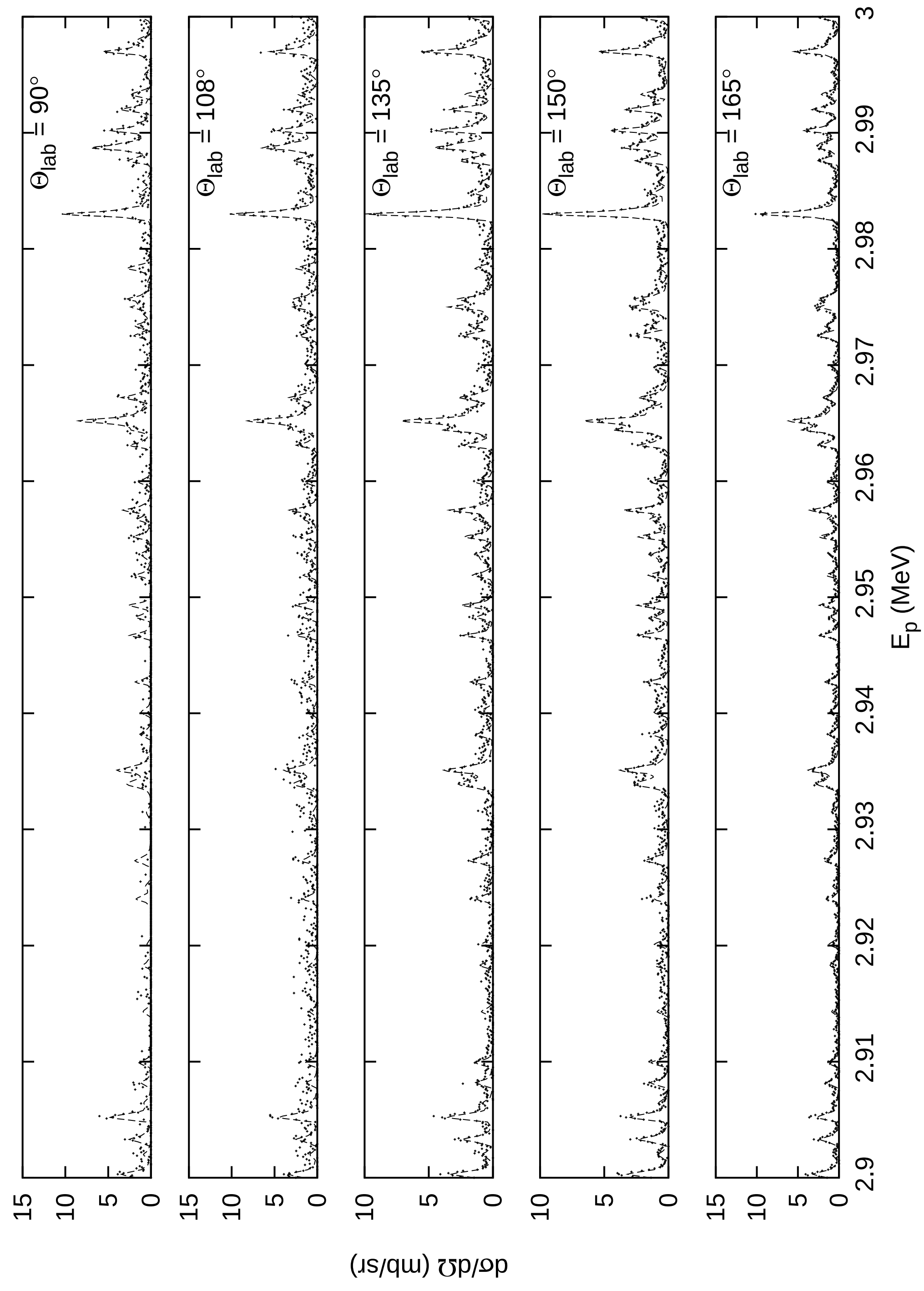

Figure A.16: The ^{44}Ca(p,p$_1$) reaction cross-sections and fits for $E_p = 2.9$–3.0 MeV.

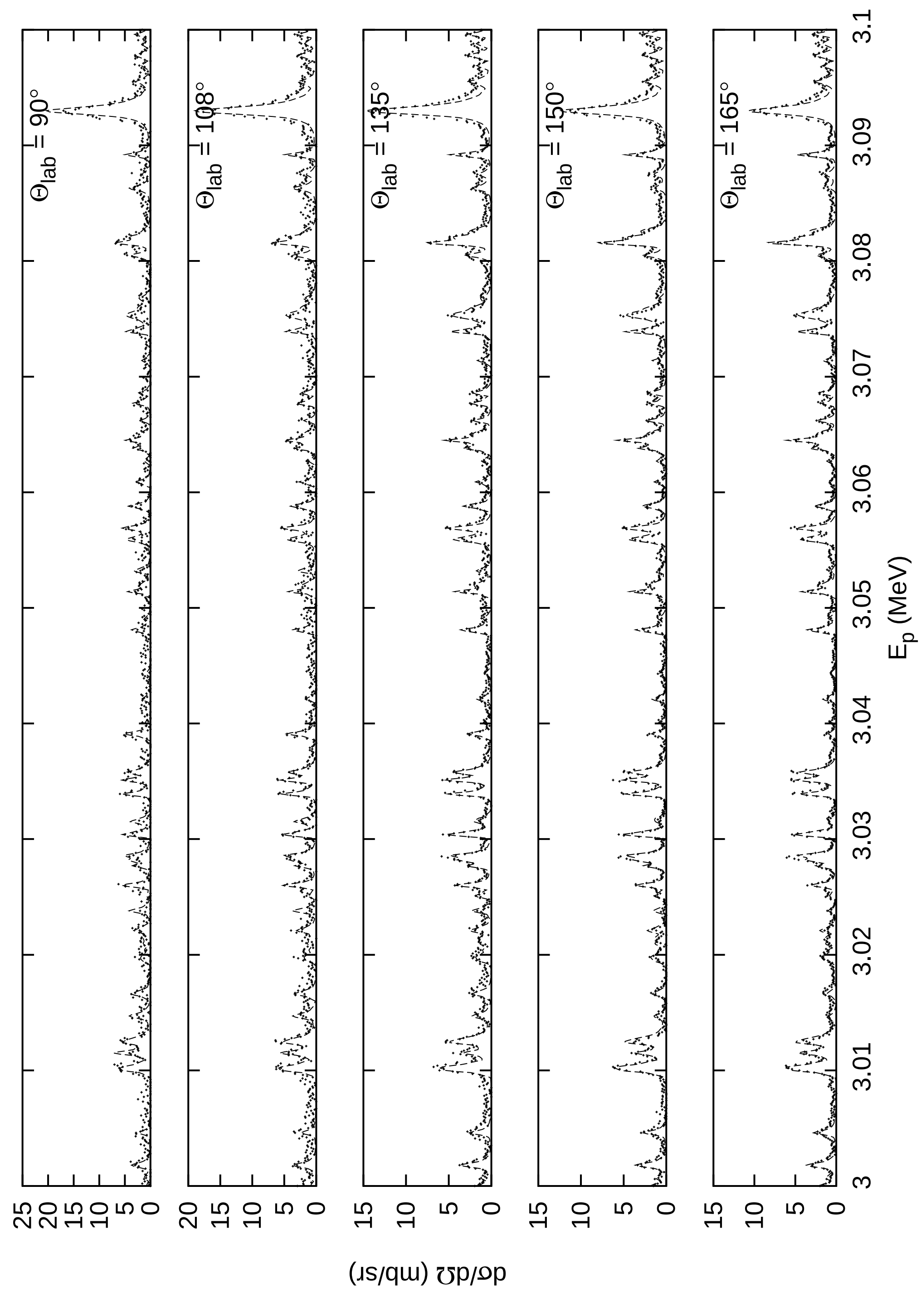

Figure A.17: The ^{44}Ca(p,p$_1$) reaction cross-sections and fits for $E_p = 3.0$–3.1 MeV.

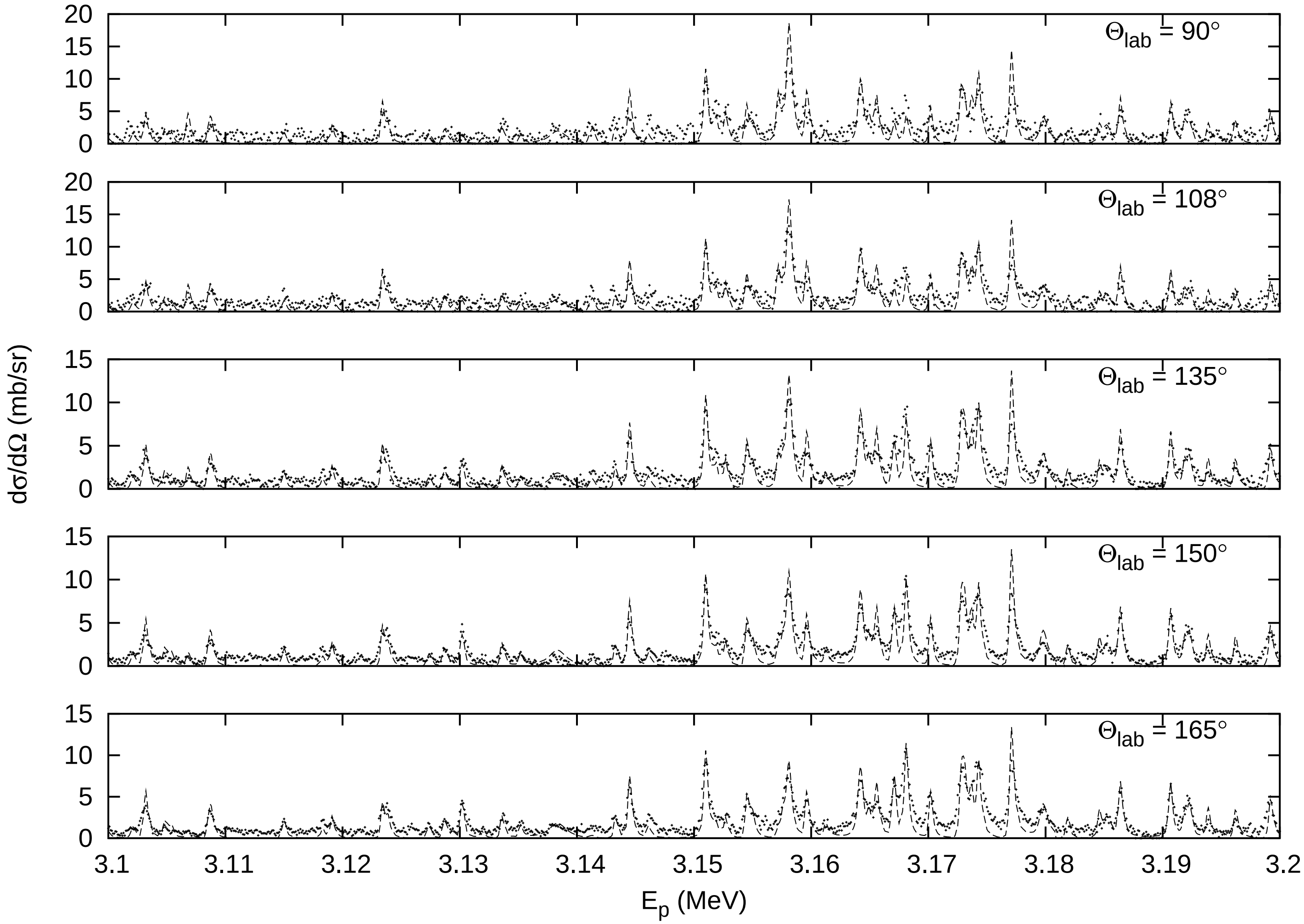

Figure A.18: The ^{44}Ca(p,p$_1$) reaction cross-sections and fits for E_p = 3.1–3.2 MeV.

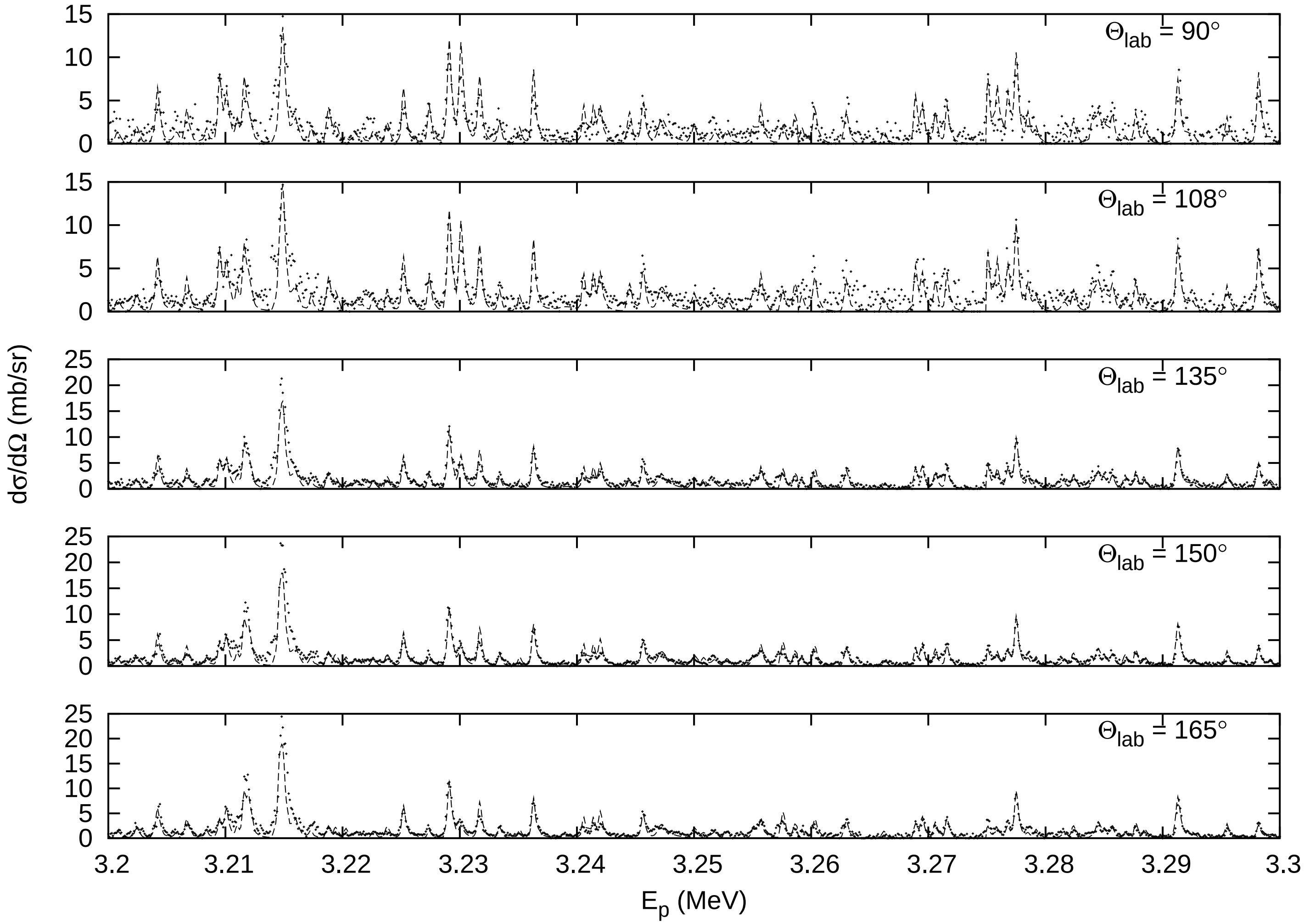

Figure A.19: The ^{44}Ca(p,p$_1$) reaction cross-sections and fits for E_p = 3.2–3.3 MeV.

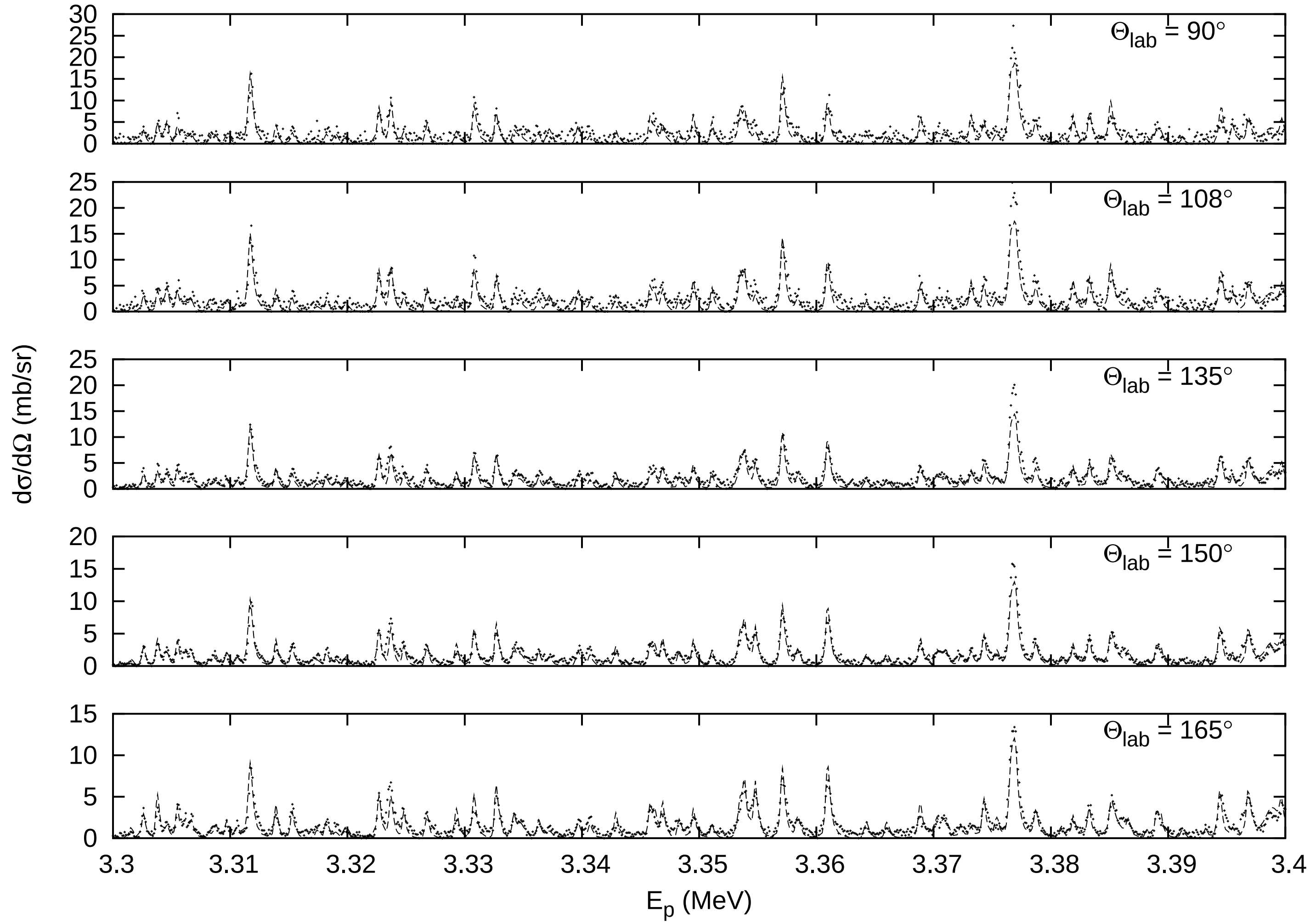

Figure A.20: The ^{44}Ca(p,p$_1$) reaction cross-sections and fits for E_p = 3.3–3.4 MeV.

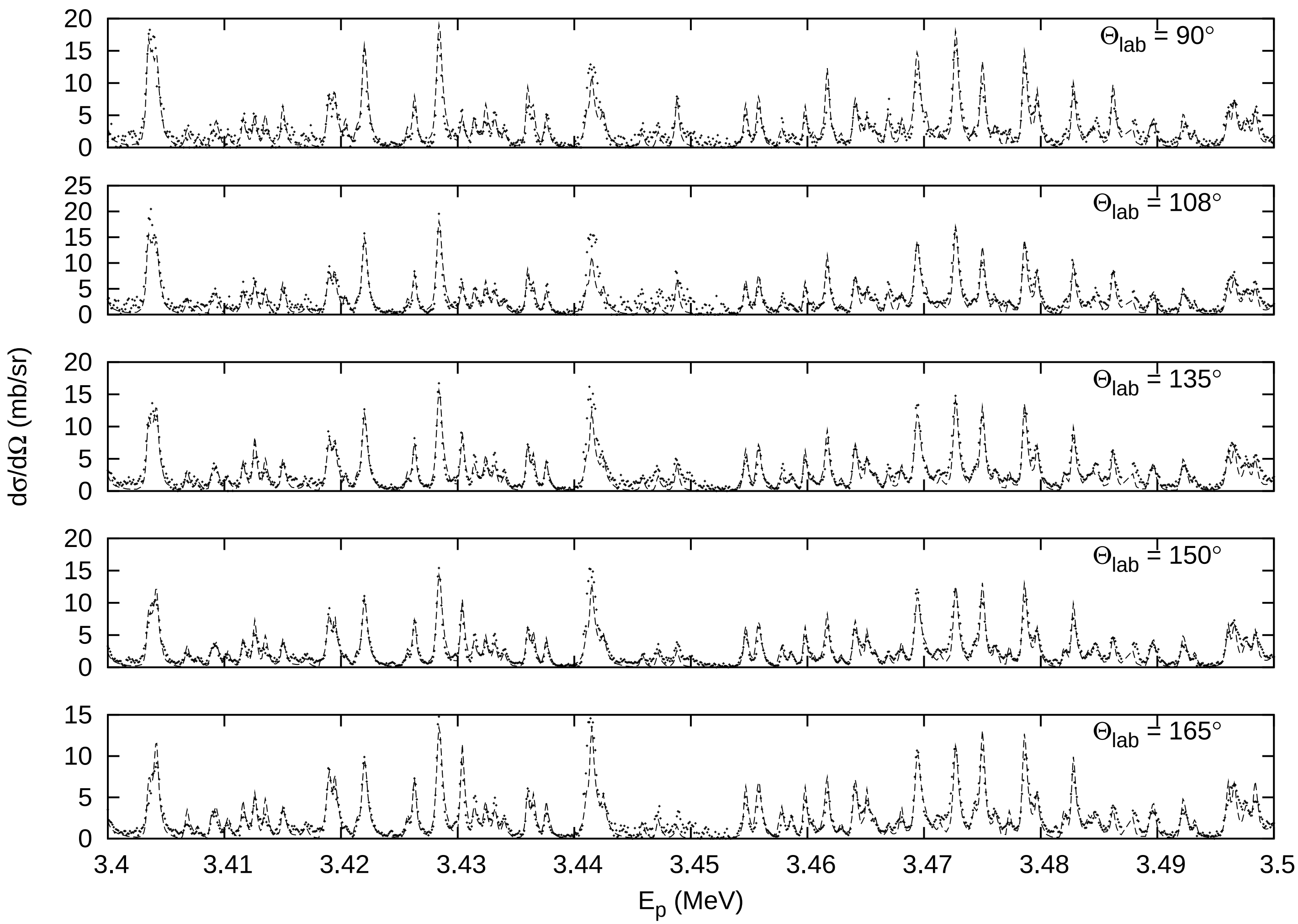

Figure A.21: The ${}^{44}Ca(p,p_1)$ reaction cross-sections and fits for $E_p = 3.4$–3.5 MeV.

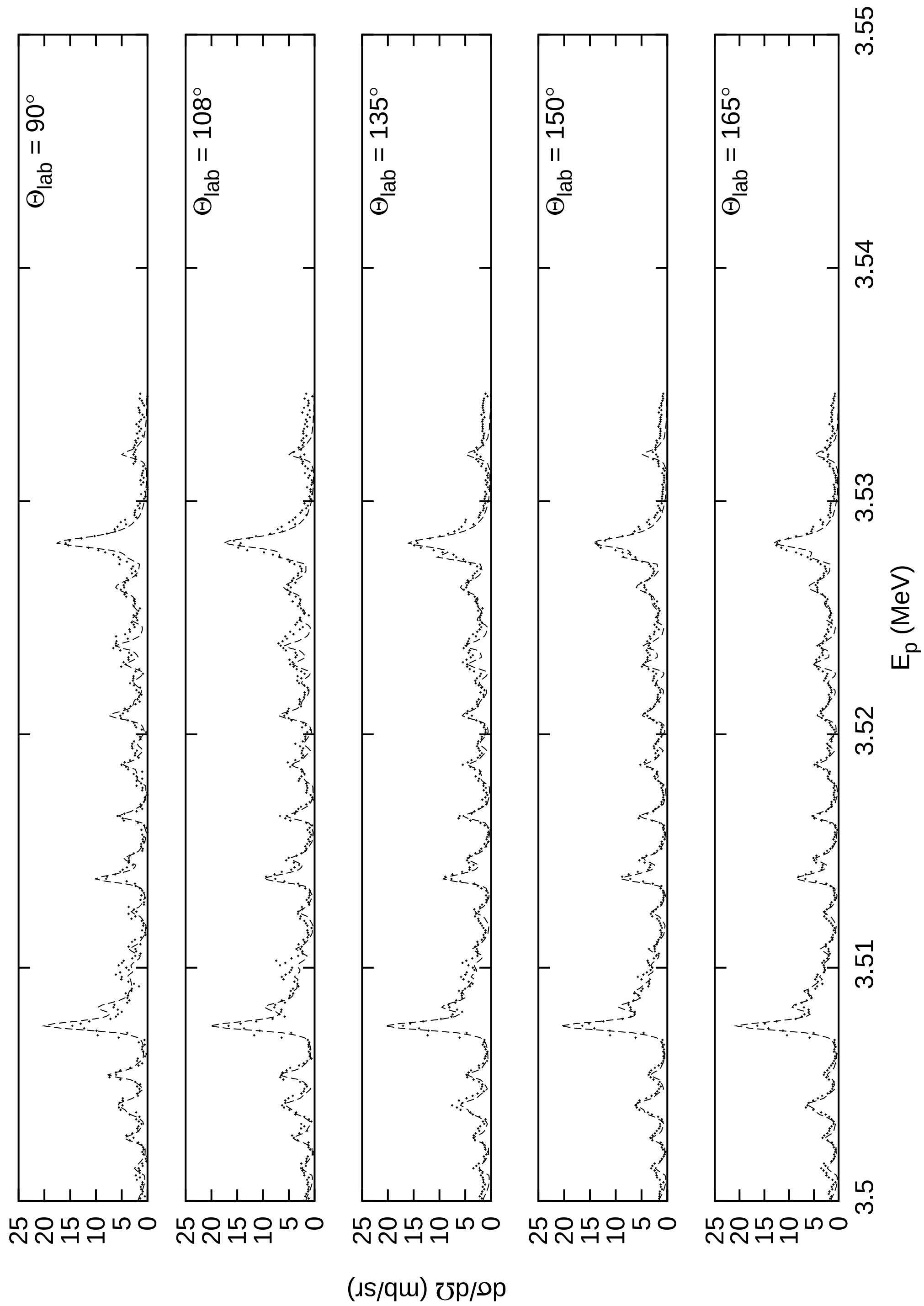

Figure A.22: The ^{44}Ca(p,p$_1$) reaction cross-sections and fits for E_p = 3.50–3.53 MeV.

Appendix B

^{45}Sc Resonance Parameters

This appendix presents the resonance parameters extracted during the analysis of the cross-section data. The resonance parameters are presented in seven tables. Table B.1 lists all the observed resonances in order of E_p. Each resonance in Table B.1 has been numbered to allow easy reference between all tables. In Tables B.2–B.8, the resonances are sorted by J^π and listed in order of E_p.

Table B.1: ^{45}Sc Resonance Parameters

Res. #	E_p (MeV)	J^π	Γ_p (eV)	γ_p^2 (keV)	s'	ℓ'	$\Gamma_{p'}$ (eV)	$\gamma_{p'}^2$ (keV)
1	2.5014	$\frac{3}{2}^+$	4	0.14				
2†	2.5022	$\frac{5}{2}^-$	3	0.65	1.5	1	2	1.14
					2.5	1	2	1.14
3†	2.5037	$\frac{5}{2}^+$	3	0.11	2.5	0	2	0.40
4	2.5045	$\frac{3}{2}^+$	15	0.53				
5	2.5094	$\frac{3}{2}^-$	35	0.27	1.5	1	2	1.09
					2.5	1	3	1.63
6*	2.5104	$\frac{1}{2}^-$	30	0.23				

† Newly observed resonance.

* Resonance with J^π assignment changed from previous work [Wil75, Shr82, Shr83, Smi89].

Table B.1(*continued*)

Res. #	E_p (MeV)	J^π	Γ_p (eV)	γ_p^2 (keV)	s′	ℓ′	$\Gamma_{p'}$ (eV)	$\gamma_{p'}^2$ (keV)
7	2.5141	$\frac{3}{2}^+$	5	0.17	1.5	0	1	0.19
8	2.5161	$\frac{3}{2}^+$	12	0.41	1.5	0	1	0.18
					2.5	2	1	3.69
9	2.5166	$\frac{1}{2}^+$	70	0.25				
10*	2.5186	$\frac{1}{2}^-$	30	0.23				
11*	2.5197	$\frac{3}{2}^+$	20	0.68	1.5	0	2	0.36
12	2.5205	$\frac{1}{2}^-$	70	0.52	1.5	1	5	2.54
13	2.5218	$\frac{1}{2}^+$	200	0.70				
14	2.5233	$\frac{3}{2}^+$	10	0.34				
15	2.5234	$\frac{3}{2}^-$	10	0.07				
16	2.5263	$\frac{3}{2}^+$	17	0.57				
17*	2.5306	$\frac{3}{2}^+$	10	0.33	1.5	0	2	0.34
					2.5	2	2	6.72
18*	2.5315	$\frac{5}{2}^+$	5	0.17	2.5	0	4	0.67
19	2.5329	$\frac{1}{2}^-$	100	0.73	1.5	1	2	0.94
20	2.5349	$\frac{1}{2}^+$	225	0.77				
21*	2.5358	$\frac{3}{2}^-$	10	0.07	1.5	1	2	0.93
					2.5	1	2	0.93
22	2.5470	$\frac{3}{2}^-$	13	0.09				
23†	2.5476	$\frac{5}{2}^+$	10	0.32				
24*	2.5512	$\frac{3}{2}^+$	40	1.27	1.5	0	2	0.30
					2.5	2	2	5.90
25	2.5538	$\frac{1}{2}^+$	80	0.26				
26	2.5559	$\frac{3}{2}^-$	150	1.04				
27*	2.5587	$\frac{1}{2}^-$	15	0.10	1.5	1	5	2.03

† Newly observed resonance.

* Resonance with J^π assignment changed from previous work [Wil75, Shr82, Shr83, Smi89].

Table B.1(*continued*)

Res. #	E_p (MeV)	J^π	Γ_p (eV)	γ_p^2 (keV)	s'	ℓ'	$\Gamma_{p'}$ (eV)	$\gamma_{p'}^2$ (keV)
28	2.5604	$\frac{1}{2}^-$	100	0.69				
29	2.5634	$\frac{1}{2}^+$	30	0.10				
30	2.5646	$\frac{3}{2}^-$	30	0.21				
31	2.5660	$\frac{1}{2}^-$	30	0.21				
32	2.5670	$\frac{3}{2}^+$	15	0.46				
33	2.5676	$\frac{3}{2}^-$	50	0.34	1.5	1	2	0.77
					2.5	1	3	1.15
34	2.5685	$\frac{3}{2}^+$	10	0.30				
35*	2.5711	$\frac{3}{2}^+$	25	0.76				
36*	2.5770	$\frac{5}{2}^-$	4	1.04				
37	2.5789	$\frac{1}{2}^+$	60	0.19				
38*	2.5798	$\frac{5}{2}^+$	10	0.30				
39	2.5830	$\frac{3}{2}^-$	10	0.07				
40	2.5842	$\frac{1}{2}^+$	115	0.36				
41†	2.5848	$\frac{3}{2}^+$	10	0.29	1.5	0	5	0.62
42	2.5878	$\frac{1}{2}^+$	60	0.19				
43	2.5884	$\frac{3}{2}^-$	70	0.46	1.5	1	5	1.71
					2.5	1	2	0.68
44	2.5894	$\frac{3}{2}^-$	10	0.07				
45*	2.5924	$\frac{1}{2}^-$	20	0.13				
46	2.5927	$\frac{3}{2}^-$	55	0.36	1.5	1	5	1.67
47	2.5962	$\frac{1}{2}^+$	150	0.46				
48†	2.5968	$\frac{5}{2}^+$	10	0.29				
49	2.5987	$\frac{3}{2}^-$	30	0.19	1.5	1	5	1.61
					2.5	1	5	1.61

† Newly observed resonance.

* Resonance with J^π assignment changed from previous work [Wil75, Shr82, Shr83, Smi89].

Table B.1(*continued*)

Res. #	E_p (MeV)	J^π	Γ_p (eV)	γ_p^2 (keV)	s′	ℓ′	$\Gamma_{p'}$ (eV)	$\gamma_{p'}^2$ (keV)
50	2.6014	$\frac{1}{2}^-$	55	0.35				
51†	2.6035	$\frac{1}{2}^+$	20	0.06				
52	2.6038	$\frac{5}{2}^+$	35	0.98	2.5	0	4	0.45
53†	2.6043	$\frac{5}{2}^-$	2	0.48				
54†	2.6051	$\frac{5}{2}^-$	2	0.48				
55†	2.6059	$\frac{5}{2}^+$	5	0.14				
56*	2.6114	$\frac{3}{2}^+$	10	0.28	1.5	0	5	0.54
57†	2.6125	$\frac{1}{2}^-$	20	0.13	1.5	1	15	4.48
58	2.6161	$\frac{3}{2}^-$	350	2.17	1.5	1	25	7.32
					2.5	1	20	5.86
59	2.6171	$\frac{1}{2}^-$	400	2.47				
60	2.6209	$\frac{1}{2}^+$	125	0.37				
61	2.6217	$\frac{3}{2}^-$	75	0.46				
62†	2.6227	$\frac{3}{2}^-$	10	0.06				
63	2.6239	$\frac{3}{2}^-$	200	1.22	1.5	1	25	7.02
					2.5	1	5	1.40
64†	2.6252	$\frac{3}{2}^-$	15	0.09				
65	2.6260	$\frac{1}{2}^-$	350	2.12				
66	2.6319	$\frac{3}{2}^-$	250	1.50	1.5	1	60	16.13
					2.5	1	30	8.07
67*	2.6324	$\frac{1}{2}^-$	175	1.05				
68	2.6333	$\frac{3}{2}^-$	30	0.18	1.5	1	10	2.67
69†	2.6335	$\frac{5}{2}^-$	5	1.12				
70	2.6342	$\frac{1}{2}^+$	30	0.09				
71†	2.6361	$\frac{5}{2}^-$	5	1.11	1.5	1	3	0.79

† Newly observed resonance.

* Resonance with J^π assignment changed from previous work [Wil75, Shr82, Shr83, Smi89].

Table B.1(*continued*)

Res. #	E_p (MeV)	J^π	Γ_p (eV)	γ_p^2 (keV)	s'	ℓ'	$\Gamma_{p'}$ (eV)	$\gamma_{p'}^2$ (keV)
72	2.6402	$\frac{3}{2}^-$	30	0.18				
73	2.6408	$\frac{3}{2}^+$	25	0.65				
74	2.6417	$\frac{3}{2}^-$	100	0.59	1.5	1	15	3.83
					2.5	1	15	3.83
75	2.6451	$\frac{3}{2}^-$	40	0.23	1.5	1	10	2.51
					2.5	1	4	1.00
76*	2.6460	$\frac{3}{2}^+$	25	0.64	1.5	0	8	0.72
77*	2.6476	$\frac{3}{2}^-$	150	0.87				
78	2.6492	$\frac{1}{2}^-$	240	1.40				
79	2.6495	$\frac{1}{2}^+$	40	0.11				
80*	2.6516	$\frac{5}{2}^-$	5	1.07	1.5	1	2	0.48
81	2.6530	$\frac{1}{2}^+$	40	0.11				
82	2.6536	$\frac{3}{2}^-$	60	0.35	2.5	1	5	1.20
83*	2.6561	$\frac{3}{2}^-$	35	0.20	1.5	1	2	0.47
					2.5	1	4	0.95
84†	2.6567	$\frac{3}{2}^+$	20	0.50	1.5	0	6	0.51
85	2.6570	$\frac{1}{2}^-$	150	0.86				
86	2.6577	$\frac{3}{2}^+$	25	0.62	1.5	0	5	0.43
87*	2.6603	$\frac{3}{2}^+$	5	0.12				
88†	2.6623	$\frac{3}{2}^+$	8	0.20				
89†	2.6636	$\frac{3}{2}^-$	20	0.11	1.5	1	20	4.55
90†	2.6642	$\frac{5}{2}^+$	20	0.49	2.5	0	2	0.17
91†	2.6650	$\frac{5}{2}^-$	5	1.03	1.5	1	4	0.90
92†	2.6657	$\frac{3}{2}^+$	15	0.37	1.5	0	6	0.49
93	2.6681	$\frac{1}{2}^-$	200	1.12	1.5	1	8	1.78

† Newly observed resonance.

* Resonance with J^π assignment changed from previous work [Wil75, Shr82, Shr83, Smi89].

Table B.1(*continued*)

Res. #	E_p (MeV)	J^π	Γ_p (eV)	γ_p^2 (keV)	s′	ℓ'	$\Gamma_{p'}$ (eV)	$\gamma_{p'}^2$ (keV)
94†	2.6692	$\frac{3}{2}^+$	15	0.36	1.5	0	15	1.21
95*	2.6701	$\frac{3}{2}^-$	75	0.42	1.5	1	5	1.10
96†	2.6723	$\frac{3}{2}^-$	10	0.06	1.5	1	10	2.18
97	2.6757	$\frac{1}{2}^-$	600	3.32				
98	2.6761	$\frac{1}{2}^+$	125	0.34	1.5	2	10	14.20
99†	2.6767	$\frac{3}{2}^+$	10	0.24	1.5	0	5	0.39
100	2.6791	$\frac{1}{2}^+$	400	1.07	1.5	2	5	6.98
101*	2.6800	$\frac{7}{2}^+$	15	42.99				
102*	2.6829	$\frac{5}{2}^-$	5	0.98				
103†	2.6838	$\frac{3}{2}^+$	10	0.24	1.5	0	2	0.15
					2.5	2	1	1.36
104	2.6852	$\frac{3}{2}^-$	30	0.16	1.5	1	4	0.82
					2.5	1	3	0.61
105	2.6860	$\frac{3}{2}^-$	20	0.11				
106†	2.6874	$\frac{5}{2}^+$	10	0.23	2.5	0	5	0.37
107	2.6886	$\frac{1}{2}^+$	30	0.08				
108	2.6910	$\frac{1}{2}^+$	140	0.37				
109†	2.6917	$\frac{5}{2}^-$	2	0.39				
110*	2.6926	$\frac{3}{2}^+$	40	0.92	1.5	0	2	0.14
111*	2.6970	$\frac{3}{2}^-$	10	0.05	1.5	1	6	1.15
					2.5	1	5	0.96
112	2.6994	$\frac{1}{2}^+$	55	0.14	1.5	2	5	6.26
113*	2.7002	$\frac{5}{2}^+$	20	0.45				
114	2.7009	$\frac{1}{2}^-$	150	0.79	1.5	1	5	0.94
115	2.7072	$\frac{3}{2}^-$	30	0.16				

† Newly observed resonance.

* Resonance with J^π assignment changed from previous work [Wil75, Shr82, Shr83, Smi89].

Table B.1(*continued*)

Res. #	E_p (MeV)	J^π	Γ_p (eV)	γ_p^2 (keV)	s′	ℓ′	$\Gamma_{p'}$ (eV)	$\gamma_{p'}^2$ (keV)
116*	2.7086	$\frac{3}{2}^+$	8	0.18	1.5	0	5	0.33
117†	2.7104	$\frac{3}{2}^+$	13	0.29	1.5	0	5	0.66
118†	2.7112	$\frac{3}{2}^+$	6	0.13	1.5	0	10	0.66
119†	2.7125	$\frac{3}{2}^-$	20	0.10				
120	2.7129	$\frac{1}{2}^-$	125	0.65				
121	2.7178	$\frac{1}{2}^+$	120	0.30				
122†	2.7189	$\frac{3}{2}^+$	5	0.11	1.5	0	3	0.19
123*	2.7215	$\frac{1}{2}^-$	15	0.08				
124*	2.7227	$\frac{5}{2}^-$	3	0.53				
125	2.7237	$\frac{1}{2}^+$	15	0.04				
126*	2.7283	$\frac{3}{2}^-$	35	0.18	1.5	1	4	0.66
					2.5	1	1	0.17
127	2.7289	$\frac{1}{2}^-$	190	0.96				
128†	2.7293	$\frac{3}{2}^+$	10	0.21	1.5	0	4	0.24
129*	2.7321	$\frac{3}{2}^-$	20	0.10	2.5	1	3	0.49
130	2.7332	$\frac{3}{2}^-$	45	0.23	1.5	1	3	0.48
131*	2.7358	$\frac{3}{2}^+$	10	0.21				
132	2.7381	$\frac{3}{2}^+$	9	0.19	1.5	0	6	0.35
133*	2.7403	$\frac{3}{2}^+$	22	0.46	2.5	2	4	4.04
134†	2.7417	$\frac{3}{2}^+$	5	0.10	1.5	0	5	0.29
135*	2.7423	$\frac{1}{2}^-$	30	0.15				
136	2.7434	$\frac{3}{2}^+$	15	0.31	1.5	0	10	0.57
137	2.7470	$\frac{1}{2}^-$	275	1.34	1.5	1	8	1.20
138	2.7480	$\frac{1}{2}^+$	5	0.01	1.5	2	5	4.85
139†	2.7491	$\frac{3}{2}^-$	10	0.05	2.5	1	3	0.45

† Newly observed resonance.

* Resonance with J^π assignment changed from previous work [Wil75, Shr82, Shr83, Smi89].

Table B.1(*continued*)

Res. #	E_p (MeV)	J^π	Γ_p (eV)	γ_p^2 (keV)	s′	ℓ′	$\Gamma_{p'}$ (eV)	$\gamma_{p'}^2$ (keV)
140*	2.7496	$\frac{3}{2}^+$	8	0.16	1.5	0	5	0.28
141	2.7509	$\frac{3}{2}^+$	15	0.31				
142†	2.7522	$\frac{3}{2}^-$	12	0.06				
143	2.7543	$\frac{1}{2}^+$	10	0.02				
144	2.7562	$\frac{3}{2}^+$	8	0.16				
145†	2.7573	$\frac{5}{2}^-$	3	0.39	1.5	1	5	0.72
146†	2.7580	$\frac{3}{2}^-$	5	0.02	2.5	1	5	0.71
147†	2.7592	$\frac{3}{2}^-$	5	0.02	2.5	1	5	0.71
148	2.7611	$\frac{1}{2}^-$	30	0.14	1.5	1	10	1.41
149†	2.7616	$\frac{5}{2}^-$	3	0.49	1.5	1	2	0.28
150	2.7627	$\frac{5}{2}^+$	22	0.44	1.5	2	1	0.90
					2.5	0	3	0.16
					2.5	2	1	0.90
151	2.7660	$\frac{1}{2}^-$	450	2.12				
152†	2.7665	$\frac{5}{2}^-$	10	1.60				
153†	2.7683	$\frac{3}{2}^+$	10	0.20	1.5	0	5	0.25
154	2.7687	$\frac{1}{2}^+$	300	0.70				
155	2.7692	$\frac{5}{2}^+$	20	0.39				
156†	2.7695	$\frac{5}{2}^-$	8	1.27				
157†	2.7700	$\frac{3}{2}^+$	35	0.68	1.5	0	5	0.25
158†	2.7723	$\frac{3}{2}^+$	10	0.19	1.5	0	15	0.75
159	2.7727	$\frac{1}{2}^+$	30	0.07				
160	2.7760	$\frac{3}{2}^-$	50	0.23	2.5	1	2	0.26
161*	2.7766	$\frac{3}{2}^+$	20	0.39				
162*	2.7788	$\frac{3}{2}^+$	12	0.23	1.5	0	6	0.29

† Newly observed resonance.

* Resonance with J^π assignment changed from previous work [Wil75, Shr82, Shr83, Smi89].

Table B.1(*continued*)

Res. #	E_p (MeV)	J^π	Γ_p (eV)	γ_p^2 (keV)	s′	ℓ′	$\Gamma_{p'}$ (eV)	$\gamma_{p'}^2$ (keV)
163*	2.7809	$\frac{5}{2}^+$	5	0.10				
164	2.7842	$\frac{1}{2}^-$	45	0.21	1.5	1	5	0.63
165*	2.7868	$\frac{3}{2}^+$	25	0.47	1.5	0	5	0.23
166	2.7892	$\frac{3}{2}^-$	35	0.16				
167*	2.7895	$\frac{3}{2}^+$	5	0.09	1.5	0	5	0.23
168†	2.7911	$\frac{3}{2}^+$	45	0.84	1.5	0	10	0.46
169	2.7916	$\frac{1}{2}^-$	40	0.18				
170	2.7940	$\frac{5}{2}^+$	45	0.84	2.5	0	2	0.09
171	2.7953	$\frac{3}{2}^-$	25	0.11	1.5	1	10	1.20
					2.5	1	3	0.36
172	2.7965	$\frac{3}{2}^-$	30	0.13				
173	2.7983	$\frac{3}{2}^-$	25	0.11				
174	2.7999	$\frac{1}{2}^+$	20	0.05				
175	2.8008	$\frac{5}{2}^+$	45	0.83	2.5	0	2	0.09
176	2.8043	$\frac{1}{2}^+$	500	1.11				
177*	2.8065	$\frac{1}{2}^-$	400	1.76	1.5	1	10	1.15
178	2.8073	$\frac{3}{2}^-$	85	0.37	1.5	1	3	0.34
					2.5	1	3	0.34
179*	2.8082	$\frac{1}{2}^-$	50	0.22				
180	2.8111	$\frac{3}{2}^-$	15	0.07	1.5	1	5	0.56
					2.5	1	2	0.22
181	2.8120	$\frac{1}{2}^+$	100	0.22				
182*	2.8131	$\frac{3}{2}^+$	20	0.36	1.5	0	7	0.29
183*	2.8145	$\frac{3}{2}^+$	20	0.36	1.5	0	20	0.83
184†	2.8174	$\frac{3}{2}^+$	5	0.09	1.5	0	4	0.16

† Newly observed resonance.

* Resonance with J^π assignment changed from previous work [Wil75, Shr82, Shr83, Smi89].

Table B.1(*continued*)

Res. #	E_p (MeV)	J^π	Γ_p (eV)	γ_p^2 (keV)	s′	ℓ′	$\Gamma_{p'}$ (eV)	$\gamma_{p'}^2$ (keV)
185†	2.8188	$\frac{3}{2}^-$	5	0.02	2.5	1	5	0.54
186	2.8212	$\frac{3}{2}^-$	65	0.28				
187	2.8239	$\frac{3}{2}^-$	5	0.02	2.5	1	5	0.53
188†	2.8236	$\frac{5}{2}^-$	3	0.42				
189	2.8248	$\frac{3}{2}^-$	45	0.19	1.5	1	4	0.42
					2.5	1	2	0.21
190†	2.8252	$\frac{3}{2}^+$	10	0.18				
191*	2.8261	$\frac{3}{2}^+$	30	0.52	1.5	0	15	0.59
192	2.8284	$\frac{1}{2}^-$	70	0.30				
193†	2.8291	$\frac{3}{2}^+$	10	0.17	1.5	0	5	0.20
194*	2.8299	$\frac{3}{2}^-$	8	0.03	1.5	1	8	0.83
					2.5	1	5	0.52
195†	2.8310	$\frac{3}{2}^+$	10	0.17				
196	2.8321	$\frac{1}{2}^+$	30	0.06				
197	2.8329	$\frac{3}{2}^+$	25	0.43				
198	2.8347	$\frac{3}{2}^-$	10	0.04				
199†	2.8362	$\frac{5}{2}^-$	5	0.68	1.5	1	2	0.20
					2.5	1	6	0.20
200*	2.8377	$\frac{3}{2}^-$	15	0.06				
201†	2.8380	$\frac{5}{2}^-$	3	0.40	1.5	1	5	0.50
202	2.8425	$\frac{1}{2}^-$	175	0.73				
203†	2.8441	$\frac{3}{2}^+$	10	0.17	1.5	0	15	0.55
204	2.8445	$\frac{3}{2}^-$	120	0.50	2.5	1	3	0.29
205†	2.8458	$\frac{3}{2}^+$	5	0.08	1.5	0	5	0.18

† Newly observed resonance.

* Resonance with J^π assignment changed from previous work [Wil75, Shr82, Shr83, Smi89].

Table B.1(*continued*)

Res. #	E_p (MeV)	J^π	Γ_p (eV)	γ_p^2 (keV)	s′	ℓ′	$\Gamma_{p'}$ (eV)	$\gamma_{p'}^2$ (keV)
206	2.8476	$\frac{3}{2}^-$	30	0.12	1.5	1	12	1.15
					2.5	1	3	0.29
207	2.8492	$\frac{5}{2}^+$	45	0.75	1.5	2	2	1.19
					2.5	0	5	0.18
					2.5	2	2	1.19
208	2.8509	$\frac{3}{2}^+$	20	0.33	1.5	0	5	0.18
209	2.8515	$\frac{1}{2}^+$	550	1.14				
210†	2.8528	$\frac{3}{2}^-$	10	0.04				
211	2.8543	$\frac{3}{2}^-$	15	0.06				
212	2.8563	$\frac{3}{2}^+$	15	0.25	1.5	0	10	0.35
					1.5	2	2	1.15
					2.5	2	2	1.15
213†	2.8571	$\frac{5}{2}^+$	5	0.08				
214*	2.8591	$\frac{3}{2}^-$	30	0.12	1.5	1	10	0.91
					2.5	1	5	0.46
215*	2.8598	$\frac{1}{2}^-$	10	0.04	1.5	1	10	0.91
216*	2.8628	$\frac{3}{2}^+$	15	0.24	1.5	0	15	0.51
217*	2.8629	$\frac{5}{2}^-$	5	0.64				
218	2.8634	$\frac{3}{2}^-$	5	0.02	2.5	1	5	0.45
219	2.8646	$\frac{3}{2}^-$	15	0.06	1.5	1	10	0.89
					2.5	1	8	0.71
220†	2.8652	$\frac{5}{2}^-$	3	0.38	1.5	1	2	0.18
221	2.8670	$\frac{3}{2}^-$	30	0.12	1.5	1	5	0.44
222	2.8677	$\frac{1}{2}^+$	180	0.37	1.5	2	5	2.72
223	2.8683	$\frac{1}{2}^-$	350	1.39	1.5	1	5	0.44

† Newly observed resonance.

* Resonance with J^π assignment changed from previous work [Wil75, Shr82, Shr83, Smi89].

Table B.1(*continued*)

Res. #	E_p (MeV)	J^π	Γ_p (eV)	γ_p^2 (keV)	s′	ℓ′	$\Gamma_{p'}$ (eV)	$\gamma_{p'}^2$ (keV)
224†	2.8687	$\frac{3}{2}^+$	10	0.16	1.5	0	5	0.17
225	2.8703	$\frac{1}{2}^-$	10	0.04	1.5	1	5	0.44
226*	2.8718	$\frac{3}{2}^-$	8	0.03	2.5	1	5	0.43
227	2.8736	$\frac{1}{2}^+$	350	0.70				
228	2.8745	$\frac{5}{2}^+$	10	0.16				
229†	2.8754	$\frac{3}{2}^-$	20	0.08	1.5	1	10	0.85
					2.5	1	5	0.43
230*	2.8770	$\frac{3}{2}^+$	10	0.16	1.5	0	4	0.13
231	2.8792	$\frac{3}{2}^+$	15	0.24	1.5	0	10	0.32
232	2.8800	$\frac{1}{2}^-$	45	0.18	1.5	1	10	0.84
233*	2.8827	$\frac{3}{2}^+$	30	0.47	1.5	0	5	0.16
234*	2.8842	$\frac{1}{2}^-$	160	0.62	1.5	1	5	0.41
235†	2.8862	$\frac{5}{2}^-$	3	0.36				
236	2.8882	$\frac{1}{2}^-$	115	0.44	1.5	1	5	0.40
237	2.8897	$\frac{1}{2}^+$	250	0.49				
238†	2.8902	$\frac{3}{2}^+$	10	0.15	1.5	0	3	0.09
239*	2.8905	$\frac{5}{2}^+$	25	0.38				
240†	2.8908	$\frac{5}{2}^-$	5	0.60	1.5	1	2	0.16
					2.5	1	2	0.16
241	2.8917	$\frac{3}{2}^+$	10	0.15	1.5	0	5	0.15
242	2.8919	$\frac{1}{2}^+$	90	0.18				
243	2.8924	$\frac{3}{2}^-$	70	0.27	2.5	1	8	0.64
244†	2.8929	$\frac{3}{2}^+$	5	0.08	1.5	0	3	0.09
245†	2.8940	$\frac{3}{2}^+$	5	0.08	1.5	0	5	0.15
246*	2.8970	$\frac{3}{2}^+$	22	0.33	1.5	0	5	0.15

† Newly observed resonance.

* Resonance with J^π assignment changed from previous work [Wil75, Shr82, Shr83, Smi89].

Table B.1(*continued*)

Res. #	E_p (MeV)	J^π	Γ_p (eV)	γ_p^2 (keV)	s′	ℓ′	$\Gamma_{p'}$ (eV)	$\gamma_{p'}^2$ (keV)
247†	2.8989	$\frac{5}{2}^+$	5	0.08				
248	2.8995	$\frac{1}{2}^-$	60	0.23	1.5	1	10	0.77
249*	2.9003	$\frac{3}{2}^+$	15	0.23	1.5	0	20	0.59
250	2.9020	$\frac{1}{2}^+$	60	0.12	1.5	2	5	2.34
251*	2.9033	$\frac{3}{2}^+$	15	0.23	1.5	0	12	0.35
252	2.9051	$\frac{3}{2}^+$	10	0.15				
253†	2.9052	$\frac{5}{2}^-$	15	1.73	1.5	1	5	0.38
					2.5	1	10	0.75
254	2.9064	$\frac{1}{2}^-$	10	0.04	1.5	1	5	0.38
255†	2.9082	$\frac{3}{2}^-$	5	0.02	2.5	1	10	0.74
256*	2.9084	$\frac{1}{2}^-$	40	0.15				
257†	2.9099	$\frac{3}{2}^+$	5	0.07	1.5	0	10	0.28
258	2.9104	$\frac{3}{2}^-$	45	0.17				
259†	2.9143	$\frac{3}{2}^+$	4	0.06	1.5	0	5	0.14
260	2.9183	$\frac{3}{2}^-$	30	0.11	2.5	1	3	0.21
261†	2.9201	$\frac{5}{2}^-$	2	0.22	1.5	1	2	0.14
262†	2.9240	$\frac{3}{2}^+$	5	0.07	1.5	0	10	0.27
					2.5	2	10	4.24
263*	2.9251	$\frac{3}{2}^-$	5	0.02	2.5	1	2	0.14
264†	2.9273	$\frac{1}{2}^-$	40	0.15	1.5	1	15	1.03
265	2.9315	$\frac{1}{2}^+$	450	0.84	1.5	2	5	2.05
266†	2.9321	$\frac{5}{2}^+$	10	0.14				
267	2.9339	$\frac{1}{2}^+$	400	0.74	1.5	2	30	12.19
268†	2.9351	$\frac{5}{2}^+$	50	0.71	2.5	0	8	0.21
269*	2.9382	$\frac{3}{2}^+$	10	0.14	1.5	0	5	0.13

† Newly observed resonance.

* Resonance with J^π assignment changed from previous work [Wil75, Shr82, Shr83, Smi89].

Table B.1(*continued*)

Res. #	E_p (MeV)	J^π	Γ_p (eV)	γ_p^2 (keV)	s′	ℓ′	$\Gamma_{p'}$ (eV)	$\gamma_{p'}^2$ (keV)
270*	2.9401	$\frac{3}{2}^+$	7	0.10	1.5	0	5	0.13
271	2.9412	$\frac{1}{2}^+$	15	0.03				
272	2.9427	$\frac{1}{2}^-$	75	0.27	1.5	1	10	0.65
273*	2.9467	$\frac{1}{2}^-$	50	0.18	1.5	1	15	0.96
274*	2.9483	$\frac{3}{2}^+$	20	0.28	1.5	0	2	0.05
					2.5	2	2	0.76
275†	2.9493	$\frac{3}{2}^+$	10	0.14	1.5	0	10	0.25
276	2.9498	$\frac{1}{2}^+$	150	0.27				
277*	2.9519	$\frac{1}{2}^-$	70	0.25	1.5	1	10	0.63
278	2.9531	$\frac{5}{2}^+$	12	0.16	1.5	2	1	0.37
279*	2.9537	$\frac{1}{2}^+$	8	0.01	1.5	2	20	7.47
280†	2.9552	$\frac{3}{2}^-$	10	0.04	2.5	1	10	0.62
281	2.9567	$\frac{1}{2}^-$	150	0.52	1.5	1	10	0.62
282	2.9575	$\frac{3}{2}^-$	30	0.10	1.5	1	1	0.06
					2.5	1	10	0.61
283*	2.9593	$\frac{1}{2}^+$	10	0.02				
284†	2.9599	$\frac{3}{2}^+$	5	0.97	1.5	2	10	3.64
285	2.9631	$\frac{3}{2}^+$	25	0.34	1.5	0	8	0.19
286*	2.9644	$\frac{5}{2}^-$	8	0.81	1.5	1	8	0.48
287	2.9648	$\frac{1}{2}^+$	200	0.36	1.5	2	12	4.28
288	2.9652	$\frac{3}{2}^-$	125	0.43	1.5	1	10	0.60
					2.5	1	15	0.89
289†	2.9662	$\frac{5}{2}^+$	5	0.07	1.5	2	3	1.06
290*	2.9672	$\frac{3}{2}^-$	10	0.03	1.5	1	15	0.89
					2.5	1	15	0.89

† Newly observed resonance.

* Resonance with J^π assignment changed from previous work [Wil75, Shr82, Shr83, Smi89].

Table B.1(*continued*)

Res. #	E_p (MeV)	J^π	Γ_p (eV)	γ_p^2 (keV)	s′	ℓ′	$\Gamma_{p'}$ (eV)	$\gamma_{p'}^2$ (keV)
291	2.9698	$\frac{3}{2}^+$	13	0.17	1.5	0	2	0.05
292*	2.9725	$\frac{5}{2}^-$	5	0.50	1.5	1	10	0.58
					2.5	1	5	0.29
293*	2.9734	$\frac{5}{2}^+$	5	0.07	2.5	0	5	0.11
294	2.9744	$\frac{1}{2}^+$	200	0.35	1.5	2	5	1.71
295	2.9750	$\frac{5}{2}^+$	10	0.13	1.5	2	3	1.02
					2.5	0	4	0.09
296	2.9757	$\frac{1}{2}^-$	40	0.14	1.5	1	20	1.14
297	2.9771	$\frac{1}{2}^-$	50	0.17	1.5	1	2	0.11
298*	2.9783	$\frac{5}{2}^-$	8	0.79	2.5	1	5	0.28
299	2.9830	$\frac{5}{2}^+$	50	0.65	2.5	0	30	0.65
300*	2.9848	$\frac{3}{2}^+$	7	0.09	1.5	0	5	0.11
301	2.9858	$\frac{1}{2}^-$	50	0.17	1.5	1	5	0.28
302	2.9876	$\frac{5}{2}^+$	12	0.15	2.5	0	7	0.15
303*	2.9887	$\frac{3}{2}^-$	40	0.13	1.5	1	15	0.82
					2.5	1	5	0.27
304*	2.9891	$\frac{1}{2}^-$	100	0.33	1.5	1	10	0.54
305	2.9902	$\frac{5}{2}^+$	10	0.13	2.5	0	25	0.53
306	2.9908	$\frac{1}{2}^+$	100	0.17	1.5	2	5	1.60
307*	2.9920	$\frac{3}{2}^+$	20	0.25	1.5	0	15	0.32
308	2.9933	$\frac{5}{2}^+$	12	0.15	2.5	0	5	0.20
309	2.9950	$\frac{1}{2}^+$	220	0.38	1.5	2	5	1.57
310	2.9970	$\frac{3}{2}^+$	20	0.25	1.5	0	70	1.45
311	2.9979	$\frac{3}{2}^+$	10	0.13	1.5	0	5	0.10
312*	2.9999	$\frac{5}{2}^-$	4	0.38	1.5	1	5	0.26

† Newly observed resonance.

* Resonance with J^π assignment changed from previous work [Wil75, Shr82, Shr83, Smi89].

Table B.1(*continued*)

Res. #	E_p (MeV)	J^π	Γ_p (eV)	γ_p^2 (keV)	s′	ℓ′	$\Gamma_{p'}$ (eV)	$\gamma_{p'}^2$ (keV)
313	3.0007	$\frac{5}{2}^+$	15	0.19	2.5	0	2	0.04
314	3.0018	$\frac{1}{2}^-$	30	0.10	1.5	1	100	5.19
315†	3.0041	$\frac{3}{2}^+$	10	0.12				
316	3.0042	$\frac{1}{2}^-$	1400	4.54	1.5	1	5	0.26
317	3.0046	$\frac{3}{2}^-$	15	0.05	2.5	1	8	0.41
318	3.0085	$\frac{1}{2}^+$	15	0.03				
319	3.0100	$\frac{5}{2}^+$	15	0.19	2.5	0	15	0.30
320	3.0103	$\frac{3}{2}^-$	40	0.13	2.5	1	15	0.75
321	3.0115	$\frac{5}{2}^+$	70	0.86	2.5	2	10	2.94
322*	3.0124	$\frac{5}{2}^+$	10	0.12	2.5	0	15	0.30
323†	3.0126	$\frac{5}{2}^-$	10	0.91				
324	3.0127	$\frac{1}{2}^-$	250	0.80	1.5	1	20	1.00
325	3.0147	$\frac{3}{2}^-$	175	0.56	1.5	1	10	0.50
326	3.0166	$\frac{3}{2}^-$	20	0.06	1.5	1	10	0.49
					2.5	1	2	0.10
327	3.0195	$\frac{1}{2}^-$	140	0.44	1.5	1	10	0.49
328†	3.0198	$\frac{3}{2}^+$	5	0.06	1.5	0	5	0.10
329	3.0204	$\frac{3}{2}^-$	50	0.16	1.5	1	1	0.05
					2.5	1	1	0.05
330†	3.0210	$\frac{1}{2}^+$	20	0.03	1.5	2	8	2.27
331*	3.0215	$\frac{5}{2}^+$	5	0.06	2.5	0	2	0.04
332	3.0221	$\frac{3}{2}^-$	10	0.03	1.5	1	10	0.48
					2.5	1	10	0.48
333*	3.0238	$\frac{3}{2}^+$	30	0.36	2.5	2	10	2.80
334	3.0251	$\frac{5}{2}^+$	20	0.24	1.5	2	2	0.56

† Newly observed resonance.

* Resonance with J^π assignment changed from previous work [Wil75, Shr82, Shr83, Smi89].

Table B.1(*continued*)

Res. #	E_p (MeV)	J^π	Γ_p (eV)	γ_p^2 (keV)	s′	ℓ′	$\Gamma_{p'}$ (eV)	$\gamma_{p'}^2$ (keV)
335*	3.0260	$\frac{3}{2}^+$	40	0.48	1.5	0	7	0.13
					2.5	2	7	1.95
336	3.0266	$\frac{1}{2}^+$	55	0.09				
337*	3.0277	$\frac{3}{2}^-$	50	0.16	1.5	1	3	0.14
					2.5	1	5	0.24
338	3.0282	$\frac{5}{2}^+$	25	0.30	2.5	0	6	0.11
339*	3.0286	$\frac{3}{2}^+$	70	0.83	1.5	0	12	0.22
340	3.0304	$\frac{5}{2}^+$	20	0.24	2.5	0	15	0.28
341*	3.0315	$\frac{5}{2}^-$	10	0.88	2.5	1	5	0.23
342	3.0318	$\frac{1}{2}^+$	40	0.07	1.5	2	5	1.36
343*	3.0339	$\frac{5}{2}^-$	10	0.87	1.5	1	20	0.92
					2.5	1	20	0.92
344	3.0351	$\frac{1}{2}^+$	50	0.08	1.5	2	60	16.08
345*	3.0358	$\frac{5}{2}^+$	10	0.12	2.5	0	10	0.18
346	3.0362	$\frac{1}{2}^-$	230	0.71	1.5	1	5	0.23
347	3.0391	$\frac{3}{2}^-$	12	0.04	1.5	1	30	1.36
348	3.0401	$\frac{1}{2}^-$	20	0.06	1.5	1	5	0.23
349	3.0421	$\frac{3}{2}^+$	5	0.06	1.5	0	20	0.36
350†	3.0436	$\frac{3}{2}^+$	10	0.12				
351†	3.0443	$\frac{1}{2}^+$	5	0.01	1.5	2	20	5.17
352	3.0481	$\frac{5}{2}^+$	18	0.21	2.5	0	8	0.14
353	3.0491	$\frac{1}{2}^+$	100	0.16	1.5	2	5	1.27
354	3.0507	$\frac{1}{2}^-$	20	0.06				
355	3.0514	$\frac{5}{2}^+$	17	0.20	2.5	0	10	0.17
356†	3.0520	$\frac{3}{2}^+$	5	0.06	1.5	0	20	0.34

† Newly observed resonance.

* Resonance with J^π assignment changed from previous work [Wil75, Shr82, Shr83, Smi89].

Table B.1(*continued*)

Res. #	E_p (MeV)	J^π	Γ_p (eV)	γ_p^2 (keV)	s′	ℓ'	$\Gamma_{p'}$ (eV)	$\gamma_{p'}^2$ (keV)
357*	3.0532	$\frac{3}{2}^-$	10	0.03	1.5	1	10	0.43
358	3.0559	$\frac{1}{2}^+$	275	0.44	1.5	2	20	4.94
					2.5	2	20	4.94
359*	3.0569	$\frac{1}{2}^-$	50	0.15	1.5	1	50	2.13
360	3.0573	$\frac{5}{2}^+$	30	0.34				
361	3.0588	$\frac{3}{2}^-$	15	0.05	1.5	1	10	0.42
					2.5	1	10	0.42
362†	3.0589	$\frac{5}{2}^-$	4	0.33				
363*	3.0609	$\frac{5}{2}^-$	4	0.33	1.5	1	5	0.21
					2.5	1	20	0.84
364	3.0627	$\frac{5}{2}^+$	3	0.03	2.5	0	3	0.05
365	3.0638	$\frac{3}{2}^+$	35	0.39	1.5	0	10	0.17
366	3.0645	$\frac{3}{2}^-$	27	0.08	2.5	1	20	0.83
367†	3.0651	$\frac{3}{2}^-$	5	0.02	2.5	1	10	0.41
368	3.0660	$\frac{1}{2}^+$	250	0.39				
369†	3.0662	$\frac{3}{2}^-$	5	0.02	2.5	1	30	1.24
370†	3.0677	$\frac{3}{2}^-$	10	0.03	1.5	1	10	0.41
					2.5	1	7	0.29
371*	3.0686	$\frac{3}{2}^+$	8	0.09	1.5	0	10	0.16
372	3.0714	$\frac{1}{2}^+$	40	0.06	1.5	2	10	2.33
373	3.0739	$\frac{5}{2}^+$	25	0.28	2.5	0	10	0.16
374	3.0753	$\frac{1}{2}^+$	550	0.86	1.5	2	30	6.88
					2.5	2	30	6.88
375	3.0760	$\frac{3}{2}^+$	35	0.38	1.5	0	2	0.03
376*	3.0768	$\frac{5}{2}^-$	5	0.40	2.5	1	2	0.08

† Newly observed resonance.

* Resonance with J^π assignment changed from previous work [Wil75, Shr82, Shr83, Smi89].

Table B.1(*continued*)

Res. #	E_p (MeV)	J^π	Γ_p (eV)	γ_p^2 (keV)	s′	ℓ′	$\Gamma_{p'}$ (eV)	$\gamma_{p'}^2$ (keV)
377	3.0805	$\frac{3}{2}^-$	150	0.44	1.5	1	5	0.20
					2.5	1	5	0.20
378	3.0816	$\frac{3}{2}^-$	105	0.31	2.5	1	25	0.98
379†	3.0821	$\frac{3}{2}^+$	10	0.11	1.5	0	20	0.31
380*	3.0826	$\frac{5}{2}^-$	10	0.79	1.5	1	3	0.12
381	3.0839	$\frac{1}{2}^+$	25	0.04				
382	3.0863	$\frac{3}{2}^-$	225	0.65	1.5	1	10	0.39
383	3.0875	$\frac{1}{2}^-$	225	0.65	1.5	1	10	0.38
384*	3.0883	$\frac{5}{2}^+$	15	0.16				
385	3.0892	$\frac{5}{2}^+$	30	0.32	2.5	0	10	0.15
386*	3.0927	$\frac{5}{2}^+$	5	0.05				
387	3.0930	$\frac{3}{2}^-$	450	1.29	1.5	1	70	2.63
					2.5	1	50	1.88
388	3.0944	$\frac{1}{2}^-$	30	0.09				
389†	3.0955	$\frac{5}{2}^-$	5	0.38	1.5	1	10	0.37
					2.5	1	10	0.37
390	3.0969	$\frac{1}{2}^-$	25	0.07	1.5	1	10	0.37
391*	3.0978	$\frac{3}{2}^+$	10	0.11	1.5	0	20	0.30
392†	3.0988	$\frac{3}{2}^+$	5	0.05	1.5	0	20	0.30
393	3.0996	$\frac{5}{2}^+$	45	0.47	2.5	0	5	0.07
394	3.1007	$\frac{1}{2}^-$	150	0.42				
395	3.1021	$\frac{1}{2}^+$	200	0.30	1.5	2	10	2.07
396	3.1032	$\frac{3}{2}^-$	20	0.06	2.5	1	30	1.09
397†	3.1048	$\frac{5}{2}^+$	5	0.05	2.5	0	10	0.15
398	3.1054	$\frac{1}{2}^-$	20	0.06	1.5	1	10	0.36

† Newly observed resonance.

* Resonance with J^π assignment changed from previous work [Wil75, Shr82, Shr83, Smi89].

Table B.1(*continued*)

Res. #	E_p (MeV)	J^π	Γ_p (eV)	γ_p^2 (keV)	s′	ℓ'	$\Gamma_{p'}$ (eV)	$\gamma_{p'}^2$ (keV)
399	3.1058	$\frac{3}{2}^+$	12	0.13				
400	3.1068	$\frac{3}{2}^-$	125	0.35	1.5	1	10	0.36
401*	3.1086	$\frac{5}{2}^+$	5	0.05	2.5	0	10	0.14
402	3.1088	$\frac{3}{2}^+$	10	0.10	1.5	0	20	0.29
403	3.1128	$\frac{1}{2}^+$	50	0.08				
404†	3.1150	$\frac{3}{2}^-$	5	0.01	2.5	1	30	1.05
405	3.1154	$\frac{3}{2}^+$	20	0.21				
406	3.1161	$\frac{1}{2}^-$	100	0.28				
407†	3.1183	$\frac{3}{2}^+$	3	0.03	1.5	0	40	0.56
408	3.1191	$\frac{1}{2}^+$	40	0.06	1.5	2	20	3.89
409	3.1230	$\frac{1}{2}^+$	25	0.04				
410*	3.1232	$\frac{5}{2}^-$	10	0.72				
411	3.1234	$\frac{3}{2}^-$	60	0.17	1.5	1	8	0.27
					2.5	1	10	0.34
412†	3.1239	$\frac{1}{2}^-$	15	0.04	1.5	1	40	1.36
413†	3.1274	$\frac{3}{2}^+$	5	0.05	1.5	0	10	0.14
414	3.1287	$\frac{5}{2}^+$	5	0.05	2.5	0	10	0.14
415	3.1294	$\frac{1}{2}^+$	30	0.04	1.5	2	5	0.94
416†	3.1298	$\frac{3}{2}^-$	10	0.03				
417*	3.1302	$\frac{5}{2}^-$	5	0.36	1.5	1	10	0.33
418	3.1307	$\frac{3}{2}^+$	25	0.25				
419	3.1390	$\frac{3}{2}^+$	10	0.10	1.5	0	2	0.03
420	3.1332	$\frac{3}{2}^-$	30	0.11				
421	3.1336	$\frac{5}{2}^+$	5	0.05	2.5	0	30	0.40
422	3.1343	$\frac{1}{2}^+$	20	0.03				

† Newly observed resonance.

* Resonance with J^π assignment changed from previous work [Wil75, Shr82, Shr83, Smi89].

Table B.1(*continued*)

Res. #	E_p (MeV)	J^π	Γ_p (eV)	γ_p^2 (keV)	s′	ℓ′	$\Gamma_{p'}$ (eV)	$\gamma_{p'}^2$ (keV)
423	3.1352	$\frac{3}{2}^-$	5	0.01	2.5	1	5	0.16
424†	3.1360	$\frac{3}{2}^-$	20	0.05				
425	3.1362	$\frac{1}{2}^+$	175	0.26				
426	3.1383	$\frac{1}{2}^-$	1500	4.04	1.5	1	50	1.62
427*	3.1413	$\frac{5}{2}^-$	5	0.35	2.5	1	5	0.16
428	3.1433	$\frac{5}{2}^+$	20	0.20	2.5	0	5	0.07
429	3.1445	$\frac{3}{2}^+$	50	0.49	1.5	0	35	0.45
430*	3.1461	$\frac{1}{2}^-$	10	0.03	1.5	1	20	0.63
431	3.1510	$\frac{3}{2}^-$	50	0.13	1.5	1	20	0.62
					2.5	1	70	2.17
432*	3.1519	$\frac{5}{2}^-$	6	0.41	1.5	1	5	0.16
					2.5	1	10	0.46
433	3.1527	$\frac{3}{2}^-$	15	0.04	1.5	1	15	0.46
					2.5	1	10	0.31
434	3.1545	$\frac{3}{2}^+$	20	0.19	1.5	0	40	0.50
435	3.1548	$\frac{1}{2}^-$	50	0.13				
436	3.1550	$\frac{1}{2}^+$	200	0.29	1.5	2	20	3.42
437	3.1563	$\frac{3}{2}^+$	25	0.24				
438	3.1572	$\frac{3}{2}^-$	30	0.08	1.5	1	20	0.61
439	3.1576	$\frac{1}{2}^-$	100	0.26	1.5	1	20	0.61
440	3.1581	$\frac{3}{2}^-$	75	0.20	1.5	1	100	3.04
					2.5	1	60	1.82
441	3.1595	$\frac{5}{2}^+$	20	0.19				
442	3.1596	$\frac{3}{2}^-$	100	0.26	1.5	1	10	0.30
					2.5	1	15	0.45

† Newly observed resonance.

* Resonance with J^π assignment changed from previous work [Wil75, Shr82, Shr83, Smi89].

Table B.1(*continued*)

Res. #	E_p (MeV)	J^π	Γ_p (eV)	γ_p^2 (keV)	s′	ℓ′	$\Gamma_{p'}$ (eV)	$\gamma_{p'}^2$ (keV)
443	3.1611	$\frac{3}{2}^+$	25	0.24				
444	3.1612	$\frac{1}{2}^+$	100	0.14	1.5	2	10	1.67
445	3.1629	$\frac{1}{2}^+$	300	0.42				
446	3.1636	$\frac{3}{2}^+$	15	0.14				
447	3.1642	$\frac{1}{2}^-$	150	0.39	1.5	1	150	4.47
448	3.1649	$\frac{1}{2}^-$	40	0.10	1.5	1	25	0.74
449	3.1656	$\frac{5}{2}^+$	20	0.19	2.5	0	20	0.24
450*	3.1671	$\frac{5}{2}^-$	10	0.66	1.5	1	25	0.74
451*	3.1681	$\frac{5}{2}^-$	15	0.99	1.5	1	40	1.18
452	3.1693	$\frac{1}{2}^-$	1250	3.23				
453*	3.1702	$\frac{3}{2}^+$	25	0.23	1.5	0	25	0.30
454	3.1707	$\frac{1}{2}^-$	350	0.90				
455	3.1720	$\frac{1}{2}^-$	60	0.15				
456	3.1728	$\frac{3}{2}^+$	70	0.65	1.5	0	30	0.36
457	3.1731	$\frac{3}{2}^-$	100	0.26	2.5	1	15	0.43
458	3.1734	$\frac{3}{2}^-$	60	0.15				
459	3.1737	$\frac{1}{2}^+$	150	0.21	1.5	2	50	8.00
460	3.1743	$\frac{5}{2}^+$	75	0.70	2.5	0	20	0.24
461	3.1771	$\frac{5}{2}^+$	75	0.69	2.5	0	40	0.47
462	3.1798	$\frac{1}{2}^-$	500	1.27	1.5	1	50	1.42
463†	3.1819	$\frac{3}{2}^-$	10	0.03	2.5	1	10	0.28
464	3.1846	$\frac{3}{2}^-$	40	0.10	2.5	1	8	0.22
465	3.1852	$\frac{1}{2}^+$	500	0.69	1.5	2	30	4.61
466	3.1859	$\frac{3}{2}^+$	15	0.14				
467	3.1864	$\frac{5}{2}^+$	15	0.14	2.5	0	40	0.46

† Newly observed resonance.

* Resonance with J^π assignment changed from previous work [Wil75, Shr82, Shr83, Smi89].

Table B.1(*continued*)

Res. #	E_p (MeV)	J^π	Γ_p (eV)	γ_p^2 (keV)	s$'$	ℓ'	$\Gamma_{p'}$ (eV)	$\gamma_{p'}^2$ (keV)
468	3.1907	$\frac{3}{2}^+$	25	0.23	1.5	0	40	0.45
469	3.1919	$\frac{1}{2}^-$	115	0.29	1.5	1	25	0.68
470†	3.1923	$\frac{3}{2}^-$	15	0.04	2.5	1	15	0.41
471	3.1931	$\frac{1}{2}^+$	50	0.07				
472	3.1939	$\frac{3}{2}^+$	15	0.14	1.5	0	10	0.11
473	3.1947	$\frac{1}{2}^-$	1500	3.75	1.5	1	20	0.54
474	3.1953	$\frac{1}{2}^+$	300	0.41				
475*	3.1956	$\frac{5}{2}^-$	20	1.25				
476	3.1962	$\frac{3}{2}^+$	100	0.90	1.5	0	10	0.11
477*	3.1992	$\frac{1}{2}^-$	40	0.10	1.5	1	100	2.67
478	3.2008	$\frac{1}{2}^+$	225	0.31	1.5	2	10	1.46
479*	3.2011	$\frac{5}{2}^-$	10	0.62				
480†	3.2024	$\frac{3}{2}^+$	10	0.09	1.5	0	10	0.11
481	3.2030	$\frac{5}{2}^+$	18	0.16				
482	3.2042	$\frac{3}{2}^-$	20	0.05	1.5	1	10	0.26
					2.5	1	40	1.05
483	3.2058	$\frac{1}{2}^+$	300	0.41	1.5	2	10	1.43
484	3.2067	$\frac{5}{2}^+$	15	0.13	2.5	0	10	0.11
485	3.2084	$\frac{1}{2}^-$	60	0.15	1.5	1	10	0.26
486	3.2095	$\frac{3}{2}^-$	25	0.06	1.5	1	25	0.65
					2.5	1	15	0.39
487	3.2101	$\frac{3}{2}^+$	15	0.13	1.5	0	50	0.53
488†	3.2110	$\frac{3}{2}^+$	10	0.09	1.5	0	10	0.11
489	3.2112	$\frac{1}{2}^-$	500	1.22				
490*	3.2116	$\frac{3}{2}^-$	40	0.10	2.5	1	40	1.03

† Newly observed resonance.

* Resonance with J^π assignment changed from previous work [Wil75, Shr82, Shr83, Smi89].

Table B.1(*continued*)

Res. #	E_p (MeV)	J^π	Γ_p (eV)	γ_p^2 (keV)	s′	ℓ′	$\Gamma_{p'}$ (eV)	$\gamma_{p'}^2$ (keV)
491*	3.2120	$\frac{5}{2}^-$	10	0.61	1.5	1	20	0.51
492†	3.2137	$\frac{5}{2}^+$	10	0.09				
493†	3.2146	$\frac{5}{2}^-$	20	1.21	1.5	1	20	0.51
494*	3.2149	$\frac{3}{2}^+$	70	0.61	1.5	0	70	0.74
495†	3.2160	$\frac{3}{2}^-$	20	0.05	2.5	1	10	0.25
496	3.2173	$\frac{1}{2}^+$	100	0.13	1.5	2	10	1.38
497†	3.2175	$\frac{5}{2}^-$	15	0.90				
498†	3.2188	$\frac{3}{2}^-$	15	0.04	1.5	1	10	0.25
					2.5	1	10	0.25
499†	3.2194	$\frac{5}{2}^+$	10	0.09	2.5	0	5	0.05
500†	3.2203	$\frac{5}{2}^-$	2	0.12	1.5	1	5	0.13
501	3.2211	$\frac{5}{2}^+$	40	0.35	2.5	0	2	0.02
502	3.2217	$\frac{3}{2}^-$	15	0.04	2.5	1	2	0.05
503†	3.2226	$\frac{3}{2}^+$	10	0.09	1.5	0	5	0.05
504*	3.2238	$\frac{5}{2}^+$	15	0.13	2.5	0	5	0.05
505	3.2249	$\frac{5}{2}^+$	10	0.09				
506*	3.2252	$\frac{3}{2}^-$	30	0.07	1.5	1	5	0.12
					2.5	1	30	0.74
507†	3.2261	$\frac{5}{2}^+$	8	0.07	1.5	2	2	0.27
508	3.2266	$\frac{1}{2}^+$	700	0.93				
509†	3.2274	$\frac{3}{2}^-$	10	0.02	1.5	1	30	0.73
					2.5	1	10	0.25
510	3.2285	$\frac{3}{2}^-$	25	0.06				
511	3.2291	$\frac{5}{2}^+$	50	0.43	2.5	0	35	0.35
512	3.2301	$\frac{3}{2}^-$	75	0.18	1.5	1	30	0.73

† Newly observed resonance.

* Resonance with J^π assignment changed from previous work [Wil75, Shr82, Shr83, Smi89].

Table B.1(*continued*)

Res. #	E_p (MeV)	J^π	Γ_p (eV)	γ_p^2 (keV)	s′	ℓ′	$\Gamma_{p'}$ (eV)	$\gamma_{p'}^2$ (keV)
513†	3.2311	$\frac{5}{2}^-$	5	0.29				
514*	3.2317	$\frac{3}{2}^+$	30	0.25	1.5	0	50	0.50
515	3.2324	$\frac{1}{2}^-$	3500	8.35				
516†	3.2334	$\frac{3}{2}^+$	10	0.09	1.5	0	10	0.10
517	3.2339	$\frac{1}{2}^+$	90	0.12				
518*	3.2351	$\frac{3}{2}^+$	20	0.17	1.5	0	5	0.05
519*	3.2356	$\frac{1}{2}^-$	250	0.59				
520	3.2363	$\frac{5}{2}^+$	40	0.34	2.5	0	20	0.20
521†	3.2365	$\frac{5}{2}^-$	20	1.16				
522	3.2390	$\frac{1}{2}^+$	2000	2.61	1.5	2	20	2.56
523	3.2406	$\frac{5}{2}^+$	10	0.08	2.5	0	20	0.20
524†	3.2414	$\frac{5}{2}^+$	30	0.25	2.5	0	8	0.08
525	3.2420	$\frac{3}{2}^-$	30	0.07	2.5	1	15	0.35
526	3.2436	$\frac{1}{2}^-$	8000	18.81				
527*	3.2445	$\frac{5}{2}^-$	15	0.85	2.5	1	5	0.12
528	3.2457	$\frac{1}{2}^-$	150	0.35	1.5	1	80	1.85
529	3.2476	$\frac{1}{2}^-$	1750	4.10	1.5	1	50	1.15
530	3.2488	$\frac{1}{2}^+$	30	0.04				
531†	3.2500	$\frac{3}{2}^+$	10	0.08	1.5	0	10	0.10
532†	3.2508	$\frac{5}{2}^+$	2	0.02	1.5	2	5	0.62
533*	3.2517	$\frac{5}{2}^-$	30	1.69				
534	3.2518	$\frac{1}{2}^+$	300	0.39	1.5	2	10	1.23
535†	3.2528	$\frac{3}{2}^+$	5	0.04	1.5	0	10	0.10
536	3.2537	$\frac{3}{2}^+$	40	0.33				
537†	3.2550	$\frac{3}{2}^+$	10	0.08	1.5	0	10	0.09

† Newly observed resonance.

* Resonance with J^π assignment changed from previous work [Wil75, Shr82, Shr83, Smi89].

Table B.1(*continued*)

Res. #	E_p (MeV)	J^π	Γ_p (eV)	γ_p^2 (keV)	s′	ℓ'	$\Gamma_{p'}$ (eV)	$\gamma_{p'}^2$ (keV)
538†	3.2557	$\frac{5}{2}^+$	10	0.08	2.5	0	20	0.19
539*	3.2576	$\frac{5}{2}^-$	10	0.56	1.5	1	10	0.22
540†	3.2586	$\frac{5}{2}^-$	10	0.55	1.5	1	5	0.11
					2.5	1	5	0.11
541	3.2592	$\frac{5}{2}^+$	5	0.04	2.5	0	5	0.05
542	3.2601	$\frac{3}{2}^+$	15	0.12				
543	3.2603	$\frac{1}{2}^+$	125	0.16	1.5	2	15	1.79
					2.5	2	15	1.79
544	3.2606	$\frac{5}{2}^+$	15	0.12				
545*	3.2630	$\frac{3}{2}^+$	13	0.11	1.5	0	30	0.28
546	3.2662	$\frac{1}{2}^+$	25	0.03	1.5	2	10	1.17
547*	3.2689	$\frac{3}{2}^-$	20	0.05	1.5	1	15	0.33
					2.5	1	10	0.22
548	3.2695	$\frac{3}{2}^+$	25	0.20	1.5	0	15	0.14
549	3.2706	$\frac{1}{2}^-$	50	0.11	1.5	1	25	0.54
550	3.2711	$\frac{1}{2}^+$	150	0.19				
551	3.2716	$\frac{3}{2}^+$	15	0.12	1.5	0	30	0.27
552	3.2746	$\frac{1}{2}^-$	300	0.68				
553†	3.2751	$\frac{3}{2}^-$	20	0.05	1.5	1	40	0.85
					2.5	1	10	0.21
554*	3.2759	$\frac{3}{2}^+$	30	0.24	2.5	2	20	2.26
555*	3.2768	$\frac{3}{2}^-$	15	0.03	1.5	1	30	0.64
					2.5	1	15	0.32
556	3.2775	$\frac{5}{2}^+$	25	0.20	2.5	0	50	0.44
557	3.2782	$\frac{1}{2}^-$	400	0.90				

† Newly observed resonance.

* Resonance with J^π assignment changed from previous work [Wil75, Shr82, Shr83, Smi89].

Table B.1(*continued*)

Res. #	E_p (MeV)	J^π	Γ_p (eV)	γ_p^2 (keV)	s′	ℓ'	$\Gamma_{p'}$ (eV)	$\gamma_{p'}^2$ (keV)
558†	3.2785	$\frac{3}{2}^+$	10	0.08	2.5	2	10	1.12
559	3.2792	$\frac{1}{2}^+$	75	0.09	1.5	2	10	1.12
560	3.2816	$\frac{1}{2}^-$	350	0.79	1.5	1	10	0.21
561*	3.2824	$\frac{5}{2}^+$	5	0.04	2.5	0	20	0.18
562†	3.2840	$\frac{3}{2}^-$	10	0.02	1.5	1	10	0.21
563†	3.2845	$\frac{5}{2}^+$	10	0.08	2.5	0	10	0.09
564†	3.2850	$\frac{5}{2}^-$	5	0.26	1.5	1	5	0.10
					2.5	1	5	0.10
565†	3.2857	$\frac{3}{2}^-$	10	0.02	1.5	1	10	0.21
					2.5	1	10	0.21
566†	3.2868	$\frac{5}{2}^+$	5	0.04	1.5	2	5	0.55
567*	3.2877	$\frac{5}{2}^-$	10	0.53	1.5	1	5	0.10
					2.5	1	5	0.10
568	3.2883	$\frac{1}{2}^+$	125	0.16				
569	3.2885	$\frac{3}{2}^+$	20	0.16	1.5	0	5	0.04
570	3.2892	$\frac{1}{2}^-$	35	0.08				
571	3.2913	$\frac{3}{2}^-$	30	0.07	1.5	1	10	0.20
					2.5	1	120	2.44
572	3.2922	$\frac{1}{2}^+$	10	0.01	1.5	2	5	0.54
573†	3.2926	$\frac{3}{2}^+$	10	0.08	1.5	0	2	0.02
574	3.2932	$\frac{1}{2}^-$	60	0.13				
575	3.2955	$\frac{3}{2}^+$	10	0.08	1.5	0	30	0.25
576*	3.2982	$\frac{3}{2}^-$	50	0.11	1.5	1	20	0.40
					2.5	1	5	0.10
577*	3.2992	$\frac{5}{2}^+$	15	0.12	1.5	2	2	0.21

† Newly observed resonance.

* Resonance with J^π assignment changed from previous work [Wil75, Shr82, Shr83, Smi89].

Table B.1(*continued*)

Res. #	E_p (MeV)	J^π	Γ_p (eV)	γ_p^2 (keV)	s′	ℓ′	$\Gamma_{p'}$ (eV)	$\gamma_{p'}^2$ (keV)
578†	3.3015	$\frac{5}{2}^-$	3	0.15	1.5	1	2	0.04
579	3.3026	$\frac{3}{2}^+$	25	0.19	1.5	0	10	0.08
580	3.3030	$\frac{1}{2}^+$	275	0.34				
581	3.3034	$\frac{3}{2}^+$	35	0.27				
582†	3.3038	$\frac{5}{2}^+$	8	0.06	2.5	0	5	0.04
					2.5	2	20	2.07
583*	3.3046	$\frac{3}{2}^+$	15	0.11	2.5	2	20	2.06
584	3.3049	$\frac{1}{2}^+$	125	0.15				
585	3.3055	$\frac{5}{2}^+$	14	0.11	2.5	0	10	0.08
586†	3.3062	$\frac{3}{2}^-$	8	0.02	2.5	1	10	0.20
587†	3.3067	$\frac{3}{2}^+$	8	0.06	1.5	0	10	0.08
588	3.3082	$\frac{3}{2}^+$	25	0.19	2.5	2	5	0.51
589	3.3088	$\frac{1}{2}^+$	35	0.04	1.5	2	10	1.02
590†	3.3097	$\frac{3}{2}^+$	10	0.08	1.5	0	10	0.08
591†	3.3106	$\frac{3}{2}^+$	5	0.04	1.5	0	5	0.04
592	3.3117	$\frac{3}{2}^-$	75	0.16	1.5	1	60	1.15
					2.5	1	50	0.96
593†	3.3139	$\frac{3}{2}^+$	30	0.22	1.5	0	15	0.12
594	3.3141	$\frac{1}{2}^+$	350	0.42				
595*	3.3153	$\frac{3}{2}^-$	10	0.02	2.5	1	20	0.38
596	3.3174	$\frac{1}{2}^+$	10	0.01	1.5	2	10	0.99
597†	3.3182	$\frac{3}{2}^+$	10	0.07	1.5	0	10	0.08
598†	3.3190	$\frac{3}{2}^+$	5	0.04	2.5	2	15	1.48
599*	3.3199	$\frac{5}{2}^+$	15	0.11	2.5	0	3	0.02

† Newly observed resonance.

* Resonance with J^π assignment changed from previous work [Wil75, Shr82, Shr83, Smi89].

Table B.1(*continued*)

Res. #	E_p (MeV)	J^π	Γ_p (eV)	γ_p^2 (keV)	s′	ℓ'	$\Gamma_{p'}$ (eV)	$\gamma_{p'}^2$ (keV)
600	3.3227	$\frac{3}{2}^-$	60	0.13	1.5	1	15	0.28
					2.5	1	15	0.28
601	3.3237	$\frac{3}{2}^-$	50	0.11	1.5	1	20	0.37
					2.5	1	15	0.28
602	3.3245	$\frac{1}{2}^+$	1250	1.50				
603*	3.3248	$\frac{3}{2}^-$	15	0.03	2.5	1	10	0.19
604*	3.3268	$\frac{3}{2}^-$	15	0.03	1.5	1	15	0.28
					2.5	1	15	0.28
605†	3.3271	$\frac{1}{2}^-$	40	0.09				
606	3.3293	$\frac{3}{2}^-$	85	0.18	2.5	1	10	0.18
607*	3.3308	$\frac{3}{2}^-$	30	0.06	1.5	1	40	0.73
					2.5	1	40	0.73
608	3.3322	$\frac{1}{2}^+$	100	0.12				
609*	3.3327	$\frac{5}{2}^+$	20	0.15	2.5	0	30	0.23
610	3.3342	$\frac{5}{2}^+$	15	0.11	2.5	0	5	0.04
611	3.3347	$\frac{1}{2}^+$	500	0.59	1.5	2	10	0.94
					2.5	2	10	0.94
612	3.3363	$\frac{5}{2}^+$	50	0.36	2.5	0	4	0.03
613	3.3364	$\frac{1}{2}^-$	100	0.21				
614*	3.3372	$\frac{3}{2}^-$	15	0.03	1.5	1	10	0.18
615	3.3397	$\frac{3}{2}^+$	20	0.14	1.5	0	5	0.04
					2.5	2	10	0.92
616	3.3407	$\frac{3}{2}^+$	5	0.04	1.5	0	50	0.38
617	3.3429	$\frac{3}{2}^+$	50	0.36	1.5	0	10	0.08
618	3.3458	$\frac{5}{2}^+$	20	0.14	2.5	2	10	0.91

† Newly observed resonance.

* Resonance with J^π assignment changed from previous work [Wil75, Shr82, Shr83, Smi89].

Table B.1(*continued*)

Res. #	E_p (MeV)	J^π	Γ_p (eV)	γ_p^2 (keV)	s′	ℓ′	$\Gamma_{p'}$ (eV)	$\gamma_{p'}^2$ (keV)
619	3.3462	$\frac{1}{2}^+$	30	0.04	1.5	2	20	2.72
620	3.3469	$\frac{3}{2}^+$	15	0.11	1.5	0	30	0.22
621*	3.3483	$\frac{5}{2}^+$	5	0.04	2.5	0	20	0.15
622	3.3495	$\frac{3}{2}^+$	50	0.35	1.5	0	10	0.07
					2.5	2	10	0.90
623	3.3509	$\frac{1}{2}^+$	150	0.18				
624†	3.3511	$\frac{3}{2}^-$	15	0.03	1.5	1	20	0.34
					2.5	1	5	0.09
625	3.3532	$\frac{1}{2}^+$	150	0.18	1.5	2	10	0.89
626*	3.3535	$\frac{3}{2}^-$	30	0.06	1.5	1	20	0.34
					2.5	1	10	0.17
627	3.3539	$\frac{3}{2}^+$	25	0.18	1.5	0	50	0.37
628*	3.3548	$\frac{5}{2}^-$	10	0.46	1.5	1	20	0.34
629*	3.3571	$\frac{5}{2}^+$	100	0.70	1.5	2	10	0.88
					2.5	0	5	0.04
					2.5	2	-20	1.75
630†	3.3584	$\frac{3}{2}^-$	15	0.03	2.5	1	10	0.17
631	3.3609	$\frac{3}{2}^+$	15	0.10	1.5	0	8	0.06
					2.5	2	15	1.30
632	3.3610	$\frac{1}{2}^-$	50	0.10	1.5	1	100	1.67
633	3.3626	$\frac{3}{2}^+$	50	0.35				
634	3.3628	$\frac{1}{2}^+$	400	0.46				
635	3.3633	$\frac{5}{2}^+$	14	0.10				
636	3.3637	$\frac{3}{2}^+$	15	0.10				
637†	3.3643	$\frac{5}{2}^+$	5	0.04	2.5	0	10	0.07

† Newly observed resonance.

* Resonance with J^π assignment changed from previous work [Wil75, Shr82, Shr83, Smi89].

Table B.1(*continued*)

Res. #	E_p (MeV)	J^π	Γ_p (eV)	γ_p^2 (keV)	s′	ℓ′	$\Gamma_{p'}$ (eV)	$\gamma_{p'}^2$ (keV)
638*	3.3660	$\frac{5}{2}^+$	10	0.07	2.5	0	5	0.04
639	3.3686	$\frac{3}{2}^+$	30	0.21				
640	3.3688	$\frac{1}{2}^+$	350	0.40	1.5	2	10	0.85
641†	3.3689	$\frac{5}{2}^-$	8	0.36	1.5	1	20	0.33
					2.5	1	60	0.98
642*	3.3696	$\frac{5}{2}^+$	10	0.07	1.5	2	2	0.17
643	3.3703	$\frac{3}{2}^+$	15	0.10	1.5	0	10	0.07
644†	3.3708	$\frac{5}{2}^+$	5	0.03	2.5	0	5	0.04
645	3.3711	$\frac{1}{2}^-$	30	0.06	1.5	1	15	0.24
646	3.3723	$\frac{1}{2}^-$	35	0.07	1.5	1	10	0.16
647	3.3732	$\frac{3}{2}^-$	100	0.20	1.5	1	15	0.24
648*	3.3743	$\frac{3}{2}^+$	35	0.24	1.5	0	20	0.14
649†	3.3754	$\frac{3}{2}^-$	10	0.02	2.5	1	10	0.16
650	3.3760	$\frac{1}{2}^-$	20	0.04				
651	3.3766	$\frac{3}{2}^+$	65	0.44	1.5	0	100	0.69
					2.5	2	100	8.26
652†	3.3769	$\frac{5}{2}^-$	8	0.36				
653	3.3770	$\frac{3}{2}^-$	50	0.10	1.5	1	100	1.60
					2.5	1	80	1.28
654†	3.3787	$\frac{5}{2}^-$	10	0.44	1.5	1	80	1.28
					2.5	1	80	1.28
655	3.3809	$\frac{1}{2}^+$	40	0.05	1.5	2	10	0.82
656	3.3819	$\frac{3}{2}^+$	30	0.20	1.5	0	5	0.03
					2.5	2	20	1.63

† Newly observed resonance.

* Resonance with J^π assignment changed from previous work [Wil75, Shr82, Shr83, Smi89].

Table B.1(*continued*)

Res. #	E_p (MeV)	J^π	Γ_p (eV)	γ_p^2 (keV)	s′	ℓ′	$\Gamma_{p'}$ (eV)	$\gamma_{p'}^2$ (keV)
657*	3.3833	$\frac{3}{2}^-$	20	0.04	1.5	1	40	0.63
					2.5	1	25	0.39
658	3.3851	$\frac{3}{2}^+$	50	0.34	2.5	2	20	1.61
659	3.3852	$\frac{1}{2}^+$	1000	1.13	1.5	2	25	2.01
					2.5	2	25	2.01
660†	3.3857	$\frac{5}{2}^-$	5	0.22				
661	3.3866	$\frac{3}{2}^+$	10	0.07	1.5	0	10	0.07
662	3.3882	$\frac{5}{2}^+$	40	0.27	2.5	2	2	0.16
663†	3.3890	$\frac{1}{2}^-$	30	0.06	1.5	1	30	0.47
664	3.3894	$\frac{1}{2}^+$	75	0.09	1.5	2	15	1.19
665†	3.3912	$\frac{1}{2}^-$	10	0.02	1.5	1	10	0.15
666†	3.3932	$\frac{3}{2}^+$	5	0.03	1.5	0	5	0.03
667	3.3944	$\frac{3}{2}^-$	45	0.09	2.5	1	20	0.31
668†	3.3946	$\frac{3}{2}^+$	20	0.13	2.5	2	20	1.56
669*	3.3955	$\frac{3}{2}^+$	15	0.10	2.5	2	15	1.17
670	3.3968	$\frac{5}{2}^+$	40	0.26	2.5	0	10	0.07
671†	3.3970	$\frac{1}{2}^-$	20	0.04	1.5	1	20	0.30
672	3.3988	$\frac{1}{2}^+$	1350	1.51	1.5	2	50	3.86
					2.5	2	50	3.86
673*	3.3997	$\frac{3}{2}^+$	15	0.10	1.5	0	20	0.13
674	3.4035	$\frac{3}{2}^-$	75	0.15	1.5	1	75	1.12
					2.5	1	25	0.37
675†	3.4038	$\frac{3}{2}^-$	25	0.05	1.5	1	50	0.75
676	3.4042	$\frac{3}{2}^+$	40	0.26	1.5	0	100	0.65
677	3.4050	$\frac{1}{2}^-$	25	0.05				

† Newly observed resonance.

* Resonance with J^π assignment changed from previous work [Wil75, Shr82, Shr83, Smi89].

Table B.1(*continued*)

Res. #	E_p (MeV)	J^π	Γ_p (eV)	γ_p^2 (keV)	s′	ℓ′	$\Gamma_{p'}$ (eV)	$\gamma_{p'}^2$ (keV)
678†	3.4068	$\frac{3}{2}^-$	10	0.02	2.5	1	40	0.59
679†	3.4077	$\frac{3}{2}^+$	10	0.07	1.5	0	5	0.03
680†	3.4089	$\frac{3}{2}^-$	15	0.03	2.5	1	10	0.15
681*	3.4093	$\frac{5}{2}^-$	15	0.63	1.5	1	5	0.07
					2.5	1	5	0.07
682†	3.4103	$\frac{3}{2}^-$	10	0.02	2.5	1	10	0.15
683	3.4116	$\frac{3}{2}^+$	20	0.13	1.5	0	30	0.19
684	3.4126	$\frac{5}{2}^+$	15	0.10	1.5	2	30	2.23
					2.5	0	30	0.19
685	3.4131	$\frac{1}{2}^+$	50	0.06				
686	3.4135	$\frac{5}{2}^+$	80	0.52	2.5	0	10	0.06
687*	3.4150	$\frac{3}{2}^-$	20	0.04	1.5	1	30	0.44
					2.5	1	25	0.36
688*	3.4158	$\frac{7}{2}^+$	20	9.35				
689	3.4170	$\frac{1}{2}^-$	250	0.48	1.5	1	10	0.14
690	3.4190	$\frac{1}{2}^+$	100	0.11	1.5	2	100	7.28
					2.5	2	100	7.28
691*	3.4195	$\frac{5}{2}^+$	20	0.13	2.5	0	20	0.13
692†	3.4204	$\frac{3}{2}^-$	10	0.02	1.5	1	20	0.29
693†	3.4214	$\frac{3}{2}^+$	10	0.06	1.5	0	10	0.06
694*	3.4220	$\frac{3}{2}^-$	75	0.14	1.5	1	100	1.43
					2.5	1	100	1.43
695	3.4223	$\frac{1}{2}^+$	150	0.16				
696*	3.4257	$\frac{5}{2}^+$	40	0.25	2.5	0	5	0.03
697	3.4263	$\frac{3}{2}^+$	60	0.38	1.5	0	30	0.18

† Newly observed resonance.

* Resonance with J^π assignment changed from previous work [Wil75, Shr82, Shr83, Smi89].

Table B.1(*continued*)

Res. #	E_p (MeV)	J^π	Γ_p (eV)	γ_p^2 (keV)	s'	ℓ'	$\Gamma_{p'}$ (eV)	$\gamma_{p'}^2$ (keV)
698	3.4267	$\frac{1}{2}^+$	200	0.22				
699	3.4278	$\frac{1}{2}^-$	25	0.05				
700	3.4284	$\frac{3}{2}^+$	200	1.26	1.5	0	30	0.18
					1.5	2	30	2.12
					2.5	2	60	4.25
701*	3.4295	$\frac{1}{2}^+$	25	0.03				
702*	3.4304	$\frac{5}{2}^-$	35	1.42	1.5	1	20	0.28
703	3.4314	$\frac{3}{2}^+$	40	0.25	1.5	0	10	0.06
704	3.4322	$\frac{1}{2}^+$	1300	1.41	1.5	2	20	1.40
					2.5	2	20	1.40
705†	3.4324	$\frac{3}{2}^+$	20	0.13	1.5	0	20	0.12
706	3.4329	$\frac{5}{2}^+$	15	0.09				
707	3.4332	$\frac{1}{2}^-$	35	0.07	1.5	1	35	0.49
708	3.4336	$\frac{3}{2}^+$	14	0.09				
709	3.4340	$\frac{1}{2}^-$	20	0.04	1.5	1	20	0.28
710	3.4360	$\frac{3}{2}^-$	50	0.09	1.5	1	20	0.28
					2.5	1	20	0.28
711	3.4365	$\frac{5}{2}^+$	17	0.11	2.5	0	15	0.09
712*	3.4376	$\frac{5}{2}^+$	10	0.06	2.5	0	40	0.24
713	3.4411	$\frac{1}{2}^-$	50	0.09	1.5	1	100	1.36
714*	3.4415	$\frac{3}{2}^-$	50	0.09	2.5	1	100	1.36
715	3.4420	$\frac{1}{2}^-$	850	1.59	1.5	1	50	0.68
716	3.4425	$\frac{5}{2}^+$	10	0.06	2.5	0	8	0.05
717	3.4458	$\frac{3}{2}^+$	10	0.06	1.5	0	10	0.06
718	3.4465	$\frac{1}{2}^-$	150	0.28				

† Newly observed resonance.

* Resonance with J^π assignment changed from previous work [Wil75, Shr82, Shr83, Smi89].

Table B.1(*continued*)

Res. #	E_p (MeV)	J^π	Γ_p (eV)	γ_p^2 (keV)	s'	ℓ'	$\Gamma_{p'}$ (eV)	$\gamma_{p'}^2$ (keV)
719†	3.4472	$\frac{1}{2}^+$	20	0.02	2.5	2	30	2.01
720*	3.4488	$\frac{3}{2}^-$	50	0.09	1.5	1	20	0.27
721	3.4492	$\frac{1}{2}^+$	100	0.11				
722	3.4496	$\frac{5}{2}^+$	10	0.06				
723	3.4502	$\frac{1}{2}^-$	100	0.19				
724	3.4547	$\frac{3}{2}^+$	80	0.49	1.5	0	25	0.14
725	3.4555	$\frac{3}{2}^-$	80	0.15				
726	3.4557	$\frac{1}{2}^+$	60	0.06	1.5	2	20	1.31
					2.5	2	20	1.31
727	3.4559	$\frac{5}{2}^+$	40	0.24	2.5	0	10	0.96
728†	3.4578	$\frac{5}{2}^+$	10	0.06	2.5	0	5	0.03
					2.5	2	5	0.33
729†	3.4586	$\frac{5}{2}^-$	3	0.12	1.5	1	10	0.13
730	3.4598	$\frac{3}{2}^+$	50	0.30	1.5	0	25	0.14
731	3.4600	$\frac{1}{2}^+$	450	0.48				
732*	3.4605	$\frac{3}{2}^+$	30	0.18	1.5	0	5	0.03
733†	3.4607	$\frac{5}{2}^-$	8	0.31				
734	3.4613	$\frac{1}{2}^-$	100	0.18	1.5	1	10	0.13
735*	3.4617	$\frac{3}{2}^-$	50	0.09	1.5	1	40	0.52
					2.5	1	40	0.52
736	3.4629	$\frac{3}{2}^+$	20	0.12	1.5	0	5	0.03
737†	3.4631	$\frac{1}{2}^-$	25	0.05				
738*	3.4641	$\frac{5}{2}^+$	20	0.12	2.5	0	200	1.13
739*	3.4651	$\frac{3}{2}^-$	20	0.04	2.5	1	35	0.45
740†	3.4658	$\frac{3}{2}^+$	10	0.06	1.5	0	10	0.06

† Newly observed resonance.

* Resonance with J^π assignment changed from previous work [Wil75, Shr82, Shr83, Smi89].

Table B.1(*continued*)

Res. #	E_p (MeV)	J^π	Γ_p (eV)	γ_p^2 (keV)	s′	ℓ′	$\Gamma_{p'}$ (eV)	$\gamma_{p'}^2$ (keV)
741†	3.4669	$\frac{3}{2}^-$	15	0.03	1.5	1	20	0.26
742	3.4676	$\frac{1}{2}^+$	150	0.16				
743*	3.4677	$\frac{3}{2}^+$	10	0.06				
744	3.4681	$\frac{1}{2}^-$	80	0.15	1.5	1	30	0.38
745	3.4694	$\frac{3}{2}^+$	300	1.79	1.5	0	60	0.34
					2.5	2	20	1.26
746†	3.4702	$\frac{3}{2}^-$	10	0.02	1.5	1	10	0.13
747	3.4706	$\frac{3}{2}^+$	50	0.30				
748	3.4708	$\frac{1}{2}^+$	500	0.52	1.5	2	10	0.63
749	3.4714	$\frac{3}{2}^+$	30	0.18	1.5	0	5	0.03
750†	3.4715	$\frac{5}{2}^-$	10	0.38				
751	3.4727	$\frac{3}{2}^-$	100	0.18	1.5	1	80	1.01
					2.5	1	80	1.01
752†	3.4743	$\frac{3}{2}^-$	10	0.02	2.5	1	20	0.25
753	3.4750	$\frac{3}{2}^+$	100	0.59	1.5	0	80	0.44
754	3.4752	$\frac{1}{2}^+$	300	0.31				
755	3.4761	$\frac{5}{2}^+$	10	0.06	2.5	0	10	0.06
756	3.4773	$\frac{3}{2}^-$	30	0.05	2.5	1	10	0.12
757	3.4786	$\frac{3}{2}^+$	100	0.59	1.5	0	100	0.55
					2.5	2	10	0.61
758*	3.4797	$\frac{3}{2}^-$	50	0.09	1.5	1	15	0.19
					2.5	1	15	0.19
759*	3.4820	$\frac{5}{2}^-$	10	0.37	1.5	1	5	0.06
760*	3.4828	$\frac{3}{2}^+$	80	0.47	1.5	0	50	0.27
761†	3.4841	$\frac{3}{2}^-$	10	0.02	2.5	1	10	0.12

† Newly observed resonance.

* Resonance with J^π assignment changed from previous work [Wil75, Shr82, Shr83, Smi89].

Table B.1(*continued*)

Res. #	E_p (MeV)	J^π	Γ_p (eV)	γ_p^2 (keV)	s′	ℓ'	$\Gamma_{p'}$ (eV)	$\gamma_{p'}^2$ (keV)
762*	3.4845	$\frac{5}{2}^+$	35	0.20	2.5	0	5	0.03
763†	3.4849	$\frac{3}{2}^+$	10	0.06	1.5	0	10	0.05
764	3.4862	$\frac{3}{2}^-$	30	0.05	1.5	1	100	1.22
					2.5	1	30	0.37
765	3.4876	$\frac{5}{2}^+$	20	0.12	2.5	0	30	0.16
					2.5	1	10	0.12
766†	3.4894	$\frac{3}{2}^+$	10	0.06	1.5	0	10	0.05
767	3.4897	$\frac{1}{2}^+$	125	0.13	1.5	2	15	0.89
					2.5	2	15	0.89
768	3.4922	$\frac{5}{2}^+$	10	0.06	2.5	0	30	0.16
769†	3.4924	$\frac{5}{2}^-$	5	0.18	1.5	1	5	0.06
					2.5	1	5	0.06
770†	3.4932	$\frac{3}{2}^+$	10	0.06	1.5	0	10	0.05
771†	3.4961	$\frac{3}{2}^-$	25	0.04	2.5	1	50	0.59
772	3.4966	$\frac{3}{2}^-$	25	0.04	1.5	1	25	0.30
					2.5	1	100	1.19
773	3.4974	$\frac{3}{2}^+$	30	0.17				
774	3.4976	$\frac{1}{2}^+$	400	0.41	1.5	2	50	2.91
775	3.4984	$\frac{5}{2}^+$	15	0.09	2.5	0	5	0.03
					2.5	2	10	0.58
776	3.5000	$\frac{1}{2}^-$	700	1.23	1.5	1	25	0.29
777*	3.5014	$\frac{3}{2}^+$	10	0.06	1.5	0	15	0.08
778	3.5027	$\frac{3}{2}^-$	15	0.03	1.5	1	15	0.18
					2.5	1	15	0.18
779	3.5038	$\frac{3}{2}^-$	45	0.08	2.5	1	10	0.12

† Newly observed resonance.

* Resonance with J^π assignment changed from previous work [Wil75, Shr82, Shr83, Smi89].

Table B.1(*continued*)

Res. #	E_p (MeV)	J^π	Γ_p (eV)	γ_p^2 (keV)	s'	ℓ'	$\Gamma_{p'}$ (eV)	$\gamma_{p'}^2$ (keV)
780	3.5040	$\frac{1}{2}^+$	20	0.02	1.5	2	60	3.43
781†	3.5042	$\frac{3}{2}^-$	20	0.04	2.5	1	20	0.23
782	3.5054	$\frac{3}{2}^+$	40	0.23	2.5	2	25	1.42
783	3.5069	$\frac{1}{2}^-$	60	0.11				
784	3.5075	$\frac{5}{2}^+$	100	0.57	2.5	0	80	0.41
785	3.5083	$\frac{3}{2}^-$	250	0.44	1.5	1	10	0.12
					2.5	1	25	0.29
786†	3.5090	$\frac{5}{2}^-$	10	0.35	1.5	1	10	0.12
787	3.5096	$\frac{5}{2}^+$	10	0.06	2.5	0	10	0.05
788	3.5101	$\frac{1}{2}^+$	200	0.20	1.5	2	20	1.12
789†	3.5108	$\frac{5}{2}^+$	10	0.06	2.5	0	10	0.05
790†	3.5124	$\frac{3}{2}^+$	10	0.06	1.5	0	50	0.25
791	3.5138	$\frac{3}{2}^-$	50	0.09	1.5	1	20	0.23
					2.5	1	50	0.57
792*	3.5142	$\frac{5}{2}^-$	5	0.18				
793	3.5147	$\frac{3}{2}^+$	12	0.08	1.5	0	30	0.15
794	3.5165	$\frac{3}{2}^+$	25	0.14	1.5	0	40	0.20
795†	3.5181	$\frac{3}{2}^+$	10	0.06	1.5	0	10	0.05
796	3.5187	$\frac{3}{2}^+$	25	0.14	1.5	0	25	0.13
797†	3.5196	$\frac{3}{2}^-$	10	0.02	2.5	1	10	0.11
798	3.5208	$\frac{3}{2}^+$	150	0.83	1.5	0	15	0.08
					2.5	2	10	0.55
799	3.5214	$\frac{1}{2}^+$	200	0.20	1.5	2	10	0.55
800†	3.5222	$\frac{3}{2}^+$	10	0.06	1.5	0	10	0.05
801	3.5226	$\frac{1}{2}^-$	20	0.03				

† Newly observed resonance.

* Resonance with J^π assignment changed from previous work [Wil75, Shr82, Shr83, Smi89].

Table B.1(*continued*)

Res. #	E_p (MeV)	J^π	Γ_p (eV)	γ_p^2 (keV)	s'	ℓ'	$\Gamma_{p'}$ (eV)	$\gamma_{p'}^2$ (keV)
802†	3.5230	$\frac{5}{2}^-$	10	0.35	1.5	1	20	0.22
					2.5	1	10	0.11
803*	3.5238	$\frac{3}{2}^-$	20	0.03	1.5	1	20	0.22
					2.5	1	30	0.33
804	3.5249	$\frac{1}{2}^+$	90	0.09	1.5	2	20	1.08
805†	3.5263	$\frac{5}{2}^+$	5	0.03	2.5	0	5	0.03
806	3.5263	$\frac{1}{2}^-$	350	0.60	1.5	1	75	0.83
807	3.5276	$\frac{5}{2}^+$	15	0.08	1.5	2	20	1.07
808	3.5282	$\frac{3}{2}^-$	100	0.17	1.5	1	80	0.88
					2.5	1	120	1.32
809	3.5320	$\frac{1}{2}^-$	60	0.10	1.5	1	60	0.65

† Newly observed resonance.

* Resonance with J^π assignment changed from previous work [Wil75, Shr82, Shr83, Smi89].

Table B.2: ^{45}Sc Resonance Parameters–$J^\pi = \frac{1}{2}^+$

Res. #	E_p (MeV)	J^π	Γ_p (eV)	γ_p^2 (keV)	s'	ℓ'	$\Gamma_{p'}$ (eV)	$\gamma_{p'}^2$ (keV)
9	2.5166	$\frac{1}{2}^+$	70	0.25				
13	2.5218	$\frac{1}{2}^+$	200	0.70				
20	2.5349	$\frac{1}{2}^+$	225	0.77				
25	2.5538	$\frac{1}{2}^+$	80	0.26				
29	2.5634	$\frac{1}{2}^+$	30	0.10				
37	2.5789	$\frac{1}{2}^+$	60	0.19				
40	2.5842	$\frac{1}{2}^+$	115	0.36				
42	2.5878	$\frac{1}{2}^+$	60	0.19				
47	2.5962	$\frac{1}{2}^+$	150	0.46				
51	2.6035	$\frac{1}{2}^+$	20	0.06				
60	2.6209	$\frac{1}{2}^+$	125	0.37				
70	2.6342	$\frac{1}{2}^+$	30	0.09				
79	2.6495	$\frac{1}{2}^+$	40	0.11				
81	2.6530	$\frac{1}{2}^+$	40	0.11				
98	2.6761	$\frac{1}{2}^+$	125	0.34	1.5	2	10	14.20
100	2.6791	$\frac{1}{2}^+$	400	1.07	1.5	2	5	6.98
107	2.6886	$\frac{1}{2}^+$	30	0.08				
108	2.6910	$\frac{1}{2}^+$	140	0.37				
112	2.6994	$\frac{1}{2}^+$	55	0.14	1.5	2	5	6.26
121	2.7178	$\frac{1}{2}^+$	120	0.30				
125	2.7237	$\frac{1}{2}^+$	15	0.04				
138	2.7480	$\frac{1}{2}^+$	5	0.01	1.5	2	5	4.85
143	2.7543	$\frac{1}{2}^+$	10	0.02				
154	2.7687	$\frac{1}{2}^+$	300	0.70				
159	2.7727	$\frac{1}{2}^+$	30	0.07				
174	2.7999	$\frac{1}{2}^+$	20	0.05				

Table B.2(*continued*)

Res. #	E_p (MeV)	J^π	Γ_p (eV)	γ_p^2 (keV)	s′	ℓ′	$\Gamma_{p'}$ (eV)	$\gamma_{p'}^2$ (keV)
176	2.8043	$\frac{1}{2}^+$	500	1.11				
181	2.8120	$\frac{1}{2}^+$	100	0.22				
196	2.8321	$\frac{1}{2}^+$	30	0.06				
209	2.8515	$\frac{1}{2}^+$	550	1.14				
222	2.8677	$\frac{1}{2}^+$	180	0.37	1.5	2	5	2.72
227	2.8736	$\frac{1}{2}^+$	350	0.70				
237	2.8897	$\frac{1}{2}^+$	250	0.49				
242	2.8919	$\frac{1}{2}^+$	90	0.18				
250	2.9020	$\frac{1}{2}^+$	60	0.12	1.5	2	5	2.34
265	2.9315	$\frac{1}{2}^+$	450	0.84	1.5	2	5	2.05
267	2.9339	$\frac{1}{2}^+$	400	0.74	1.5	2	30	12.19
271	2.9412	$\frac{1}{2}^+$	15	0.03				
276	2.9498	$\frac{1}{2}^+$	150	0.27				
279	2.9537	$\frac{1}{2}^+$	8	0.01	1.5	2	20	7.47
283	2.9593	$\frac{1}{2}^+$	10	0.02				
287	2.9648	$\frac{1}{2}^+$	200	0.36	1.5	2	12	4.28
294	2.9744	$\frac{1}{2}^+$	200	0.35	1.5	2	5	1.71
306	2.9908	$\frac{1}{2}^+$	100	0.17	1.5	2	5	1.60
309	2.9950	$\frac{1}{2}^+$	220	0.38	1.5	2	5	1.57
318	3.0085	$\frac{1}{2}^+$	15	0.03				
330	3.0210	$\frac{1}{2}^+$	20	0.03	1.5	2	8	2.27
336	3.0266	$\frac{1}{2}^+$	55	0.09				
342	3.0318	$\frac{1}{2}^+$	40	0.07	1.5	2	5	1.36
344	3.0351	$\frac{1}{2}^+$	50	0.08	1.5	2	60	16.08
351	3.0443	$\frac{1}{2}^+$	5	0.01	1.5	2	20	5.17
353	3.0491	$\frac{1}{2}^+$	100	0.16	1.5	2	5	1.27

Table B.2(*continued*)

Res. #	E_p (MeV)	J^π	Γ_p (eV)	γ_p^2 (keV)	s′	ℓ′	$\Gamma_{p'}$ (eV)	$\gamma_{p'}^2$ (keV)
358	3.0559	$\frac{1}{2}^+$	275	0.44	1.5	2	20	4.94
					2.5	2	20	4.94
368	3.0660	$\frac{1}{2}^+$	250	0.39				
372	3.0714	$\frac{1}{2}^+$	40	0.06	1.5	2	10	2.33
374	3.0753	$\frac{1}{2}^+$	550	0.86	1.5	2	30	6.88
					2.5	2	30	6.88
381	3.0839	$\frac{1}{2}^+$	25	0.04				
395	3.1021	$\frac{1}{2}^+$	200	0.30	1.5	2	10	2.07
403	3.1128	$\frac{1}{2}^+$	50	0.08				
408	3.1191	$\frac{1}{2}^+$	40	0.06	1.5	2	20	3.89
409	3.1230	$\frac{1}{2}^+$	25	0.04				
415	3.1294	$\frac{1}{2}^+$	30	0.04	1.5	2	5	0.94
422	3.1343	$\frac{1}{2}^+$	20	0.03				
425	3.1362	$\frac{1}{2}^+$	175	0.26				
436	3.1550	$\frac{1}{2}^+$	200	0.29	1.5	2	20	3.42
444	3.1612	$\frac{1}{2}^+$	100	0.14	1.5	2	10	1.67
445	3.1629	$\frac{1}{2}^+$	300	0.42				
459	3.1737	$\frac{1}{2}^+$	150	0.21	1.5	2	50	8.00
465	3.1852	$\frac{1}{2}^+$	500	0.69	1.5	2	30	4.61
471	3.1931	$\frac{1}{2}^+$	50	0.07				
474	3.1953	$\frac{1}{2}^+$	300	0.41				
478	3.2008	$\frac{1}{2}^+$	225	0.31	1.5	2	10	1.46
483	3.2058	$\frac{1}{2}^+$	300	0.41	1.5	2	10	1.43
496	3.2173	$\frac{1}{2}^+$	100	0.13	1.5	2	10	1.38
508	3.2266	$\frac{1}{2}^+$	700	0.93				
517	3.2339	$\frac{1}{2}^+$	90	0.12				
522	3.2390	$\frac{1}{2}^+$	2000	2.61	1.5	2	20	2.56

Table B.2(*continued*)

Res. #	E_p (MeV)	J^π	Γ_p (eV)	γ_p^2 (keV)	s′	ℓ′	$\Gamma_{p'}$ (eV)	$\gamma_{p'}^2$ (keV)
530	3.2488	$\frac{1}{2}^+$	30	0.04				
534	3.2518	$\frac{1}{2}^+$	300	0.39	1.5	2	10	1.23
543	3.2603	$\frac{1}{2}^+$	125	0.16	1.5	2	15	1.79
					2.5	2	15	1.79
546	3.2662	$\frac{1}{2}^+$	25	0.03	1.5	2	10	1.17
550	3.2711	$\frac{1}{2}^+$	150	0.19				
559	3.2792	$\frac{1}{2}^+$	75	0.09	1.5	2	10	1.12
568	3.2883	$\frac{1}{2}^+$	125	0.16				
572	3.2922	$\frac{1}{2}^+$	10	0.01	1.5	2	5	0.54
580	3.3030	$\frac{1}{2}^+$	275	0.34				
584	3.3049	$\frac{1}{2}^+$	125	0.15				
589	3.3088	$\frac{1}{2}^+$	35	0.04	1.5	2	10	1.02
594	3.3141	$\frac{1}{2}^+$	350	0.42				
596	3.3174	$\frac{1}{2}^+$	10	0.01	1.5	2	10	0.99
602	3.3245	$\frac{1}{2}^+$	1250	1.50				
608	3.3322	$\frac{1}{2}^+$	100	0.12				
611	3.3347	$\frac{1}{2}^+$	500	0.59	1.5	2	10	0.94
					2.5	2	10	0.94
619	3.3462	$\frac{1}{2}^+$	30	0.04	1.5	2	20	2.72
623	3.3509	$\frac{1}{2}^+$	150	0.18				
625	3.3532	$\frac{1}{2}^+$	150	0.18	1.5	2	10	0.89
634	3.3628	$\frac{1}{2}^+$	400	0.46				
640	3.3688	$\frac{1}{2}^+$	350	0.40	1.5	2	10	0.85
655	3.3809	$\frac{1}{2}^+$	40	0.05	1.5	2	10	0.82
659	3.3852	$\frac{1}{2}^+$	1000	1.13	1.5	2	25	2.01
					2.5	2	25	2.01
664	3.3894	$\frac{1}{2}^+$	75	0.09	1.5	2	15	1.19

Table B.2(*continued*)

Res. #	E_p (MeV)	J^π	Γ_p (eV)	γ_p^2 (keV)	s′	ℓ′	$\Gamma_{p'}$ (eV)	$\gamma_{p'}^2$ (keV)
672	3.3988	$\frac{1}{2}^+$	1350	1.51	1.5	2	50	3.86
					2.5	2	50	3.86
685	3.4131	$\frac{1}{2}^+$	50	0.06				
690	3.4190	$\frac{1}{2}^+$	100	0.11	1.5	2	100	7.28
					2.5	2	100	7.28
695	3.4223	$\frac{1}{2}^+$	150	0.16				
698	3.4267	$\frac{1}{2}^+$	200	0.22				
701	3.4295	$\frac{1}{2}^+$	25	0.03				
704	3.4322	$\frac{1}{2}^+$	1300	1.41	1.5	2	20	1.40
					2.5	2	20	1.40
719	3.4472	$\frac{1}{2}^+$	20	0.02	2.5	2	30	2.01
721	3.4492	$\frac{1}{2}^+$	100	0.11				
726	3.4557	$\frac{1}{2}^+$	60	0.06	1.5	2	20	1.31
					2.5	2	20	1.31
731	3.4600	$\frac{1}{2}^+$	450	0.48				
742	3.4676	$\frac{1}{2}^+$	150	0.16				
748	3.4708	$\frac{1}{2}^+$	500	0.52	1.5	2	10	0.63
754	3.4752	$\frac{1}{2}^+$	300	0.31				
767	3.4897	$\frac{1}{2}^+$	125	0.13	1.5	2	15	0.89
					2.5	2	15	0.89
774	3.4976	$\frac{1}{2}^+$	400	0.41	1.5	2	50	2.91
780	3.5040	$\frac{1}{2}^+$	20	0.02	1.5	2	60	3.43
788	3.5101	$\frac{1}{2}^+$	200	0.20	1.5	2	20	1.12
799	3.5214	$\frac{1}{2}^+$	200	0.20	1.5	2	10	0.55
804	3.5249	$\frac{1}{2}^+$	90	0.09	1.5	2	20	1.08

Table B.3: ^{45}Sc Resonance Parameters–$J^\pi = \frac{1}{2}^-$

Res. #	E_p (MeV)	J^π	Γ_p (eV)	γ_p^2 (keV)	$s_{p'}$	$\ell'_{p'}$	$\Gamma_{p'}$ (eV)	$\gamma_{p'}^2$ (keV)
6	2.5104	$\frac{1}{2}^-$	30	0.23				
10	2.5186	$\frac{1}{2}^-$	30	0.23				
12	2.5205	$\frac{1}{2}^-$	70	0.52	1.5	1	5	2.54
19	2.5329	$\frac{1}{2}^-$	100	0.73	1.5	1	2	0.94
27	2.5587	$\frac{1}{2}^-$	15	0.10	1.5	1	5	2.03
28	2.5604	$\frac{1}{2}^-$	100	0.69				
31	2.5660	$\frac{1}{2}^-$	30	0.21				
45	2.5924	$\frac{1}{2}^-$	20	0.13				
50	2.6014	$\frac{1}{2}^-$	55	0.35				
57	2.6125	$\frac{1}{2}^-$	20	0.13	1.5	1	15	4.48
59	2.6171	$\frac{1}{2}^-$	400	2.47				
65	2.6260	$\frac{1}{2}^-$	350	2.12				
67	2.6324	$\frac{1}{2}^-$	175	1.05				
78	2.6492	$\frac{1}{2}^-$	240	1.40				
85	2.6570	$\frac{1}{2}^-$	150	0.86				
93	2.6681	$\frac{1}{2}^-$	200	1.12	1.5	1	8	1.78
97	2.6757	$\frac{1}{2}^-$	600	3.32				
114	2.7009	$\frac{1}{2}^-$	150	0.79	1.5	1	5	0.94
120	2.7129	$\frac{1}{2}^-$	125	0.65				
123	2.7215	$\frac{1}{2}^-$	15	0.08				
127	2.7289	$\frac{1}{2}^-$	190	0.96				
135	2.7423	$\frac{1}{2}^-$	30	0.15				
137	2.7470	$\frac{1}{2}^-$	275	1.34	1.5	1	8	1.20
148	2.7611	$\frac{1}{2}^-$	30	0.14	1.5	1	10	1.41
151	2.7660	$\frac{1}{2}^-$	450	2.12				
164	2.7842	$\frac{1}{2}^-$	45	0.21	1.5	1	5	0.63

‡ Identified as a fragment of the analog of the state in ^{45}Ca at E_x = 3.442 MeV.

Table B.3(*continued*)

Res. #	E_p (MeV)	J^π	Γ_p (eV)	γ_p^2 (keV)	s'	ℓ'	$\Gamma_{p'}$ (eV)	$\gamma_{p'}^2$ (keV)
169	2.7916	$\frac{1}{2}^-$	40	0.18				
177	2.8065	$\frac{1}{2}^-$	400	1.76	1.5	1	10	1.15
179	2.8082	$\frac{1}{2}^-$	50	0.22				
192	2.8284	$\frac{1}{2}^-$	70	0.30				
202	2.8425	$\frac{1}{2}^-$	175	0.73				
215	2.8598	$\frac{1}{2}^-$	10	0.04	1.5	1	10	0.91
223	2.8683	$\frac{1}{2}^-$	350	1.39	1.5	1	5	0.44
225	2.8703	$\frac{1}{2}^-$	10	0.04	1.5	1	5	0.44
232	2.8800	$\frac{1}{2}^-$	45	0.18	1.5	1	10	0.84
234	2.8842	$\frac{1}{2}^-$	160	0.62	1.5	1	5	0.41
236	2.8882	$\frac{1}{2}^-$	115	0.44	1.5	1	5	0.40
248	2.8995	$\frac{1}{2}^-$	60	0.23	1.5	1	10	0.77
254	2.9064	$\frac{1}{2}^-$	10	0.04	1.5	1	5	0.38
256	2.9084	$\frac{1}{2}^-$	40	0.15				
264	2.9273	$\frac{1}{2}^-$	40	0.15	1.5	1	15	1.03
272	2.9427	$\frac{1}{2}^-$	75	0.27	1.5	1	10	0.65
273	2.9467	$\frac{1}{2}^-$	50	0.18	1.5	1	15	0.96
277	2.9519	$\frac{1}{2}^-$	70	0.25	1.5	1	10	0.63
281	2.9567	$\frac{1}{2}^-$	150	0.52	1.5	1	10	0.62
296	2.9757	$\frac{1}{2}^-$	40	0.14	1.5	1	20	1.14
297	2.9771	$\frac{1}{2}^-$	50	0.17	1.5	1	2	0.11
301	2.9858	$\frac{1}{2}^-$	50	0.17	1.5	1	5	0.28
304	2.9891	$\frac{1}{2}^-$	100	0.33	1.5	1	10	0.54
314	3.0018	$\frac{1}{2}^-$	30	0.10	1.5	1	100	5.19
316	3.0042	$\frac{1}{2}^-$	1400	4.54	1.5	1	5	0.26
324	3.0127	$\frac{1}{2}^-$	250	0.80	1.5	1	20	1.00

‡ Identified as a fragment of the analog of the state in ^{45}Ca at $E_x = 3.442$ MeV.

Table B.3(*continued*)

Res. #	E_p (MeV)	J^π	Γ_p (eV)	γ_p^2 (keV)	s′	ℓ′	$\Gamma_{p'}$ (eV)	$\gamma_{p'}^2$ (keV)
327	3.0195	$\frac{1}{2}^-$	140	0.44	1.5	1	10	0.49
346	3.0362	$\frac{1}{2}^-$	230	0.71	1.5	1	5	0.23
348	3.0401	$\frac{1}{2}^-$	20	0.06	1.5	1	5	0.23
354	3.0507	$\frac{1}{2}^-$	20	0.06				
359	3.0569	$\frac{1}{2}^-$	50	0.15	1.5	1	50	2.13
383	3.0875	$\frac{1}{2}^-$	225	0.65	1.5	1	10	0.38
388	3.0944	$\frac{1}{2}^-$	30	0.09				
390	3.0969	$\frac{1}{2}^-$	25	0.07	1.5	1	10	0.37
394	3.1007	$\frac{1}{2}^-$	150	0.42				
398	3.1054	$\frac{1}{2}^-$	20	0.06	1.5	1	10	0.36
406	3.1161	$\frac{1}{2}^-$	100	0.28				
412	3.1239	$\frac{1}{2}^-$	15	0.04	1.5	1	40	1.36
426‡	3.1383	$\frac{1}{2}^-$	1500	4.04	1.5	1	50	1.62
430‡	3.1461	$\frac{1}{2}^-$	10	0.03	1.5	1	20	0.63
435‡	3.1548	$\frac{1}{2}^-$	50	0.13				
439‡	3.1576	$\frac{1}{2}^-$	100	0.26	1.5	1	20	0.61
447‡	3.1642	$\frac{1}{2}^-$	150	0.39	1.5	1	150	4.47
448‡	3.1649	$\frac{1}{2}^-$	40	0.10	1.5	1	25	0.74
452‡	3.1693	$\frac{1}{2}^-$	1250	3.23				
454‡	3.1707	$\frac{1}{2}^-$	350	0.90				
455‡	3.1720	$\frac{1}{2}^-$	60	0.15				
462‡	3.1798	$\frac{1}{2}^-$	500	1.27	1.5	1	50	1.42
469‡	3.1919	$\frac{1}{2}^-$	115	0.29	1.5	1	25	0.68
473‡	3.1947	$\frac{1}{2}^-$	1500	3.75	1.5	1	20	0.54
477‡	3.1992	$\frac{1}{2}^-$	40	0.10	1.5	1	100	2.67
485‡	3.2084	$\frac{1}{2}^-$	60	0.15	1.5	1	10	0.26

‡ Identified as a fragment of the analog of the state in ^{45}Ca at $E_x = 3.442$ MeV.

Table B.3(*continued*)

Res. #	E_p (MeV)	J^π	Γ_p (eV)	γ_p^2 (keV)	s'	ℓ'	$\Gamma_{p'}$ (eV)	$\gamma_{p'}^2$ (keV)
489‡	3.2112	$\frac{1}{2}^-$	500	1.22				
515‡	3.2324	$\frac{1}{2}^-$	3500	8.35				
519‡	3.2356	$\frac{1}{2}^-$	250	0.59				
526‡	3.2436	$\frac{1}{2}^-$	8000	18.81				
528‡	3.2457	$\frac{1}{2}^-$	150	0.35	1.5	1	80	1.85
529‡	3.2476	$\frac{1}{2}^-$	1750	4.10	1.5	1	50	1.15
549	3.2706	$\frac{1}{2}^-$	50	0.11	1.5	1	25	0.54
552	3.2746	$\frac{1}{2}^-$	300	0.68				
557	3.2782	$\frac{1}{2}^-$	400	0.90				
560	3.2816	$\frac{1}{2}^-$	350	0.79	1.5	1	10	0.21
570	3.2892	$\frac{1}{2}^-$	35	0.08				
574	3.2932	$\frac{1}{2}^-$	60	0.13				
605	3.3271	$\frac{1}{2}^-$	40	0.09				
613	3.3364	$\frac{1}{2}^-$	100	0.21				
632	3.3610	$\frac{1}{2}^-$	50	0.10	1.5	1	100	1.67
645	3.3711	$\frac{1}{2}^-$	30	0.06	1.5	1	15	0.24
646	3.3723	$\frac{1}{2}^-$	35	0.07	1.5	1	10	0.16
650	3.3760	$\frac{1}{2}^-$	20	0.04				
663	3.3890	$\frac{1}{2}^-$	30	0.06	1.5	1	30	0.47
665	3.3912	$\frac{1}{2}^-$	10	0.02	1.5	1	10	0.15
671	3.3970	$\frac{1}{2}^-$	20	0.04	1.5	1	20	0.30
677	3.4050	$\frac{1}{2}^-$	25	0.05				
689	3.4170	$\frac{1}{2}^-$	250	0.48	1.5	1	10	0.14
699	3.4278	$\frac{1}{2}^-$	25	0.05				
707	3.4332	$\frac{1}{2}^-$	35	0.07	1.5	1	35	0.49
709	3.4340	$\frac{1}{2}^-$	20	0.04	1.5	1	20	0.28

‡ Identified as a fragment of the analog of the state in ^{45}Ca at $E_x = 3.442$ MeV.

Table B.3(*continued*)

Res. #	E_p (MeV)	J^π	Γ_p (eV)	γ_p^2 (keV)	s'	ℓ'	$\Gamma_{p'}$ (eV)	$\gamma_{p'}^2$ (keV)
713	3.4411	$\frac{1}{2}^-$	50	0.09	1.5	1	100	1.36
715	3.4420	$\frac{1}{2}^-$	850	1.59	1.5	1	50	0.68
718	3.4465	$\frac{1}{2}^-$	150	0.28				
723	3.4502	$\frac{1}{2}^-$	100	0.19				
734	3.4613	$\frac{1}{2}^-$	100	0.18	1.5	1	10	0.13
737	3.4631	$\frac{1}{2}^-$	25	0.05				
744	3.4681	$\frac{1}{2}^-$	80	0.15	1.5	1	30	0.38
776	3.5000	$\frac{1}{2}^-$	700	1.23	1.5	1	25	0.29
783	3.5069	$\frac{1}{2}^-$	60	0.11				
801	3.5226	$\frac{1}{2}^-$	20	0.03				
806	3.5263	$\frac{1}{2}^-$	350	0.60	1.5	1	75	0.83
809	3.5320	$\frac{1}{2}^-$	60	0.10	1.5	1	60	0.65

‡ Identified as a fragment of the analog of the state in ^{45}Ca at $E_x = 3.442$ MeV.

Table B.4: ^{45}Sc Resonance Parameters–J$^{\pi}$ = $\frac{3}{2}^-$

Res. #	E_p (MeV)	J^{π}	Γ_p (eV)	γ_p^2 (keV)	s′	ℓ′	$\Gamma_{p'}$ (eV)	$\gamma_{p'}^2$ (keV)
5	2.5094	$\frac{3}{2}^-$	35	0.27	1.5	1	2	1.09
					2.5	1	3	1.63
15	2.5234	$\frac{3}{2}^-$	10	0.07				
21	2.5358	$\frac{3}{2}^-$	10	0.07	1.5	1	2	0.93
					2.5	1	2	0.93
22	2.5470	$\frac{3}{2}^-$	13	0.09				
26§	2.5559	$\frac{3}{2}^-$	150	1.04				
30§	2.5646	$\frac{3}{2}^-$	30	0.21				
33§	2.5676	$\frac{3}{2}^-$	50	0.34	1.5	1	2	0.77
					2.5	1	3	1.15
39§	2.5830	$\frac{3}{2}^-$	10	0.07				
43§	2.5884	$\frac{3}{2}^-$	70	0.46	1.5	1	5	1.71
					2.5	1	2	0.68
44§	2.5894	$\frac{3}{2}^-$	10	0.07				
46§	2.5927	$\frac{3}{2}^-$	55	0.36	1.5	1	5	1.67
49§	2.5987	$\frac{3}{2}^-$	30	0.19	1.5	1	5	1.61
					2.5	1	5	1.61
58§	2.6161	$\frac{3}{2}^-$	350	2.17	1.5	1	25	7.32
					2.5	1	20	5.86
61§	2.6217	$\frac{3}{2}^-$	75	0.46				
62§	2.6227	$\frac{3}{2}^-$	10	0.06				
63§	2.6239	$\frac{3}{2}^-$	200	1.22	1.5	1	25	7.02
					2.5	1	5	1.40
64§	2.6252	$\frac{3}{2}^-$	15	0.09				

§ Identified as a fragment of the analog of the state in ^{45}Ca at E_x = 2.842 MeV.

** Identified as a fragment of the analog of the state in ^{45}Ca at E_x = 3.241 MeV.

Table B.4(*continued*)

Res. #	E_p (MeV)	J^π	Γ_p (eV)	γ_p^2 (keV)	s′	ℓ′	$\Gamma_{p'}$ (eV)	$\gamma_{p'}^2$ (keV)
66§	2.6319	$\frac{3}{2}^-$	250	1.50	1.5	1	60	16.13
					2.5	1	30	8.07
68§	2.6333	$\frac{3}{2}^-$	30	0.18	1.5	1	10	2.67
72§	2.6402	$\frac{3}{2}^-$	30	0.18				
74§	2.6417	$\frac{3}{2}^-$	100	0.59	1.5	1	15	3.83
					2.5	1	15	3.83
75§	2.6451	$\frac{3}{2}^-$	40	0.23	1.5	1	10	2.51
					2.5	1	4	1.00
77§	2.6476	$\frac{3}{2}^-$	150	0.87				
82	2.6536	$\frac{3}{2}^-$	60	0.35	2.5	1	5	1.20
83	2.6561	$\frac{3}{2}^-$	35	0.20	1.5	1	2	0.47
					2.5	1	4	0.95
89	2.6636	$\frac{3}{2}^-$	20	0.11	1.5	1	20	4.55
95	2.6701	$\frac{3}{2}^-$	75	0.42	1.5	1	5	1.10
96	2.6723	$\frac{3}{2}^-$	10	0.06	1.5	1	10	2.18
104	2.6852	$\frac{3}{2}^-$	30	0.16	1.5	1	4	0.82
					2.5	1	3	0.61
105	2.6860	$\frac{3}{2}^-$	20	0.11				
111	2.6970	$\frac{3}{2}^-$	10	0.05	1.5	1	6	1.15
					2.5	1	5	0.96
115	2.7072	$\frac{3}{2}^-$	30	0.16				
119	2.7125	$\frac{3}{2}^-$	20	0.10				
126	2.7283	$\frac{3}{2}^-$	35	0.18	1.5	1	4	0.66
					2.5	1	1	0.17
129	2.7321	$\frac{3}{2}^-$	20	0.10	2.5	1	3	0.49

§ Identified as a fragment of the analog of the state in ^{45}Ca at E_x = 2.842 MeV.

** Identified as a fragment of the analog of the state in ^{45}Ca at E_x = 3.241 MeV.

Table B.4(*continued*)

Res. #	E_p (MeV)	J^π	Γ_p (eV)	γ_p^2 (keV)	s′	ℓ′	$\Gamma_{p'}$ (eV)	$\gamma_{p'}^2$ (keV)
130	2.7332	$\frac{3}{2}^-$	45	0.23	1.5	1	3	0.48
139	2.7491	$\frac{3}{2}^-$	10	0.05	2.5	1	3	0.45
142	2.7522	$\frac{3}{2}^-$	12	0.06				
146	2.7580	$\frac{3}{2}^-$	5	0.02	2.5	1	5	0.71
147	2.7592	$\frac{3}{2}^-$	5	0.02	2.5	1	5	0.71
160	2.7760	$\frac{3}{2}^-$	50	0.23	2.5	1	2	0.26
166	2.7892	$\frac{3}{2}^-$	35	0.16				
171	2.7953	$\frac{3}{2}^-$	25	0.11	1.5	1	10	1.20
					2.5	1	3	0.36
172	2.7965	$\frac{3}{2}^-$	30	0.13				
173	2.7983	$\frac{3}{2}^-$	25	0.11				
178	2.8073	$\frac{3}{2}^-$	85	0.37	1.5	1	3	0.34
					2.5	1	3	0.34
180	2.8111	$\frac{3}{2}^-$	15	0.07	1.5	1	5	0.56
					2.5	1	2	0.22
185	2.8188	$\frac{3}{2}^-$	5	0.02	2.5	1	5	0.54
186	2.8212	$\frac{3}{2}^-$	65	0.28				
187	2.8239	$\frac{3}{2}^-$	5	0.02	2.5	1	5	0.53
189	2.8248	$\frac{3}{2}^-$	45	0.19	1.5	1	4	0.42
					2.5	1	2	0.21
194	2.8299	$\frac{3}{2}^-$	8	0.03	1.5	1	8	0.83
					2.5	1	5	0.52
198	2.8347	$\frac{3}{2}^-$	10	0.04				
200	2.8377	$\frac{3}{2}^-$	15	0.06				
204	2.8445	$\frac{3}{2}^-$	120	0.50	2.5	1	3	0.29

§ Identified as a fragment of the analog of the state in ^{45}Ca at E_x = 2.842 MeV.

** Identified as a fragment of the analog of the state in ^{45}Ca at E_x = 3.241 MeV.

Table B.4(*continued*)

Res. #	E_p (MeV)	J^π	Γ_p (eV)	γ_p^2 (keV)	s′	ℓ′	$\Gamma_{p'}$ (eV)	$\gamma_{p'}^2$ (keV)
206	2.8476	$\frac{3}{2}^-$	30	0.12	1.5	1	12	1.15
					2.5	1	3	0.29
210	2.8528	$\frac{3}{2}^-$	10	0.04				
211	2.8543	$\frac{3}{2}^-$	15	0.06				
214	2.8591	$\frac{3}{2}^-$	30	0.12	1.5	1	10	0.91
					2.5	1	5	0.46
218	2.8634	$\frac{3}{2}^-$	5	0.02	2.5	1	5	0.45
219	2.8646	$\frac{3}{2}^-$	15	0.06	1.5	1	10	0.89
					2.5	1	8	0.71
221	2.8670	$\frac{3}{2}^-$	30	0.12	1.5	1	5	0.44
226	2.8718	$\frac{3}{2}^-$	8	0.03	2.5	1	5	0.43
229	2.8754	$\frac{3}{2}^-$	20	0.08	1.5	1	10	0.85
					2.5	1	5	0.43
243	2.8924	$\frac{3}{2}^-$	70	0.27	2.5	1	8	0.64
255	2.9082	$\frac{3}{2}^-$	5	0.02	2.5	1	10	0.74
258	2.9104	$\frac{3}{2}^-$	45	0.17				
260	2.9183	$\frac{3}{2}^-$	30	0.11	2.5	1	3	0.21
263	2.9251	$\frac{3}{2}^-$	5	0.02	2.5	1	2	0.14
280	2.9552	$\frac{3}{2}^-$	10	0.04	2.5	1	10	0.62
282	2.9575	$\frac{3}{2}^-$	30	0.10	1.5	1	1	0.06
					2.5	1	10	0.61
288	2.9652	$\frac{3}{2}^-$	125	0.43	1.5	1	10	0.60
					2.5	1	15	0.89
290	2.9672	$\frac{3}{2}^-$	10	0.03	1.5	1	15	0.89
					2.5	1	15	0.89

§ Identified as a fragment of the analog of the state in ^{45}Ca at E_x = 2.842 MeV.

** Identified as a fragment of the analog of the state in ^{45}Ca at E_x = 3.241 MeV.

Table B.4(*continued*)

Res. #	E_p (MeV)	J^π	Γ_p (eV)	γ_p^2 (keV)	s′	ℓ′	$\Gamma_{p'}$ (eV)	$\gamma_{p'}^2$ (keV)
303	2.9887	$\frac{3}{2}^-$	40	0.13	1.5	1	15	0.82
					2.5	1	5	0.27
317	3.0046	$\frac{3}{2}^-$	15	0.05	2.5	1	8	0.41
320	3.0103	$\frac{3}{2}^-$	40	0.13	2.5	1	15	0.75
325	3.0147	$\frac{3}{2}^-$	175	0.56	1.5	1	10	0.50
326	3.0166	$\frac{3}{2}^-$	20	0.06	1.5	1	10	0.49
					2.5	1	2	0.10
329	3.0204	$\frac{3}{2}^-$	50	0.16	1.5	1	1	0.05
					2.5	1	1	0.05
332	3.0221	$\frac{3}{2}^-$	10	0.03	1.5	1	10	0.48
					2.5	1	10	0.48
337	3.0277	$\frac{3}{2}^-$	50	0.16	1.5	1	3	0.14
					2.5	1	5	0.24
347	3.0391	$\frac{3}{2}^-$	12	0.04	1.5	1	30	1.36
357	3.0532	$\frac{3}{2}^-$	10	0.03	1.5	1	10	0.43
361	3.0588	$\frac{3}{2}^-$	15	0.05	1.5	1	10	0.42
					2.5	1	10	0.42
366	3.0645	$\frac{3}{2}^-$	27	0.08	2.5	1	20	0.83
367	3.0651	$\frac{3}{2}^-$	5	0.02	2.5	1	10	0.41
369	3.0662	$\frac{3}{2}^-$	5	0.02	2.5	1	30	1.24
370	3.0677	$\frac{3}{2}^-$	10	0.03	1.5	1	10	0.41
					2.5	1	7	0.29
377**	3.0805	$\frac{3}{2}^-$	150	0.44	1.5	1	5	0.20
					2.5	1	5	0.20
378**	3.0816	$\frac{3}{2}^-$	105	0.31	2.5	1	25	0.98

§ Identified as a fragment of the analog of the state in ^{45}Ca at $E_x = 2.842$ MeV.

** Identified as a fragment of the analog of the state in ^{45}Ca at $E_x = 3.241$ MeV.

Table B.4(*continued*)

Res. #	E_p (MeV)	J^π	Γ_p (eV)	γ_p^2 (keV)	s′	ℓ′	$\Gamma_{p'}$ (eV)	$\gamma_{p'}^2$ (keV)
382**	3.0863	$\frac{3}{2}^-$	225	0.65	1.5	1	10	0.39
387**	3.0930	$\frac{3}{2}^-$	450	1.29	1.5	1	70	2.63
					2.5	1	50	1.88
396**	3.1032	$\frac{3}{2}^-$	20	0.06	2.5	1	30	1.09
400**	3.1068	$\frac{3}{2}^-$	125	0.35	1.5	1	10	0.36
404**	3.1150	$\frac{3}{2}^-$	5	0.01	2.5	1	30	1.05
411	3.1234	$\frac{3}{2}^-$	60	0.17	1.5	1	8	0.27
					2.5	1	10	0.34
416	3.1298	$\frac{3}{2}^-$	10	0.03				
420	3.1332	$\frac{3}{2}^-$	30	0.11				
423	3.1352	$\frac{3}{2}^-$	5	0.01	2.5	1	5	0.16
424	3.1360	$\frac{3}{2}^-$	20	0.05				
431	3.1510	$\frac{3}{2}^-$	50	0.13	1.5	1	20	0.62
					2.5	1	70	2.17
433	3.1527	$\frac{3}{2}^-$	15	0.04	1.5	1	15	0.46
					2.5	1	10	0.31
438	3.1572	$\frac{3}{2}^-$	30	0.08	1.5	1	20	0.61
440	3.1581	$\frac{3}{2}^-$	75	0.20	1.5	1	100	3.04
					2.5	1	60	1.82
442	3.1596	$\frac{3}{2}^-$	100	0.26	1.5	1	10	0.30
					2.5	1	15	0.45
457	3.1731	$\frac{3}{2}^-$	100	0.26	2.5	1	15	0.43
458	3.1734	$\frac{3}{2}^-$	60	0.15				
463	3.1819	$\frac{3}{2}^-$	10	0.03	2.5	1	10	0.28
464	3.1846	$\frac{3}{2}^-$	40	0.10	2.5	1	8	0.22

§ Identified as a fragment of the analog of the state in ^{45}Ca at E_x = 2.842 MeV.

** Identified as a fragment of the analog of the state in ^{45}Ca at E_x = 3.241 MeV.

Table B.4(*continued*)

Res. #	E_p (MeV)	J^π	Γ_p (eV)	γ_p^2 (keV)	s′	ℓ′	$\Gamma_{p'}$ (eV)	$\gamma_{p'}^2$ (keV)
470	3.1923	$\frac{3}{2}^-$	15	0.04	2.5	1	15	0.41
482	3.2042	$\frac{3}{2}^-$	20	0.05	1.5	1	10	0.26
					2.5	1	40	1.05
486	3.2095	$\frac{3}{2}^-$	25	0.06	1.5	1	25	0.65
					2.5	1	15	0.39
490	3.2116	$\frac{3}{2}^-$	40	0.10	2.5	1	40	1.03
495	3.2160	$\frac{3}{2}^-$	20	0.05	2.5	1	10	0.25
498	3.2188	$\frac{3}{2}^-$	15	0.04	1.5	1	10	0.25
					2.5	1	10	0.25
502	3.2217	$\frac{3}{2}^-$	15	0.04	2.5	1	2	0.05
506	3.2252	$\frac{3}{2}^-$	30	0.07	1.5	1	5	0.12
					2.5	1	30	0.74
509	3.2274	$\frac{3}{2}^-$	10	0.02	1.5	1	30	0.73
					2.5	1	10	0.25
510	3.2285	$\frac{3}{2}^-$	25	0.06				
512	3.2301	$\frac{3}{2}^-$	75	0.18	1.5	1	30	0.73
525	3.2420	$\frac{3}{2}^-$	30	0.07	2.5	1	15	0.35
547	3.2689	$\frac{3}{2}^-$	20	0.05	1.5	1	15	0.33
					2.5	1	10	0.22
553	3.2751	$\frac{3}{2}^-$	20	0.05	1.5	1	40	0.85
					2.5	1	10	0.21
555	3.2768	$\frac{3}{2}^-$	15	0.03	1.5	1	30	0.64
					2.5	1	15	0.32
562	3.2840	$\frac{3}{2}^-$	10	0.02	1.5	1	10	0.21

§ Identified as a fragment of the analog of the state in ^{45}Ca at E_x = 2.842 MeV.

** Identified as a fragment of the analog of the state in ^{45}Ca at E_x = 3.241 MeV.

Table B.4(*continued*)

Res. #	E_p (MeV)	J^π	Γ_p (eV)	γ_p^2 (keV)	s′	ℓ′	$\Gamma_{p'}$ (eV)	$\gamma_{p'}^2$ (keV)
565	3.2857	$\frac{3}{2}^-$	10	0.02	1.5	1	10	0.21
					2.5	1	10	0.21
571	3.2913	$\frac{3}{2}^-$	30	0.07	1.5	1	10	0.20
					2.5	1	120	2.44
576	3.2982	$\frac{3}{2}^-$	50	0.11	1.5	1	20	0.40
					2.5	1	5	0.10
586	3.3062	$\frac{3}{2}^-$	8	0.02	2.5	1	10	0.20
592	3.3117	$\frac{3}{2}^-$	75	0.16	1.5	1	60	1.15
					2.5	1	50	0.96
595	3.3153	$\frac{3}{2}^-$	10	0.02	2.5	1	20	0.38
600	3.3227	$\frac{3}{2}^-$	60	0.13	1.5	1	15	0.28
					2.5	1	15	0.28
601	3.3237	$\frac{3}{2}^-$	50	0.11	1.5	1	20	0.37
					2.5	1	15	0.28
603	3.3248	$\frac{3}{2}^-$	15	0.03	2.5	1	10	0.19
604	3.3268	$\frac{3}{2}^-$	15	0.03	1.5	1	15	0.28
					2.5	1	15	0.28
606	3.3293	$\frac{3}{2}^-$	85	0.18	2.5	1	10	0.18
607	3.3308	$\frac{3}{2}^-$	30	0.06	1.5	1	40	0.73
					2.5	1	40	0.73
614	3.3372	$\frac{3}{2}^-$	15	0.03	1.5	1	10	0.18
624	3.3511	$\frac{3}{2}^-$	15	0.03	1.5	1	20	0.34
					2.5	1	5	0.09
626	3.3535	$\frac{3}{2}^-$	30	0.06	1.5	1	20	0.34
					2.5	1	10	0.17

§ Identified as a fragment of the analog of the state in ^{45}Ca at E_x = 2.842 MeV.

** Identified as a fragment of the analog of the state in ^{45}Ca at E_x = 3.241 MeV.

Table B.4(*continued*)

Res. #	E_p (MeV)	J^π	Γ_p (eV)	γ_p^2 (keV)	s′	ℓ′	$\Gamma_{p'}$ (eV)	$\gamma_{p'}^2$ (keV)
630	3.3584	$\frac{3}{2}^-$	15	0.03	2.5	1	10	0.17
647	3.3732	$\frac{3}{2}^-$	100	0.20	1.5	1	15	0.24
649	3.3754	$\frac{3}{2}^-$	10	0.02	2.5	1	10	0.16
651	3.3766	$\frac{3}{2}^+$	65	0.44	1.5	0	100	0.69
					2.5	2	100	8.26
653	3.3770	$\frac{3}{2}^-$	50	0.10	1.5	1	100	1.60
					2.5	1	80	1.28
657	3.3833	$\frac{3}{2}^-$	20	0.04	1.5	1	40	0.63
					2.5	1	25	0.39
667	3.3944	$\frac{3}{2}^-$	45	0.09	2.5	1	20	0.31
674	3.4035	$\frac{3}{2}^-$	75	0.15	1.5	1	75	1.12
					2.5	1	25	0.37
675	3.4038	$\frac{3}{2}^-$	25	0.05	1.5	1	50	0.75
678	3.4068	$\frac{3}{2}^-$	10	0.02	2.5	1	40	0.59
680	3.4089	$\frac{3}{2}^-$	15	0.03	2.5	1	10	0.15
682	3.4103	$\frac{3}{2}^-$	10	0.02	2.5	1	10	0.15
687	3.4150	$\frac{3}{2}^-$	20	0.04	1.5	1	30	0.44
					2.5	1	25	0.36
692	3.4204	$\frac{3}{2}^-$	10	0.02	1.5	1	20	0.29
694	3.4220	$\frac{3}{2}^-$	75	0.14	1.5	1	100	1.43
					2.5	1	100	1.43
710	3.4360	$\frac{3}{2}^-$	50	0.09	1.5	1	20	0.28
					2.5	1	20	0.28
714	3.4415	$\frac{3}{2}^-$	50	0.09	2.5	1	100	1.36
720	3.4488	$\frac{3}{2}^-$	50	0.09	1.5	1	20	0.27

§ Identified as a fragment of the analog of the state in ^{45}Ca at E_x = 2.842 MeV.

** Identified as a fragment of the analog of the state in ^{45}Ca at E_x = 3.241 MeV.

Table B.4(*continued*)

Res. #	E_p (MeV)	J^π	Γ_p (eV)	γ_p^2 (keV)	s′	ℓ′	$\Gamma_{p'}$ (eV)	$\gamma_{p'}^2$ (keV)
725	3.4555	$\frac{3}{2}^-$	80	0.15				
735	3.4617	$\frac{3}{2}^-$	50	0.09	1.5	1	40	0.52
					2.5	1	40	0.52
739	3.4651	$\frac{3}{2}^-$	20	0.04	2.5	1	35	0.45
741	3.4669	$\frac{3}{2}^-$	15	0.03	1.5	1	20	0.26
746	3.4702	$\frac{3}{2}^-$	10	0.02	1.5	1	10	0.13
751	3.4727	$\frac{3}{2}^-$	100	0.18	1.5	1	80	1.01
					2.5	1	80	1.01
752	3.4743	$\frac{3}{2}^-$	10	0.02	2.5	1	20	0.25
756	3.4773	$\frac{3}{2}^-$	30	0.05	2.5	1	10	0.12
758	3.4797	$\frac{3}{2}^-$	50	0.09	1.5	1	15	0.19
					2.5	1	15	0.19
761	3.4841	$\frac{3}{2}^-$	10	0.02	2.5	1	10	0.12
764	3.4862	$\frac{3}{2}^-$	30	0.05	1.5	1	100	1.22
					2.5	1	30	0.37
771	3.4961	$\frac{3}{2}^-$	25	0.04	2.5	1	50	0.59
772	3.4966	$\frac{3}{2}^-$	25	0.04	1.5	1	25	0.30
					2.5	1	100	1.19
778	3.5027	$\frac{3}{2}^-$	15	0.03	1.5	1	15	0.18
					2.5	1	15	0.18
779	3.5038	$\frac{3}{2}^-$	45	0.08	2.5	1	10	0.12
781	3.5042	$\frac{3}{2}^-$	20	0.04	2.5	1	20	0.23
785	3.5083	$\frac{3}{2}^-$	250	0.44	1.5	1	10	0.12
					2.5	1	25	0.29

§ Identified as a fragment of the analog of the state in ^{45}Ca at E_x = 2.842 MeV.

** Identified as a fragment of the analog of the state in ^{45}Ca at E_x = 3.241 MeV.

Table B.4(*continued*)

Res. #	E_p (MeV)	J^π	Γ_p (eV)	γ_p^2 (keV)	s′	ℓ'	$\Gamma_{p'}$ (eV)	$\gamma_{p'}^2$ (keV)
791	3.5138	$\frac{3}{2}^-$	50	0.09	1.5	1	20	0.23
					2.5	1	50	0.57
797	3.5196	$\frac{3}{2}^-$	10	0.02	2.5	1	10	0.11
803	3.5238	$\frac{3}{2}^-$	20	0.03	1.5	1	20	0.22
					2.5	1	30	0.33
808	3.5282	$\frac{3}{2}^-$	100	0.17	1.5	1	80	0.88
					2.5	1	120	1.32

§ Identified as a fragment of the analog of the state in ^{45}Ca at E_x = 2.842 MeV.

** Identified as a fragment of the analog of the state in ^{45}Ca at E_x = 3.241 MeV.

Table B.5: ^{45}Sc Resonance Parameters–J$^{\pi}$ = $\frac{3}{2}^{+}$

Res. #	E_p (MeV)	J^{π}	Γ_p (eV)	γ_p^2 (keV)	s′	ℓ′	$\Gamma_{p'}$ (eV)	$\gamma_{p'}^2$ (keV)
1	2.5014	$\frac{3}{2}^{+}$	4	0.14				
4	2.5045	$\frac{3}{2}^{+}$	15	0.53				
7	2.5141	$\frac{3}{2}^{+}$	5	0.17	1.5	0	1	0.19
8	2.5161	$\frac{3}{2}^{+}$	12	0.41	1.5	0	1	0.18
					2.5	2	1	3.69
11	2.5197	$\frac{3}{2}^{+}$	20	0.68	1.5	0	2	0.36
14	2.5233	$\frac{3}{2}^{+}$	10	0.34				
16	2.5263	$\frac{3}{2}^{+}$	17	0.57				
17	2.5306	$\frac{3}{2}^{+}$	10	0.33	1.5	0	2	0.34
					2.5	2	2	6.72
24	2.5512	$\frac{3}{2}^{+}$	40	1.27	1.5	0	2	0.30
					2.5	2	2	5.90
32	2.5670	$\frac{3}{2}^{+}$	15	0.46				
34	2.5685	$\frac{3}{2}^{+}$	10	0.30				
35	2.5711	$\frac{3}{2}^{+}$	25	0.76				
41	2.5848	$\frac{3}{2}^{+}$	10	0.29	1.5	0	5	0.62
56	2.6114	$\frac{3}{2}^{+}$	10	0.28	1.5	0	5	0.54
73	2.6408	$\frac{3}{2}^{+}$	25	0.65				
76	2.6460	$\frac{3}{2}^{+}$	25	0.64	1.5	0	8	0.72
84	2.6567	$\frac{3}{2}^{+}$	20	0.50	1.5	0	6	0.51
86	2.6577	$\frac{3}{2}^{+}$	25	0.62	1.5	0	5	0.43
87	2.6603	$\frac{3}{2}^{+}$	5	0.12				
88	2.6623	$\frac{3}{2}^{+}$	8	0.20				
92	2.6657	$\frac{3}{2}^{+}$	15	0.37	1.5	0	6	0.49
94	2.6692	$\frac{3}{2}^{+}$	15	0.36	1.5	0	15	1.21
99	2.6767	$\frac{3}{2}^{+}$	10	0.24	1.5	0	5	0.39

Table B.5(*continued*)

Res. #	E_p (MeV)	J^π	Γ_p (eV)	γ_p^2 (keV)	s′	ℓ′	$\Gamma_{p'}$ (eV)	$\gamma_{p'}^2$ (keV)
103	2.6838	$\frac{3}{2}^+$	10	0.24	1.5	0	2	0.15
					2.5	2	1	1.36
110	2.6926	$\frac{3}{2}^+$	40	0.92	1.5	0	2	0.14
116	2.7086	$\frac{3}{2}^+$	8	0.18	1.5	0	5	0.33
117	2.7104	$\frac{3}{2}^+$	13	0.29	1.5	0	5	0.66
118	2.7112	$\frac{3}{2}^+$	6	0.13	1.5	0	10	0.66
122	2.7189	$\frac{3}{2}^+$	5	0.11	1.5	0	3	0.19
128	2.7293	$\frac{3}{2}^+$	10	0.21	1.5	0	4	0.24
131	2.7358	$\frac{3}{2}^+$	10	0.21				
132	2.7381	$\frac{3}{2}^+$	9	0.19	1.5	0	6	0.35
133	2.7403	$\frac{3}{2}^+$	22	0.46	2.5	2	4	4.04
134	2.7417	$\frac{3}{2}^+$	5	0.10	1.5	0	5	0.29
136	2.7434	$\frac{3}{2}^+$	15	0.31	1.5	0	10	0.57
140	2.7496	$\frac{3}{2}^+$	8	0.16	1.5	0	5	0.28
141	2.7509	$\frac{3}{2}^+$	15	0.31				
144	2.7562	$\frac{3}{2}^+$	8	0.16				
153	2.7683	$\frac{3}{2}^+$	10	0.20	1.5	0	5	0.25
157	2.7700	$\frac{3}{2}^+$	35	0.68	1.5	0	5	0.25
158	2.7723	$\frac{3}{2}^+$	10	0.19	1.5	0	15	0.75
161	2.7766	$\frac{3}{2}^+$	20	0.39				
162	2.7788	$\frac{3}{2}^+$	12	0.23	1.5	0	6	0.29
165	2.7868	$\frac{3}{2}^+$	25	0.47	1.5	0	5	0.23
167	2.7895	$\frac{3}{2}^+$	5	0.09	1.5	0	5	0.23
168	2.7911	$\frac{3}{2}^+$	45	0.84	1.5	0	10	0.46
182	2.8131	$\frac{3}{2}^+$	20	0.36	1.5	0	7	0.29
183	2.8145	$\frac{3}{2}^+$	20	0.36	1.5	0	20	0.83
184	2.8174	$\frac{3}{2}^+$	5	0.09	1.5	0	4	0.16

Table B.5(*continued*)

Res. #	E_p (MeV)	J^π	Γ_p (eV)	γ_p^2 (keV)	s'	ℓ'	$\Gamma_{p'}$ (eV)	$\gamma_{p'}^2$ (keV)
190	2.8252	$\frac{3}{2}^+$	10	0.18				
191	2.8261	$\frac{3}{2}^+$	30	0.52	1.5	0	15	0.59
193	2.8291	$\frac{3}{2}^+$	10	0.17	1.5	0	5	0.20
195	2.8310	$\frac{3}{2}^+$	10	0.17				
197	2.8329	$\frac{3}{2}^+$	25	0.43				
203	2.8441	$\frac{3}{2}^+$	10	0.17	1.5	0	15	0.55
205	2.8458	$\frac{3}{2}^+$	5	0.08	1.5	0	5	0.18
208	2.8509	$\frac{3}{2}^+$	20	0.33	1.5	0	5	0.18
212	2.8563	$\frac{3}{2}^+$	15	0.25	1.5	0	10	0.35
					1.5	2	2	1.15
					2.5	2	2	1.15
216	2.8628	$\frac{3}{2}^+$	15	0.24	1.5	0	15	0.51
224	2.8687	$\frac{3}{2}^+$	10	0.16	1.5	0	5	0.17
230	2.8770	$\frac{3}{2}^+$	10	0.16	1.5	0	4	0.13
231	2.8792	$\frac{3}{2}^+$	15	0.24	1.5	0	10	0.32
233	2.8827	$\frac{3}{2}^+$	30	0.47	1.5	0	5	0.16
238	2.8902	$\frac{3}{2}^+$	10	0.15	1.5	0	3	0.09
241	2.8917	$\frac{3}{2}^+$	10	0.15	1.5	0	5	0.15
244	2.8929	$\frac{3}{2}^+$	5	0.08	1.5	0	3	0.09
245	2.8940	$\frac{3}{2}^+$	5	0.08	1.5	0	5	0.15
246	2.8970	$\frac{3}{2}^+$	22	0.33	1.5	0	5	0.15
249	2.9003	$\frac{3}{2}^+$	15	0.23	1.5	0	20	0.59
251	2.9033	$\frac{3}{2}^+$	15	0.23	1.5	0	12	0.35
252	2.9051	$\frac{3}{2}^+$	10	0.15				
257	2.9099	$\frac{3}{2}^+$	5	0.07	1.5	0	10	0.28
259	2.9143	$\frac{3}{2}^+$	4	0.06	1.5	0	5	0.14

Table B.5(*continued*)

Res. #	E_p (MeV)	J^π	Γ_p (eV)	γ_p^2 (keV)	s′	ℓ'	$\Gamma_{p'}$ (eV)	$\gamma_{p'}^2$ (keV)
262	2.9240	$\frac{3}{2}^+$	5	0.07	1.5	0	10	0.27
					2.5	2	10	4.24
269	2.9382	$\frac{3}{2}^+$	10	0.14	1.5	0	5	0.13
270	2.9401	$\frac{3}{2}^+$	7	0.10	1.5	0	5	0.13
274	2.9483	$\frac{3}{2}^+$	20	0.28	1.5	0	2	0.05
					2.5	2	2	0.76
275	2.9493	$\frac{3}{2}^+$	10	0.14	1.5	0	10	0.25
284	2.9599	$\frac{3}{2}^+$	5	0.97	1.5	2	10	3.64
285	2.9631	$\frac{3}{2}^+$	25	0.34	1.5	0	8	0.19
291	2.9698	$\frac{3}{2}^+$	13	0.17	1.5	0	2	0.05
300	2.9848	$\frac{3}{2}^+$	7	0.09	1.5	0	5	0.11
307	2.9920	$\frac{3}{2}^+$	20	0.25	1.5	0	15	0.32
310	2.9970	$\frac{3}{2}^+$	20	0.25	1.5	0	70	1.45
311	2.9979	$\frac{3}{2}^+$	10	0.13	1.5	0	5	0.10
315	3.0041	$\frac{3}{2}^+$	10	0.12				
328	3.0198	$\frac{3}{2}^+$	5	0.06	1.5	0	5	0.10
333	3.0238	$\frac{3}{2}^+$	30	0.36	2.5	2	10	2.80
335	3.0260	$\frac{3}{2}^+$	40	0.48	1.5	0	7	0.13
					2.5	2	7	1.95
339	3.0286	$\frac{3}{2}^+$	70	0.83	1.5	0	12	0.22
349	3.0421	$\frac{3}{2}^+$	5	0.06	1.5	0	20	0.36
350	3.0436	$\frac{3}{2}^+$	10	0.12				
356	3.0520	$\frac{3}{2}^+$	5	0.06	1.5	0	20	0.34
365	3.0638	$\frac{3}{2}^+$	35	0.39	1.5	0	10	0.17
371	3.0686	$\frac{3}{2}^+$	8	0.09	1.5	0	10	0.16
375	3.0760	$\frac{3}{2}^+$	35	0.38	1.5	0	2	0.03
379	3.0821	$\frac{3}{2}^+$	10	0.11	1.5	0	20	0.31

Table B.5(*continued*)

Res. #	E_p (MeV)	J^π	Γ_p (eV)	γ_p^2 (keV)	s′	ℓ′	$\Gamma_{p'}$ (eV)	$\gamma_{p'}^2$ (keV)
391	3.0978	$\frac{3}{2}^+$	10	0.11	1.5	0	20	0.30
392	3.0988	$\frac{3}{2}^+$	5	0.05	1.5	0	20	0.30
399	3.1058	$\frac{3}{2}^+$	12	0.13				
402	3.1088	$\frac{3}{2}^+$	10	0.10	1.5	0	20	0.29
405	3.1154	$\frac{3}{2}^+$	20	0.21				
407	3.1183	$\frac{3}{2}^+$	3	0.03	1.5	0	40	0.56
413	3.1274	$\frac{3}{2}^+$	5	0.05	1.5	0	10	0.14
418	3.1307	$\frac{3}{2}^+$	25	0.25				
419	3.1390	$\frac{3}{2}^+$	10	0.10	1.5	0	2	0.03
429	3.1445	$\frac{3}{2}^+$	50	0.49	1.5	0	35	0.45
434	3.1545	$\frac{3}{2}^+$	20	0.19	1.5	0	40	0.50
437	3.1563	$\frac{3}{2}^+$	25	0.24				
443	3.1611	$\frac{3}{2}^+$	25	0.24				
446	3.1636	$\frac{3}{2}^+$	15	0.14				
453	3.1702	$\frac{3}{2}^+$	25	0.23	1.5	0	25	0.30
456	3.1728	$\frac{3}{2}^+$	70	0.65	1.5	0	30	0.37
466	3.1859	$\frac{3}{2}^+$	15	0.14				
468	3.1907	$\frac{3}{2}^+$	25	0.23	1.5	0	40	0.45
472	3.1939	$\frac{3}{2}^+$	15	0.14	1.5	0	10	0.11
476	3.1962	$\frac{3}{2}^+$	100	0.90	1.5	0	10	0.11
480	3.2024	$\frac{3}{2}^+$	10	0.09	1.5	0	10	0.11
487	3.2101	$\frac{3}{2}^+$	15	0.13	1.5	0	50	0.53
488	3.2110	$\frac{3}{2}^+$	10	0.09	1.5	0	10	0.11
494	3.2149	$\frac{3}{2}^+$	70	0.61	1.5	0	70	0.74
503	3.2226	$\frac{3}{2}^+$	10	0.09	1.5	0	5	0.05
514	3.2317	$\frac{3}{2}^+$	30	0.25	1.5	0	50	0.50
516	3.2334	$\frac{3}{2}^+$	10	0.09	1.5	0	10	0.10

Table B.5(*continued*)

Res. #	E_p (MeV)	J^π	Γ_p (eV)	γ_p^2 (keV)	s′	ℓ′	$\Gamma_{p'}$ (eV)	$\gamma_{p'}^2$ (keV)
518	3.2351	$\frac{3}{2}^+$	20	0.17	1.5	0	5	0.05
531	3.2500	$\frac{3}{2}^+$	10	0.08	1.5	0	10	0.10
535	3.2528	$\frac{3}{2}^+$	5	0.04	1.5	0	10	0.10
536	3.2537	$\frac{3}{2}^+$	40	0.33				
537	3.2550	$\frac{3}{2}^+$	10	0.08	1.5	0	10	0.09
542	3.2601	$\frac{3}{2}^+$	15	0.12				
545	3.2630	$\frac{3}{2}^+$	13	0.11	1.5	0	30	0.28
548	3.2695	$\frac{3}{2}^+$	25	0.20	1.5	0	15	0.14
551	3.2716	$\frac{3}{2}^+$	15	0.12	1.5	0	30	0.27
554	3.2759	$\frac{3}{2}^+$	30	0.24	2.5	2	20	2.26
558	3.2785	$\frac{3}{2}^+$	10	0.08	2.5	2	10	1.12
569	3.2885	$\frac{3}{2}^+$	20	0.16	1.5	0	5	0.04
573	3.2926	$\frac{3}{2}^+$	10	0.08	1.5	0	2	0.02
575	3.2955	$\frac{3}{2}^+$	10	0.08	1.5	0	30	0.25
579	3.3026	$\frac{3}{2}^+$	25	0.19	1.5	0	10	0.08
581	3.3034	$\frac{3}{2}^+$	35	0.27				
583	3.3046	$\frac{3}{2}^+$	15	0.11	2.5	2	20	2.06
587	3.3067	$\frac{3}{2}^+$	8	0.06	1.5	0	10	0.08
588	3.3082	$\frac{3}{2}^+$	25	0.19	2.5	2	5	0.51
590	3.3097	$\frac{3}{2}^+$	10	0.08	1.5	0	10	0.08
591	3.3106	$\frac{3}{2}^+$	5	0.04	1.5	0	5	0.04
593	3.3139	$\frac{3}{2}^+$	30	0.22	1.5	0	15	0.12
597	3.3182	$\frac{3}{2}^+$	10	0.07	1.5	0	10	0.08
598	3.3190	$\frac{3}{2}^+$	5	0.04	2.5	2	15	1.48
615	3.3397	$\frac{3}{2}^+$	20	0.14	1.5	0	5	0.04
					2.5	2	10	0.92
616	3.3407	$\frac{3}{2}^+$	5	0.04	1.5	0	50	0.38

Table B.5(*continued*)

Res. #	E_p (MeV)	J^π	Γ_p (eV)	γ_p^2 (keV)	s′	ℓ′	$\Gamma_{p'}$ (eV)	$\gamma_{p'}^2$ (keV)
617	3.3429	$\frac{3}{2}^+$	50	0.36	1.5	0	10	0.08
620	3.3469	$\frac{3}{2}^+$	15	0.11	1.5	0	30	0.22
622	3.3495	$\frac{3}{2}^+$	50	0.35	1.5	0	10	0.07
					2.5	2	10	0.90
627	3.3539	$\frac{3}{2}^+$	25	0.18	1.5	0	50	0.37
631	3.3609	$\frac{3}{2}^+$	15	0.10	1.5	0	8	0.06
					2.5	2	15	1.30
633	3.3626	$\frac{3}{2}^+$	50	0.35				
636	3.3637	$\frac{3}{2}^+$	15	0.10				
639	3.3686	$\frac{3}{2}^+$	30	0.21				
643	3.3703	$\frac{3}{2}^+$	15	0.10	1.5	0	10	0.07
648	3.3743	$\frac{3}{2}^+$	35	0.24	1.5	0	20	0.14
656	3.3819	$\frac{3}{2}^+$	30	0.20	1.5	0	5	0.03
					2.5	2	20	1.63
658	3.3851	$\frac{3}{2}^+$	50	0.34	2.5	2	20	1.61
661	3.3866	$\frac{3}{2}^+$	10	0.07	1.5	0	10	0.07
666	3.3932	$\frac{3}{2}^+$	5	0.03	1.5	0	5	0.03
668	3.3946	$\frac{3}{2}^+$	20	0.13	2.5	2	20	1.56
669	3.3955	$\frac{3}{2}^+$	15	0.10	2.5	2	15	1.17
673	3.3997	$\frac{3}{2}^+$	15	0.10	1.5	0	20	0.13
676	3.4042	$\frac{3}{2}^+$	40	0.26	1.5	0	100	0.65
679	3.4077	$\frac{3}{2}^+$	10	0.07	1.5	0	5	0.03
683	3.4116	$\frac{3}{2}^+$	20	0.13	1.5	0	30	0.19
693	3.4214	$\frac{3}{2}^+$	10	0.06	1.5	0	10	0.06
697	3.4263	$\frac{3}{2}^+$	60	0.38	1.5	0	30	0.18

Table B.5(*continued*)

Res. #	E_p (MeV)	J^π	Γ_p (eV)	γ_p^2 (keV)	s′	ℓ′	$\Gamma_{p'}$ (eV)	$\gamma_{p'}^2$ (keV)
700	3.4284	$\frac{3}{2}^+$	200	1.26	1.5	0	30	0.18
					1.5	2	30	2.12
					2.5	2	60	4.25
703	3.4314	$\frac{3}{2}^+$	40	0.25	1.5	0	10	0.06
705	3.4324	$\frac{3}{2}^+$	20	0.13	1.5	0	20	0.12
708	3.4336	$\frac{3}{2}^+$	14	0.09				
717	3.4458	$\frac{3}{2}^+$	10	0.06	1.5	0	10	0.06
724	3.4547	$\frac{3}{2}^+$	80	0.49	1.5	0	25	0.14
730	3.4598	$\frac{3}{2}^+$	50	0.30	1.5	0	25	0.14
732	3.4605	$\frac{3}{2}^+$	30	0.18	1.5	0	5	0.03
736	3.4629	$\frac{3}{2}^+$	20	0.12	1.5	0	5	0.03
740	3.4658	$\frac{3}{2}^+$	10	0.06	1.5	0	10	0.06
743	3.4677	$\frac{3}{2}^+$	10	0.06				
745	3.4694	$\frac{3}{2}^+$	300	1.79	1.5	0	60	0.34
					2.5	2	20	1.26
747	3.4706	$\frac{3}{2}^+$	50	0.30				
749	3.4714	$\frac{3}{2}^+$	30	0.18	1.5	0	5	0.03
753	3.4750	$\frac{3}{2}^+$	100	0.59	1.5	0	80	0.44
757	3.4786	$\frac{3}{2}^+$	100	0.59	1.5	0	100	0.55
					2.5	2	10	0.61
760	3.4828	$\frac{3}{2}^+$	80	0.47	1.5	0	50	0.27
763	3.4849	$\frac{3}{2}^+$	10	0.06	1.5	0	10	0.05
766	3.4894	$\frac{3}{2}^+$	10	0.06	1.5	0	10	0.05
770	3.4932	$\frac{3}{2}^+$	10	0.06	1.5	0	10	0.05
773	3.4974	$\frac{3}{2}^+$	30	0.17				
777	3.5014	$\frac{3}{2}^+$	10	0.06	1.5	0	15	0.08
782	3.5054	$\frac{3}{2}^+$	40	0.23	2.5	2	25	1.42

Table B.5(*continued*)

Res. #	E_p (MeV)	J^π	Γ_p (eV)	γ_p^2 (keV)	s′	ℓ′	$\Gamma_{p'}$ (eV)	$\gamma_{p'}^2$ (keV)
790	3.5124	$\frac{3}{2}^+$	10	0.06	1.5	0	50	0.25
793	3.5147	$\frac{3}{2}^+$	12	0.08	1.5	0	30	0.15
794	3.5165	$\frac{3}{2}^+$	25	0.14	1.5	0	40	0.20
795	3.5181	$\frac{3}{2}^+$	10	0.06	1.5	0	10	0.05
796	3.5187	$\frac{3}{2}^+$	25	0.14	1.5	0	25	0.13
798	3.5208	$\frac{3}{2}^+$	150	0.83	1.5	0	15	0.08
					2.5	2	10	0.55
800	3.5222	$\frac{3}{2}^+$	10	0.06	1.5	0	10	0.05

Table B.6: ^{45}Sc Resonance Parameters–J$^{\pi}$ = $\frac{5}{2}^{+}$

Res. #	E_p (MeV)	J^{π}	Γ_p (eV)	γ_p^2 (keV)	s'	ℓ'	$\Gamma_{p'}$ (eV)	$\gamma_{p'}^2$ (keV)
3	2.5037	$\frac{5}{2}^{+}$	3	0.11	2.5	0	2	0.40
18	2.5315	$\frac{5}{2}^{+}$	5	0.17	2.5	0	4	0.67
23	2.5476	$\frac{5}{2}^{+}$	10	0.32				
38	2.5798	$\frac{5}{2}^{+}$	10	0.30				
48	2.5968	$\frac{5}{2}^{+}$	10	0.29				
52	2.6038	$\frac{5}{2}^{+}$	35	0.98	2.5	0	4	0.45
55	2.6059	$\frac{5}{2}^{+}$	5	0.14				
90	2.6642	$\frac{5}{2}^{+}$	20	0.49	2.5	0	2	0.17
106	2.6874	$\frac{5}{2}^{+}$	10	0.23	2.5	0	5	0.37
113	2.7002	$\frac{5}{2}^{+}$	20	0.45				
150	2.7627	$\frac{5}{2}^{+}$	22	0.44	1.5	2	1	0.90
					2.5	0	3	0.16
					2.5	2	1	0.90
155	2.7692	$\frac{5}{2}^{+}$	20	0.39				
163	2.7809	$\frac{5}{2}^{+}$	5	0.10				
170	2.7940	$\frac{5}{2}^{+}$	45	0.84	2.5	0	2	0.09
175	2.8008	$\frac{5}{2}^{+}$	45	0.83	2.5	0	2	0.09
207	2.8492	$\frac{5}{2}^{+}$	45	0.75	1.5	2	2	1.19
					2.5	0	5	0.18
					2.5	2	2	1.19
213	2.8571	$\frac{5}{2}^{+}$	5	0.08				
228	2.8745	$\frac{5}{2}^{+}$	10	0.16				
239	2.8905	$\frac{5}{2}^{+}$	25	0.38				
247	2.8989	$\frac{5}{2}^{+}$	5	0.08				
266	2.9321	$\frac{5}{2}^{+}$	10	0.14				
268	2.9351	$\frac{5}{2}^{+}$	50	0.71	2.5	0	8	0.21

Table B.6(*continued*)

Res. #	E_p (MeV)	J^π	Γ_p (eV)	γ_p^2 (keV)	s′	ℓ′	$\Gamma_{p'}$ (eV)	$\gamma_{p'}^2$ (keV)
278	2.9531	$\frac{5}{2}^+$	12	0.16	1.5	2	1	0.37
289	2.9662	$\frac{5}{2}^+$	5	0.07	1.5	2	3	1.06
293	2.9734	$\frac{5}{2}^+$	5	0.07	2.5	0	5	0.11
295	2.9750	$\frac{5}{2}^+$	10	0.13	1.5	2	3	1.03
					2.5	0	4	0.09
299	2.9830	$\frac{5}{2}^+$	50	0.65	2.5	0	30	0.65
302	2.9876	$\frac{5}{2}^+$	12	0.15	2.5	0	7	0.15
305	2.9902	$\frac{5}{2}^+$	10	0.13	2.5	0	25	0.53
308	2.9933	$\frac{5}{2}^+$	12	0.15	2.5	0	5	0.20
313	3.0007	$\frac{5}{2}^+$	15	0.19	2.5	0	2	0.04
319	3.0100	$\frac{5}{2}^+$	15	0.19	2.5	0	15	0.30
321	3.0115	$\frac{5}{2}^+$	70	0.86	2.5	2	10	2.94
322	3.0124	$\frac{5}{2}^+$	10	0.12	2.5	0	15	0.30
331	3.0215	$\frac{5}{2}^+$	5	0.06	2.5	0	2	0.04
334	3.0251	$\frac{5}{2}^+$	20	0.24	1.5	2	2	0.56
338	3.0282	$\frac{5}{2}^+$	25	0.30	2.5	0	6	0.11
340	3.0304	$\frac{5}{2}^+$	20	0.24	2.5	0	15	0.28
345	3.0358	$\frac{5}{2}^+$	10	0.12	2.5	0	10	0.18
352	3.0481	$\frac{5}{2}^+$	18	0.21	2.5	0	8	0.14
355	3.0514	$\frac{5}{2}^+$	17	0.20	2.5	0	10	0.17
360	3.0573	$\frac{5}{2}^+$	30	0.34				
364	3.0627	$\frac{5}{2}^+$	3	0.03	2.5	0	3	0.05
373	3.0739	$\frac{5}{2}^+$	25	0.28	2.5	0	10	0.16
384	3.0883	$\frac{5}{2}^+$	15	0.16				
385	3.0892	$\frac{5}{2}^+$	30	0.32	2.5	0	10	0.15
386	3.0927	$\frac{5}{2}^+$	5	0.05				
393	3.0996	$\frac{5}{2}^+$	45	0.47	2.5	0	5	0.07

Table B.6(*continued*)

Res. #	E_p (MeV)	J^π	Γ_p (eV)	γ_p^2 (keV)	s′	ℓ′	$\Gamma_{p'}$ (eV)	$\gamma_{p'}^2$ (keV)
397	3.1048	$\frac{5}{2}^+$	5	0.05	2.5	0	10	0.15
401	3.1086	$\frac{5}{2}^+$	5	0.05	2.5	0	10	0.14
414	3.1287	$\frac{5}{2}^+$	5	0.05	2.5	0	10	0.14
421	3.1336	$\frac{5}{2}^+$	5	0.05	2.5	0	30	0.40
428	3.1433	$\frac{5}{2}^+$	20	0.20	2.5	0	5	0.07
441	3.1595	$\frac{5}{2}^+$	20	0.19				
449	3.1656	$\frac{5}{2}^+$	20	0.19	2.5	0	20	0.24
460	3.1743	$\frac{5}{2}^+$	75	0.70	2.5	0	20	0.24
461	3.1771	$\frac{5}{2}^+$	75	0.69	2.5	0	40	0.47
467	3.1864	$\frac{5}{2}^+$	15	0.14	2.5	0	40	0.46
481	3.2030	$\frac{5}{2}^+$	18	0.16				
484	3.2067	$\frac{5}{2}^+$	15	0.13	2.5	0	10	0.11
492	3.2137	$\frac{5}{2}^+$	10	0.09				
499	3.2194	$\frac{5}{2}^+$	10	0.09	2.5	0	5	0.05
501	3.2211	$\frac{5}{2}^+$	40	0.35	2.5	0	2	0.02
504	3.2238	$\frac{5}{2}^+$	15	0.13	2.5	0	5	0.05
505	3.2249	$\frac{5}{2}^+$	10	0.09				
507	3.2261	$\frac{5}{2}^+$	8	0.07	1.5	2	2	0.27
511	3.2291	$\frac{5}{2}^+$	50	0.43	2.5	0	35	0.35
520	3.2363	$\frac{5}{2}^+$	40	0.34	2.5	0	20	0.20
523	3.2406	$\frac{5}{2}^+$	10	0.08	2.5	0	20	0.20
524	3.2414	$\frac{5}{2}^+$	30	0.25	2.5	0	8	0.08
532	3.2508	$\frac{5}{2}^+$	2	0.02	1.5	2	5	0.62
538	3.2557	$\frac{5}{2}^+$	10	0.08	2.5	0	20	0.19
541	3.2592	$\frac{5}{2}^+$	5	0.04	2.5	0	5	0.05
544	3.2606	$\frac{5}{2}^+$	15	0.12				
556	3.2775	$\frac{5}{2}^+$	25	0.20	2.5	0	50	0.44

Table B.6(*continued*)

Res. #	E_p (MeV)	J^π	Γ_p (eV)	γ_p^2 (keV)	s'	ℓ'	$\Gamma_{p'}$ (eV)	$\gamma_{p'}^2$ (keV)
561	3.2824	$\frac{5}{2}^+$	5	0.04	2.5	0	20	0.18
563	3.2845	$\frac{5}{2}^+$	10	0.08	2.5	0	10	0.09
566	3.2868	$\frac{5}{2}^+$	5	0.04	1.5	2	5	0.55
577	3.2992	$\frac{5}{2}^+$	15	0.12	1.5	2	2	0.21
582	3.3038	$\frac{5}{2}^+$	8	0.06	2.5	0	5	0.04
					2.5	2	20	2.07
585	3.3055	$\frac{5}{2}^+$	14	0.11	2.5	0	10	0.08
599	3.3199	$\frac{5}{2}^+$	15	0.11	2.5	0	3	0.02
609	3.3327	$\frac{5}{2}^+$	20	0.15	2.5	0	30	0.23
610	3.3342	$\frac{5}{2}^+$	15	0.11	2.5	0	5	0.04
612	3.3363	$\frac{5}{2}^+$	50	0.36	2.5	0	4	0.03
618	3.3458	$\frac{5}{2}^+$	20	0.14	2.5	2	10	0.91
621	3.3483	$\frac{5}{2}^+$	5	0.04	2.5	0	20	0.15
629	3.3571	$\frac{5}{2}^+$	100	0.70	1.5	2	10	0.88
					2.5	0	5	0.04
					2.5	2	-20	1.75
635	3.3633	$\frac{5}{2}^+$	14	0.10				
637	3.3643	$\frac{5}{2}^+$	5	0.04	2.5	0	10	0.07
638	3.3660	$\frac{5}{2}^+$	10	0.07	2.5	0	5	0.04
642	3.3696	$\frac{5}{2}^+$	10	0.07	1.5	2	2	0.17
644	3.3708	$\frac{5}{2}^+$	5	0.03	2.5	0	5	0.04
662	3.3882	$\frac{5}{2}^+$	40	0.27	2.5	2	2	0.16
670	3.3968	$\frac{5}{2}^+$	40	0.26	2.5	0	10	0.07
684	3.4126	$\frac{5}{2}^+$	15	0.10	1.5	2	30	2.23
					2.5	0	30	0.19
686	3.4135	$\frac{5}{2}^+$	80	0.52	2.5	0	10	0.06
691	3.4195	$\frac{5}{2}^+$	20	0.13	2.5	0	20	0.13

Table B.6(*continued*)

Res. #	E_p (MeV)	J^π	Γ_p (eV)	γ_p^2 (keV)	s'	ℓ'	$\Gamma_{p'}$ (eV)	$\gamma_{p'}^2$ (keV)
696	3.4257	$\frac{5}{2}^+$	40	0.25	2.5	0	5	0.03
706	3.4329	$\frac{5}{2}^+$	15	0.09				
711	3.4365	$\frac{5}{2}^+$	17	0.11	2.5	0	15	0.09
712	3.4376	$\frac{5}{2}^+$	10	0.06	2.5	0	40	0.24
716	3.4425	$\frac{5}{2}^+$	10	0.06	2.5	0	8	0.05
722	3.4496	$\frac{5}{2}^+$	10	0.06				
727	3.4559	$\frac{5}{2}^+$	40	0.24	2.5	0	10	0.96
728	3.4578	$\frac{5}{2}^+$	10	0.06	2.5	0	5	0.03
					2.5	2	5	0.33
738	3.4641	$\frac{5}{2}^+$	20	0.12	2.5	0	200	1.13
755	3.4761	$\frac{5}{2}^+$	10	0.06	2.5	0	10	0.06
762	3.4845	$\frac{5}{2}^+$	35	0.20	2.5	0	5	0.03
765	3.4876	$\frac{5}{2}^+$	20	0.12	2.5	0	30	0.16
					2.5	1	10	0.12
768	3.4922	$\frac{5}{2}^+$	10	0.06	2.5	0	30	0.16
775	3.4984	$\frac{5}{2}^+$	15	0.09	2.5	0	5	0.03
					2.5	2	10	0.58
784	3.5075	$\frac{5}{2}^+$	100	0.57	2.5	0	80	0.41
787	3.5096	$\frac{5}{2}^+$	10	0.06	2.5	0	10	0.05
789	3.5108	$\frac{5}{2}^+$	10	0.06	2.5	0	10	0.05
805	3.5263	$\frac{5}{2}^+$	5	0.03	2.5	0	5	0.03
807	3.5276	$\frac{5}{2}^+$	15	0.08	1.5	2	20	1.07

Table B.7: ^{45}Sc Resonance Parameters–J$^{\pi}$ = $\frac{5}{2}^{-}$

Res. #	E_p (MeV)	J^{π}	Γ_p (eV)	γ_p^2 (keV)	s′	ℓ′	$\Gamma_{p'}$ (eV)	$\gamma_{p'}^2$ (keV)
2	2.5022	$\frac{5}{2}^{-}$	3	0.65	1.5	1	2	1.14
					2.5	1	2	1.14
36	2.5770	$\frac{5}{2}^{-}$	4	1.04				
53	2.6043	$\frac{5}{2}^{-}$	2	0.48				
54	2.6051	$\frac{5}{2}^{-}$	2	0.48				
69	2.6335	$\frac{5}{2}^{-}$	5	1.12				
71	2.6361	$\frac{5}{2}^{-}$	5	1.11	1.5	1	3	0.79
80	2.6516	$\frac{5}{2}^{-}$	5	1.07	1.5	1	2	0.48
91	2.6650	$\frac{5}{2}^{-}$	5	1.03	1.5	1	4	0.90
102	2.6829	$\frac{5}{2}^{-}$	5	0.98				
109	2.6917	$\frac{5}{2}^{-}$	2	0.39				
124	2.7227	$\frac{5}{2}^{-}$	3	0.53				
145	2.7573	$\frac{5}{2}^{-}$	3	0.39	1.5	1	5	0.72
149	2.7616	$\frac{5}{2}^{-}$	3	0.49	1.5	1	2	0.28
152	2.7665	$\frac{5}{2}^{-}$	10	1.60				
156	2.7695	$\frac{5}{2}^{-}$	8	1.27				
188	2.8236	$\frac{5}{2}^{-}$	3	0.42				
199	2.8362	$\frac{5}{2}^{-}$	5	0.68	1.5	1	2	0.20
					2.5	1	6	0.20
201	2.8380	$\frac{5}{2}^{-}$	3	0.40	1.5	1	5	0.50
217	2.8629	$\frac{5}{2}^{-}$	5	0.64				
220	2.8652	$\frac{5}{2}^{-}$	3	0.38	1.5	1	2	0.18
235	2.8862	$\frac{5}{2}^{-}$	3	0.36				
240	2.8908	$\frac{5}{2}^{-}$	5	0.60	1.5	1	2	0.16
					2.5	1	2	0.16

All observed f-wave resonances are arbitrarily assigned J = $\frac{5}{2}$.

Table B.7(*continued*)

Res. #	E_p (MeV)	J^π	Γ_p (eV)	γ_p^2 (keV)	s'	ℓ'	$\Gamma_{p'}$ (eV)	$\gamma_{p'}^2$ (keV)
253	2.9052	$\frac{5}{2}^-$	15	1.73	1.5	1	5	0.38
					2.5	1	10	0.75
261	2.9201	$\frac{5}{2}^-$	2	0.22	1.5	1	2	0.14
286	2.9644	$\frac{5}{2}^-$	8	0.81	1.5	1	8	0.48
292	2.9725	$\frac{5}{2}^-$	5	0.50	1.5	1	10	0.58
					2.5	1	5	0.29
298	2.9783	$\frac{5}{2}^-$	8	0.79	2.5	1	5	0.28
312	2.9999	$\frac{5}{2}^-$	4	0.38	1.5	1	5	0.26
323	3.0126	$\frac{5}{2}^-$	10	0.91				
341	3.0315	$\frac{5}{2}^-$	10	0.88	2.5	1	5	0.23
343	3.0339	$\frac{5}{2}^-$	10	0.87	1.5	1	20	0.92
					2.5	1	20	0.92
362	3.0589	$\frac{5}{2}^-$	4	0.33				
363	3.0609	$\frac{5}{2}^-$	4	0.33	1.5	1	5	0.21
					2.5	1	20	0.84
376	3.0768	$\frac{5}{2}^-$	5	0.40	2.5	1	2	0.08
380	3.0826	$\frac{5}{2}^-$	10	0.79	1.5	1	3	0.12
389	3.0955	$\frac{5}{2}^-$	5	0.38	1.5	1	10	0.37
					2.5	1	10	0.37
410	3.1232	$\frac{5}{2}^-$	10	0.72				
417	3.1302	$\frac{5}{2}^-$	5	0.36	1.5	1	10	0.33
427	3.1413	$\frac{5}{2}^-$	5	0.35	2.5	1	5	0.16
432	3.1519	$\frac{5}{2}^-$	6	0.41	1.5	1	5	0.16
					2.5	1	10	0.46
450	3.1671	$\frac{5}{2}^-$	10	0.66	1.5	1	25	0.74
451	3.1681	$\frac{5}{2}^-$	15	0.99	1.5	1	40	1.18

All observed f-wave resonances are arbitrarily assigned J = $\frac{5}{2}$.

Table B.7(*continued*)

Res. #	E_p (MeV)	J^π	Γ_p (eV)	γ_p^2 (keV)	s′	ℓ′	$\Gamma_{p'}$ (eV)	$\gamma_{p'}^2$ (keV)
475	3.1956	$\frac{5}{2}^-$	20	1.25				
479	3.2011	$\frac{5}{2}^-$	10	0.62				
491	3.2120	$\frac{5}{2}^-$	10	0.61	1.5	1	20	0.51
493	3.2146	$\frac{5}{2}^-$	20	1.21	1.5	1	20	0.51
497	3.2175	$\frac{5}{2}^-$	15	0.90				
500	3.2203	$\frac{5}{2}^-$	2	0.12	1.5	1	5	0.13
513	3.2311	$\frac{5}{2}^-$	5	0.29				
521	3.2365	$\frac{5}{2}^-$	20	1.16				
527	3.2445	$\frac{5}{2}^-$	15	0.85	2.5	1	5	0.12
533	3.2517	$\frac{5}{2}^-$	30	1.69				
539	3.2576	$\frac{5}{2}^-$	10	0.56	1.5	1	10	0.22
540	3.2586	$\frac{5}{2}^-$	10	0.55	1.5	1	5	0.11
					2.5	1	5	0.11
564	3.2850	$\frac{5}{2}^-$	5	0.26	1.5	1	5	0.10
					2.5	1	5	0.10
567	3.2877	$\frac{5}{2}^-$	10	0.53	1.5	1	5	0.10
					2.5	1	5	0.10
578	3.3015	$\frac{5}{2}^-$	3	0.15	1.5	1	2	0.04
628	3.3548	$\frac{5}{2}^-$	10	0.46	1.5	1	20	0.34
641	3.3689	$\frac{5}{2}^-$	8	0.36	1.5	1	20	0.33
					2.5	1	60	0.98
652	3.3769	$\frac{5}{2}^-$	8	0.36				
654	3.3787	$\frac{5}{2}^-$	10	0.44	1.5	1	80	1.28
					2.5	1	80	1.28
660	3.3857	$\frac{5}{2}^-$	5	0.22				

All observed f-wave resonances are arbitrarily assigned J = $\frac{5}{2}$.

Table B.7(*continued*)

Res. #	E_p (MeV)	J^π	Γ_p (eV)	γ_p^2 (keV)	s'	ℓ'	$\Gamma_{p'}$ (eV)	$\gamma_{p'}^2$ (keV)
681	3.4093	$\frac{5}{2}^-$	15	0.63	1.5	1	5	0.07
					2.5	1	5	0.07
702	3.4304	$\frac{5}{2}^-$	35	1.42	1.5	1	20	0.28
729	3.4586	$\frac{5}{2}^-$	3	0.12	1.5	1	10	0.13
733	3.4607	$\frac{5}{2}^-$	8	0.31				
750	3.4715	$\frac{5}{2}^-$	10	0.38				
759	3.4820	$\frac{5}{2}^-$	10	0.37	1.5	1	5	0.06
769	3.4924	$\frac{5}{2}^-$	5	0.18	1.5	1	5	0.06
					2.5	1	5	0.06
786	3.5090	$\frac{5}{2}^-$	10	0.35	1.5	1	10	0.12
792	3.5142	$\frac{5}{2}^-$	5	0.18				
802	3.5230	$\frac{5}{2}^-$	10	0.35	1.5	1	20	0.22
					2.5	1	10	0.11

All observed f-wave resonances are arbitrarily assigned J = $\frac{5}{2}$.

Table B.8: ^{45}Sc Resonance Parameters–J$^{\pi}$ = $\frac{7}{2}^{+}$

Res. #	E$_p$ (MeV)	J$^{\pi}$	Γ_p (eV)	γ_p^2 (keV)	s$'$	ℓ'	$\Gamma_{p'}$ (eV)	$\gamma_{p'}^2$ (keV)
101	2.6800	$\frac{7}{2}^{+}$	15	42.99				
688	3.4158	$\frac{7}{2}^{+}$	20	9.35				

Appendix C

^{45}Ca Adopted Levels

This appendix presents the spectroscopic information for the levels in ^{45}Ca as adopted in Nuclear Data Sheets [Bur92, Bur83]. The information about the levels in ^{45}Ca is necessary to identify analog resonances in ^{45}Sc.

Table C.1: ^{45}Ca Adopted Levels

E_x (keV)†	$J^{\pi\dagger}$	$T_{\frac{1}{2}}{}^\dagger$	$S_{dp}{}^\ddagger$
0.0	$\frac{7}{2}^-$	163.8 d	2.9
174.269	$\frac{5}{2}^-$	0.40 ns	0.65
1434.74	$\frac{3}{2}^-$	1.10 ps	0.40
1554.37	$\left(\frac{11}{2}^-\right)$	>2.1 ps	
1558			
1584			
1879.91	$\frac{3}{2}^+$	0.05 ps	
1884.3			0.12
1899.90	$\frac{3}{2}^-$	1.12 ps	2.2
1940.19			
1973	$\frac{5}{2}^-, \frac{7}{2}^-$	0.08	
2249.08	$\frac{1}{2}^-$	0.43 ps	0.30

† [Bur92]

‡ [Bur83]

Table C.1(*continued*)

E_x (keV)†	J^{π}†	$T_{\frac{1}{2}}$†	S_{dp}‡
2353.81	$\frac{1}{2}^+, \frac{3}{2}^+, \frac{5}{2}^+$	4.7 ns	
2392.38	$\frac{1}{2}^+$	0.19 ps	0.10
2523.1	$\left(\frac{3}{2}, \frac{5}{2}, \frac{7}{2}\right)$		
2599			
2683	$\left(\frac{3}{2}, \frac{5}{2}\right)$		
2771.12	$\frac{1}{2}^+, \frac{3}{2}^+, \frac{5}{2}^+$		
2786			
2842.07	$\frac{3}{2}^-$	22 fs	0.34
2877.99	$\left(\frac{15}{2}^-\right)$	>2.1 ps	
2953			
2976.8	$\frac{5}{2}^-$	42 fs	0.34
3023.7	$\frac{1}{2}, \frac{3}{2}, \frac{5}{2}$		
3035			
3151			
3241.35	$\frac{3}{2}^-$	36 fs	0.14
3278			
3294.5	$\left(\frac{3}{2}^+, \frac{5}{2}^+\right)$		(0.01)
3322	$\frac{5}{2}^-, \frac{7}{2}^-$		0.28
3348			
3418.34	$\frac{1}{2}^-$	35 fs	
3442	$\frac{1}{2}^-, \frac{3}{2}^-$		0.49
3463			
3490.8	$\frac{3}{2}^-, \frac{5}{2}^+$		
3556.01			
3560	$\left(\frac{1}{2}^+\right)$		
3654.0	$\frac{1}{2}, \frac{3}{2}, \frac{5}{2}$		

† [Bur92]

‡ [Bur83]

Table C.1(*continued*)

E_x (keV)[†]	J^{π}[†]	$T_{\frac{1}{2}}$[†]	S_{dp}[‡]
3675			
3705.0	$\frac{1}{2}, \frac{3}{2}, \frac{5}{2}$		
3753			
3783.28	$\frac{1}{2}^{-}, \frac{3}{2}^{-}$	<26 fs	0.08
3838.03	$\left(\frac{1}{2}\right)^{-}$	<15 fs	0.19

† [Bur92]

‡ [Bur83]

Appendix D

Unfolded Sequences

In this appendix, the effects of unfolding the energy dependence of the level density are shown. In each of the following figures, the cumulative number of levels N(E) is plotted for both the experimental excitation energies and the unfolded values of those energies. The upper curve in each plot shows N(E) for the unfolded energies while the lower curve shows N(E) for the true energies. The unfolding procedure is described in Section 6.1.

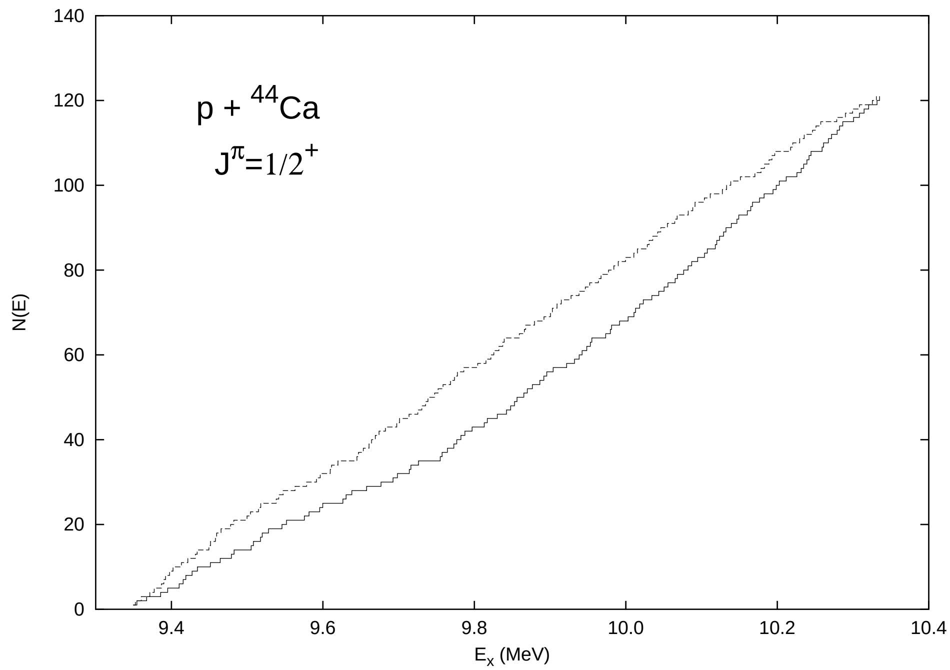

Figure D.1: N(E) plots for experimental and unfolded values of E_x for the s-wave resonance sequence.

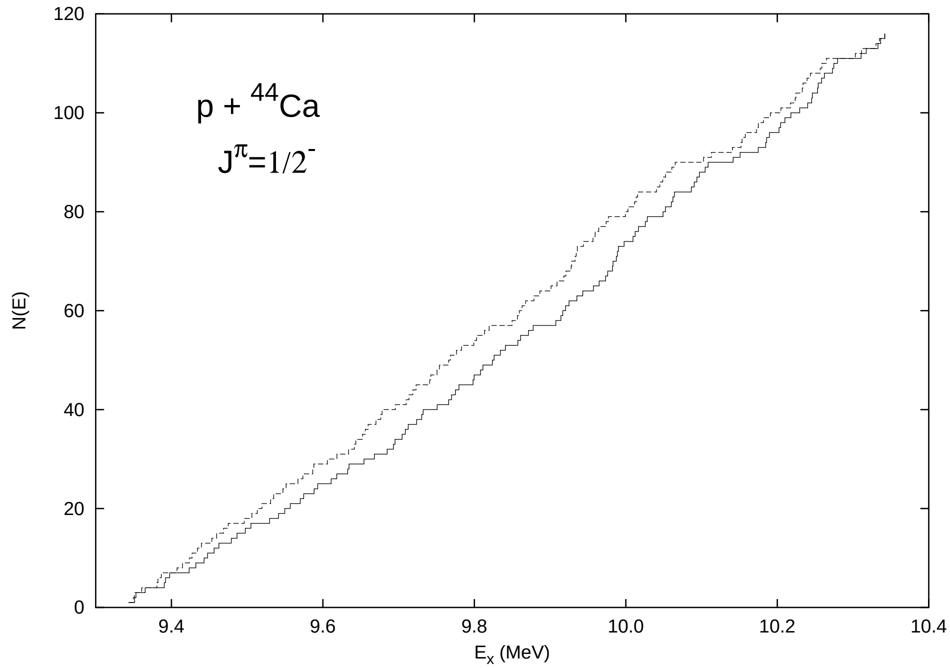

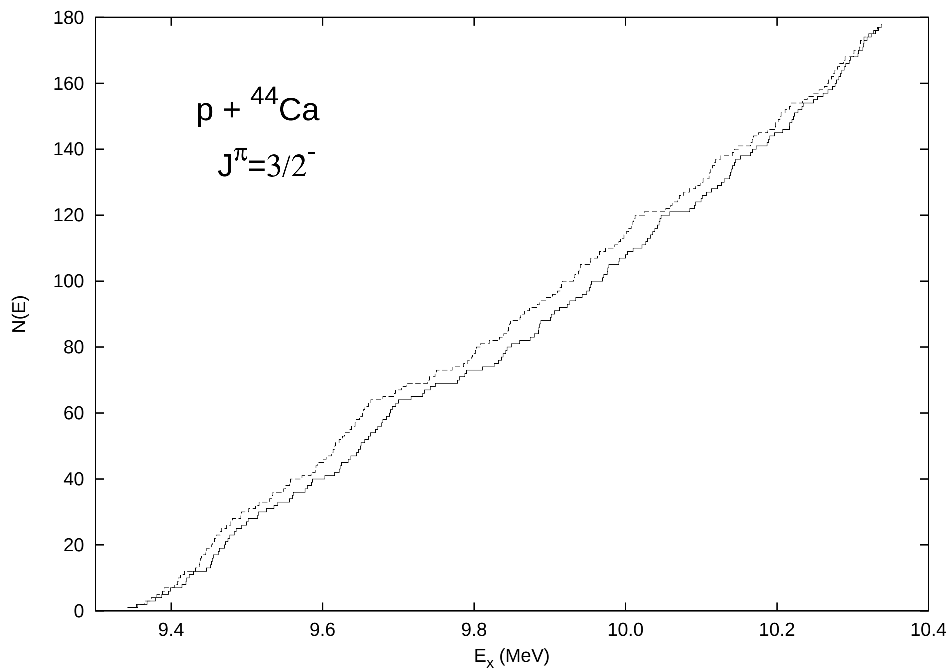

Figure D.2: N(E) plots for experimental and unfolded values of E_x for p-wave resonance sequences.

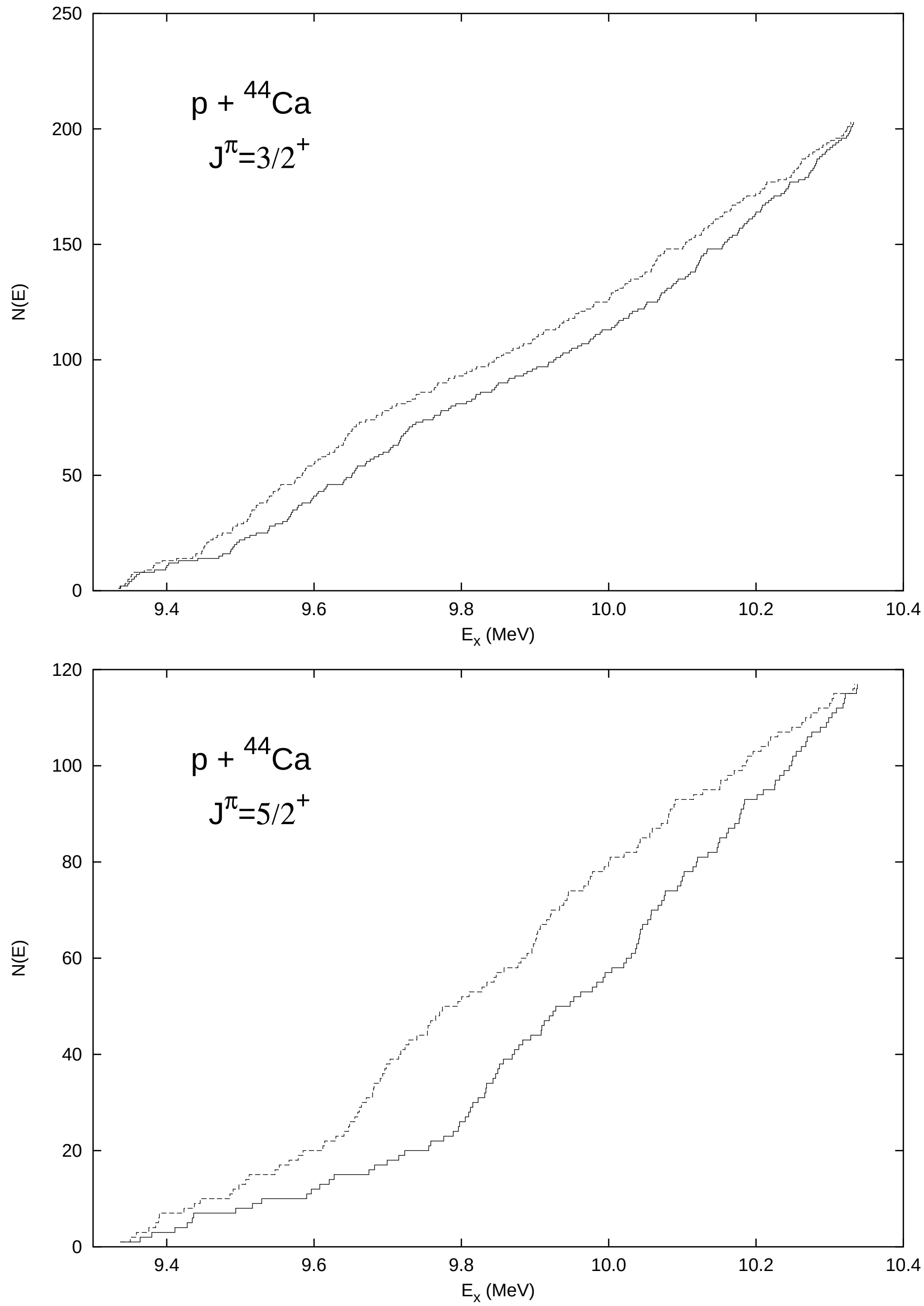

Figure D.3: N(E) plots for experimental and unfolded values of E_x for d-wave resonance sequences.

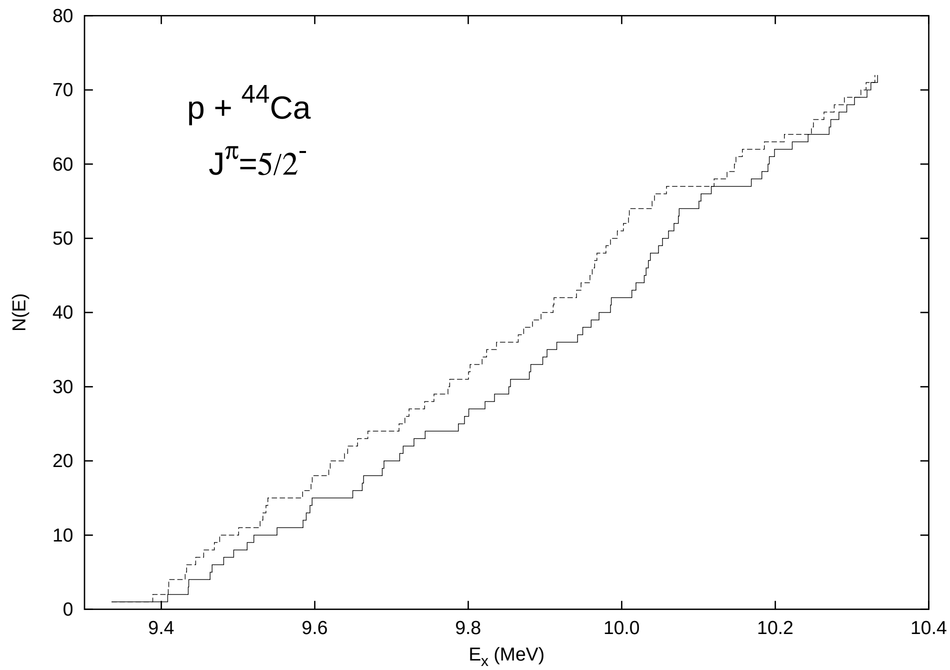

Figure D.4: N(E) plots for experimental and unfolded values of E_x for the f-wave resonance sequence.

Bibliography

[Agv02] U. Agvaanluvsan, *Level Density Analysis of Nuclear Resonances*, Ph.D. thesis, North Carolina State University, 2002.

[Agv03a] U. Agvaanluvsan, G. E. Mitchell, J. F. Shriner, Jr., and M. Pato, "Parity Dependence of Nuclear Level Densities", Physical Review **C67**, 064608 (2003).

[Agv03b] U. Agvaanluvsan, G. E. Mitchell, J. F. Shriner, Jr., and M. P. Pato, "Missing Level Corrections in Nuclear Resonances", Nuclear Instruments and Methods in Physics Research **A498**, 459 (2003).

[Bie52] L. C. Biedenharn, J. M. Blatt, and M. E. Rose, "Some Properties of the Racah and Associated Coefficients", Review of Modern Physics **24**, 249 (1952).

[Bil76] E. G. Bilpuch, A. M. Lane, G. E. Mitchell, and J. D. Moses, "Fine Structure of Analog States", Physics Reports **28**, 145 (1976).

[Bur83] T. Burrows, "Nuclear Data Sheets for A=45", Nuclear Data Sheets **40**, 149 (1983).

[Bur92] T. Burrows, "Nuclear Data Sheets Update for A=45", Nuclear Data Sheets **65**, 1 (1992).

[Con51] E. U. Condon and G. H. Shortley, *The Theory of Atomic Spectra*, Cambridge University Press, Cambridge, 1951.

[Dys63] F. J. Dyson and M. L. Mehta, "Statistical Theory of the Energy Levels of Complex Systems. IV", Journal of Mathematical Physics **4**, 701 (1963).

[Frö80] F. H. Fröhner, "Nuclear Theory and Applications", IAEA-SMR- **43**, 59 (1980).

[Gil65] A. Gilbert and A. G. W. Cameron, "A Composite Nuclear-Level Density Formula with Shell Model Corrections", Canadian Journal of Physics **43**, 1446 (1965).

[Guh98] T. Guhr, A. Müller-Groeling, and H. A. Weidenmüller, "Random Matrix Theories in Quantum Physics: Common Concepts", Physics Reports **299**, 190 (1998).

[Hub54] R. Huby, "Phase of Matrix Elements in Nuclear Reactions and Radioactive Decay", Proceedings of the Physical Society, Section A **67**, 1103 (1954).

[Jah60] E. Jahnke, F. Emde, and F. Lösch, *Tables of Higher Functions*, McGraw-Hill, New York, 1960.

[Jän69] J. Jänecke, "Systematics of Coulomb Energies and Excitation Energies of Isobaric Analog States", in *Isospin in Nuclear Physics*, edited by D. H. Wilkinson, North-Holland, Amsterdam, 1969.

[Lan58] A. M. Lane and R. G. Thomas, "R-Matrix Theory of Nuclear Reactions", Reviews of Modern Physics **30**, 257 (1958).

[Lyn68] J. E. Lynn, *The Theory of Neutron Resonance Reactions*, Clarendon, Oxford, 1968.

[Meh91] M. L. Mehta, *Random Matrices*, Academic Press, New York, second edition, 1991.

[Nel83] R. O. Nelson, *Proton Resonance Spectroscopy in* ^{28}Si *and* ^{30}P, Ph.D. thesis, Duke University, 1983.

[Nud03] National Nuclear Data Center, www.nndc.bnl.gov, 2003.

[Por56] C. E. Porter and R. G. Thomas, "Fluctuations of Nuclear Reaction Widths", Physical Review **104**, 483 (1956).

[Shr82] J. F. Shriner, Jr., K. M. Whatley, E. G. Bilpuch, C. R. Westerfeldt, and G. E. Mitchell, "Amplitude Correlations for Inelastic Proton Scattering from ^{44}Ca", Zeitschrift für Physik **A305**, 307 (1982).

[Shr83] J. F. Shriner, Jr., K. M. Whatley, E. G. Bilpuch, C. R. Westerfeldt, and G. E. Mitchell, "Statistical Properties of $3/2^-$ Resonances in ^{45}Sc and ^{51}Mn", Zeitschrift für Physik **A313**, 51 (1983).

[Shr90] J. F. Shriner, Jr., E. G. Bilpuch, P. Endt, and G. E. Mitchell, "Fluctuation Properties of States in ^{26}Al", Zeitschrift für Physik **A335**, 393 (1990).

[Smi89] B. W. Smith, *Level Density Studies in* ^{45}Sc, Ph.D. thesis, Duke University, 1989.

[Wat80] W. A. Watson, III, *A High Resolution Study of Proton Resonances in* ^{57}Co, Ph.D. thesis, Duke University, 1980.

[Wes82] C. R. Westerfeldt, Triangle Universities Nuclear Laboratory Annual Report — TUNL XXI, 1982.

[Wes83] C. R. Westerfeldt, Triangle Universities Nuclear Laboratory Annual Report — TUNL XXII, 1983.

[Wes88] C. R. Westerfeldt, R. O. Nelson, E. G. Bilpuch, and G. E. Mitchell, "A Microcomputer-Based System for Measuring Excitation Functions with Good Energy Resolution", Nuclear Instruments and Methods in Physics Research **A270**, 467 (1988).

[Wes95] C. R. Westerfeldt, J. F. Shriner, Jr., and G. A. Vavrina, *The TUNL High Resolution Laboratory System and Operating Procedures*, Triangle Universities Nuclear Laboratory, Durham, NC, third edition, 1995.

[Wig46a] E. P. Wigner, "Resonance Reactions", Physical Review **70**, 606 (1946).

[Wig46b] E. P. Wigner, "Resonance Reactions and Anomalous Scattering", Physical Review **70**, 15 (1946).

[Wig47] E. P. Wigner and L. Eisenbud, "Higher Angular Momenta and Long Range Interaction in Resonance Reactions", Physical Review **72**, 29 (1947).

[Wig57] E. P. Wigner, "Results and Theory of Resonance Absorption", Oak Ridge National Laboratory Report ORNL-2309, 1957.

[Wil73] W. M. Wilson, Jr., *A High Resolution Study of Proton Resonances in* ^{41}Sc, ^{43}Sc, *and* ^{45}Sc, Ph.D. thesis, Duke University, 1973.

[Wil75] W. M. Wilson, E. G. Bilpuch, and G. E. Mitchell, "Fine Structure of Analogue States in ^{45}Sc", Nuclear Physics **A245**, 262 (1975).